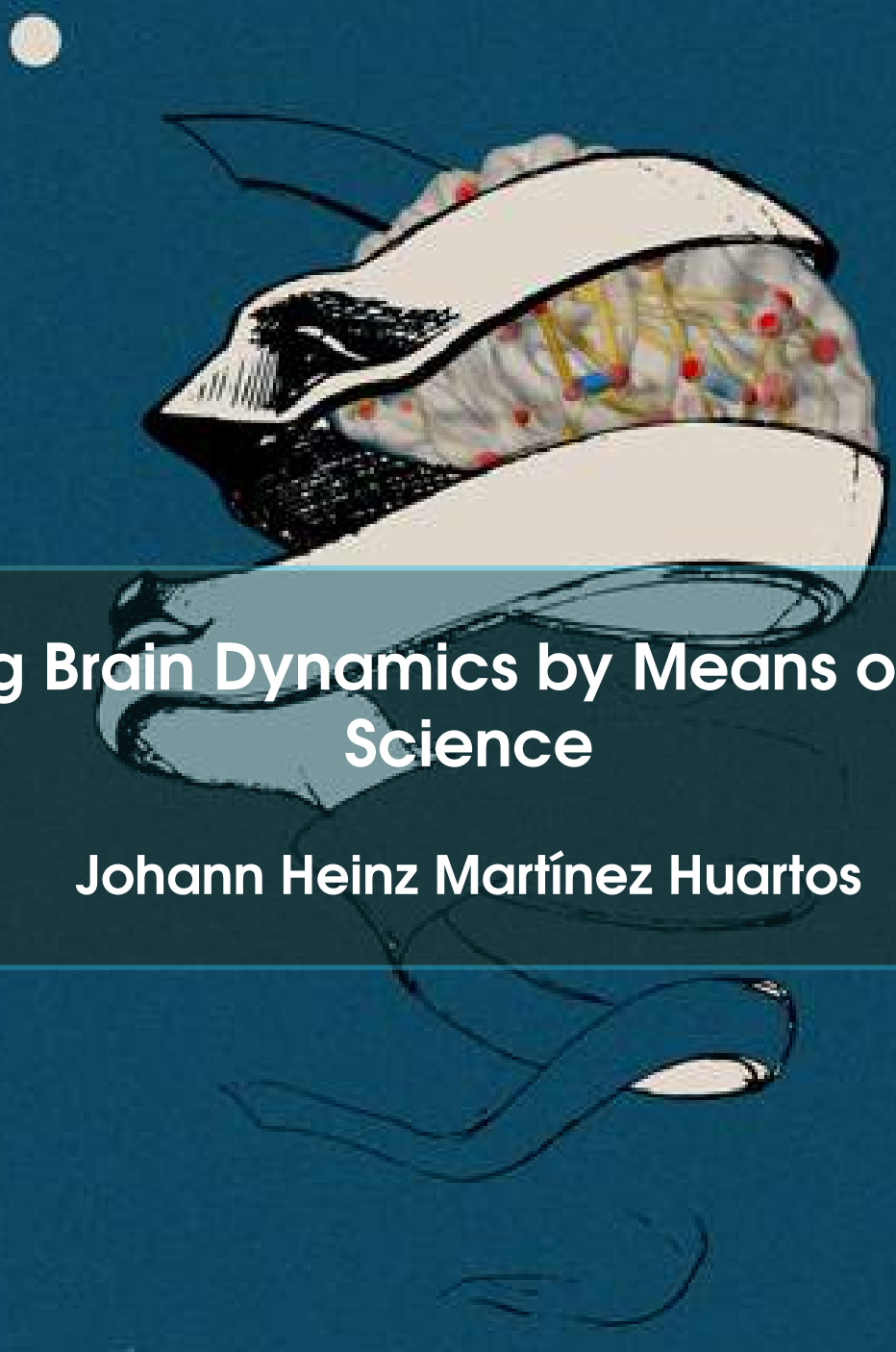

Analysing Brain Dynamics by Means of Networks Science

Johann Heinz Martínez Huartos

A dissertation submitted to the Technical University of Madrid. Spain, in accordance with the requirements of the degree of DOCTOR OF PHILOSOPHY in the Physics of Complex Systems.

Copyright © 2015 Johann H. Martínez
PUBLISHED BY UPM EDITORIAL PRESS
www.johemart.wix.com/neurocomplexity

I declare that the work in this dissertation was carried out in accordance with the requirements of the University's Regulations and Code of Practice for Research Degree Programmes and that it has not been submitted for any other academic award. Except where indicated by specific reference in the text, the work is the candidate's own work, with the advisory of professors Dr. Juan Manuel Pastor Ph.D and Dr. Javier Martín Buldú Ph.D. Any views expressed in the dissertation are those of the author.

First printing, July 2015

Dedication

All the good efforts and the excellent results of this work belong to my beloved parents, sisters and brothers. Without you all, it would have not been possible to arrive here.

Dedicated to

Maria Roquelia Huartos
Cruz Alcibiades Martínez

Alcibiades
Esperanza
Javier
Susana
Roquelia
Rodrigo

Acknowledgements

Las cosas claras. Absolutamente todo lo positivo de esta tesis, los buenos resultados, los objetivos cumplidos y los grandes esfuerzos pertenecen completamente a mi familia y al conjunto de personas que han creído en mi a lo largo de estos años. Los errores y faltas competen enteramente a mi. Gracias a todos los que de una y otra forma colaboraron y se preocuparon por mí en esta etapa.

En primera instancia quiero agradecer a mi gran abuelo Maximo Huartos, quien me infundió el hábito de la lectura y me mostró la relevancia de las matemáticas. A mis padres, Cruz Martínez y Maria Roquelia Huartos, a él, que me cuidó con calma y me enseñó a reír inclusive en momentos difíciles, a ella, que delicadamente me enseñó el valor del trabajo cumplido. A ellos, mis más bellos campesinos que me enseñaron a apreciar la naturaleza y de quienes me siento completamente orgulloso. Ellos son implícitamente los verdaderos autores de esta tesis.

De igual manera agradezco con mucho cariño a mis hermanos. A Alci, por haberme enseñado la diferencia entre un trueno, un rayo y un relámpago, cuando era niño. Esto fue el inicio de mi interés por la ciencia. Gracias por enseñarme lo sorprendente de la naturaleza cuando era niño. A las Panchas por haberme consentido tanto, Gracias por ser ese nicho de amor en el que me puedo refugiar siempre. A Javier, quien me enseñó a tener ambiciones en la vida. Gracias por haberme dicho que me centrara en programar y en el Inglés. A Susi, de quien aprendí a tener siempre una mentalidad joven y alegre. Gracias por ser mi confidente. A Roqui, de quien recibí mucha disciplina que me ha ayudado a llegar hasta este punto. Gracias por corregirme y amarme. A kikín, quien me guió, me aconsejó y me alentó muchas veces en todos mis problemas. Gracias por ser mi protector. A mi tío Emigdio, quien siempre ayudó a mi familia y procuró por el bienestar de todos nosotros. Gracias por tu apoyo a mi carrera y la confianza en mí.

Por un lado, también quiero agradecer y hacer mención a quienes me ayudaron a formarme académicamente. A ellos, de quienes recibí consejos, opiniones, ayudas e inclusive desaprobaciones y, además, me alentaron a seguir mis objetivos sin importar las bases que tuviese. A Bernardo Gómez, Carlos Ávila, Alonso Botero, de la Universidad de los Andes en Bogotá. A Ramón Fayad de la Universidad Nacional de Colombia, A Carlos Moreno Benavides y Carlos Maldonado de la

Universidad del Rosario de Colombia. A Filena Jimenez, mi profesora de física en la secundaria. Mis bases académicas y científicas fueron plantadas por ustedes.

De la misma forma, quiero expresar mi sincera gratitud al profesor Esteban Duran y la directora Gisele Becerra del CESA en Bogotá. Aun me pregunto qué vieron ellos en mí para apoyar las ideas locas que tenía. De alguna manera, este viaje implícitamente empezó al meterme en el lago de aquella finca. Gracias a Fernando Restrepo y Fernando Locano, ex decanos de la escuela de administración de la Universidad del Rosario en Bogotá. A Gabriel Silgado, decano del medio universitario. Gracias por la confianza depositada en mí al presentarme al comité de becas, gracias por apoyarme en esta estadía.

A las personas que colateralmente ayudaron, de manera personal, a que este trabajo viera la luz. A la familia Navas Garrido por todo su apoyo y su calidez. A Juan Carlos Sanchez, por su gran soporte al escribir este documento. A Diana Martínez, por su apoyo incondicional desde los inicios de mi carrera y a José David Romero por estar presente siempre.

Así mismo, una especial mención a la Fundación Carolina de España y su programa iberoamericano de becas doctorales para jóvenes profesores de Latinoamérica. Gracias por apoyarnos. A Piedad Martín Díez de Baldeon y Juan Torres Minondo, coordinadores de dicho programa de becas. Gracias por su apoyo a mi llegada a España y a lo largo de estos cinco años. Mi reconocimiento también para el programa de becas doctorales 568 de Colciencias en Colombia, al comité de becas de la universidad del Rosario y al ministerio de economía y competitividad español. Gracias por creer en las aptitudes de los jóvenes colombianos. Mi completo agradecimiento a mi director de tesis en la Universidad Politécnica de Madrid (UPM), profesor Dr. Juan Manuel Pastor Ruíz. Gracias por creer en mí y dedicar gran parte de su tiempo a ayudarme en todo lo que yo quería hacer con mi vida académica. Gracias por siempre estar pendiente y preocuparte por mí. Sus guías y apoyo fueron enteramente relevantes para poder llegar a este punto desde mis inicios en el grupo de investigación. Gracias al profesor Javier Galeano, quien siempre tuvo la puerta de su oficina abierta para ayudarme con preguntas. En general, gracias al Grupo de Sistemas Complejos de la UPM. A su directora, profesora Rosa Maria Benito, por su eficiente labor administrativa, al profesor Juan Carlos Losada, por sus recomendaciones, al profesor Luis Seidel, quien nunca se librará de mis preguntas sobre LaTeX. Gracias a todos ellos por contestar con detenimiento mis largos correos de preguntas.

De igual forma, deseo agradecer al profesor Dr. Alex Arenas, de la Universitat Rovira i Virgili de Tarragona. Gracias, no solamente por las referencias y libros que me recomendó cuando lo conocí, sino también por aquel consejo que me dio en Natal. Eso marcó el curso de mi carrera. Al profesor Dr. Jesús Gómez Gardeñes, de la Universidad de Zaragoza. Gracias por creer en mi, apoyarme, aconsejarme y ayudar a delinear parte de una vida científica. Al profesor Dr. Ernesto Estrada, de "*Strathclyde University*" por sus clases sobre la *"eigenvector centrality*", pero en especial, por su alegría, por los buenos deseos y consejos y la forma en la que él tiene de incentivar a las personas. Al investigador Ricardo Bajo, del Centro de Tecnología Biomédica de Madrid. Gracias por ayudarme a resolver dudas al llegar al centro.

Al grupo de París de Mario Chavez. Gracias por darme la oportunidad de trabajar con ustedes. A Xavier, por sus traducciones del Francés-Inglés-Catalán al Español. A Fabrizio de Vico Fallani, por sus múltiples correcciones y ayudas. Quedó en mi mente la frase: "*[...] when I started, I started like you, so keep calm that you are doing it right*. En especial, gracias al profesor Dr. Mario Chavez, cabeza del grupo de investigación en redes complejas cerebrales en el "*L'institut du cerveau et de la Moelle Épinère, Hôpital Universitarie Pitié-Salpêtrière et Universite Pierre et Marie Curie-Paris*

VI". Gracias Dr. Mario por permitirme trabajar en su laboratorio. Mas allá de ser un gran científico, eres es una excelente persona y un gran amigo que me apoyó durante mi vida en Francia. De manera general, ustedes son mis co asesores implícitos de este trabajo.

Por otro lado, deseo agradecer también al Dr. Massimiliano Zanin del "*Innaxis Research Foundation*". Gracias por sus clases en SVM. Gracias también al profesor Dr. Stefano Boccaletti, de la embajada de Italia en Israel y a la profesora Dra. Irene Sendiña Nadal de la Universidad Rey Juan Carlos (URJC) por sus comentarios, correcciones y opiniones de esta tesis. Definitivamente sus aportes enriquecieron este trabajo. Gracias a los profesores Inmaculada Leyva y Juan Almendral miembros del "*Biological Network Group*" de la URJC, y a profesor Jacobo Aguirre, por las dudas, correcciones y discusiones a lo largo de estos últimos dos años.

A mis compañeros de doctorado: Daniel, Eliezer, Ricardo Sevilla, Jose Pineda, Ricardo Gutierrez, por los momentos compartidos. A Alfredo Morales, Maximiliano Fernandez, Bettina y Paco, por haberme sacado de problemas miles de veces. En especial a Adrian Santo-Tomas, quien particularmente me ayudó muchísimo en la etapa final de la tesis. Los últimos capítulos avanzaron por él. Gracias también a Mathias Legrand de "*McGill University*" por sus comentarios, ayudas y discusiones en el uso de su plantilla LaTeX. Todo un maestro de la estética.

En especial, mi inmensa gratitud al profesor Dr. David Papo, uno de los científicos mas excepcionales que he podido conocer. Alguien que se ha leído casi todos los artículos publicados de neurociencia y complejidad, una biblioteca ambulante. Alguien que, sin importar el área de conocimiento, siempre tiene una respuesta a cada pregunta, una buena pregunta para cada idea, una buena idea para cualquier empresa y una palabra alentadora para cada mal momento. Esta tesis, sin él, no hubiese llegado a buen término. ¡Muchas Gracias David, eres un gran amigo y un excelente mentor!

Finalmente, deseo dedicar especialmente este párrafo para agradecer a quien está detrás de esta tesis. A aquel que llevó el timón en estos dos últimos años y medio, que marcó la pauta de lo que debería ser, -no solo los tópicos de esta tesis-, sino también lo que es ser un buen científico. Alguien que valora mucho la forma en que las personas luchan para conseguir sus propósitos, sin importar lo que tenían al empezar sus batallas. Gracias por tanta paciencia que tuviste conmigo, gracias por buscar miles de formas de explicarme la misma respuesta una y otra vez. Gracias por guiarme, inclusive en cálculos simples, por soportar las correcciones de esta tesis, por confiar en mi trabajo, por corregirlo y criticarlo fuertemente, por querer sacar al mundo un buen investigador. Gracias por la oportunidad que me diste de trabajar en tu grupo, los eventos asistidos, las discusiones. Gracias por creer en mí, por incentivar mi trabajo, por fortalecer mi conocimiento. Gracias por estar siempre en las buenas y darme aliento en los momentos más difíciles de estos años. Gracias por ser mi mentor, mi director de tesis, y además mi amigo, creo que nunca te vas a librar de mi. Gracias profesor Dr. Javier Martín Buldú.

Resumen

El cerebro humano es probablemente uno de los sistemas más complejos a los que nos enfrentamos en la actualidad, si bien es también uno de los más fascinantes. Sin embargo, la compresión de cómo el cerebro organiza su actividad para llevar a cabo tareas complejas es un problema plagado de restos y obstáculos.

En sus inicios la neuroimagen y la electrofisiología tenían como objetivo la identificación de regiones asociadas a activaciones relacionadas con tareas especificas, o con patrones locales que variaban en el tiempo dada cierta actividad. Sin embargo, actualmente existe un consenso acerca de que la actividad cerebral tiene un carácter temporal multiescala y espacialmente extendido, lo que lleva a considerar el cerebro como una gran red de áreas cerebrales coordinadas, cuyas conexiones funcionales son continuamente creadas y destruidas. Hasta hace poco, el énfasis de los estudios de la actividad cerebral funcional se han centrado en la identidad de los nodos particulares que forman estas redes, y en la caracterización de métricas de conectividad entre ellos: la hipótesis subyacente es que cada nodo, que es una representación mas bien aproximada de una región cerebral dada, ofrece a una única contribución al total de la red. Por tanto, la neuroimagen funcional integra los dos ingredientes básicos de la neuropsicología: la localización de la función cognitiva en módulos cerebrales especializados y el rol de las fibras de conexión en la integración de dichos módulos. Sin embargo, recientemente, la estructura y la función cerebral han empezado a ser investigadas mediante la Ciencia de la Redes, una interpretación mecánico-estadística de una antigua rama de las matemáticas: La teoría de grafos. La Ciencia de las Redes permite dotar a las redes funcionales de una gran cantidad de propiedades cuantitativas (robustez, centralidad, eficiencia, ...), y así enriquecer el conjunto de elementos que describen objetivamente la estructura y la función cerebral a disposición de los neurocientíficos.

La conexión entre la Ciencia de las Redes y la Neurociencia ha aportado nuevos puntos de vista en la comprensión de la intrincada anatomía del cerebro, y de cómo las patrones de actividad cerebral se pueden sincronizar para generar las denominadas redes funcionales cerebrales, el principal objeto de estudio de esta Tesis Doctoral. Dentro de este contexto, la complejidad emerge como el puente entre las propiedades topológicas y dinámicas de los sistemas biológicos y, específicamente, en la relación entre la organización y la dinámica de las redes funcionales

cerebrales. Esta Tesis Doctoral es, en términos generales, un estudio de cómo la actividad cerebral puede ser entendida como el resultado de una red de un sistema dinámico íntimamente relacionado con los procesos que ocurren en el cerebro. Con este fin, he realizado cinco estudios que tienen en cuenta ambos aspectos de dichas redes funcionales: el topológico y el dinámico.

De esta manera, la Tesis está dividida en tres grandes partes: Introducción, Resultados y Discusión. En la primera parte, que comprende los Capítulos 1, 2 y 3, se hace un resumen de los conceptos más importantes de la Ciencia de las Redes relacionados al análisis de imágenes cerebrales. Concretamente, el Capitulo 1 está dedicado a introducir al lector en el mundo de la complejidad, en especial, a la complejidad topológica y dinámica de sistemas acoplados en red. El Capítulo 2 tiene como objetivo desarrollar los fundamentos biológicos, estructurales y funcionales del cerebro, cuando éste es interpretado como una red compleja. En el Capítulo 3, se resumen los objetivos esenciales y tareas que serán desarrolladas a lo largo de la segunda parte de la Tesis.

La segunda parte es el núcleo de la Tesis, ya que contiene los resultados obtenidos a lo largo de los últimos cuatro años. Esta parte está dividida en cinco Capítulos, que contienen una versión detallada de las publicaciones llevadas a cabo durante esta Tesis. El Capítulo 4 está relacionado con la topología de las redes funcionales y, específicamente, con la detección y cuantificación de los nodos mas importantes: aquellos denominados “hubs” de la red. En el Capítulo 5 se muestra como las redes funcionales cerebrales pueden ser vistas no como una única red, sino más bien como una red-de-redes donde sus componentes tienen que coexistir en una situación de balance funcional. De esta forma, se investiga cómo los hemisferios cerebrales compiten para adquirir centralidad en la red-de-redes, y cómo esta interacción se mantiene (o no) cuando se introducen fallos deliberadamente en la red funcional. El Capítulo 6 va un paso mas allá al considerar las redes funcionales como sistemas vivos. En este Capítulo se muestra cómo al analizar la evolución de la topología de las redes, en vez de tratarlas como si estas fueran un sistema estático, podemos caracterizar mejor su estructura. Este hecho es especialmente relevante cuando se quiere tratar de encontrar diferencias entre grupos que desempeñan una tarea de memoria, en la que las redes funcionales tienen fuertes fluctuaciones. En el Capítulo 7 defino cómo crear redes parenclíticas a partir de bases de datos de actividad cerebral. Este nuevo tipo de redes, recientemente introducido para estudiar las anormalidades entre grupos de control y grupos anómalos, no ha sido implementado nunca en datos cerebrales y, en este Capítulo explico cómo hacerlo cuando se quiere evaluar la consistencia de la dinámica cerebral. Para concluir esta parte de la Tesis, el Capítulo 8 se centra en la relación entre las propiedades topológicas de los nodos dentro de una red y sus características dinámicas. Como mostraré más adelante, existe una relación entre ellas que revela que la posición de un nodo dentro una red está íntimamente correlacionada con sus propiedades dinámicas.

Finalmente, la última parte de esta Tesis Doctoral está compuesta únicamente por el Capítulo 9, el cual contiene las conclusiones y perspectivas futuras que pueden surgir de los trabajos expuestos.

En vista de todo lo anterior, espero que esta Tesis aporte una perspectiva complementaria sobre uno de los más extraordinarios sistemas complejos frente a los que nos encontramos: El cerebro humano.

Abstract

The human brain is probably one of the most complex systems we are facing, thus being a timely and fascinating object of study. Characterizing how the brain organizes its activity to carry out complex tasks is highly non-trivial. While early neuroimaging and electrophysiological studies typically aimed at identifying patches of task-specific activations or local time-varying patterns of activity, there has now been consensus that task-related brain activity has a temporally multiscale, spatially extended character, as networks of coordinated brain areas are continuously formed and destroyed. Up until recently, though, the emphasis of functional brain activity studies has been on the identity of the particular nodes forming these networks, and on the characterization of connectivity metrics between them, the underlying covert hypothesis being that each node, constituting a coarse-grained representation of a given brain region, provides a unique contribution to the whole. Thus, functional neuroimaging initially integrated the two basic ingredients of early neuropsychology: localization of cognitive function into specialized brain modules and the role of connection fibres in the integration of various modules. Lately, brain structure and function have started being investigated using Network Science, a statistical mechanics understanding of an old branch of pure mathematics: graph theory. Network Science allows endowing networks with a great number of quantitative properties, thus vastly enriching the set of objective descriptors of brain structure and function at neuroscientists' disposal.

The link between Network Science and Neuroscience has shed light about how the entangled anatomy of the brain is, and how cortical activations may synchronize to generate the so-called functional brain networks, the principal object under study along this PhD Thesis. Within this context, complexity appears to be the bridge between the topological and dynamical properties of biological systems and, more specifically, the interplay between the organization and dynamics of functional brain networks. This PhD Thesis is, in general terms, a study of how cortical activations can be understood as the output of a network of dynamical systems that are intimately related with the processes occurring in the brain. In order to do that, I performed five studies that encompass both the topological and the dynamical aspects of such functional brain networks.

In this way, the Thesis is divided into three major parts: Introduction, Results and Discussion. In the first part, comprising Chapters 1, 2 and 3, I make an overview of the main concepts of

Network Science related to the analysis of brain imaging. More specifically, Chapter 1 is devoted to introducing the reader to the world of complexity, specially to the topological and dynamical complexity of networked systems. Chapter 2 aims to develop the biological, topological and functional fundamentals of the brain when it is seen as a complex network. Next, Chapter 3 summarizes the main objectives and tasks that will be developed along the forthcoming Chapters.

The second part of the Thesis is, in turn, its core, since it contains the results obtained along these last four years. This part is divided into five Chapters, containing a detailed version of the publications carried out during the Thesis. Chapter 4 is related to the topology of functional networks and, more specifically, to the detection and quantification of the leading nodes of the network: the hubs. In Chapter 5 I will show that functional brain networks can be viewed not as a single network, but as a network-of-networks, where its components have to co-exist in a trade-off situation. In this way, I investigate how the brain hemispheres compete for acquiring the centrality of the network-of-networks and how this interplay is maintained (or not) when failures are introduced in the functional network. Chapter 6 goes one step beyond by considering functional networks as living systems. In this Chapter I show how analyzing the evolution of the network topology instead of treating it as a static system allows to better characterize functional networks. This fact is especially relevant when trying to find differences between groups performing certain memory tasks, where functional networks have strong fluctuations. In Chapter 7 I define how to create parenclitic networks from brain imaging datasets. This new kind of networks, recently introduced to study abnormalities between control and anomalous groups, have not been implemented with brain datasets and I explain in this Chapter how to do it when evaluating the consistency of brain dynamics. To conclude with this part of the Thesis, Chapter 8 is devoted to the interplay between the topological properties of the nodes within a network and their dynamical features. As I will show, there is an interplay between them which reveals that the position of a node in a network is intimately related with its dynamical properties.

Finally, the last part of this PhD Thesis is composed only by Chapter 9, which contains the conclusions and future perspectives that may arise from the exposed results.

In view of all, I hope that reading this Thesis will give a complementary perspective of one of the most extraordinary complex systems: The human brain.

Declaration

I declare that the work in this dissertation was carried out in accordance with the requirements of the University's Regulations and Code of Practice for Research Degree Programmes and that it has not been submitted for any other academic award. Except where indicated by specific reference in the text, the work is the candidate's own work. with the advisory of professors Dr. Juan Manuel Pastor and Dr. Javier Martín Buldú. Any views expressed in the dissertation are those of the author.

SIGNED: ..... DATE: .....

Authorization

TECHNICAL UNIVERSITY OF MADRID
Applied Physics II Department
Higher Technical School of Agronomic Engineers
(E. T. S. I. Agrónomos)

The undersigned hereby certify that they have read and recommend to the Faculty of doctoral committe in Agronomic Engineer of Universidad Politécnica de Madrid. (Spain) the acceptance of the Thesis entitled *Analysing Brain Dynamics by Means of Networks Science*, by Johann Heinz Martínez Huartos in fulfillment of the requirements for the degree of *philosophiae doctor* in science.

Dated: October 2015

SUPERVISOR: .....
Professor Dr. Juan Manuel Pastor Ph.D.

CO ADVISOR: .....
Professor Dr. Javier Martín Buldú. Ph.D.

EXTERNAL EXAMINER: .....
Professor Dr. Stefano Boccaletti Ph.D.

EXTERNAL EXAMINER: .....
Professor Dr. Guillermo Huerta Cuellar Ph.D.

Permissions

TECHNICAL UNIVERSITY OF MADRID

Date: September 2015

Author: **Johann Heinz Martínez Huartos**.
Title: **Analysing Brain Dynamics by Means of Networks Science.**
Department: **Applied Physics II**.

Degree: **Ph. D** Convocation: **October** Year: **2015**

Permission is herewith granted to Technical University of Madrid to circulate and to have copied for non-commercial purposes, at its discretion, the above title upon the request of individuals or institutions.

SIGNATURE OF AUTHOR: .....
Johann Heinz Martínez Huartos.

THE AUTHOR RESERVES OTHER PUBLICATION RIGHTS, AND NEITHER THE THESIS NOR EXTENSIVE EXTRACTS FROM IT MAY BE PRINTED OR OTHERWISE REPRODUCED WITHOUT THE AUTHOR'S WRITTEN PERMISSION.

THE AUTHOR ATTESTS THAT PERMISSION HAS BEEN OBTAINED FOR THE USE OF ANY COPYRIGHTED MATERIAL APPEARING IN THIS THESIS (OTHER THAN BRIEF EXCERPTS REQUIRING ONLY PROPER ACKNOWLEDGEMENT IN SCHOLARLY WRITING) AND THAT ALL SUCH USE IS CLEARLY ACKNOWLEDGED.

Contents

List of Figures

List of Tables

Introduction

1 Complexity of Interconnected Systems

Regardless the success of reductionism in science, the later half of the previous century came with the so called complexity paradigm, putting under the spotlight the perspective of *"how we study"* nature, more than *"what we study"* in nature. This PhD Thesis is an illustration of how complexity sciences can lead to the enhancement of our knowledge of, perhaps, the most extraordinary complex system we are dealing with: The human brain.

In order to contextualize the reader, this first Chapter puts the emphasis on complexity as one of the main and novel perspectives in science devoted to understand how systems in nature behave. With this aim, I will develop an abbreviated summary of *Complex Networks Theory* (also known as *Network Science*), which is concerned about the understanding of the organization of interacting systems, being one of the most fruitful approaches in complexity sciences. In this way, this Chapter reviews the basic models and main properties describing the topology of networked systems and explains how the structural properties of networks are related to different dynamical aspects of the dynamical units but also to the network as a whole. Nevertheless, even though it is necessary to fathom the scaffolding of networked systems, it is also important to realize that nature, -specially biological systems-, is in continuous evolution. This means that the time variable plays a crucial role and, as a consequence, I will also overview some mathematical tools to evaluate the dynamical properties of biological systems, specifically, those quantifying the amount of order/disorder of their temporal evolution.

All of the above, with the aim of better understanding how brain works. Here we go.

1.1 Complex Systems and the Brain

Imagine an airplane and the world wide web (WWW) network. Both of them are composed by a extremely high number of composite elements. In turn, all these elements are, somehow, connected with each other. In principle, one can think that they are not so different. Multiple routers or parts connected with each other so as to a achieve a specific outcome evokes the idea of complicated systems, but it is more than this. Although both systems seem not to be different, they have fundamental differences: The airplane is an example of a complicated system, while the WWW is a paradigm of complex systems [B1]. In this sense, complicated systems are, indeed, assembled by a

high number of elements, but they are engineered in the sense that they are strategically organized for a specific blueprint. On the other hand, complex systems functioning is based on the interactions among their constituents (and the environment) generating a spontaneous organization that leads to emergent behaviours with unexpected properties and regularities that, in turn, could never be explained by the behaviour of their fundamental parts. This means that in complex systems the interactions among elements are more important than the elements themselves, being useless to analyze their fundamental units in isolation. Complex systems have self-organized principles that rely on a collective behaviour and unsupervised dynamics, something different from the complicated ones, where a supervised hierarchical organization is the responsible of the collective functioning.

Regarding to their output, complex systems live in-between ordered and random states and also combine heterogeneous structures and fluctuations along different scales. They are capable of exhibit critical behaviours, where microscopic and localized perturbations can propagate and trigger a macro-rearrangement across the entire system. Those mechanisms entail certain processes that are intimately linked to the complex systems nature, such as adaptation, evolution or robustness. For example, imagine what would happen if some elements of the aforementioned systems were randomly removed. The common sense would predict a malfunctioning both in a complicated and a complex system, but only the first one (e.g., the airplane) contemplate the worst panorama, while the latter can adapt to changes. We can randomly remove (or add) some routers and the WWW network can still operate, but the absence of a part of an airplane not only may result in an inoperative system, but in a dangerous one.

Complex systems are not only present in nature, they can be found in man-made systems like the previously mentioned WWW, but also in economical systems or social interactions, among others. The complexity of the interactions within these systems, no matter the type we are dealing with, has been studied by several approximations and methodologies during the last years [B7], [A37].

Although the classification of complex systems is out of the scope of this thesis, I would like to call the attention of the reader to three kinds of dynamical systems that are related to the main characteristics of the brain: Chaotic, stochastic and excitable systems.

Chaotic systems are characterized for being deterministic systems[1] with a high sensitivity to the initial conditions [B11]. Their dynamics, like complex systems in general, combine both order and disorder. Interestingly, despite being deterministic systems, the high sensibility to the initial conditions make chaotic systems to be highly unpredictable when found in nature, due to the unavoidable presence of noise and external perturbations. Some classical examples of chaotic systems in the literature are the Chua's circuit, the double pendulum, the logistic map or the Rössler attractor. Nevertheless, beyond theoretical models, chaotic behaviour has been reported in a diversity of real systems and the brain is not an exception [A71].

On the other hand, stochastic systems are those susceptible to evolve according to random behaviour. Their output can not be explicitly defined by equations like the deterministic ones, which means that the response of those systems is not the same for a given input. In other words, the output of a stochastic system not only depends on the previous states of the system but also on the underlying random process. Stochastic systems present random delays in time, noise and different levels of uncertainty about the values of their measured variables, something that is also typical in the brain.

Finally, excitable systems are also fundamental to understand brain dynamics, since its fundamental bricks, the neurons, are a paradigmatic example of an excitable system. They are typically characterized by a "rest" state, an "excited" (or "firing") state, and a "refractory" (or "recovery") state. If unperturbed, the excitable system resides in the rest state. If a small perturbation is applied, only a small-amplitude linear response is observed. For sufficiently strong perturbations, however,

[1] Systems whose behaviour in the past determines perfectly its future due to a definite rules.

the system can leave the rest state, going through the firing and refractory states before it comes back to rest again . This response is strongly nonlinear and accompanied by a large excursion of the system's variables through phase space, which corresponds to a "spike". The system is refractory after such a spike, which means that it takes a certain recovery time before another excitation can evoke a second spike. Neurons behave exactly in this way, generating short-length responses called action potentials if the membrane potential is above a certain threshold, otherwise, they remain intrinsically quiescent [B17], [B4].

1.1.1 Complexity in the brain

What can the academy say about the complexity of living systems, in special, the human brain? Among the diversity of approaches to understand human brain complexity, it is worth to highlight the early works developed by Scott Kelso in the upper middle of the 80s and the decade of 90s. His works were focused on the dynamics of pattern formation in the brain [B12]. Kelso and collaborators analysed the behavioural patterns observed in neuronal, electromyographic or kinematic recordings, by means of microscopic collective variables that could be lumped together in high dimensional mathematical objects. In his arguments, those mathematical objects depended exclusively on nonlinear functions of microscopic states and noise [A197].

In a similar way, other approximations that involved the fundamental role of noise in the brain were put forward around the 90s by Deco. He defended the idea of a noisy brain that can be modelled by means of mean-field approximations, bifurcation analysis and, in general, mathematical tools that belong to nonlinear dynamics and statistical physics [B20]. The basis of Deco's works are the relative random activation times of neurons, and how these random excitations lead to stochastic dynamical effects that are relevant for brain functioning [A63].

On the other hand, since the beginning of the first decade of the XXI, the paradigm of the brain complexity has been analyzed under the scope of an early and influential branch of graph theory, namely, the complex networks theory [B23]. In this case, the complexity of the brain, again, does not rely on the complicatedness of million of neural components apparently working in independent ways. If the existence of either structural, behavioural, or dynamical patterns is one of the fingerprints of complex systems, in the brain, the existence of hierarchical, structural and functional patterns reveals part of its complexity. Those patterns are relevant since they can conform associations of groups of neurons regarding to specific functions by means of cooperative processes. At the same time, a great variety of dynamics and different kind of relations between the brain and its environment leads to enhanced functional characteristics like flexibility and robustness under different circumstances. Furthermore, the complexity of the brain goes beyond spatial and temporal scales, showing a hierarchical organization that, among other mechanisms, is fundamental to simultaneously segregate and integrate the information a brain deals with. This particular approach is the one I will consider along this PhD Thesis and, as we will see, will give us important information about how the brain operates.

1.1.2 Why networks?

To understand the brain, it is important to know what happens at the local scale of neuronal units, but also to comprehend the way in which those components interact between each other forming different patterns of connectivity which, in turn, occur at different spatial and temporal scales. Brain patterns are the result of structured and self-organized couplings of excitable systems in a series of networked representations that deserve quantitative analysis and sophisticated statistical techniques that only Network Science can offer through a combination of nonlinear dynamics, statistical physics and graph theory. In this context, Network Science is able to characterize the topological features of brain regions organization, as well as to provide fundamental insights about how dynamical patterns arise. On the other hand, if one contemplates the idea that thoughts,

reasoning, behaviour, memories, even consciousness are consequences of collective actions of individual neuron units, Network Science comprises a series of methodologies that could be an adequate approach to understand how these units correlate regarding to different cognitive or motor processes.

Furthermore, this new approach can be useful to understand interactions from a microscale level of few individual cells and their synapses up to a macroscale state of correlated cortical areas . In sum, the connectivity of brain structures plays an important role in many branch of neuroscience and, for this reason, this PhD Thesis deals with the use of Network Science as a mathematical tool to address different open questions about how the brain is organized.

In view of all and taking into account the brain as a complex system, the goal of this PhD Thesis is to further analyze the classical problem of the brain *dynamical and topological aspects* and their possible correlation. In what follows, I will overview several fundamental aspects of complex networks theory, since part of the methodology introduced in this Chapter will be used along the PhD Thesis. Finally, I will give a brief explanation about time varying networks and time series analysis and enumerate a series of measures to evaluate the dynamical complexity of a system.

1.2 What is a Network?

Historically, Network Science is associated to the mathematical branch of graph theory founded by Leonhard Euler. Euler solved the seven bridge problem, one of the defiant problems for mathematicians of the XVIII century, through a mathematical demonstration that proved the impossibility of crossing all bridges just once (See Box 1).

Box 1: The Seven Bridge Problem

The seven bridge problem consists on answering if it were possible to walk across the seven bridges of the city of Könisberg (nowadays Kaliningrad, Russia), which was divided by the river Pregel into four parcels, just crossing one time over each bridge. Euler transformed each of the four parcels of land into nodes of a network where a moving agent could depart-from/arrive-to. Likewise, each of the bridges of the city was considered as a link connecting two nodes of the network. This simplistic model of vertices (nodes) connected through edges (links) is basically the sketch of a graph. At the end, Euler computed all possible paths among nodes that accomplished the situation of "*once at time*" and, obtained the necessary condition to find such a path. The condition was that the network must (i) be connected (no isolated nodes are permitted) and (ii) only two nodes could have odd number of links. Since the Könisberg had three end-points, then such a route did not exist[a] [B9].

[a] The interested reader can find an extended explanation of this solution in the book of E. Estrada [B9].

Mathematically speaking, a network, also known as a graph $\mathscr{G}$ on its mathematical side, is defined as a finite set of nodes (or vertices) $\mathscr{N}$ combined with another finite set of links (or edges) $\mathscr{L}$, such that $\mathscr{L} \subseteq \mathscr{N} \otimes \mathscr{N}$. This way, a network, $\mathscr{G}$, is the combination of both sets $\mathscr{G} = \{\mathscr{N}, \mathscr{L}\}$. $\mathscr{G}$ is defined symmetric if any element $(v_i, v_j) \in \mathscr{L} \Longleftrightarrow (v_j, v_i) \in \mathscr{L}$, otherwise is defined nonsymmetric. Nodes v_i, v_j, $\in \mathscr{N}$, can be joined by edges from $\mathscr{L}$ forming undirected networks if $\mathscr{L}$ is bidirectional and directed ones if $\mathscr{L}$ has direction [B16] [B9].

In order to analyze the properties of networks, the former definitions allow to implement the use of matrix algebra so as to simplify and manage the information contained in the network. A formal matrix definition of a network stands for the adjacency matrix $A = (a_{ij})$:

$$a_{i,j} = \begin{cases} 1, \text{ if } i \text{ links } j \\ 0, \text{ otherwise} \end{cases} \tag{1.1}$$

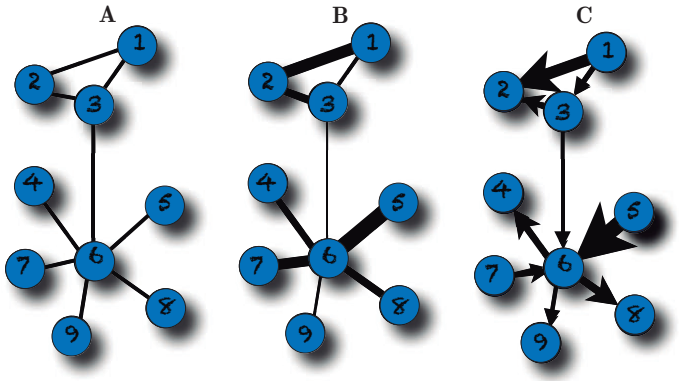

Figure 1.1: **Schematic representation of networks based on their kind of links**. **A**, Binary network with all links equal to one. **B**, Undirected weighted network with the links width according to their value. **C**, Directed weighted network where links indicate the direction and level of causality.

The adjacency matrix $A = \{a_{i,j}\}$ fully characterizes the structural properties of a binary graph of N nodes and L links (See, Fig. 1.1A) .

In the absence of self-cycling nodes, the maximum amount of possible links is obtained as $\frac{N(N-1)}{2}$ [A22], and the network is said to be complete. The application and significance of those elements can be translated into several contexts, e. g., in physics, nodes are sites and links are bonds, meanwhile in social sciences are called actors and ties, respectively. In this way, it is possible to find analogies between connected systems thanks to the matrix representation.

On the other hand, if we are concerned about the level of interaction two systems have, say, the correlation between their dynamics, the adjacency matrix is not enough. In this case, we can assign the links a weight $w_{i,j}$ that quantifies the amount of coordination and the adjacency matrix becomes a weighted connectivity matrix ($c_{i,j}$):

$$c_{i,j} = \begin{cases} w_{i,j}, & \text{if } i \text{ links } j \text{ have a certain interaction, with } w_{i,j} \in \mathbb{R} \\ 0, & \text{otherwise} \end{cases} \tag{1.2}$$

This matrix is also symmetric but, instead of being binary, each element can have different values quantifying the importance of the edges (see Fig. 1.1B for a representation of a weighted network). But correlation does not necessarily imply causality. This is the case of directed networks, in which a link indicates the level of influence a node has onto another. The mathematical representation of a directed network, usually named digraph, is a nonsymmetric matrix. In other words, the existence of a weighted link $w_{i,j}$, from node i to node j, does not necessarily imply the presence of the reverse edge $w_{j,i}$ from j to i (see Fig. 1.1C).

Finally, it is important to remark that not necessarily all networks are complex. A complex network is any networked system whose topology is neither purely ordered, -as rectangular grids-, nor completely random.

1.2.1 Structural Network Parameters

Networks are much more than a visual representation of interconnections. It is in their topology where the information about the network properties lies. The properties a network has are related to different quantifications of the connectivity, importance of nodes and edges (See Fig. 1.2), formation of segregating groups, flux mobility among links, distances of connections, preferences in connectivity nodes, robustness, etc... In general, there are plenty of topological features that

provide different kind of information from one node to the whole network, as well as information at different scales.

We can roughly classify the different node and network parameters according to the kind of information needed to compute them. In this way, we can define the local parameters as those that require information at node level without the need to analyze the whole network connectivity. For example, this is the case of the *degree* ($k(i)$), a local feature that measures the number of links attached to each node, which, in turn, is used as a primary estimation of the level of importance of a node in the network.

On the other hand, global parameters are defined as those that need the topology of the whole network for being calculated. An example of a global parameter is the eigenvector centrality $e_c(i)$, which is obtained from the eigenvector associated to the largest eigenvalue of the adjacency matrix, and it is commonly used as a proxy to determine the importance of a node within the network. In order to obtain $e_c(i)$, it is mandatory to know, not only the number of links attached to each node, but also to whom each node is connected to.

Another way of classifying network metrics is to consider the topological scale in which these metrics are calculated, no matter if they require local or global information. In this way, we can call *microscopic metrics* to those that give information at the level of nodes, e.g., the *degree* a node has. In contrast, the *macroscopic metrics* account for information about the whole network as, for example, the average shortest path (d), measuring the number of steps, in average, to go from one node of the network to any other. Finally, it is also possible to define *mesoscopic metrics*, which coexist in-between the previous scales and give information at the level of small-to-intermediate groups of nodes. That is the case of the modularity (Q), which gives the information about the existence of groups of nodes tightly linked between them.

In what follows, I will summarize the definitions of the main and most common network parameters, their corresponding equations and their underlying concepts (the reader can find a more exhaustive summary in [A22], [A161] or [A49]) .

1.2.2 "Microscale" network parameters

I will use the term "microscale" when referring to parameters at the lowest scale of the network: the nodes. Note, that the most typical microscale parameters can also be translated into a "macroscale" version just by averaging over all nodes. If it is the case, parameters will be highlighted with the symbol (‡$\mathbb{M}$). Although there are extensions to directed networks, in the following definitions I will be restricted to undirected networks with N number of nodes:

Definition 1.2.1 — (‡$\mathbb{M}$) Degree $k(i)$ and Strength $s(i)$. Number of links a node has, and total sum of link's weights w_{ij} arriving to a certain node, respectively [A160]:

$$k(i) = \sum_{j \in N} a_{i,j} \tag{1.3}$$

$$s(i) = \sum_{j \in N} w_{i,j} \tag{1.4}$$

Definition 1.2.2 — (‡$\mathbb{M}$) Outhreach $o(i)$. Sum of the link's weights w_{ij} multiplied by the link Euclidean lengths $\mathrm{l}_{i,j}$ [A29]:

$$o(i) = \sum_{j \in N} \mathrm{l}_{i,j} w_{i,j} \tag{1.5}$$

Definition 1.2.3 — (‡$\mathbb{M}$) Clustering $C(i)$. Percentage of neighbours of a certain node that, in

turn, are neighbours between them [B16, A246]. The clustering reads, in its weighted version:

$$C(i) = \frac{\sum_{j,k} w_{ij} w_{jk} w_{ik}}{\sum_{j,k} w_{ij} w_{ik}} \tag{1.6}$$

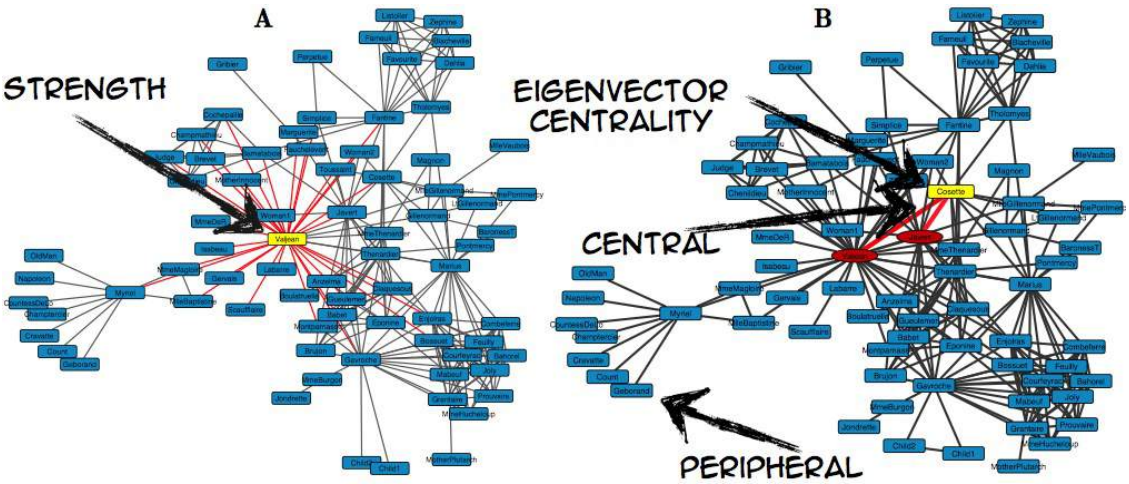

Figure 1.2: **Node strength $s(i)$ and eigenvector centrality $e_c(i)$.** In this example, all links have the same weight. In A, the node with the highest strength is highlighted. In this case the "hub" (i.e., the most important node) is the one that accumulates the highest strength. In B, the node with highest eigenvector centrality is highlighted in yellow. Note that it does not coincide with the node in A, since now, the importance of the node's neighbors (the red ones) is taken into account. Nodes with the highest centrality are said to be "central" while nodes with low centrality are called "peripheral".

Definition 1.2.4 — Eigenvector Centrality $e_c(i)$. A measure of node centrality (importance) that takes into account the importance of all neighbours a node has. It is obtained from the eigenvector associated with the largest eigenvalue of the connectivity matrix [B16]. See Fig. 1.2 for a qualitative comparison between two measures of node importance: The strength and the eigenvector centrality.

Definition 1.2.5 — Betweenness Centrality $b(i)$. Also known as node betweenness, it measures the percentage of shortest paths between any node i and k that cross through node i. n_{jk} is the number of shortest paths between nodes j and k and $n_{jk}(i)$ is the number of these paths that go through node i [B16]:

$$b(i) = \sum_{j \neq k} \frac{n_{jk}(i)}{n_{jk}} \tag{1.7}$$

Definition 1.2.6 — Node Closeness $Cn(i)$. It is defined as the mean of the inverse of the geodesic paths d_{ij} between node i and the rest of the nodes of the network. The more central a node is, the lower its average distance to the rest of the nodes and, as a consequence, its closeness [B16]:

$$Cn(i) = \frac{1}{l_i} = \frac{n}{\sum_j d_{ij}} \tag{1.8}$$

Definition 1.2.7 — Within-Module Degree $z(i)$. It measures the importance of a node inside its community [A94]:

$$z(i) = \frac{k_i(m_i) - \langle k_i(m_i) \rangle}{\sigma_{k(m_i)}} \tag{1.9}$$

where $k(m_i)$ is the degree of node i inside its community, and $\langle k_i(m_i) \rangle$ and $\sigma_{k(m_i)}$ are the average and the standard deviation of the degree inside the community, respectively.

Definition 1.2.8 — Participation Coefficient $p(i)$. Percentage of links of a node that reach other communities [A94]:

$$p(i) = 1 - \sum_m \left(\frac{k_i(m)}{k_i} \right)^2 \tag{1.10}$$

where $k_i(m)$ is the degree of node i inside community m.

1.2.3 "Mesoescale" network parameters

Although not all of the following parameters were used in this work, here we summarize those network parameters that lie between the microscale (i.e., at the level of nodes) and the macroscale (at the level of the network). The mesoscale parameters refer to low-to-intermediate number of nodes.

Definition 1.2.9 — Motifs. Subgraphs or topological patterns that appear overrepresented in real networks when compared to their random counterparts. They are considered as the building blocks of complex networks and classified into classes, according to the number of nodes forming the motif, e.g. class 3 (formed by three nodes) or class 4 (formed by four nodes). After the paper by Milo et al [A151] introducing the concept of network motifs, different methods to measure its presence in a network have been proposed such as in [A167] and [A49]. Here, we show a representation of the 13 possible class-3 motifs:

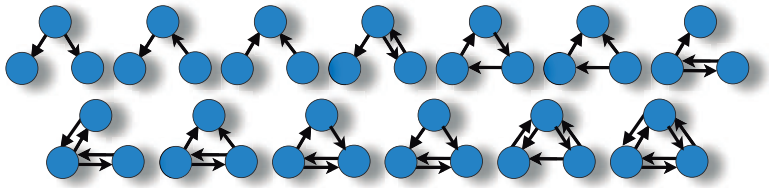

Definition 1.2.10 — Modularity Q. Modularity has been classically used as a benchmark to evaluate the output of network partition algorithms. Specifically, modularity measures how good a given partition of the network into communities is when compared to the case of random reshuffling of the links [273], [A86], [A162]:

$$\mathrm{Q} = \sum_{c=1}^{N_c} [\frac{l_c}{L} - (\frac{d_c}{2L})^2] \tag{1.11}$$

The sum is over the number of clusters N_c, l_c is the number of links joining nodes of module c and d_c is the sum of the degrees of the nodes of c. See Fig. 1.3 for an example of a network divided into communities

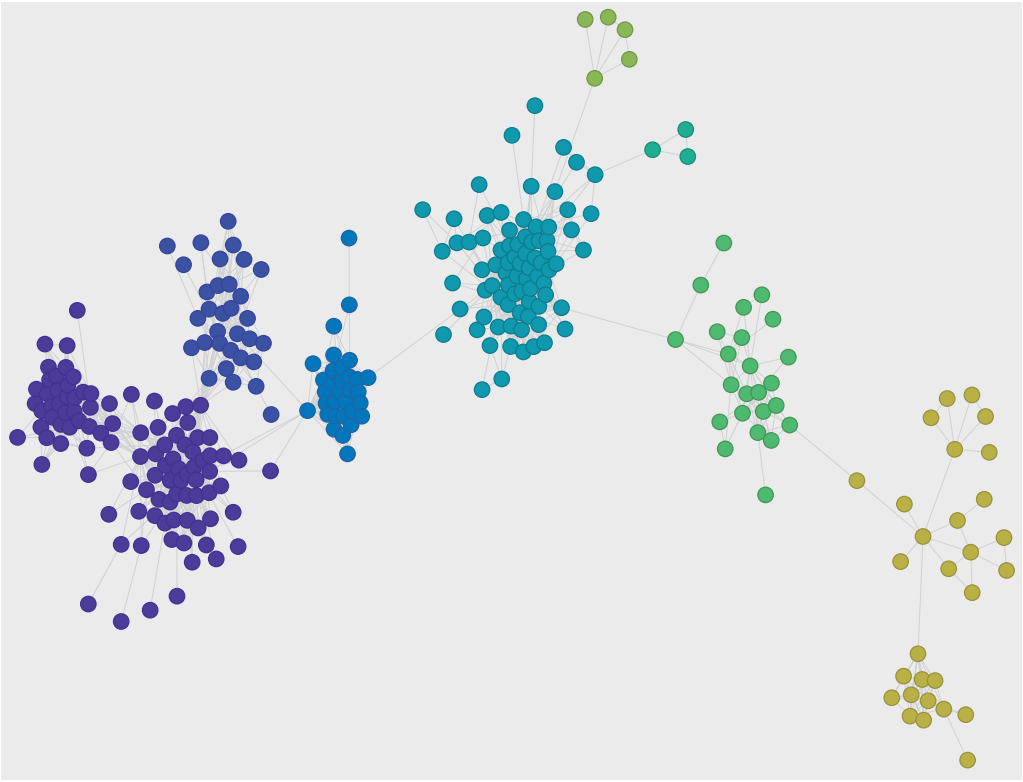

Figure 1.3: **Network communities and modularity**. Personal Facebook network of the author of this PhD Thesis. Five important communities are detected and highlighted in different colors. Nevertheless, different partition algorithms can lead to the detection of different communities. The network modularity Q allows to objectively asses which of the algorithms leads to the best partition, at least when compared with the randomized version of the network (still maintaining the number of communities).

1.2.4 "Macroscale" network parameters

Definition 1.2.11 — Average Shortest Path d**.** Average of the minimum number of nodes to be visited when going from i to j. First, we need to weight the distance between nodes D_{ij}, usually as the inverse of the elements of the connectivity matrix w_{ij}, i.e. $D_{ij} = \frac{1}{w_{ij}}$. Next, we calculate the shortest-path distance between every pair of nodes based on D_{ij} using, for example, the Dijkstra's algorithm [A65]. This way, we obtain the shortest-path matrix dis_{ij} [B16], and finally the average shortest path d is obtained as the average of the distance of each node to the rest of the network:

$$d = \frac{1}{N(N-1)} \sum_{i \neq j} dis_{ij} \tag{1.12}$$

Definition 1.2.12 — Global Efficiency E_g**.** Latora et al. introduced the global efficiency to overcome the fact that certain nodes of a network could be isolated from the others, thus leading to infinite distance between them [A131]. Mathematically, E_g is defined as the harmonic mean of the inverse of the shortest paths between all nodes of the network, with dis_{ij} being the shortest

path between nodes i and j:

$$E_g = \frac{1}{N(N-1)} \sum_{i \neq j} \frac{1}{dis_{ij}} \tag{1.13}$$

Definition 1.2.13 — Local Efficiency $E_l(i)$. It accounts for the inverse of the shortest path within the neighbourhood of node i when node i has been deleted (see definition of global efficiency [A131]). Despite measuring different things, it is strongly related to the clustering coefficient.

Definition 1.2.14 — Assortativity r. The assortativity parameter measures the degree-degree correlation of the whole network. Assortative (disassortative) networks are those with positive (negative) degree correlations [A86]:

$$r = \frac{L^{-1} \sum_i j_i k_i - [L^{-1} \sum_i \frac{1}{2}(j_i + k_i)]^2}{L^{-1} \sum_i \frac{1}{2}(j_i^2 + k_i^2) - [L^{-1} \sum_i \frac{1}{2}(j_i + k_i)]^2} \tag{1.14}$$

where j_i and k_i are the degrees of the nodes at the end of the i^{th} link, with $i = 1, ..., L$. The assortativity parameter r is bounded between the interval $(-1 \leq r \leq 1)$.

Definition 1.2.15 — Small-Worldness Sw. It measures the ratio between the normalized clustering coefficient and the normalized shortest path [A112]:

$$S_w = \frac{C/C_{rand}}{d/d_{rand}} \tag{1.15}$$

where C_{rand} and d_{rand} are the clustering and shortest path of an ensemble of randomized versions of the original network. In principle, the highest the value of Sw, the more “small-world" a networks is.

Definition 1.2.16 — Synchronizability r **and** λ_2. Both the r and λ_2 parameters evaluate the linear stability of the synchronized state of a diffusively coupled network of identical oscillators, according to the class the dynamical systems are. Dynamical systems can be classified as class I, II or III [A22], depending on the number of zeros that the Master Stability Function (MSF) has [A172]. This way, the MSF of class I systems does not have negative values and the synchronized state is always unstable. Class II systems have one zero, which leads to a stable synchronized state beyond a critical value of the coupling strength. Finally, the MSF of class III systems has two zeroes and the synchronization manifold of the network is only stable when the eigenvalues λ_2 and λ_N of the Laplacian matrix are bounded within an interval defined by the MSF. In view of all, the r parameter (obtained from the eigenvalues of the Laplacian matrix) and λ_2 (also from the Laplacian matrix) are fundamental to asses whether a network can synchronize or not, depending on the type of dynamical system:

$$\mathrm{r} = \frac{\lambda_N}{\lambda_2} \quad \text{Class III} \tag{1.16}$$

$$\mathrm{r} = \lambda_2 \quad \text{Class II} \tag{1.17}$$

Network parameters are summarized in the Tab. 1.1. The meaning of the aforementioned metrics and the optimized ways to compute them is just a part of the Network Science. Another important branch of Network Science is the study of the different network models that explain the topology and dynamical processes reported in real systems. This is what will be developed in the

	Microscale	Mesoscale	Macroscale
Local	$k(i)$	Motifs	$\langle k(i) \rangle$
	$s(i)$		$\langle s(i) \rangle$
	$o(i)$		$\langle o(i) \rangle$
	$C(i)$		$\langle C(i) \rangle$
Global	$e_c(i)$	Q	N/A
	$b(i)$		N/A
	$Cn(i)$		$\langle Cn(i) \rangle$
	$z(i)$		N/A
	$p(i)$		N/A
	E_l		$\langle E_l(i) \rangle$
			$\langle E_g(i) \rangle$
			d
			r
			Sw
			r and λ_2

Table 1.1: **Classification of Networks Parameters according to the "topological" scale.** Columns indicate the classification associated to the topological scale. Rows distinguish between local and global parameters. $\langle \bullet \rangle$ refers to those parameters whose average leads to a macroscale representation. Specifically: Degree $k(i)$, Strength $s(i)$, Outreach $o(i)$, Clustering $C(i)$, Eigenvector Centrality $e_c(i)$, Betweennes Centrality $b(i)$, Node Closeness $Cn(i)$, Within Module Degree (z-score) $z(i)$, Participation Coefficient $p(i)$, Modularity Q, Average Shortest Path d, Assortativity r, Small-Worldness Sw, Synchronizability r and λ_2. N/A refers for those microsccopic features that does not have a macroscopic representation.

next Section where I will overview the most common network structures and models.

1.3 Networks Structures

Networks can be statistically characterized by studying how some of their topological features can be described by means of the adequate network models. In this Section, I will introduce the way connections lead to: Random networks (in particular using the *Erdös-Rényi model*), *Small-world networks*, *s*cale-free networks (associated to the *Barabási-Albert model*) and the way we can construct different kind of networks while maintaining a specific degree distribution (using the *configuration model*).

1.3.1 Degree Distribution

Before describing the most common network structures and models, it is important to define what the degree distribution is together with their implications. As mentioned before, the degree of a

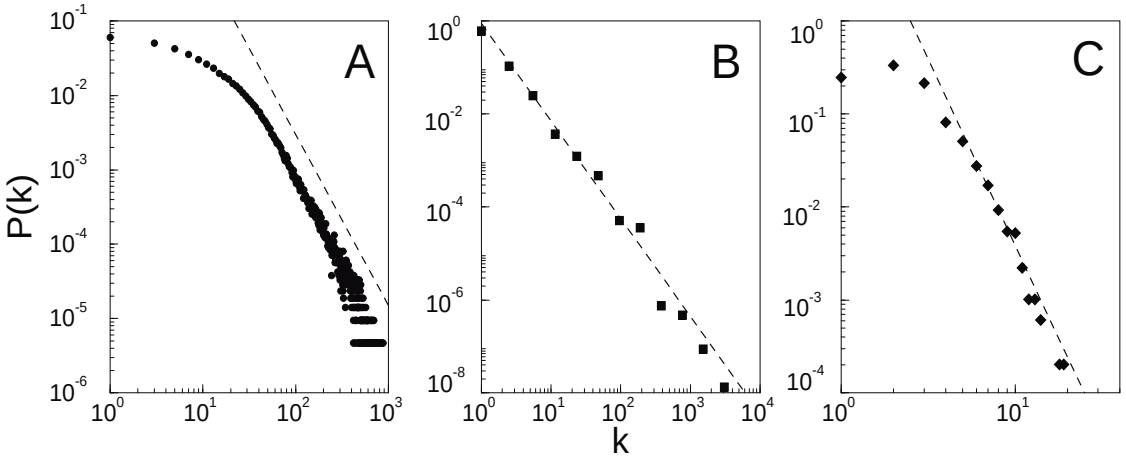

Figure 1.4: **Cummulated distribution functions for large scales networks**. γ is the slope of dashed lines. **A**. Actor collaboration networks ($\gamma_A = 2.3$), **B**. WWW graph ($\gamma_B = 2.1$), **C**. Power grid data ($\gamma_C = 4$). [A16]

node is the number of links a node has. Thus, degree distribution $p(k)$ quantifies the probability of finding a node with a certain degree k. Formally, this probability can be featured as $p(k) = M(k)/N$, where $M(k)$ is the number of nodes with degree k and the probability distribution can be traced just by plotting $p(k)$ against k. Real networks, both natural or man-made, can have many different types of degree distributions, nevertheless there are two kinds that seem to be pervasive, i.e., according to the shape of the distribution, exponential and power law. As we will see, the former distribution is normally attributed to a random process while the second one is related to a preferential attachment. Eventually, it may happen that the degree distribution of a real network is very noisy because the data finiteness. In these cases, one might calculate the Cumulative Degree Distribution as $P(k) = p(k \geq k_i)$ (e.g., see Fig. 1.4). $P(k)$ represents the probability of finding a node with a value greater or equal to k. In this way, the distribution is smoothed, specially at its tail, where the probability of finding nodes with high degree is low and the effects of noise are important [A161].

1.3.2 Random Networks

Random networks were one of the first classes of networks largely studied in the academic literature. The basic idea behind random networks is that their nodes are randomly connected. Despite there are many types of models to generate random networks, the most extended was introduced by Paul Erdös and Alfred Rényi around the 50s and 60s. Erdös-Rényi (*ER*) graphs are very practical for their simplicity, which allows different analytical treatment. But the importance of this kind of networks comes from their use as benchmarks for real networks, specifically to the construction of null cases for comparing realistic models. The simplest model starts from a finite number of disconnected nodes N that are randomly connected through a fixed set of links L. An alternative version introduces a probability p, such as $0 \leq p \leq 1$, of connecting all pair of nodes.

In an ER random network the associated probability of attaching any pair of nodes follows a binomial distribution. As it is well known from probability theory, for large N and fixed $\langle k \rangle$, this degree distribution tends to a Poisson distribution and, therefore this kind of networks are commonly called Poisson random graphs or homogeneous networks:

$$p(k) = e^{-\langle k \rangle} \frac{\langle k \rangle^k}{k!} \tag{1.18}$$

ER graphs have been exhaustively studied and their main statistical properties have been fully characterized (see [A22, B16]).

1.3.3 Small-World Networks

The idea that any individual is connected to any other through a few number of steps, no matter what the size of the population is, was first introduced in 1929 in a short story called *Láncszemek* (Chains), written by the Hungarian author Frigyes Karinthy. Later, in the 60s, this idea was made famous by Stanley Milgram through his experiment testing the concept of Six Degrees of Separation [A150]. Milgram carried out an experiment showing that the average number of steps a letter should follow to arrive to a target (unknown) person through successive acquaintances was close to six. This property, where nodes within a large network are virtually connected through a very low number of steps, is called the *Small-World property*.

This type of social experiments, were the inspiration to what Watts and Strogatz defined as *Small-World networks* (*SW*) [A246]. In *SW* networks two, supposedly, independent features are present, i.e., a high level of clustering C and small average path length d. Watts and Strogatz proposed a model to generate this kind of networks: departing from a perfect ordered structure a random rewiring of few of its connections led to a drastic reduction of the shortest path, while the clustering coefficient was still maintained at high levels. The rewiring process introduces shortcuts near the ordered state reducing the distance between nodes and leading the average shortest path d to scale with the logarithm of the network size N. Interestingly, the probability of rewiring a link does not need to be high, as shown in Fig. 1.5.

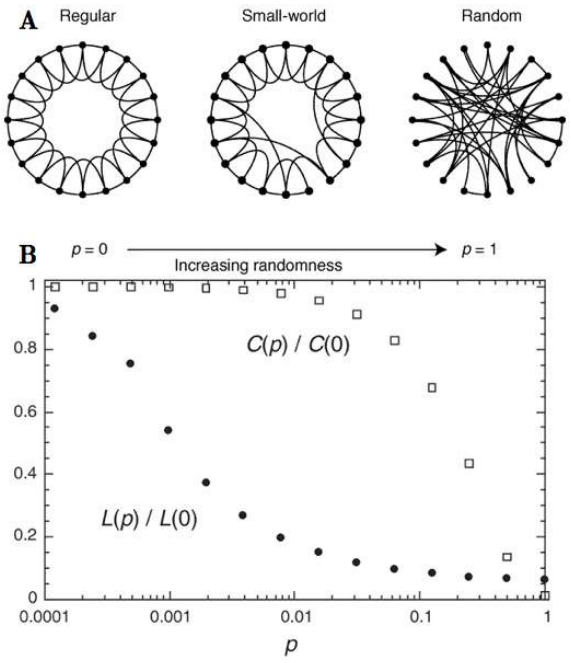

Figure 1.5: **From the regular to random networks**. Watts-Strogatz model: Average shortest path and clustering coefficient as a function of the rewiring probability p. Small-world networks, obtained with the WS model, arise at low values of the rewiring probability p. The fingerprint of a SW network combines a high clustering coefficient with a low shortest path. (Taken from [A246])

SW networks have shown its importance in biological and technological fields and have been investigated in terms of, among others, efficiency, robustness, integration/segregation of information [A225], [A130], [A28].

1.3.4 Scale-Free Networks and the Barabási-Albert Model

A diversity of real networks have a degree distribution that can not be explained by means of a random model, i.e. they do not have a degree distribution with an exponential decay. Among them,

distributions following power law functions in the form of $p(k) \sim k^{-\gamma}$ have been widely reported in a diversity of social, biological and technological systems [A160]. Networks having a power law dependence in their degree distribution are commonly called Scale-Free (*SF*) networks, because the power law distribution guarantees the existence of nodes with a high heterogeneity in the number of connections, thus making the average value of the degree not representative (i.e., it makes no sense to talk about a particular scale, at least in terms of degree). The Barabási-Albert model (*BA*) is the most extended model to generate scale-free networks [A16]. Such a model relies on the growth of a network departing from m_0 nodes (connected through l_0 links) and then, sequentially, nodes are attached to the existing ones by means of m links. Crucially, the probability of attaching a new node to the existing ones is dependent on the degree, following what is known as *preferential attachment*. This kind of attachment promotes connections to the nodes with higher degree k thanks to a probability of attachment β that is proportional to the degree a node has. In this way, the probability of attaching a new node j to an existing node i is given by:

$$\beta(j \to i) = \frac{k_i}{\sum_l k_l} \tag{1.19}$$

After adding a number of n nodes to the initial set of m_0, the network will have $m_0 + n$ nodes and $mn + l_0$ links and will follow a degree distribution close to $p(k) \sim k^{-\gamma}$. It can be proved analytically that, when $n \to \infty$, the average degree will be $\langle k \rangle \to 2m$ and the exponent $\gamma \to 3$ [A5].

1.3.5 Configuration Model

Consider the possibility to compare a real-world network to another artificial one that holds some characteristics of the former one, say, the degree distribution. Such comparison can be advantageous if, for example, one is interested in reaching some generalizations of real networks, which are unaffordable to reconstruct, may be because of the cost of collecting the data.

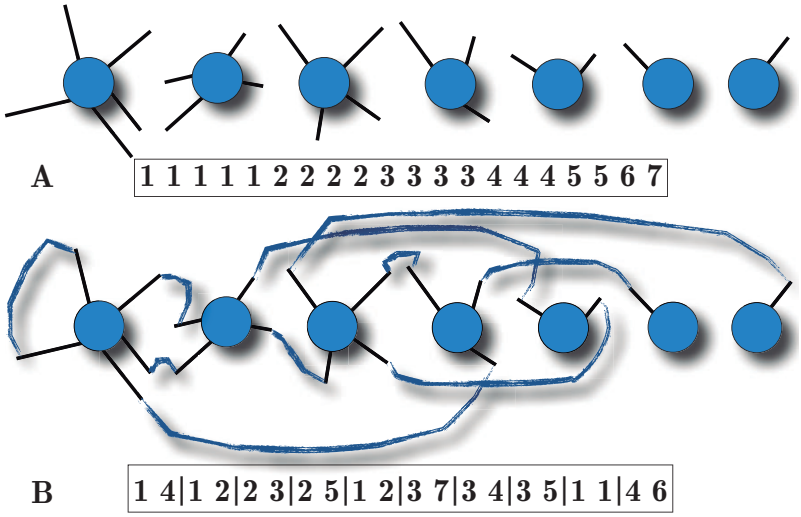

Figure 1.6: **Configuration model example**. **A**, degree sequence for 7 nodes. **B**, permuted matched spokes vector of the generated graph. Adapted from [C1].

In those cases, the existence of models available to obtain networks that follow non-Poisson degree distributions becomes useful. The most accepted model to create such a network is known as the *configuration model*. The idea behind this model is to assume a degree distribution $p(k)$, from which one can choose a certain degree sequence $\vec{k} = \{k_1, k_2, ..., k_i, ..., k_n\}$, with n as the number of nodes of the future network. This vector contains the available "spokes" or accessible edges to each node n_i, in order to be randomly matched with the stubs of the other nodes in the network. Next,

this vector is randomly permuted (see Fig. 1.6), leading to a random network that has a specific degree distribution. The configuration model, in principle, can admit the creation of self-loops and multi-edge graphs, but one can reject those kind of connectivities by adding some particular requirements to the linking algorithm.

1.4 Dynamics in/of Networks

While it is clear that the word “dynamics" implies the temporal evolution of a certain variable, the prepositions in/of importantly determine what the variable under study is. Dynamics *in* networks refers to the activity of the dynamical systems within the network (i.e., the dynamics of the nodes), while dynamics *of* the networks refers to the evolution of the network itself, in terms of how its topology changes in time.

Regarding to the dynamics occurring inside a network, there are different kinds of dynamical processes that are strongly influenced by the topology of the networks, such as, for example, spreading, traffic or synchronization.

Spreading processes mainly refer to both epidemic and rumour propagation, and Network Science is one of the fundamental methodologies to study both kind of processes. One example is the implementation of the most basic model of epidemiology, the susceptible-infected (SI) model, in which nodes (individuals) can be in two states: susceptible or non infected, and infected. Other models, such as the Susceptible-Infected-Susceptible (SIS) and Susceptible-Infected-Removed (SIR,) have also been studied assuming the nodes as dynamical entities that can adopt three states: susceptible (S), infected (I), and removed (R) (or vaccinated in the SIR).

In parallel, rumour spreading is based on the study of how individuals can adopt, create and optimize the way in which a rumour spreads over a network, and the influence of external perturbations such as marketing campaigns or propaganda actions. Models are similar to those of disease spreading [A22], [A160], but the target is basically the oposite because in epidemiology the aim is to eradicate the transmission, while in rumour spreading the goal is to improve such transmission of information. This kind of processes underlay on the individual propensity to acquire and diffuse knowledge, ideas or habits in social networks. In the case of opinion formation, the voter model [A37], is the simplest one in which an agent posses a unique opinion that can take two discrete values. Different models have been developed to take into account the possibility of having a variability of choices (trends) due to shared cultural features as it is the case of the Axelrode model [B1], and other approaches take into account even the circumstances in which agents can collaborate or cooperate, as in the prisoner dilemma [A160], [B1].

On the other hand, traffic processes are related to problems of real communication networks that take into account routing dynamics and strategies for enhancing transport efficiency based on the network topology. An example of these systems is the Internet dynamics, where packages of information flow among different nodes (routers). Another example is the problem of vehicular mobility, congestions and the development of new pathways in cities [A39]. The main aim of these models is to give insights about the physical substrate enhancing the flow of information of physical quantities [B1].

Parallel to the previous processes, the dynamics of a node, no matter what the system is, is strongly determined by the topology of the underlying networks. For example, the dynamical state of the nodes can synchronize in several ways namely, complete synchronization, phase synchronization, lag synchronization or even anti-synchronization, among many others. Beyond the synchronization properties, there are many other processes associated to complex networks like percolation, phase transitions, resilience and robustness[2], but with the aim of focusing on the scope

[2]The interested reader can find a detailed summary of the different dynamical processes in the works by Barrat [B1], Newman [A160] and Boccaletti [A22]

of this PhD thesis I will concentrate around synchronization in networks, the content of information in the dynamics of a system and the evolution of the network topology, since they are the main topics related to the methodologies used here to analyze brain networks.

In this sense, in the following Sections I summarize how one can track the synchronization in complex networks using the Kuramoto model, one of the simplest toy-models to describe the transition from an asynchronous state to a complete synchronous state. Likewise, it will be described how to extract temporal patterns from real-data signals in order to evaluate the dynamical complexity of networked systems. More precisely, a theoretical framework will be developed to explain how to capture the amount of information in those signals by the use of the permutation entropy and the statistical complexity. Finally, I will describe how time-varying networks can be used to track the evolution of the nodes' synchronization.

1.4.1 Synchronization in Complex Networks

There are a diversity of examples about the emergence of synchronization in social, biological and technological systems. For instance, under certain conditions women can synchronize their menstrual cycles, yeast cell population exhibits synchronization of glycolytic oscillations, the existence of coordinated hand clapping of an audience, breathing in mammals, predator-prey cycles in ecosystems, synchronization of neural systems, as well as lighting synchronization of fireflies swarms [B17]. Synchronization is one of the emerging dynamical processes whose understanding has benefited the most from Network Science. For example, in identical systems diffusively coupled, the spectral analysis of the Laplacian matrix of a network allows to evaluate the synchronization properties of the whole network and quantifying the stability of the synchronized state [A22], [272].

But synchronization goes beyond identical systems. In general, synchronization is a time dependent phenomenon based on the adjustment of rhythms of oscillating objects due to a weak interaction. In principle, dynamical systems may have different rhythms but it is possible to define their angular displacement through a variable called ϕ, the phase of the system. In other words, the phase can be defined as a wave-sinusoidal angle elapsed respect its origin, which increases by 2π within one cycle. Finally, the interaction (coupling strength) of such oscillating objects determines if there will be synchronization and how fast it can occur.

One of the most renowned synchronization models applied to networks is known as the Kuramoto model [A1, B13]. In general, the Kuramoto model implemented into a network reads:

$$\dot{\phi}_k = \omega_k + \lambda \sum_{j=i}^{N} a_{ij} \sin(\phi_j - \phi_k) \tag{1.20}$$

where a_{ij} are the elements of a connectivity matrix and $\lambda = \frac{K}{N}$, being K and N the coupling strength and the number of nodes, respectively (see Fig, 1.7). One of the advantages of the Kuramoto model is that it is possible to define an order parameter $r(t)e^{i\psi(t)} = (1/N)\sum_{j=1}^{N} e^{i\phi_j(t)}$. Taking into account that $\psi(t)$ is the average phase, the modulus of $r(t)$ directly measures the level of phase coherence among dynamical systems, ranging between phase locking (1) and de-coherence behaviour (0).

1.4.2 Content of Information in Natural Systems

From laser dynamics [A231] or biological data [A187], to chaotic systems [A186] or statistical physics [A270], there has been an important need of quantifying the stochasticity and the randomness of dynamical systems. Nevertheless, one of the main problems is to differentiate whether patterns appearing along time series show an exclusive random-like demeanour or are in a state between order and disorder.

For this reason, a typical way to distinguish noise from chaos in natural signals is the so-called Signal to Noise Ratio analysis (SNR). Nevertheless, in the framework of complex systems, the *SNR*

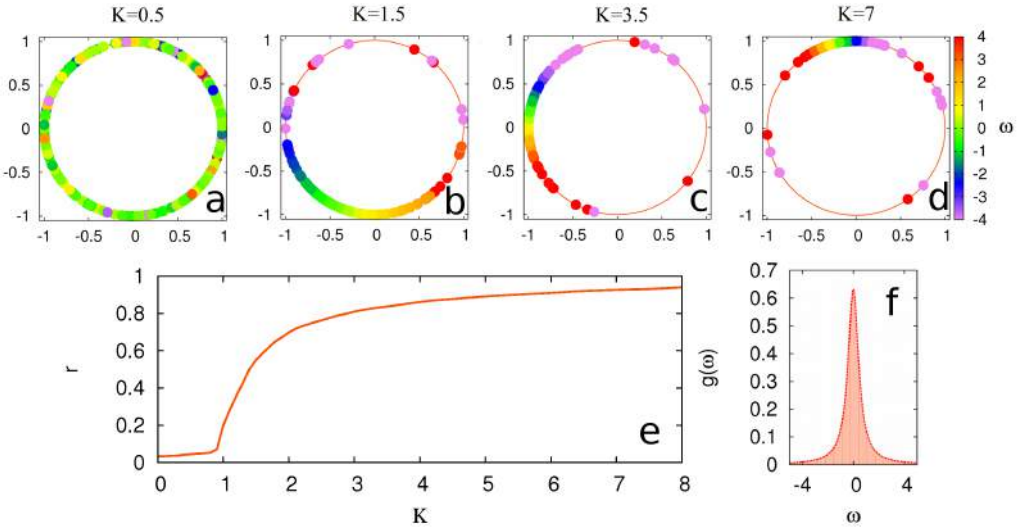

Figure 1.7: **Phase synchronization, order parameter r, coupling strength K and distribution of natural frequencies g(ω).** The upper panel (**a** to **d**) shows the evolution of the phase synchronization as function of coupling factors K. Phases are plotted in a complex unitary circle centered in the phasor $re^{i\Psi}$. Panel **e**: Order parameter r as a function of the coupling strength K. Panel **f**: Distribution of the natural frequencies $g(\omega)$ of the oscillators (figure adapted from [A107]).

is not enough to capture the interplay between stochasticity and determinism within a given time series $\{Xt\}$. To overcome this issue, several alternatives have been proposed, e.g., the calculation of the entropy or complexity of a signal, among others.

Between the several ways of accounting for these two features of time series (entropy and complexity) in this PhD Thesis I am going to focus on a recently developed methodology based on specific partitions of time series, which are used to build up an associated symbol sequence $\{St\}$ in order to evaluate the information content via a Probability Distribution Function (PDF) of $\{St\}$.

Specifically, I am going to apply the methodology developed by Bandt and Pompe [A15], which is known as the *BP* method. The *BP* method accounts for arbitrary real-world data time series with certain characteristics: low *SNR*, weak stationary behaviour (mandatory in stochastic process), and continuous distributions that attest the temporal evolution of the system. This methodology is based on the use of symbolic dynamics applied to time series, without further assumptions concerning the system under study. The *BP* methodology, successful for its simplicity, robustness and fast calculation, is based on a comparison of the neighbouring samples of a time series, extracting ordinal patterns whose probability of appearance will characterize the dynamical properties of the system.

In the following Subsections I will summarize how to obtain the ordinal patterns and their associated probability distributions from real-data time series [A180]. These ordinal patterns are useful to measure the entropy and complexity of a system. In this way, I will describe how to obtain the normalized permutation entropy [A185], the statistical disequilibrium [A128] and the statistical complexity of a system [A138].

Ordinal Patterns and Stochastic Analysis

In the matter of dynamical complexity, information plays an important role as a feature that describes the outermost bounds of periodicity, chaos and complexity. The information content of a natural signal is obtained by a largely tantamount way of characterize the PDF of real-data time series. In this sense, the *BP* method obtains the intrinsic temporal symbol sequences $\{St\}$ from the neighbouring steps of a time series. This symbol sequences depend on an embedding

dimension $D = 3,4,5,...$, which represents the amount of past information, being D the number of neighbouring samples. In this way, D characterizes each $\{Xt\}$ along $t = 1,2,...,M$ samples. To do that, $\{Xt\}$ is partitioned into $(M-D)$ overlapping vectors of dimension D.

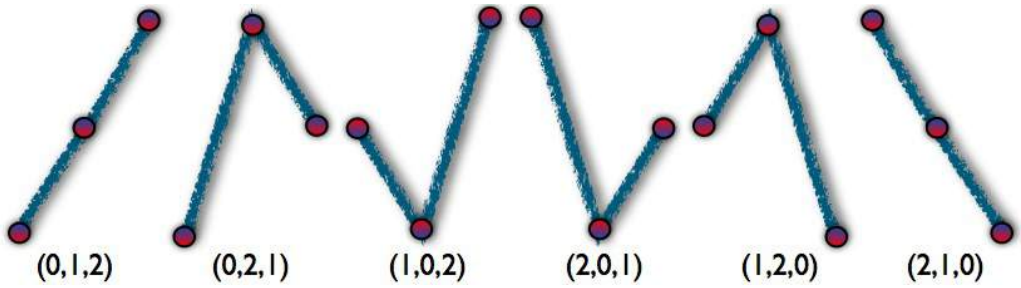

Figure 1.8: **Overlapping vectors for the case D = 3**. $D!$ is the number of patterns. This way 3! different types π of accessible states are presented. The probability of appearance of the ordinal patterns is contained in P. If an ordinal pattern never appears, it is called a forbidden pattern.

Clearly, the greater the dimension D, the more information about the past state of our system, and the longer the vectors are (containing the ordering of a set of D samples). Each of the vectors are assigned to a time t, sliding the vector at every time step, to get a total of $(M-D+1)$ overlapping vectors. Hence, for each $(M-D)$ vector, the position of the lowest value will be assigned the ordinal value zero. The position of the highest value will correspond to $(D-1)$ ordinal value (the highest in the ranking). Thus, the following positions in-between the assigned zero and $(D-1)$ will be assigned by rating the positions of the remaining samples in the respective ordinal values. When all $(M-D+1)$ different order types in $\{St\}$ are calculated, it is possible to obtain the PDF $P(\pi)$, quantifying the probability of finding a certain order pattern associated to $\{Xt\}$:

$$P(\pi) = \frac{\#\{t | t \leq M-D, (x_{t+1},...,x_{t+D}) \; has \; a \; type \; \pi\}}{M-D+1} \tag{1.21}$$

In equation 1.21, π is a possible ordinal pattern presented in the sequence $\{St\}$ and # is its number of appearances. Note that each ordinal pattern is a permutation of $\pi = (0,1,2,...,D-1)$. In other words, $D!$ represents all possible permutations π of order D of the number of accessible states $(M-D)$. As an example, consider the case of $D = 3$ in Fig. 1.8. The number of patterns or accessible states will be $D! = 3! = 6$ and the possible patterns π will be: $\{(012),(021),(102),(201),(120),(210)\}$. From the former ones, vectors that appear in $\{St\}$ are called *ordinal patterns* of $\{Xt\}$, those that do not appear in $\{St\}$, but belong to the possible accessible states are called *forbidden patterns*. Finally, the discrete PDF of the ordinal patterns $P = p_j, \; \forall \; j = 1,2,...,N \; \wedge \; N = D!$ is calculated. This PDF obtained from *BP* method carries the temporal information of $\{Xt\}$ by comparing consecutive samples. In other words, this symbolic technique incorporates the causality effects of a short-memory (of D steps) a time series has.

1.4.3 Statistical Complexity Measures

Entropy

As it was mentioned before, the information contained in the time series has been translated into a PDF. Now, if we want to deal with the computation of the uncertainty associated in a physical process described by the PDF, we need to calculate the so-called *entropy*. There are many interpretations for this quantity depending on the field of application: for example, one can consider the entropy as the level of disorder in a system or the lack of information, or can be either defined in

processes of cooling and heating. In its fundamentals, entropy is defined as an extensive functional form that stands for:

$$S[P] = -k \sum_{j=1}^{N} p_j \log(p_j) \tag{1.22}$$

Here N is the total number of accessible states j, p_j is the probability of finding a state j, k is the Boltzman constant for physical systems (in Boltzman-Gibbs entropy form): $log(2)$ for binary-information systems (in Shannon-Tukey form) or it is omitted for natural dimensionless systems (Shannon entropy), which is the case of this PhD Thesis.

When dealing with information content from dimensionless systems, Shanonn's entropy is often the most natural choice to quantify the level of uncertainty of a physical process. In turn, the amount of information is related to the level of order of the system. Thus, the lower amount of information, the higher order in the system. Here, the Shannon's entropy (S) is useful to measure the intrinsic order-disorder behaviour as a dynamical parameter of a complex system. Specifically, it measures the uncertainty of $\{Xt\}$ and ranges between zero and $\log(N)$: Zero if $\{Xt\}$ is perfectly predicable and depicts a perfect ordered system, meanwhile $\log(N)$ stands for the case in which samples in $\{Xt\}$ are independent between them. In this way, the amount of information is obtained as the logarithm of the number of available choices,'*The most freedom to choose, the more information you might convey*" [B21]. In a more general framework, the amount of information is a qualitative construct, consisting on the number of discriminable ordered sequences of symbols required to communicate the state of an uncertain event that can be encoded into signs transmitted via signals [A244].

It is worth noting that this methodology also presents some drawbacks. To begin with, this measure neglects the existence of temporal relationships among samples in time series. For instance, let $X_1 = \{0,0,1,1\}$ and $X_2 = \{0,1,1,0\}$ be two time series. If we do not assign a symbol sequence for each time point, then it holds that $S[P(X_1)] = S[P(X_2)]$, which means that the order relations in the time scales would be lost. In addition, the measure assumes a prior knowledge about the system in terms of the absence of generalization of the associated PDFs, and finally, this measure suffers from size effects. Nonetheless, taking into account the *BP* method, it is possible to capture the temporal relationships among time series elements, as well as it is feasible to measure the entropy of any system regardless the type of the associated PDF.

Therefore, Bandt and Pompe, use the PDF of the ordinal patterns to define the Normalized Permutation Entropy H [A15]:

Definition 1.4.1 — Normalized Permutation Entropy $H[P]$**.** It is given by the ratio between the entropy $S[P]$ of the ordinal patterns and $S_{max} = S[P_e]$, being P_e the uniform probability distribution:

$$H[P] = \frac{S[P]}{S_{max}} \tag{1.23}$$

The normalized permutation entropy $H[P]$ is bounded between $0 \leq H[P] \leq 1$.

Regarding the finite size effects, the normalized permutation entropy H allows to include a uniform distribution $Pe = \{1/N, 1/N, ..., 1/N\}$ making H to be an intensive property. This uniform distribution P_e, also maximizes the associate-system information entropy $S[P]$, i.e., $S_{max} = \log(N) = \log(D!)$. This way, the amount of disorder $H[P]$ based on the information measure $S[P]$ associated to P is defined as the Permutation Entropy [A185] because it runs over all $D!$ permutations π of order D [281].

Disequilibrium

On the other hand, the insertion of '*a priori*" equilibrium distribution $\{P_e\}$ as a correction for the associated entropy, leads to a discrimination between two populations. In other words, we need to evaluate the distance between both distributions P and P_e. This fact makes $S[P]$ not being enough to effectively characterize $\{Xt\}$ because there could be some ordinal patterns that belong to P as well as to Pe. This distance accounts for the "order" of the system when one of the few ordinal patterns emerge as the preferred ones [A200]. The disequilibrium between statistical populations will be the measure to distinguish this non-Euclidean distance. We quantify the disequilibrium$Q$ by adopting some statistical distance $\mathfrak{D}$ betwen the possible and accessible states of the systems in P and the equilibrium distribution P_e.

Definition 1.4.2 — Disequilibrium $Q[P]$**.** It evaluates the distance between P and P_e as:

$$Q[P] = Q_0 \mathfrak{D}[P, P_e] \tag{1.24}$$

where Q_0 is a normalization constant leading to $0 \leq Q[P] \leq 1$. A $Q \neq 0$ indicates the existence of preferred states among the accessible ones.

The normalization constant is obtained as $Q_0 = \{\frac{N+1}{N}\log(N+1) - 2\log(2N) + \log(N)\}^{-1}$. On the other hand, the statistical distance $\mathfrak{D} = J[P|P_e]$ is defined in terms of the Jensen-Shannon divergence as $J[P|P_e] = (K[P|P_e] + K[P_e|P])/2$, with $K[P|P_e]$ as the mean information for discriminating between P and P_e per observation p_j, also known as the symmetric form of the Kullback-Leibler relative entropy [A128]:

$$\begin{aligned} K[P|Pe] &= -\sum_{j=1}^{N} p * \log(p_e) + \sum_{j=1}^{N} p * \log(p) \\ &= S[P, Pe] - S[P] \end{aligned} \tag{1.25}$$

Where $S[P|Pe]$ is the Shannon cross entropy. As a consequence, $J[P, Pe]$ can be defined in terms of S as:

$$J[P|Pe] = S[(P + Pe)/2] - S[P]/2 - S[Pe]/2 \tag{1.26}$$

In this way, the disequilibrium $Q[P]$, discriminates ordinal patterns in P from the uniform distribution P_e. The zero limit or the minimum disequilibrium, implies that the lowest separation of both populations does not distinguish between ordinal patterns coming from both populations. Meanwhile the upper limit, with a high disequilibrium, is related to the fact of the existence of some privileged ordinal patterns in P.

Statistical Complexity

Hitherto, both H and Q give some sense of the understanding of what the dynamical properties of the system are. Nevertheless, we are concerned on evaluating the interplay between the order and disorder of a system. Therefore, it is also desirable to complement these measures with some metric quantifying the complexity of the system. In this sense, there exists an intense debate about what would be the better way of quantifying the complexity of a system. In fact, there are several definitions of complexity, which can be roughly classified into three main categories. The first one relates complexity to a sort of function that monotonically increases with the amount of disorder [A125], [B21]. A second category claims that complexity is a convex function of disorder. In other words, it is defined as a function with zero value as the minimum of complexity in either complete ordered and disordered states, while a maximum of complexity lays in some intermediate

level in-between those states [B18], [A138], [A200]. Finally, the last type of definitions assumes complexity to be loosely the level of self-organization of a system [A146].

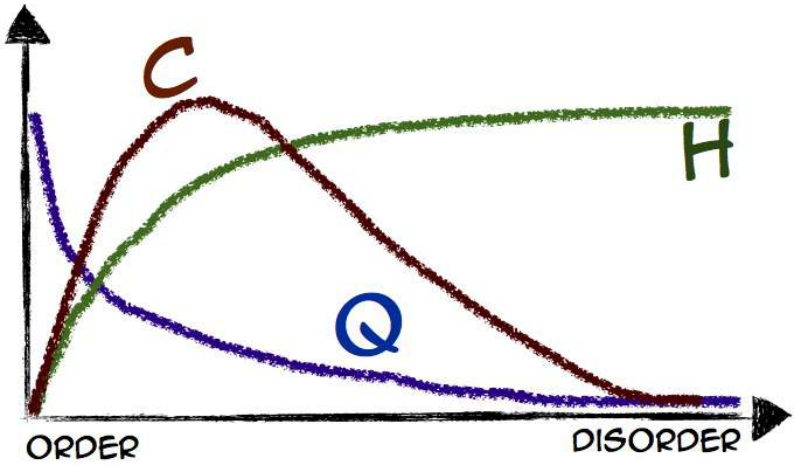

Figure 1.9: **Statistical measures based on ordinal patterns**. Schematic representation of the interplay between the normalized permutation entropy **H**[**P**], disequilibrium **Q**[**P**] and the statistical complexity **C**[**P**], in terms of a system that range from complete order to complete disorder.

Regardless many for-and-against discussions about these three categories, the results of this PhD Thesis require from a complexity measure that accomplishes the following characteristics: (i) it must be independent of size effects, since the complexity should not increase just because the system becomes larger and (ii) for non equilibrium systems, it must take into account both levels of disorder and order of the system.

In this way, Bandt and Pompe define the statistical complexity of a system as:

Definition 1.4.3 — Statistical Complexity $C[P]$. This complexity mesures is defined as the product between the permutation entropy H and the disequilibrium Q:

$$C[P] = H[P] \cdot Q[P] \tag{1.27}$$

With this definition, the statistical complexity C accomplishes the first requirement since H and Q are intensive quantities. The second requirement is also achieved since, by means of H and Q, we are measuring the disorder of a system and its distance from the equilibrium. Note that the statistical complexity vanishes either if the system is at equilibrium (maximum disorder) or if it is completely ordered (maximal distance from the equilibrium). Figure 1.9 shows a qualitative plot indicating the intreplay between the three measures.

The previous definitions of H, Q and C are usually known as *Generalized Statistical Complexity Measures* (*SCM*). *SCM* capture either, the essential details of the dynamics that allow to discern among different degrees of periodicity and randomness, as well as all possible degrees of stochasticity when the information of $\{Xt\}$ is extracted via the *BP* method. *SCM*, not only compute randomness, but a wide range of correlation structures, not already offered by a simple entropy analysis.

1.4.4 Evolving Networks

To conclude the overview of the main properties a complex network has, I am going to recall the importance of time when analyzing the topology of networks. Instead of assuming the classical approach where a network is considered as a static entity, one can choose a more realistic point of view, where network properties change along time according to the evolution of the processes

occurring inside the networks.

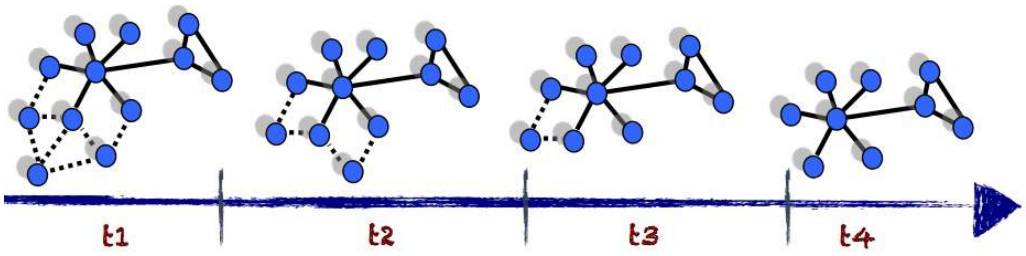

Figure 1.10: **Networks may evolve in time**. In this qualitative example, each time t_n represents the evolution of a given network $\mathscr{G}_n$. Each time step, the properties of the network can change, highlighting the importance of studying of how these changes arise.

This approximation leads to what is known as time-varying networks or *evolving networks* (*EN*). In these networks, the links and the nodes change in time (see Fig. 1.10) and the connectivity matrix is defined as a time aggregated graph:

$$a_{i,j}(t) = \begin{cases} 1, \text{if } i \text{ links } j \text{ at time } t \\ 0, \text{otherwise} \end{cases} \tag{1.28}$$

Arriving to this point it is reasonable to ask in what cases the use of *EN* offers better options than the static viewpoint? The answer is related to the time scales of both the dynamical systems and the topology of the network: if the dynamical systems evolve in a time scale much faster than that of the network evolution, it is not necessary to use the *EN* approach [A82].

Regarding the topological properties, there are several extensions of the parameters of static networks to the case of *EN* [A110]. As an example, let me take the *temporal clustering*[3], a measure of clustering along several "snapshots" of a *EN*, where certain persistence of connections is computed:

Definition 1.4.4 — Temporal clustering C^i. $(0 \leq C^i \leq 1)$. A measure of persistence of the interactions of node i^{th}. C^i approaches to one when the clustering remains fixed and C^i tends to zero if the clustering parameter is volatile [A45, A227]:

$$C^i = \frac{1}{T-1} \sum_{t=1}^{T-1} \frac{\sum_j a_{ij}^t a_{ij}^{t+1}}{\sqrt{k_i^t k_i^{t+1}}} \tag{1.29}$$

Where $T = nt$, is the total time, and t is the exact time step with $k^t = \sum_j a_{ij}^t$ representing the degree of node i at the specific time t.

Finally, regarding the paths existing in the network, temporal paths are usually named as *"sequences of contacts with non-decreasing times that connect sets of vertices"* [A109, 275]. The fact that time introduces causality, divides the nodes between the *source set* and *set of influence* of a node i. The former set contains the nodes that, in a time lapse, can reach the node i, while the latter set reflects those nodes that can be reached from node i [A41]. In general, for *EN*, the "duration" or 'temporal path length" relates to a measure of elapsed time during the first and the final contact of both set of nodes, but still, it is important to remark that static path lengths and temporal path lengths are not transitive [A170].

[3] This metric was not used in this work, notwithstanding I consider as relevant to mention the existence of this metric.

1.5 Final Remarks

In this Chapter I have overviewed the main topics of Network Science that are related to the results of this PhD Thesis, in particular, those that quantify the topology and dynamics of networked systems. I highlighted the importance of studying the brain as, "*par excellence*", the most sophisticated complex system and I enumerated the ways Network Science can help in the understanding of the brain behaviour.

First, I summarized the most common network metrics, which extract information about the topological organization of a network and I explained some of the most studied models in Network Science. Likewise, I described the most relevant dynamical processes occurring in networks, which, in turn, have some connections with the brain, such as synchronization.

Next, I over-viewed the so-called statistical complexity measures *SCM* via the *BP* methodology. This methodology has been previously applied to the analysis of brain signals, more precisely to electroencephalographic (EEG) recordings [A180]. Notwithstanding, the application of this methodology to other kind of brain signals, such as Magnetoencephalography (MEG), has not been documented yet (until this PhD Thesis). In this context, I remarked the importance of a detailed study of the brain that takes into account two properties of networks: the dynamics *of* networks as the evolution of the network topology, and the dynamics *in* networks as the inner and temporal dynamical processes of the network's nodes.

Finally, I discussed about the importance of taking into account the time variable to understand the past, present and future states of networks, the majority of them being "living systems" whose properties may evolve in time. In view of all, the topology of the complex networks, its evolution and the dynamical properties of the nodes, are proposed as candidates to analyze the properties of brain activation patterns. In this way, the following Chapter will be devoted to define what a brain network is, what kind of brain networks I will deal with, and what does the emergent properties of human brain mean.

2 Brain Networks

Solomon Shereshevski, a journalist with the ability to remember and recall long lists of data, numbers, names even entries in books, was diagnosed with Synaesthesia, a complex pathology that makes the bearer interchanges senses (coupled senses), so he was able to hear colors, see sounds, and taste objects just by touching them [276]. Unfortunately, this mnemonic "gift" led him difficulties in his everyday life, because he could not differentiate events from minutes to years (what is known as Telescoping effect).

Phineas Gage, was a rail-road worker who suffered a brain injury because an accident. A 1 meter long iron bar passed through his brain damaging his frontal lobe. Since then, he intensified his bad mood with many negative changes in his personality. Subsequent studies demonstrated that emotion, as a feature of mind, is enclosed in the brain [A51][280].

Henry Molaison, best known as the *H.M.* patient, suffered from epilepsy since an accident he had with a bicycle. During a surgery, his hippocampus was functionally removed and then he was unable to learn new things because his long time memory was affected (Anterograde amnesia) [A48].

As these people, many other subjects in the neuropsychological literature reveal the astonishing, complicated and, in some cases, strange responses of the brain under different situations. The evidences found in brain injuries and other neuronal phenomena have shed conjectures about how intangible elements, such as consciousness, perception, mind, will or thoughts could be in connection with brain processes.

An example of the first attempts to unveil this interrelation was exposed by Rene Descartes in 1637. In his treatise "*Les passions de l'âme*", he declared the pineal gland as the key structure where the soul was attached to the body and the only link between the "thinking substance" and the corporeal entity. He considered that this substance was associated with the substrate of passions, which nowadays are named emotions [B5]. Descartes established the basis of what is currently known as the dualism branch of the philosophy of mind, a perspective that demands a relationship between mind and matter despite of belonging to two different ontological categories.

Since then, several perspectives have focussed on how the brain works from interdisciplinary

angles. Nevertheless, it has not been an easy enterprise and it will not be during much time. Notwithstanding, with the use of new technologies to record brain signals combined with new mathematical approaches under the paradigm of complexity and interdisciplinary perspectives, it is possible to address new studies of the brain's nature. These studies already take into account the inner dynamics and the nonlinear features of the brain to undermine a little bit more our ignorance about the unknown entity the human brain is.

Thus, this Chapter is devoted to introduce the key topics about the brain's nature, experimental methods related to brain signals and how to construct brain networks. Specifically, I will briefly describe some of the brain features from the neuroanatomical viewpoint. Then, a short summary of functional properties will be exposed in following Sections. I will complement the previous descriptions touching slightly the brain-mind problem, the neural correlates, the mental states and how they relate as the result of neural coding. A simple revision of some of the main research fields devoted to the study of brain, and their relation with what is known as cognitive sciences will also be exposed. Next, a Section will be devoted to brain signaling, and how to gather those signals so as to built brain networks. The representation and classification of brain networks and paradigmatic examples extracted from the scientific literature will be treated at the closing sections.

2.1 The Structural and Functional Brain

From the structural point of view, the brain can be understood as a network of cells forming a massively parallel system, organized to carry out three major functions: computation, information storage and transport, and communication among computational structures. Brain tissue can be separated into (i) grey matter (neurons, unmyelinated fibers) surrounding the deeper (ii) white matter fibers connecting neurons (glial cells, myelinated axons and dendrites). The human brain consists of roughly $10^{10} - 10^{11}$ neurons. Each neuron has approximately 10^4 synapses, which directly connect to other neurons. The total wiring in human cortical grey matter is of the order of $10^5 - 10^6$ km, resulting in an overall neuronal potential band-width of the order of Terabits/second [C4]. The cortical membrane surface is about 25000 m^2, the equivalent of 4 soccer fields. Furthermore, the brain performs an estimated of 10^{15}, synaptic operations per second, but only consumes around 12 W, thus achieving an operation/joule ratio several orders of magnitude higher than the fastest available microprocessor [T5].

On the other hand, powering the human adult brain drains $\sim 20\%$ of resting energy consumption ($\sim 60\%$ in infants). Neuronal signal transmission through axons and synapses accounts for about 50% of the brain's overall consumption [A132], and due to the dense interconnected structure of its axons and synapses, cortical gray matter uses more than 75% of the total energy consumption for signalling. The energy supply limits both the total size and the amount of information that can be transmitted within the brain at a time. The brain achieves these impressively high levels of computational efficiency by adopting energy efficient architectures, involving trimming of superfluous signals and the representation of information with energy-efficient codes, distributing signals appropriately in space and time. The brain can also be seen as a two-fold trait of structure plus function, organized at different spatio-temporal scales in hierarchical dynamical modules of neurons that process information [B3]. Neurons represent the building-blocks of the nervous system, in which their spatio-temporal scales for synaptic processing ranges between ($\mu m - mm$) and ($ms - s$), respectively [B8].

The human brain anatomy is also characterized by networks of coupled neural systems across different spatial scales (see Fig. 2.1). Vertical structures divide the cortex into six main layers perpendicular to the pia matter, within them basic computational units, encoding similar features, can heuristically be defined as minicolumns, consisting of dense local interconnections between excitatory cells and inhibitory interneurons. Couplings between these local regions arise through

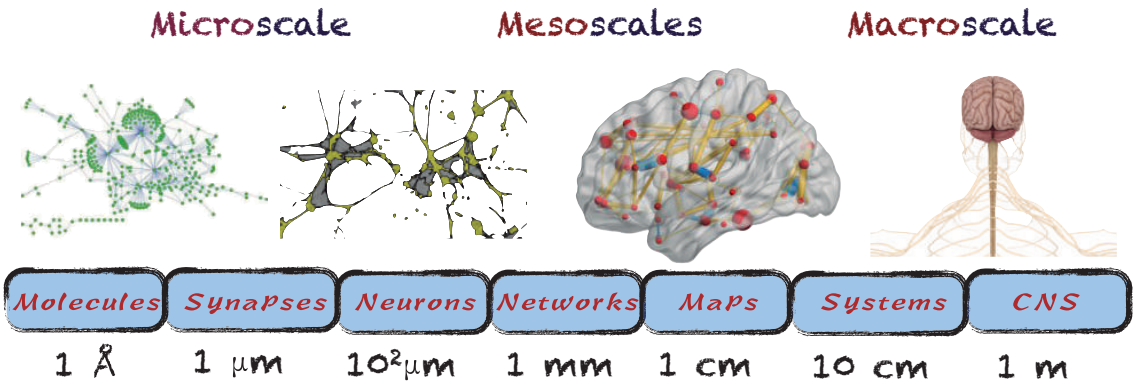

Figure 2.1: **Scales of structural brain networks**. Brain networks range between the organized interconnected systems from the microscale to the macroscale, passing through different mesoscales. **Microscale**: Functional groups of neurons depict the microscale interconnectivity, **Mesoscales**: From large functional neuron groups to cortical interconnected regions. **Macroscale**: In the context of neuroscience, this scale accounts for the large-nerves interconnections like the central nervous systems. In the plot, from left to right, we show networks of molecules (taken from [A259]), cultured networks in microscales (taken from [T2]), a brain network in one of the different mesoescales (Drawing using toolkit [A252]) and the macroscale representation of the central nervous system.

sparse long-range excitatory projections, such as cortico-cortical fibres. These couplings facilitate large-scale integrative processes involving coordination between specialized networks. In sum, there are two important facts around hierarchical modularity that are associated to the brain. First, the modules can change their functions without adversely perturbing the remainder of the system and, second, hierarchical modularity facilitates behavioural adaptation [A123].

2.1.1 Functional Background

Functional brain activity consists of transient episodes of synchronized/unsynchronized activity between different parts brain regions [A24]. Synchronization facilitates integrative functions, by transiently binding together spatially distributed neural populations in parallel networks during sensory perception and information processing [A201], [A152]. Desynchronization allows the brain to flexibly switch from one coherent state to another [A183]. Asynchronous (non-linear) couplings may also play an important role in functional integration, facilitating the creation of transient context-sensitive coherent neural assemblies between distant brain regions [A77]. On the other hand, plasticity, as a temporal functionality, occurs over multiple temporal scales, a short one in the order of seconds to minutes (related to learning and memory), and a long one that requires from days to months (related to ageing and recovery).

In this context, neurons represent the basic functional units of the brain. What actually distinguish neurons from other kinds of cells is their time-dependent fluctuations of the membrane potential. They behave like nonlinear excitable entities thanks to the dynamics of their membrane potentials, which allow the propagation of fluctuations in space. This propagation is called *Action Potential* or, more commonly, *Spikes*. They are produced near the soma when an ion imbalance appears in the membrane cell or an external stimulus affects the polarization of the neuron. The resting potential is around $\sim -70\,mV$. If the membrane potential slightly overcomes differences higher than a threshold, that is about $20-30\,\mu V$ higher than the resting potential, the action potential appears and travels along the dendrite. Its all-or-none characteristic defines the spikes as the elementary packages of information in nervous systems, in other words, the units of neural code.

Neural communication is based on the so-called synapses, which are specific inter neuronal junctions. There exist chemical and electrical synapses. In the first group, predominant in vertebrates, the separation between neurons, known as the *Synaptic Cleft*, is around tenths of *nm*. The spike, which arrives at the end of the presynaptic cell, provokes a release of thousands of neurotransmitters through a diffusion process due to the higher concentration of presynaptic vesicles filled of such neurotransmitters. Neurotransmitters released in the synaptic cleft induce chemical channel excitations in the postsynaptic neuron opening its ionic receptors and producing a new depolarization of the membrane potential. In this way, the electrical signal is transferred from one cell to another by means of neurotransmitters. Ramon y Cajal, defined the phenomenon of chemical synapses as the neuron doctrine, which characterizes the neurons as discrete entities because the intermittent character of the signal propagation. On the other hand, electrical synapses are based on the fact that there are cell membranes that are directly connected through specialized channels called *Gap Junctions*. In this case, ionic particles can cross this gap enabling bidirectional current flow between both cells, and the transferred signal to the postsynaptic cell underlays without neurotransmitters as mediators of signal propagation. This quality claimed the reticular hypothesis of Camillo Golgi, in which neural tissue is rather continuous [C2].

Anyhow, discrete and continuous phenomena leads the postsynaptic cells to reproduce large amount of spikes from different sources ($\sim 10^4$ exchanges of information per second and per neuron) [B10]. The oscillatory activity can be summed up creating what is called a bursting in postsynaptic cells. Bursting acts in short periods of time and then decays into quiescent periods. This superposition of contributions from neighbouring neurons serves as an information media that evolves multi-rhythmically along time in localized groups of neurons with more than one natural frequency [B2]. The synchrony of these rhythms drives the extracellular potentials. These potentials are associated to distinct cognitive functions as well as the healthy functioning of the brain along a wide spectrum of frequency scales, that range almost four order of magnitude ($0.05 - 500\ Hz$) characterized by several frequency bands [A33]. These brain signals carry the information about the functional demeanour of the brain and the intangible features of mind, like consciousness and cognition. Hence, albeit structure and function are important to characterize the brain behaviour, the study of such intangible features of mind is also crucial to better understand the brain and its interplay with the so-called mind.

In this sense, this interrelation accounts for intangible features like mental states. Mental states play an important role in neuroscience because refer to the way the individual feels and thinks [C5], [B15], i.e., the person's conscious experiences. The mental states associate cognitive functions that delineate what people can do with their minds, e.g. perception, memory, ideation, imagination, belief, reasoning, desire, volition, emotion, sensation, consciousness demeanour or language. Hence, mental manifestations like cover attitudes, lies, visual perception [A102], memory tasks or even introspection, among others, are also a representation of different mental states.

In summary, when one looks at the brain as a complex system, mental states arise by the hand of the brain emergent properties. These states generally identify certain neural correlates, that account for the minimal physical arrangement of constituents (neurons) and events (processes) that crucially correlate with a specific context of experience. In other words, the minimal set of neurons performing a task regarded with some conscious percept, for example, γ oscillations related to visual awareness [A50].

Finally, these emergent properties result from information processing of the neural activity, but: What does information processing mean? In fact, what does information mean? The next Section is devoted to discuss about the information sources in the brain and its interplay with the neural

coding.

2.2 Brain Information Sources

Information processing has been widely studied from different angles encompassing classical or quantum mechanics. In the same way, the conveyed neural information has been investigated at different levels that span from the quantum and molecular level of neurons up to different microscales, as far as cortical mesoscales in brain networks, even from the most challenging field of philosophy of mind.

Sataric et al, developed linear models in classical mechanics to explain the transfer of information at molecular level [A192], and the information velocity using Kink-type Solitons has given the nonlinear mechanics explanation to this phenomenon [279], [278]. Collective behaviours of proteins in the presence of Landau-Ginzburg energy functions [A235], and polymerization of neural organelles with solitary waves dynamics[A42] have been used by *Tuszynski* and *Chou* to give appropriated physical-chemical explanations. In the case of quantum approximations,*Hameroff et al* have worked on information quantum biology [274]. Electrostatic properties at quantum level in neural organelles [A236] have also been described, and biological quantum computations, where conformational states of proteins behave akin to "qbits" have been successful models in quantum information theory [A100]. Regarding to the philosophy of mind, *Díaz et al* have developed what is defined as the "Living consciousness" [B6], the pattern-process theory in aggression behaviour [A155] and the works of *Churchland* have been another attempts to associate the body-mind problem with proposals coming from mathematical models [B3]. Likewise, in microscopic and mesoscopic scales *Kostal et al.* and *Butts et al.* have been working on neuronal coding in spike trains [A126] and temporal precision in neural code for visual system [A32], respectively. The effects of conveyed "neural noise" to other neurons, as a part of neural signals, have been exposed by *Stein* [A219], the responses of stimuli encoded in neuron spikes for visual cortex have been also studied by *Monterruno et al* [A154]. Finally, *Wu et al.* have focussed on the coding of neural populations for biological computation [A251] and the structural complexity at brain mesoscale has been also investigated by *Young et al* [A255], just to name a few.

Among all of these valid approximations, one can say that there are a variety of information sources ranging from single neurons, passing through oxygen/blood dynamics and arriving to bursting groups of neurons, mesoscopic inner regions of the brain and pyramidal cortical neurons. These sources offer a wide range of brain signalling that can be acquired by different invasive and non invasive techniques, which take into account anatomical and functional information of the brain. Among these techniques, Post-Mortem Dissection and Positron Emission Tomography (PET) belong to invasive methodologies that achieve anatomical data, meanwhile intra-cranial Electroencephalography (iEEG) represents and example of an invasive technique that gives functional information. In contrast to the previous ones, the noninvasive methods accounting for functional information can be divided into two main groups: the ones that gather data coming from metabolic processes and those that are involved with the electromagnetic responses of the brain.

2.2.1 Metabolic Sources

The first group comprises the family of the Magnetic Resonance Imaging techniques (MRI)[1]. The structural MRI (sMRI) is one of the brain imaging techniques that focuses in the anatomical information. In addition, several variations like the Diffusion Tensor Imaging (DTI)[2], and Diffusion Spectrum Imaging (DSI)[3] are based on the trace, in a three dimensional space, of the course of the

[1] Also known as nuclear MRI (nMRI) or Magnetic Resonance Tomography (MRT)

[2] DTI is not enough to obtain an anatomical reconstruction in sites where neurons fibers bundles cross one into another.

[3] DSI solves the problem of DTI by assuming several diffusion directions in each white matter representation.

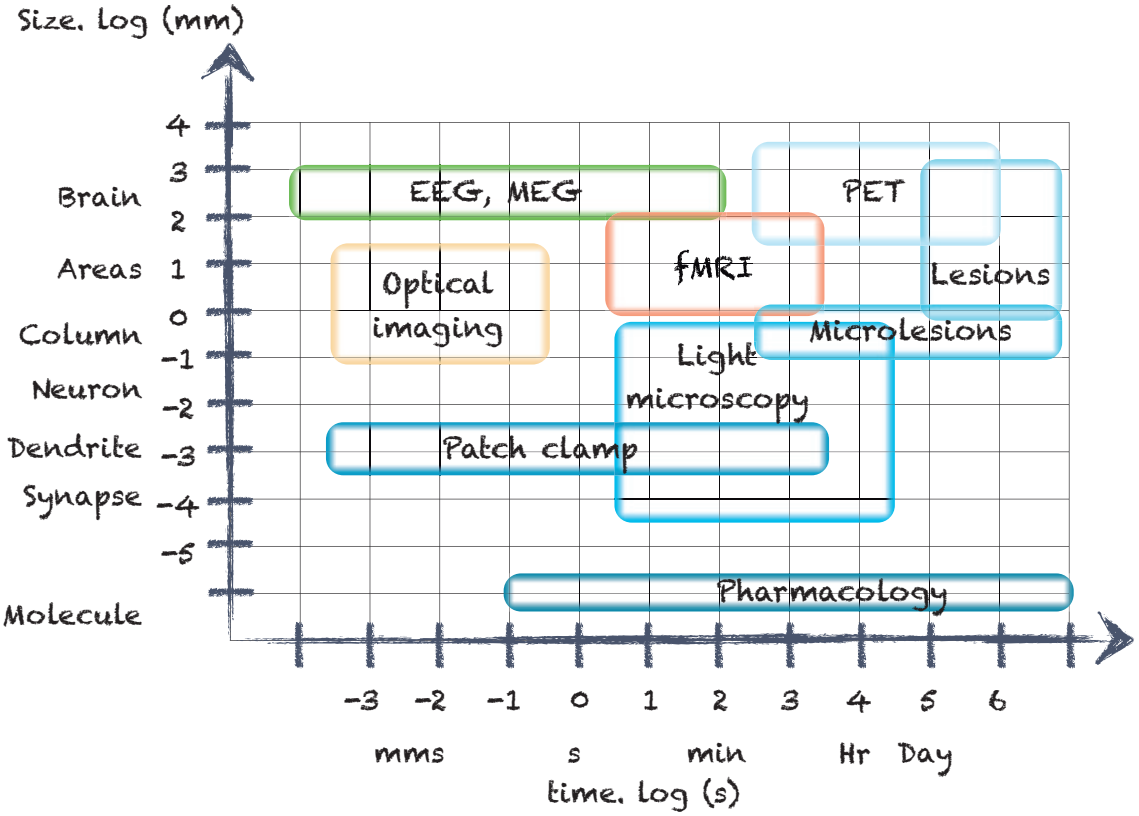

Figure 2.2: **Different techniques and their spatio-temporal resolutions**. Resolution ranges are shown in logarithmic scales. Here it can be seen how the EEG and MEG techniques guarantee the best temporal resolution at the level of mesoscales in contrast with fMRI. This way, EEG and MEG capture information about mental states and cognitive functions. The others tow methods with higher temporal resolution (Optical imaging and Patch clamp) only can be applied at the level of microscale. Figure modified from Churchland [B3]

oxygen through myelinated fibers [A242].

In parallel to these methods, functional MRI (fMRI) records hemodynamic-based brain activity by measuring blood and oxygenation fluxes. More exactly, fMRI records Blood-Oxygen-Level-Dependent signals (BOLD), which account for magnetic susceptibility changes in brain tissue. This information is coded in three dimensional pixels called voxels, which contain local changes of the oxygenated hemoglobin levels as consequence of brain activity [A175] [A102]. The main characteristic of these signals is its high (low) spatial (temporal) resolution (see Fig. 2.2). Hemodynamic-based signals do not really measure neural events, informing only metabolic processes in conglomerates of brain structures. In other words, the sources of MRI information-types remain in oxygen and hemoglobin changes of deeper brain tissues, allowing complex relationship with what is deduced from neuronal activity and pointing higher difficulties to extrapolate conclusions about the real neuronal responses. In this context, the second group of techniques offers an affordable frame to get a bit closer to the real neural activity, taking into account the electromagnetic responses of single neurons or groups of cortical neurons.

2.2.2 Electromagnetic Sources

In contrast with metabolic sources, imaging techniques based on the electromagnetic activity offer higher (lower) temporal (spatial) resolution. Here, the sources of information are groups of neurons. More exactly, the spatio-temporal superposition of many spikes at the level of cortical columns that

create variations of the electromagnetic activity.

These sources (the neurons) use the spike trains as transmitters, conveying information into a receiver, that is not much than a capture device. Nevertheless, in the time lapse required by the information to travel from one site to the other, different noise sources are present. However, the resulting information[4], recorded from the conglomerate of neurons, associates some emergent property of brain and carries information of action potentials, which are thought to be the information of brain in the context of neural dynamics [B4], [B21]. This information may elucidate some neural correlates and evidence different mental states. In this sense, cognitive, linguistic, perceptual, emotional and motor processes are associated to fast signals, so this means that techniques with high temporal resolution are the most adequate to analyze these kind of processes.

Electromagnetic Techniques

It is possible to measure the activity of neuron cultures at the microscale level using Micro-Electrode-Arrays (MEA). Nevertheless, when capturing brain rhythms, the most extended techniques are non invasive, and electroencephalography (EEG) or Magnetoencephalography (MEG) are the two that are most extended [A242], [B19]. In particular, EEG and MEG favour the extraction of sensory information, meanwhile metabolic signals can not witness these events because its temporal resolution is around two orders of magnitudes below the typical EEG or MEG accuracy [T3], [A13]. EEG and MEG measure different physical variables. On the one hand, EEG measures the electrical activity (at the scalp) in the order of μV, due to the difference of extracellular potential from cortical groups of pyramidal neurons. On the other hand, MEG measures the magnetic activity (also at the scalp), in the scale of fT, of large axons in this same group of neurons. They allow to differentiate into several frequencies that have been associated to particular cognitive events, occurring from hundreds of millisecond to periods of few seconds (see Tab. 2.1 [A191].

Band	**Band Width** (Hz)	**Associated Events**
δ	< 4	Deep dreamless sleep, Loss of proprioception, Unconsciousness
θ	$4-7$	Memory, Non-REM sleep, Deep meditation, Hypnosis
α	$8-13$	Relaxation, Resting state, Pree-Sleep(wake)-drowsiness, REM
β	$14-29$	Active concentration, Anxious, thinking, Arousal, Paranoia
γ	$30-80$	Perception, Problem solving, fear, Consciousness

Table 2.1: **Most Common Cognitive Band Frequencies.** There is no agreement in the literature about the exact frequency band limits, but certainly these frequency bands have been reported in association with several cognitive phenomena.

In this way, one can obtain information about cognitive processes by means of experiments that account for that cognitive functions and, then, filtering the obtained signals in the respective band. Moreover, one can also get another type of information about a specific stimulus response. For example, in some experiments individuals usually perform motor tasks like pressing a button or finger tapping [B14], then one can be interested in signals associated to these specific events. The Event-Related Potential (ERP) and the magnetic counterpart, Event-Related Field (ERF), are waveforms associated to such events that come from some all-trial[5] average of time series in the same cortical regions [A21]. Likewise, one can also be interested in provoking an explicit response in the brain due to a well-known stimulus. For instance, subjects may be submitted to a known visual stimulus (flashes or visual patterns), auditory excitations (clicks and tones), somatosensory

[4] In terms of Shannon's definition "*information processing is regarded to a conversion of latent information into a detectable manifest information gathered by an observer*".

[5] Trial is the fraction of a time series that contains the temporal lapse in which a complete experiment occurs.

stimulus (skin punctures) or motors stimulus like electromagnetic stimulations [A137], [A166], [A105]. In this case, the Evoked-Potential (EP) provides information about the function of that respective sensory system.

In general, EEG and MEG are the most common techniques to dig into the brain information sources, since they directly reflect the neural activity [A102], [A191]. The quality of the recorded data depends on the experimental set up and the preprocessing step, which is an important bridge between collecting and analyzing the data. It allows to pass from raw to clean data. In a rough view, the simplest preprocessing is the Epoching, which consists of a reorganization of the data into segments associated to the same response, including the removal of artifacts. In this way, preprocessing increases the SNR associated to the recorded signals. All in all, the final goal of these experiments is to gather the most cleaned brain signals possible, which includes the highest possible amount of information associated to an explicit cognitive process. Thus, these signals can be correlated in order to figure out what neural correlates and neuromarkers could be associated to these cognitive processes.

In the case of brain complex networks, the search of such signal interdependencies is the backbone in the construction of different brain networks. Specifically, the metrics of interdependencies among signals are fundamental to evaluate the interconnectivity among brain sites associated to specific signals. In the next Section, I will develop a short summary of the signal interdependencies as the way for the obtaining functional brain networks.

2.3 Measuring Coordination Between Brain Sites

Signals recorded from cortical regions can be correlated in order to extract the connectivity pattern among these regions. There are plenty of different correlations that make use of statistical analysis, extracting linear and non linear interdependencies. Some of them look at interdependencies in time, others in frequency and other in phase and/or amplitude. Likewise, some of them are based on information theory, i.e., they do not explore similar behaviours in signals, but their search is based on the amount of information that one signal can convey to another. This way, taking into account those interdependencies, one may ask: What measure of coordination between brain sites is the most adequate?

This is one of the most common question about brain signals analysis. In principle, there is not a correct, perfect or better connectivity method [A265]. However, this is not necessarily bad news, in fact, it opens the doors to a wide spectrum for custom-tailoring analyses regarding specific research questions. Based on that, this section is devoted to summarize the principal methods to evaluate the coordination between brain signals. They will be presented in a simple organization based on the type of features that can be extracted for each pairwise correlation, i.e., linear or non linear ones. Additionally, I will also present those measures that account for time series associations from the perspective of the frequency domain.

2.3.1 Linear Methods

In time domain, one of the most extended measures to evaluate correlation between time series is the *Cross-Correlation* ($C(\tau)_{XY}$), measuring linear interdependencies between zero-mean normalized $\{Xt\}$ and $\{Yt\}$, for now on, $X(t)$ and $Y(t)$ signals. It ranges between 1 and -1 and is able to extract correlations in the presence of a time lag τ. $C_{XY} > 0$ quantifies the amount of direct correlation between the two signals, while negative values reveal the existence of an anti-correlated behaviour. The renowned *Pearson Correlation* (*PC*) is subcategory of this measure, consisting on the case of $C(\tau = 0)_{XY}$.

Previous indexes only give information about dependencies but there is no information about whether one source influences the behaviour of the other. To do that, causality indexes, as *Granger*

Causality (*GC*) quantify this kind of directed interdependencies. The idea behind *GC* is that if $X(t)$ influences $Y(t)$, the addition of past terms of $X(t)$ to the regression of $Y(t)$ should yield accuracy in its prediction of $Y(t)$ [A93].

2.3.2 Non Linear Methods

The use of nonlinear time series analysis in brain signals goes back around three decades ago with the works of Babloyantz [A12]. Regarding those non linear indexes, *Non-Linear Correlation* (*NLC*) is a non parametric and nonlinear regression coefficient that measures the dependency of signals. The underlying idea is that each point in $Y(t)$ given $X(t)$ can be predicted based on a nonlinear regression curve. In addition, *Synchronization Likelihood Algorithm* (*SL*) is useful in cases where it is important to find temporal patterns among signals. *SL*, which is bounded between $[0,1]$, identifies temporal patterns in $X(t)$ that arise within a fixed time window, then it looks at signal $Y(t)$ to find the existence of coordinated (not necessarily similar) patterns within the same window, evaluating how this co-ocurrence of patterns is maintained along the whole time series [A214].

Likewise, *Information-theory based* indexes have arisen as parallel tools to correlate signals. Among them, *Mutual Information* (*MI*) is a non causal index defined as the common relative amount of information that we get from $X(t)$, knowing the past of $Y(t)$ [A267]. The analogue form of causality is the *Transfer Entropy* (*TE*), which gives clues about the mean information between the previous state Y_{n-1} and the next state of X_n [A164].

Another domain where one can find out correlations is in the *phase* of the signals. In that respect, one first must estimate the instantaneous phases. For continuous time series like those obtained in EEG or MEG, one can use the analytic concept of Hilbert transform [A229], or alternatively, by convolution of a complex wavelet [A129]. For discrete neural signals, like spikes, they can also be transformed to get instant phases by linear interpolation [B17]. Thereafter, correlations of the respective phases can be estimated by the *Stroboscopic Approach* (*SA*), which is an information-theory based index [A184]. Nonetheless, the *Mean Phase Coherence* and *Phase Locking Value* (*PLV*) are the most common indexes to measure how the mean phase or phase differences are distributed along the unit circle. In the case of *PLV*, the tendency of the relative different phases to be distributed uniformly leads to low values of the index. On the contrary, when phase differences tend to be maintained within a certain threshold along the time, the PLV is close to 1 [A129].

On the other hand, although the concept of Complete Synchronization can only be applied to identical systems [A80], something difficult to accomplish in natural systems, its relation with chaos synchronization has been the reason to its application in neuronal systems [T4], [B17]. *Generalized Synchronization* (*GS*) represents another kind of nonlinear coordination that assumes the existence of chaotic oscillators. In particular, *GS* claims for the existence of certain functional dependency between systems, which can be quantified using different nonlinear techniques [A189].

2.3.3 Spectral Methods

Coherence (*Coh*), also known as *Coherence Spectrum* [A174] is the most extended indicator of coordination based on the spectral properties of time series. Coherence is defined as the square module of a coherence function F. This function F is based on either: the Cross-Spectral Density (also called cross power spectrum) function, that is simply the Fourier transform of the classical Cross-Correlation function of $X(t)$ and $Y(t)$; or the power spectral densities of each signal. It has a zero value when both signals are linearly independent at a certain frequency, and 1 for the maximum correlation of the spectra. There is another extension of the Coherence that takes into account just the imaginary part [A165]. This *Imaginary Coherence* has proved to be successful at the time of extracting dependencies in brain signals based on their frequencies, avoiding the field spread residual effects due to the volume conduction [A81], [A56].

Another example of frequency based correlation is the *Partial Coherence* (*PC*) and *Partial*

Directed Coherence (*PDC*). The former captures the fractional coherence between X and Y, which is not shared with another signal Z under the assumption of linearity, meanwhile the latter extracts causality as the relative strength correlation a signal X has with respect to Y, as compared with all correlations of Y with the other signals in the channels [A173].

In short, let us return to the initial question about what measure is the most adequate to evaluate coordination between signals. Although the brain is a non linear system and, at least, one may have strong reasons to believe that the recorded signals contain some nonlinear interdependencies, the nonlinear methods do not necessary overcome the linear indexes. In fact, a good strategy could be to start the analysis with a linear measure, and then use some of the nonlinear methodologies in order to capture all possible correlations of the system. At the end, it depends on the kind of data and the aims of the research. For example, if we are interested on the amplitude of the signals, nonlinear Granger causality and *GS* are good candidates, otherwise *PS* indexes give correlations independently of the signal amplitudes. In this work, we have used the *Synchronization Likelihood*, the *imaginary Coherence* and the *Phase Locking-Value* in order to evaluate coordination in the time, frequency and phase domains.

Finally, once correlations between brain sites have been obtained, it is time to focus on the resulting *functional network*, which will be the target of the next section.

2.4 The Brain as a Complex Network

A network representation arises naturally both for the brain's anatomy and its functional activity. Brain networks can be defined at different scales, from the microscale up to several mesoscales of centimeters of system-level neural assemblies, corresponding to the spatial resolution of the brain imaging technique used to define them. For anatomical brain networks, it is straightforward to identify nodes with neurons or cortical areas and edges with axons or fibre tracts, in general, using the signals obtained from the MRI techniques. On the other hand, when considering functional connectivity, networks are defined as those whose edges correspond to statistical correlated activity at different brain regions using any of the correlations showed in the previous Section. The effective connectivity, goes one step beyond, leading to networks with directed edges whenever the activity at one node modulates the activity of another node [A210].

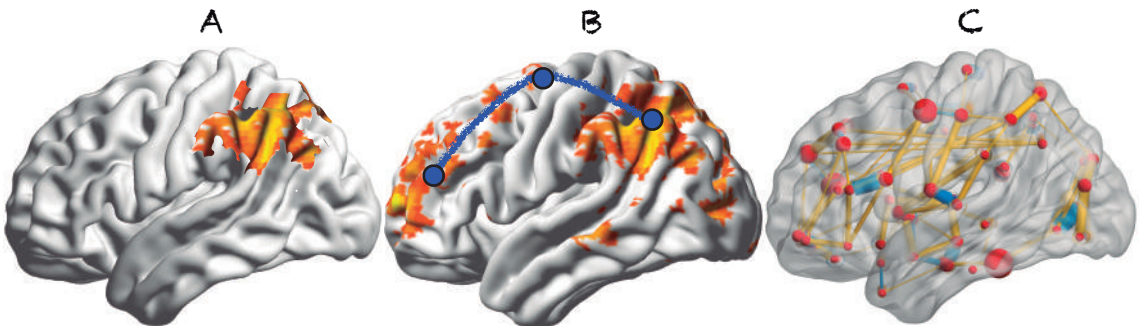

Figure 2.3: **Different perspectives for analyzing the brain activity**. **A**, Initially, studies of brain activity were concerned on the activation of single regions and its relation with different brain activities. **B**, Next, studies on brain segregation/integration evaluated the interrelation between few brain regions involved in the performance of a single task. **C**, Finally, network science focuses on the complex interactions between brain regions.

The classical view of brain connectivity is centered on the localization of a cognitive function into some brain regions due to several integrative fibres. The assumption here is that each region and fibre is associated to specifics activities of the brain. Functional Connectivity analysis considers the

brain as a computational entity in which different regions activate in a coordinated/uncoordinated way. This approximation is focused only on the activations but not on how these activations are organized from a holistic point of view. Network Science approach represents a qualitatively different view for the analysis of the brain activity and brain-behavior mapping (see Fig. 2.3). In this case, the brain is understood as a complex system, where relationships between a great number of constituent parts give rise to collective behaviors. The viewpoint of the statistical physics approach is based on understanding of observed network properties as macroscopic phenomena resulting from the microscopic interactions among a great number of individual components. Therefore, the identity of nodes and links is somehow lost. The network, rather than well-specified nodes or links, is endowed with specific properties. These network properties are not easily traced to their single nodes and links, rather, they emerge from the statistical properties of their components. With respect to prior connectivity methods, the complex networks approach presents three distinctive advantages:

1. It affords a multiscale characterization of the brain's organization.
2. It allows handling complex relationships between brain structure, dynamics and function.
3. It allows studying the brain as a biophysical machine and investigating a wide range of aspects of mechanistic brain functioning, including efficiency, resistance to failure or synchronizability, which could not directly be addressed with connectivity techniques alone.

2.4.1 Building a Brain Network

The projection of experimental data onto a network is one of the most delicate steps in the application of network theory to the analysis of biological data. Both the nature (anatomical or functional) and the scale of observation constrain the way networks are reconstructed. The experimental technique used to record brain activity determines the size of the network and, ultimately, the information that can be extracted from it. Important methodological aspects of brain network reconstruction and possible pitfalls are still a subject of debate [T1], [A262]. In general, brain networks can be classified into three main types: anatomical, functional and effective networks.

Anatomical networks

They refer to the physical connections between neuronal elements, ranging from synapses between neurons to the grid of bundles between Regions of Interest (ROIs). We can define an anatomical network of connections at the scale we are interested in (or the scale given by experimental limitations): neurons cortical columns, ROIs or any parcellation of the brain with significant meaning. There exist different experimental techniques to trace the anatomical network of connections, which rely both in the scale at the organism being studied. For example, electron microscopy has allowed extracting the complete set of connections between neurons of the nematode C. Elegans [A248], the only living system whose nervous system has been fully mapped [A243]. More recently, Micro-Optical Sectioning Tomography (MOST) has also revealed the connectivity of a mouse brain [A134]. Both the anatomical networks of the cat [A194] and the macaque [A72] cortex has been extensively studied thanks to the data obtained from different histological studies, leading to a complete cortico-cortical network of $N = 53$ cortical regions and $L = 650$ connections in the cat [A194] and the reconstruction of the macaque visual area ($N = 32$ and $L = 305$) [A72]. DTI technique [A115], [A88] allowed to reconstruct the human brain anatomical network, with the limitation of inferring the fibre bundle orientation. The use of DSI has overcome this constraint [A97] allowing an anatomical reconstruction of the human brain anatomical network formed by up to $N \sim 1.000$ nodes and $L \sim 100.000$ link [A96].

Although the anatomical networks provide a substrate for the dynamical processes occurring on them, they are not necessarily linked to the functional activity occurring between different brain regions. Anatomical and functional networks may differ depending on the specific cognitive process that an individual is carrying out: while at short time scales the anatomical network

is essentially static, the functional network associated with the execution of a cognitive task is inherently dynamical.

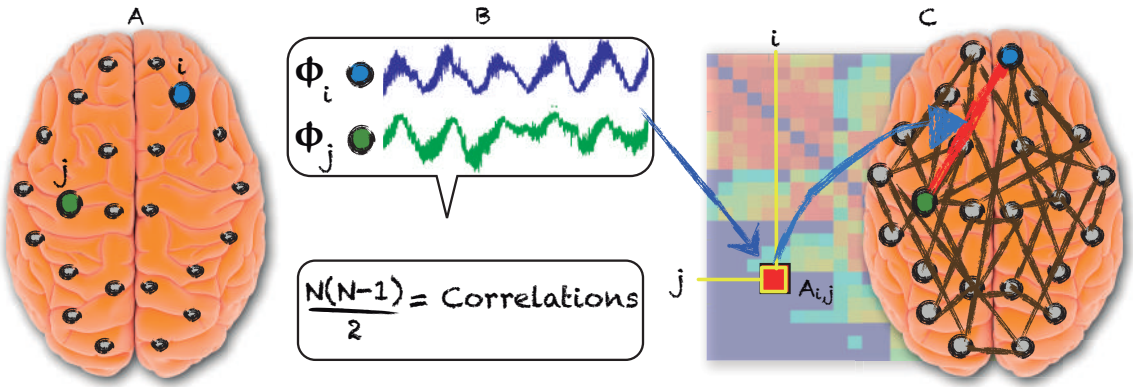

Figure 2.4: **How to obtain functional brain networks**. **A**. Sensors spread through the scalp to record the cortical activity. **B**. Next, the coordination between the times series of every pair of channels, e.g. ϕ_i and ϕ_j, is calculated with the use of the aforementioned metrics. **C**. Each correlation will be an element of the weighted adjacency matrix, i.e. the weight of the link between two nodes (brain regions).

Functional Networks

They account for the neurodynamical interactions between neural regions. Functional networks measures statistical interdependences between the dynamics of large amount of pairs of the network nodes without taking into account causal effects. The more correlated the activity between two regions, the higher the weight of the functional connections between them. Note that despite functional connectivity requires the existence of an underlying anatomical connection, both functional and anatomical networks do not necessary need to resemble each other[6]. As we will see, functional networks share common features between them, despite each network is task dependent. In Fig. 2.4 we have qualitatively shown the procedure to obtain a functional network from a brain signal.

Effective Networks

Nevertheless, one of the main drawbacks of functional networks is the lack of directionality of their links. The fact that correlation does not imply causality, leads to the necessity of defining an additional kind of brain networks. Effective networks, which are constructed from the analysis of the dynamical response of the different brain sites, assign directionality to the links based on causality analysis [A26]. This kind of networks is the most mathematically demanding [A220] but also the most accurate approximation to evaluate the real relations between brain sites (See Fig. 2.5 for a general framework of functional and effective brain networks).

2.4.2 Brain Networks Features

In the following Section we are going to overview what are the main properties of functional brain networks and how Network Science is able to capture and quantify the main features of this kind of brain networks.

Degree and Strength Distributions

In the case of the brain, different kinds of distributions have been reported depending on the spatial scale at which the system is analysed, since the scale determines the number of nodes N and links L of the network which, in turn, constrain the width of the degree distribution. In cultured neural

[6] As the map of the road connections does not necessary reveal the traffic moving through them.

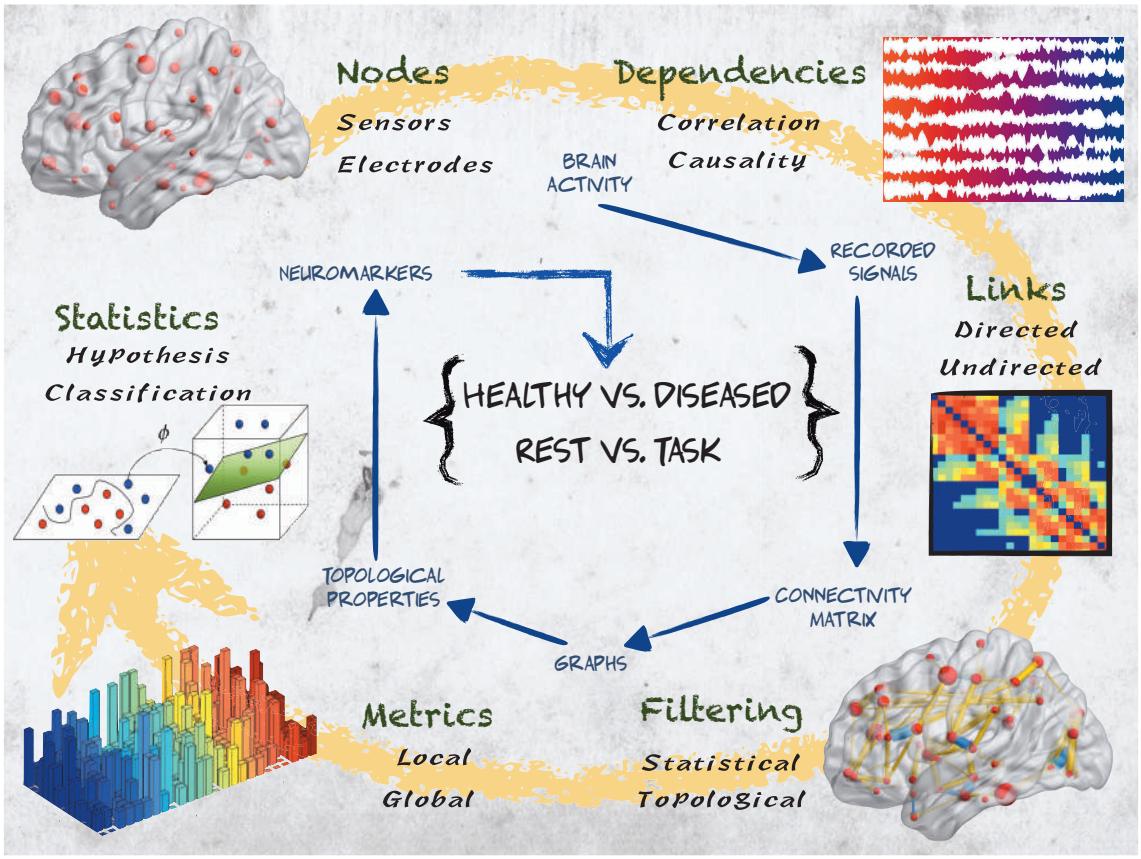

Figure 2.5: **The general framework of brain networks**. Clockwise guideline. Nodes can be regarded as sensor or electrodes recording the electromagnetic signals of the brain, which may contain dependencies based on correlation or causality. These interdependencies, or link weights, lead to a weighted connectivity matrix, which is the mathematical representation of a network. This network is usually filtered using statistical thresholds to work only with the relevant links. Network metrics can be classified into local (degree, clustering,...) and global (average shortest path, global efficiency, ...). The previous topological properties allow to compare, to establish hypothesis and to classify different brain networks in order to obtain neuromarkers for either: healthy vs. diseased subjects, and resting state vs. cognitive/motor tasks (figure adapted from [A53].

networks, the fact that neurons primarily connect through a random process leads to exponential distributions [A62] [A199]. This kind of distribution is also reported in the in-degree and the out-degree of the anatomical connections of *C.Elegans* nematode, the only living system with a whole reconstruction of its neural network [A8]. In human brain networks, the degree distribution strongly depends on the experimental technique used to acquire the data, the scale at which the system is observed and the nature of the network that its being analysed (anatomical, functional or effective).

In functional networks, Eguíluz et al, [A70], showed that functional brain networks from fMRI had scale-free distributions for different tasks [A70] which could be related to their resistance to failure, facility of synchronization, and fast signal processing [A130]. Van den Heuvel et al, also reported a scale-free distribution. Nevertheless, other results showed some discrepancies at the tail of the degree distribution, which was better fitted with an exponential decay leading to a power-law, exponentially truncated distribution [A240], [A3]. In summary, there is no typical behaviour that describes the degree or strength distribution in brain networks. The number of nodes and links of the network, the experimental technique used to obtain the data and the task performed during the

recordings restrict the width of the distribution.

Hubs and Rich Clubs

The existence of hubs in both anatomical and functional brain networks has been related to a reduction of the wiring cost of the network, since hubs behave as integrators and distributors of information through the network when combined with a few long-range connections to other brain modules. Several studies have focused on the identification of these hubs and both their role inside their respective community and as connectors between different brain modules [A97]. The tracking of hub connectivity during aging has shown an alteration of both its importance within its community and its participation in other network modules [A148]. Particularly, hub failure, quantified in terms of loss of connectivity, has been associated to the emergence of different brain diseases [A18].

In the context of Network Science, the *rich club* refers to the existence of tight connections between the hubs of the network, leading to groups that retain the majority of the importance along the whole network. In the human brain, the rich club seems to encompass regions including the superior parietal cortex, the precuneus, both posterior and anterior cingulate cortices, and the insula [A239]. The brain's rich club appears as a "super hub" where information converges from and is broadcast back to segregated communities and networks, allowing for integrated processing, offering a potential network substrate for the 'global neuronal workspace' proposed in recent influential theories of cognition [A198].

Assortavity

Assortativity is one of the mechanisms promoting the emergence of rich-clubs. Regarding assortativity in the brain, functional networks obtained from fMRI recordings during music listening and finger tapping were shown to be assortative [A70]. Interestingly, the majority of biological networks seem to be disassortative, with clusters organized around local hubs [B16].

Brain Efficiency

Efficiency in brain networks is related to the cost of creating and maintaining the network, and its interplay with the performance in executing a given task. Note that the concept of efficiency introduced by Latora et al [A131], measures a different thing, since it is essentially a way of evaluating the (inverse of the) topological distance between nodes. Different studies have shown that, in brain anatomical networks, the number of steps between any pair of nodes in the network [A121] and the physical cost of their placement in a three-dimensional space [A19] are reasonably close to their optimal value. Functional networks can enhance their topological efficiency during a demanding cognitive process, paying the price of an extra-cost and recovering the initial state after finalizing the task [A124]. In this sense, impaired networks show the deviation from a cost-efficiency balance in the brain, for example in schizophrenia and Alzheimer's disease [A139], [A217].

2.5 Brain Networks Organization

Network Science also offers a diversity of tools to evaluate the organization of the whole functional network and its interplay with different cognitive processes.

2.5.1 Modularity and Hierarchy

Detecting modular structure of a brain network is a complex task, nonetheless is completely necessary since it gives information about the segregated activity of the brain [A169]. Interestingly, anatomical networks exhibit a modular [A108] and hierarchical organization [A258]. Additionally, different algorithms of community detection upon anatomical networks have shown high correlations of the obtained communities with known functional areas in the human brain [A40], [A98].

Parallel to this, hierarchical organization of functional communities has been reported in the human brain showing that hierarchically modular structures facilitate the embedding of complex topologies into low-dimensional physical space [A147], [A19].

2.5.2 Integration and segregation

Regarded to this point, there are evidences that show that cognitive functions require an optimal balance between global integrative and local functionally specialized processes [A232], [A241], for instance, the local and global collaboration in the phenomena of gestalt-like perception by Singer et al [A201]. An appropriate balance between these two tendencies has been shown to be necessary for efficient functioning, particularly in neural systems [A232] ; in fact, exceedingly segregated or integrated brains have been associated with various pathological conditions, e.g. autism [A118] , or schizophrenia [A74], [A233], [A74]. The functional organization of the human brain presents an essential balance: On the one hand, modules present sufficient independence to guarantee functional specialization and parallel computing; on the other hand, modules are sufficiently connected to bind multiple sources of information so as to benefit a coordinated activity.

2.5.3 Small-world structure

It has consistently been shown that brain anatomical networks have characteristically small-world properties of clustered local connectivity with relatively few long-range connections mediating a short path length between any pair of neurons or brain regions [A208], [A103], [A96]. The small world structure seems to be pervasive both across scales of brain activity and across species, for example: in mammal [A206], [A256], and the simplest system of C. Elegans [A247]. The modifications of small world structure in disease [A212], normal aging, and by pharmacological blockade of dopamine neurotransmission [A2] may be functionally interpreted in the light of theoretical studies showing that small-world architecture optimizes information processing [A225], facilitates synchronization [A28] and rapid response and emergence of coherent oscillations conferring resilience against pathological attacks [A130].

2.5.4 Brain Diseases

Graph theoretical measures have proven to be adequate indicators of the emergence and evolution of a series of brain diseases, an aspect that renders them of enormous practical applications. The emergence of brain dysfunction can be quantified using network metrics, which are altered in a disease-specific way [A215]. For example, during epileptic seizures, functional brain networks become more regular, modifying their degree distribution and losing part of their modular structure [A181], [A119]. On the contrary, functional networks of schizophrenic patients become more random, with a consequent decrease of both the normalized clustering coefficient and shortest path [A149]. Mild cognitive impairment, a condition sometimes evolving into Alzheimer's dementia, also shows increased functional network randomness, but in this case it is associated to increased network synchronization and a propensity to enhance long-range connections [A29]. Network analysis of Alzheimer's disease indicates a disconnection syndrome leading to an increased shortest path and decreased network clustering, both leading to a severe impairment of the desirable properties afforded by small-world networks [A218] , [A213]. The epilepsy as neural disorder was investigated with MEG techniques in the works by Chavez et al. [A38] and the brain plasticity problem and strokes injuries using EEG data have been better understood through the works by De Vico Fallani et al. [A54], [A57]. Regarding brain resilience, cats [A122] and macaques [A120] brains had been analysed from the optics of robustness showing a robust behaviour due to their scale-free organization.

2.6 Final Remarks

In summary, tools coming from Network Science have been widely applied to better understand different problems in neuroscience, ranging form normal functioning of a brain to the impairment due to different diseases. Notwithstanding, there are a diversity of open problems and future lines of research in the field. The problem of how to link structure and function in the brain, the application of concepts like control and targeting of a functional network or the debate around what should be a node (neuron, groups of them, cortical regions,...) and a link (functional or anatomical) in brain networks. Among them, I will be ultimately interested in the interplay between the topology of a brain network and the dynamics occurring in it. The possibility of figuring out a correlation between both the topological features and the dynamical properties of functional networks will be investigated along this PhD Thesis through a series of results using, all of them, different methodological tools coming from Network Science.

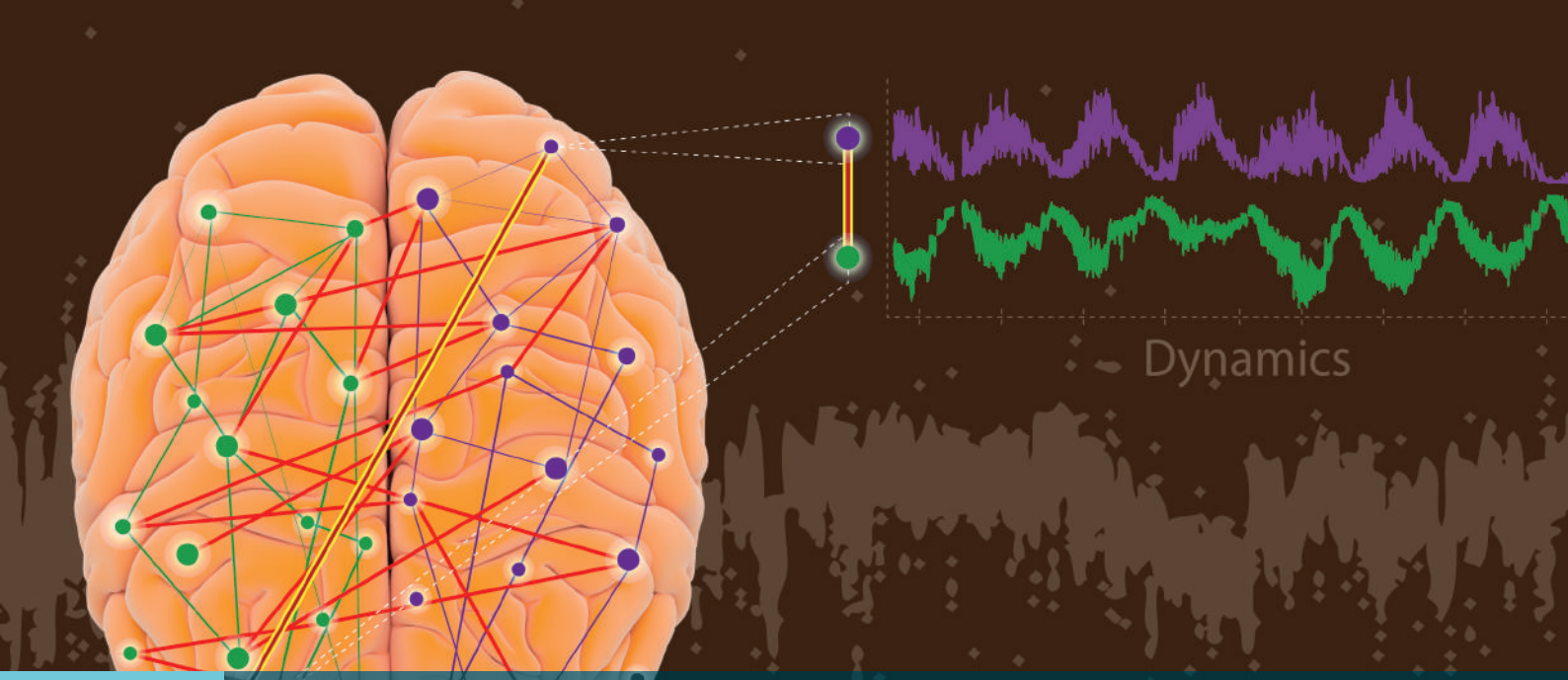

3 Topology & Dynamics of Brain Networks

In this (short) Chapter I will summarize the specific problems that have been addressed during this PhD Thesis. The five forthcoming Chapters, each of them targeting a specific problem, make up the second part of the Thesis, were the results obtained during the last four years will be exposed. Obviously, there are several links between all of them, but they are organized in a time line departing from the most fundamental problems to the most general ones. All of that, by the hand of Network Science.

3.1 Quantifying Functional Hubs

The first results of this Thesis refer to the quantification of the importance of a node within a functional network. With this aim, I will investigate what is the more adequate network measure capturing the importance of brain regions in both healthy individuals and patients suffering from a neurodegenerative disease. In this Chapter 4 will introduce the way functional networks can be obtained from brain imaging and how network metrics can help us to discriminate between groups.

3.2 Hemispherical Balance

In the previous Chapter I investigated the properties (in that case centrality) of functional networks when they are considered as *single networks*. In this Chapter, I will explicitly take into account that networks are not isolated systems, and they are in continuous contact with other networks. In neuroscience, the task-differentiation between brain hemispheres has been deeply studied. Nevertheless, concepts coming from Network Science, such as the existence of networks-of-networks have been scarcely developed in the context of functional brain networks. Thus, I will consider functional networks as an interplay between two sub-networks, each one accounting for the activity of each of the hemispheres a brain has. Chapter 5 is completely devoted to study the problem of hemisphere competition/cooperation using a EEG datasets recorded from a group of individuals under two base-line conditions: (i) open eyes resting state and (ii) closed eyes resting state. Here, I will evaluate to what extent the centrality of the whole network is shared between both

hemispheres, and how the robustness of functional brain networks relies on the inter-hemispherical connections.

3.3 Evolving Networks

Hitherto, previous Chapters answer different questions related to the topology of the networks. However, those functional networks only capture the dynamics of the system during a specific moment, i.e., networks are a snapshot of what is really happening in the brain. Nevertheless, functional networks are intrinsically dynamical and its topology unavoidably changes as time goes by. Based on this fact, in this Chapter 6 investigate what happens when the topology of a functional network is tracked during several time-steps? In other words, I investigate how functional brain networks evolve in time. In this way, in Chapter 6, I put forward the evolution of the topological properties of functional networks associated to two groups of people (young and old subjects). The idea is to define specific time windows in MEG signals in order to create dynamical networks corresponding to different temporal lapses. I will show how the statistical comparisons of the topological features of the time-evolving networks lead to discriminate the brain performance in young and old individuals who are facing an interrupted memory task.

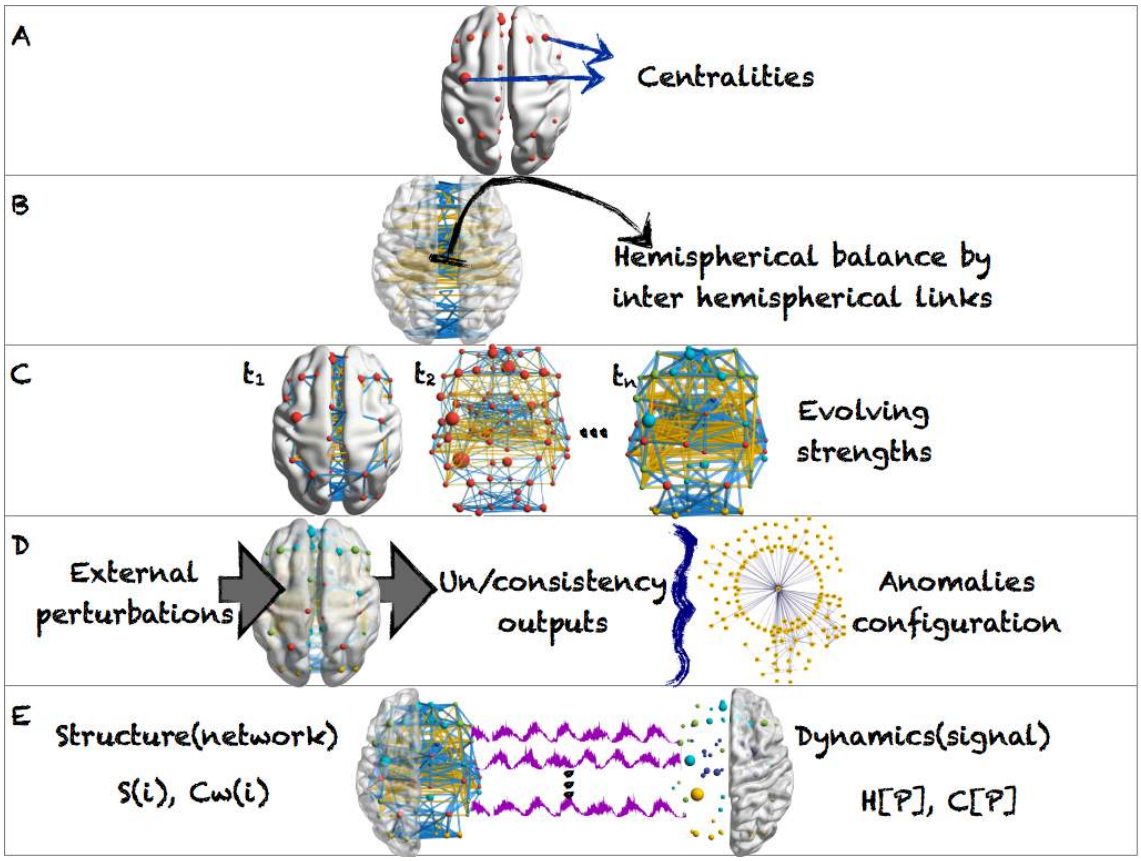

Figure 3.1: **Five Studies on topology and dynamics of functional brain networks**. **A**. Quantifying Functional Hubs. **B**. Hemispherical Balance. **C**. Evolving Networks. **D**. Anomalous Networks. **E**. Cognitive Reserve.

3.4 Anomalous Networks

In this Chapter 7 I will show how it is possible to obtain a new type of functional network from the recording of the brain activity, what is called "parenclitic network". The main aim will be to investigate the consistency of the brain signals and how it deteriorates in a group of individuals suffering from mild cognitive impairment. The phenomenon of consistency is based on the identical response of a dynamical system when the same external perturbation is applied, no matter what the initial conditions of the system are. What I will show is that the differences of the consistency of the brain activity in a group of patients diagnosed with mild cognitive impairment can be captured by a parenclitic network, which is defined as the network projection of the differences between the features of two different groups. In this study, the reader will find how the consistency, measured by means of MEG, can be translated into a network, which can be analyzed with the aim of determining where are the focal nodes of "anomalous networks".

3.5 Cognitive Reserve

In the last Chapter devoted to the new findings of this PhD Thesis, I will be concerned about the interplay between the topological features of a node and its dynamical properties. Specifically, on the one hand, I will characterize the inner dynamics of the nodes through the use of several statistical complexity measures. In this way, the complexity and the level of disorder will be assessed by means of temporal ordinal patterns obtained from MEG signals. These signals will be recorded from two groups of healthy people performing a well defined memory task, being the level of studies the key difference between both groups. The idea behind this experiment is to evaluate the level of cognitive reserve, a term that was widely associated with the stability of brain function during ageing. MEG signals will be correlated to reconstruct the respective functional networks to seek for some their topological features. Next, the dynamical properties of cortical signals and their corresponding topological features will be correlated. The results contained in Chapter 8 will show certain type of hub reorganization regarding the level of complexity and permutation entropy.

Study	**Type**	**Phenomena**	**Activity**	**Emphasis**	**Correlation**
1	Topology	Node importance	Short-term memory task	Centralities	SL(t)
2	Topology of *NoN*	Hemisphere balance	Resting state	Eigenvector centrality	i-Coh(f)
3	Topology in time	Age-related memory	Working memory task	Strength	PLV(ϕ)
4	Dynamics of nodes	Brain consistency	Short-term memory task	Anomalies organization	SL(t) & Z-scores
5	Dynamics & topology	Cognitive reserve	Short-term memory task	Hubs reorganization	SL(t)

Table 3.1: **Summary of the results contained in the PhD Thesis.** Rows corresponds to the problems investigated in each chapter. I present the type of study, the associated phenomenon, the task-related activity, the associated key information and the kind of correlation used. Regarding short-term memory tasks, it was performed using the Sternberg test. It is important to highlight that the experiment datasets consists on MEG signals in Study 1, 3, 4 and 5 (Chapters 4, 6, 7 and 8), while Study 2 (Chapter 4) is based on EEG recordings.

3.6 Final Remarks

In view of all, this PhD Thesis contains a series of complementary studies with the common objective of characterizing the topology and dynamics of functional networks. As shown in Tab. 3.1, in this PhD Thesis I address different problems, all of them with the common tool of Network Science. Despite the results concern very specific and applied problems, the methodology I use could inspire future research on the field of brain networks, simply by analyzing different cases of study. In this way, although a neuroscience-based network theory has not been developed yet, I hope to have helped in its future arrival. Definitely, we deserve more efforts to develop a set of well established methodologies aiming to fully describe the behaviour of brain networks.

II Results

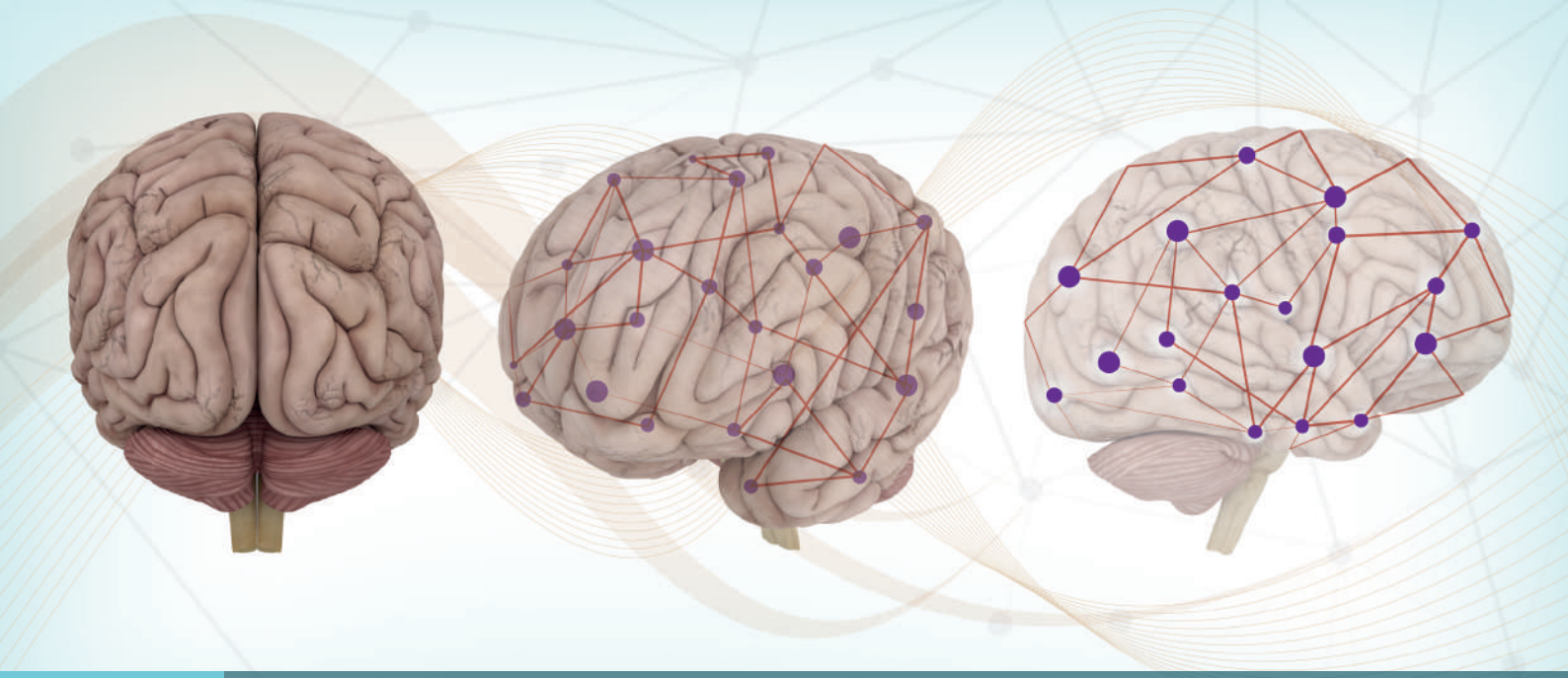

4 Functional Hubs

§

In this first study about topology of functional brain networks, we investigate how hubs of functional brain networks are modified as a result of mild cognitive impairment (MCI), a condition causing a slight but noticeable decline in cognitive abilities, which sometimes precedes the onset of Alzheimer's disease. We used MEG to investigate the dynamics of the networks of a group of patients suffering from MCI and a control group of healthy subjects, during the execution of a short-term memory task. Couplings between brain sites were evaluated using synchronization likelihood, from which a network of functional interdependencies was constructed and the *centrality* quantified. The results showed that, with respect to healthy controls, MCI patients were associated with decreases and increases in hub centrality respectively in occipital and central scalp regions, supporting the hypothesis that MCI modifies functional brain network topology, leading to more random structures.

4.1 Introduction

Characterizing how the brain organizes its activity to carry out complex cognitive tasks is a highly non trivial pursuit. While early neuroimaging studies typically aimed at identifying patches of task-specific activation or local time-varying patterns of activity, it is now recognized that both at rest and during behaviour, that brain activity is characterized by the formation and dissolution of functionally meaningful integrated activity [A24].

The existence of central regions in brain functional networks and the way of quantifying their importance in the network structure has been the object of numerous studies [A209], [A3], [A27], [A258] [A117], [A136], [A114], [A127]. The importance of a node i, can *prima facie* be measured by the number of connections $k(i)$ (degree), indicating how many regions are coordinated with it during a certain task. Likewise in weighted networks, the node strength $S(i)$, becomes a more accurate indicator of the importance of a node. Nevertheless, both the degree and the strength are

§This chapter is based on my published paper: ***Functional Hubs in Mild Cognitive Impairment***. *International Journal of Bifurcation and Chaos*. **25**, 10 (July 2015). [A158]

local measures, which do not take into account the global topology of the functional network. To overcome this issue, global measures of centrality have been proposed. Node closeness $C(i)$, takes into account the number of steps that we have to do to go from one to another: the lower number of steps, the higher closeness a node has. The eigenvector centrality $E(i)$, is another indicator of the global relevance of a node and it is measured by computing the eigenvector v_1 associated to the largest eigenvalue of the connectivity matrix. A more intuitive measure is represented by node betweenness $B(i)$, which quantifies the number of shortest paths that cross a certain node, thus reflecting its importance in the transmission of information in the whole network. Closeness, eigenvector centrality and betweenness, make use of information about the structure of the whole network, nevertheless node centrality could be restricted solely to a certain community. To measure the community importance of nodes, Guimerà *et al.* [A94] introduced two indicators, the within-module-degree z_i and the participation coefficient p_i. The combination of both parameters not only measures the importance of a node inside its community but allows classifying the role played by the central nodes (hubs) in the overall community structure.

The application of these measures to functional brain networks may help in quantifying how relevant nodes are impaired by the emergence of different brain diseases. Here, we analyse the alteration of functional networks' hubs caused by MCI, a brain syndrome involving cognitive impairments beyond those expected based on the age and education of the individual often representing a transitional stage between normal aging and dementia. The progressive accumulation of the beta amyloid protein and the loss of cells and synapses along the Alzheimer's disease (AD) continuum impair cognitive function as a reflection of network malfunctioning. Thus, although hubs organization has been studied for fully-fledged AD [A27], [A218], [A60], whether hub organization impairment at the early stages of the disease such as in MCI still remains unclear.

In Buldu et al. [A29], the attention was devoted to the global properties of the functional networks. Nevertheless, how hub organization is affected by the disease was not considered. In the present work we focus on how the role of the hubs is distorted by MCI. Our hub characterization relies on various parameters, but we show how the eigenvector centrality $E(i)$ of the nodes is the more adequate indicator, in contrast with local measures such as degree or strength centrality. Therefore, we use this measure of centrality to identify (and quantify) network hubs. Eigenvector centrality allows detecting the dominant regions in the functional connectivity network and, next, how these regions are affected by the disease. Our results show that the leading role played by network hubs is attenuated by MCI, which transforms the network into a more homogeneous one. These results are consistent with previously reported analyses showing that MCI increases the randomness of the global structure of the functional network [A30], thus, leading to a more homogeneous connectivity network.

4.2 Materials and Methods

The MEG signal of seventeen patients suffering from MCI and seventeen control subjects (Box, 2 and [A14]), was recorded (Box, 3) during the execution of a memory task (Box, 4 and [A30] for details). Next, we measured the synchronization likelihood (*SL*) between all pairs of nodes, and obtained a weighted correlation matrix.

In this case we chose Synchronization Likelihood (*SL*) [A214] to correlate the MEG signals. *SL* is a nonlinear measure of the synchronized activity that has been proven to be a suitable quantifier for datasets obtained from magnetoencephalographic recordings [A216], [A30]. This index, which is closely related to the concept of generalized mutual information [A34], relies on the detection of simultaneously occurring patterns, which can be complex and widely different for every pair of signals. Specifically, the *SL* algorithm detects windows of repeated patterns within the time series of a channel A and, next, checks whether the channel B also shows a repeated pattern at the same time windows, no matter if it is the same or different to that observed in channel A.

The idea behind this algorithm proceeds as follows. Let$\mathbf{X}$ denote the matrix containing all the M signals (one per each channel that measures a certain cortical region) of n time steps, and let $X_n = [x_n, y_n, ..., z_n]$, where $X_{1,n} = x_n$, $X_{2,n} = y_n$ and so on. In the time series of a given channel, for each time step n, we define the probability that embedded vectors are closer to each other than a distance ε:

$$P_n^{\varepsilon}(X) = \frac{1}{2(w_2 - w_1)} \sum_{\substack{m=1 \\ w_1 < |n-m| < w_2}}^{N} \theta(\varepsilon - |x_n - x_m|) \tag{4.1}$$

where $|.|$ is the Euclidean distance and θ is the Heaviside step function, being $\theta(x) = 0$ if $x \leq 0$ and $\theta(x) = 1$ for $x > 0$. Here w_1 and w_2 are two windows: w_1 is the Theiler correction for autocorrelation effects and should be at least of the order of the autocorrelation time; w_2 is a window that sharpens the time resolution of the synchronization measure and is chosen such that $w_1 \ll w_2 \ll N$.

Box 2: Subjects

All recruited subjects or legal representatives provided written consent to participate in the study, which was approved by the local ethics committee of the Hospital Clínico Universitario San Carlos (Madrid, Spain). MCI patients fulfilled the following criteria:

- Cognitive complaint corroborated by an informant (a person who stays with the patient at least for half a day for 4 days a week). Additionally, relatively preserved daily living activities was measured by the Lawton scale.
- In addition to age, years of education were matched to the MCI group: 10 years for the MCI group and 11 years for controls. Objective cognitive impairment, documented by delayed recall in the logical memory II sub-test of the revised Wechsler Memory Scale (score $\leq 16/50$ for patients with more than 15 years of education; score $\leq 8/50$ for patients with $8-15$ years of education). Memory impairment was assessed using the Logical Memory immediate (LM1) and delayed (LM2) subtests of the Wechsler Memory Scale-III-Revised.
- Normal general cognitive function, as assessed by a clinician during a structured interview with the patient and an informant and, additionally, a mini mental state examination (MMSE) scored greater than 24. Specifically, two scales of cognitive and functional status were applied as well: the Spanish version of the Mini Mental State Exam (MMSE) [A135], and the Global Deterioration Scale/Functional Assessment Staging (GDS/FAST).
- Not sufficiently impaired, cognitively and functionally to meet criteria for dementia. Age and years of education were matched to the SMC group. According to their clinical and neuropsychological profile, all patients in this group were considered multi-domain MCI patients (see [A177]). As for the geriatric depression scale, none of the MCI showed depression (score lower than 9) [A253]. To confirm the absence of memory complaints, a score of 0 was required in a 4-question questionnaire [A153]. None of the participants had a clinic history of neurological or psychiatric condition.

Box 3: Recordings

The MEG signal was recorded with a 256 Hz sampling frequency and a band pass of $[0.5, 50]$ Hz, using a 148-channel whole-head magnetometer (MAGNES©2500 WH, $4-D$ Neuroimaging) confined in a magnetically shielded room. An environmental noise reduction algorithm using reference channels at a distance from the MEG sensors was applied to the data. Letters of the Sternberg test were projected through a LCD videoprojector (SONY VPLX600E), situated outside of a magnetically-shielded room, onto a series of in-room mirrors, the last of which was suspended approximately 1 meter above the participant's face. The letters subtended 1.8 and 3 degrees of horizontal and vertical visual angle respectively.

Box 4: Task & Preprocessing

Task Subjects' responses were classified into four different categories: hits, false alarms, correct rejections and omissions. Only hits were considered for further analysis because we were interested in evaluating the functional connectivity patterns which support recognition success. The percentage of hits (80% control group and 84% MCI group) and correct rejections (92% control group and 89% MCI group) was high enough in both groups, indicating that participants actively engaged in the task.

Preprocessing Thereafter, single trial epochs were visually inspected by an experienced investigator, and epochs containing visible blinks, eye movements or muscular artifacts were excluded from further analysis. Thirty-five epochs corresponding to each subject were used in order to calculate the functional connectivity values (i.e., their synchronization likelihood). This lower bound was determined by the participant with the least epochs. To have an equal number of epochs across participants, thirty-five epochs were randomly chosen from each of the other participants. The effect of plasticity in the evaluation of network synchronization is not dealt with in this work, although it could be a subject of analysis in future ones.

Now, for each signal and each time n, the critical distance ε_n is determined for which $P_n^{\varepsilon}(x) = p_{ref}$, where $p_{ref} \ll 1$. We can determine for each discrete time pair (n,m) within our considered window $(w_1 < |n-m| < w_2)$ the number of channels $H_{n,m}$ where the embedded vectors $x_{k,n}$ and $x_{k,m}$ will be closer together than this critical distance $\varepsilon_{k,i}$:

$$H_{n,m} = \sum_{k=1}^{M} \theta\left(\varepsilon_{k,n} - |x_{k,n} - x_{k,m}|\right) \tag{4.2}$$

This number lies in a range between 0 and M, and reflects how many of the embedded signals "resemble" each other. We can now define a *synchronization likelihood* $SL_{n,m}(X)$ for each channel k and each discrete time pair (n,m) as:

$$SL_{n,m}(X) = \begin{cases} \dfrac{H_{n,m}-1}{M-1}, & \text{if } |x_n - x_m| < \varepsilon_n \\ 0, & \text{if } |x_n - x_m| \geq \varepsilon_n \end{cases} \tag{4.3}$$

By averaging over all m, we finally obtain the synchronization likelihood, $SL_n(X)$ who stands for :

$$SL_n(X) = \frac{1}{2(w_2 - w_1)} \sum_{\substack{m=1 \\ w_1 < |n-m| < w_2}}^{N} SL_{n,m}(X) \tag{4.4}$$

Synchronization likelihood $SL_n(X)$ describes how strongly channel x at time n is synchronized to all the other $M-1$ channels. The range of values of SL is $0 \leq SL \leq 1$, being (p_{ref}) when all M time series are uncorrelated, and 1 for maximal synchronization of all M time series. The value of p_{ref} can be set at an arbitrarily low level, and does not depend on the properties of the time series, nor it is influenced by the embedding parameters [A214]. The SL yields a symmetric and weighted correlation matrix w_{ij}, then we follow the normalization technique proposed in [A29] in order to avoid intrinsic differences from different individuals. The off-diagonal weights in the correlation matrices are rescaled to the interval $[0,1]$ by means of

$$SL_{ij} = \frac{w_{ij} - min(w_{ij})}{max(w_{ij}) - min(w_{ij})} \tag{4.5}$$

Figure 4.1 shows an example of a functional brain network obtained from the control group. The normalized weighted correlation matrix W_{ij} leads to a fully connected network (since all pair of nodes have a $SL > 0$), so only the 5% of the links with higher weights have been plotted to ease visualization of the network. The size of a node i is proportional to its strength $S(i)$, defined as the sum of the weights of all its connections. We can observe how the density of connections is higher at the peripheral regions and, specially, at the occipital lobe, while the central cortical region is sparsely connected (note that we are only considering the links with higher correlations). Interestingly, nodes with higher strengths, i.e., the network hubs, are mainly localized in the occipital lobe.

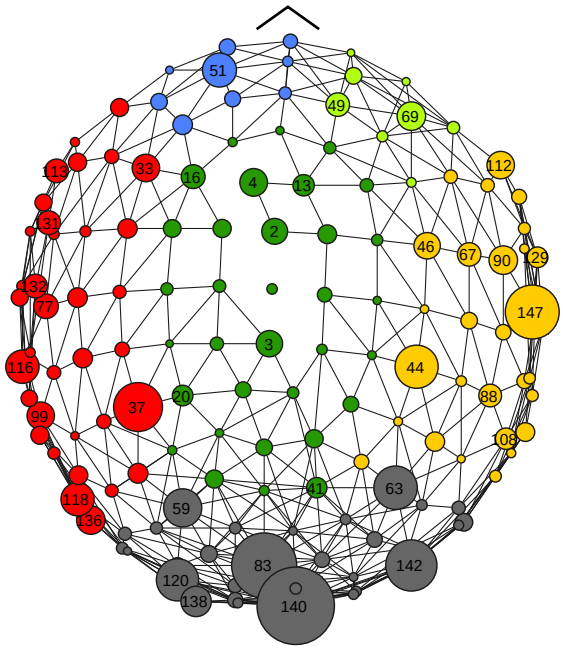

Figure 4.1: **Averaged functional network of the control group**. Only 5% of the links with higher weights have been plotted. Colors indicate the lobe that a node belongs to: frontal-left (blue), frontal-right (light green), central (dark green), temporal left (red), temporal-right (light orange) and occipital (dark grey). Node size is proportional to the node strength S(i). Note the higher density of connections at the occipital and frontal lobes. Node number is indicated for those nodes with higher strength.

4.3 Results

4.3.1 Measuring node centrality

The emergence and evolution of MCI has been studied extensively during the last years [A177], [A64], [A11], [A195], [A196], [A13] since it is known to be related to prodromal Alzheimer's disease (AD). Neuropathological studies indicate that MCI patients have clear pathophysiological characteristics, such as the presence of neurofibrillary tangles, loss of dendritic spines and the accumulation of beta-amyloid protein in the associative cortex [A142]. From the point of view of brain connectivity, MEG recordings of patients suffering from MCI revealed an enhancement of the synchronization between cortical regions when memory tasks were performed [A13]. The increase of the synchronized behaviour was accompanied with a change of the topological structure of the associated functional network, which turned into more random configurations [A30]. A reduction of the modular behaviour of the network together with an increase of the long-range functional

connections has also been associated with the appearance of MCI [A30].

Nevertheless, how functional hubs are affected by the disease is still unclear. It is known that network hubs are strongly affected by brain diseases like schizophrenia [A18] or Alzheimer's disease [A27], [A218], [A60]. This is bad news, since the targeted attack to leading nodes leads to a fast damage of the whole network properties [A6] and, eventually, to cascading failures [A156]. We used four different centrality measures from complex weighted-network theory to detect network hubs and to evaluate how their topological roles are affected by the disease.

The most straightforward centrality measure is the strength of nodes, $S(i)$. If a node has strong connections with its neighbors, it will have higher influence on the functional network, i.e. it will be more central. Figure 4.2A shows the strength $S(i)$ of both control and MCI groups, averaged over the whole groups. Network hubs can be easily identified as those with higher network strength, while the influence of the disease in the hubs is directly the difference of $S(i)$ between both groups. We can observe that the strength of the network hubs (highest peaks of the $S(i)$ distribution) is not specially altered, while from node 1 to 40 (localized at the central lobe) there is a significant increase of strength, although they are not hubs of the network. Therefore, node strength seems to indicate that MCI is not especially severe with the hubs.

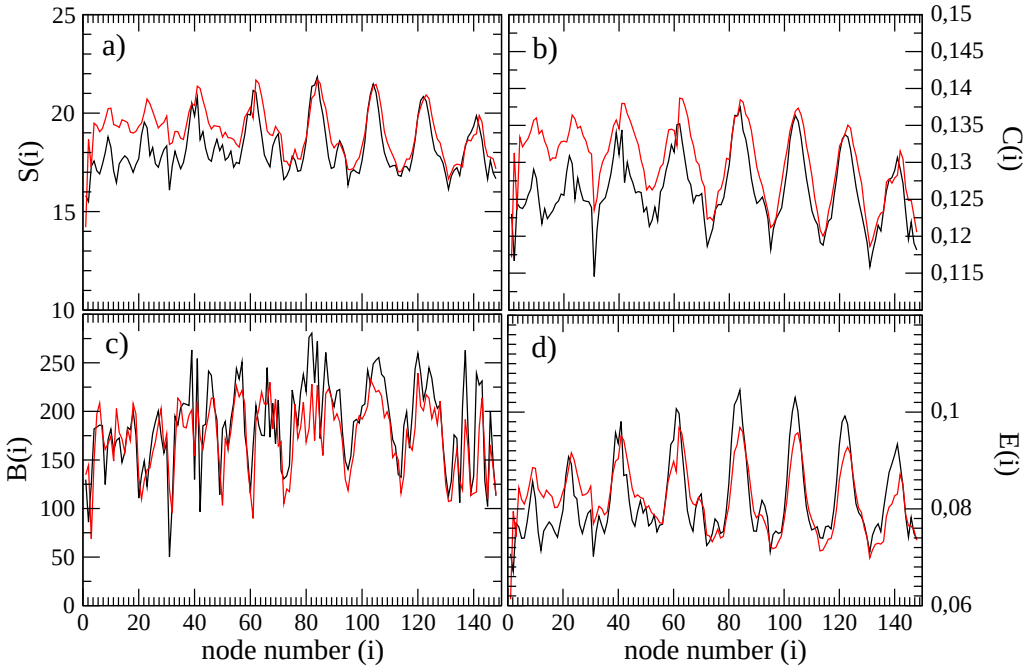

Figure 4.2: **Averaged centrality measures for the control (black) and MCI (red) groups**. Specifically, we calculate the node strength $S(i)$ (a), node closeness $C(i)$ (b), node betweenness $B(i)$ (c) and node eigenvector centrality $E(i)$ (d). All measures have been calculated and averaged over each epoch and for each subject of both groups. Note that $E(i)$ is the measure that better captures the differences between groups in those nodes with higher centrality. The periodicity reported in the four figures is only a consequence of the node numbering. See Fig. 4.1 for details on where relevant nodes are placed in the Euclidean space.

Nevertheless, as the strength $S(i)$ is a local measure, it does not account for correlations of link strength or specific structural distributions of the weights in the network. To overcome this issue, two measures of centrality have been applied, with the aim of including the influence of the network structure from a point of view of information transfer: the node closeness $C(i)$ and the node betweenness $B(i)$, which are measures based on the geodesic distance d_{ij} from node (i) to

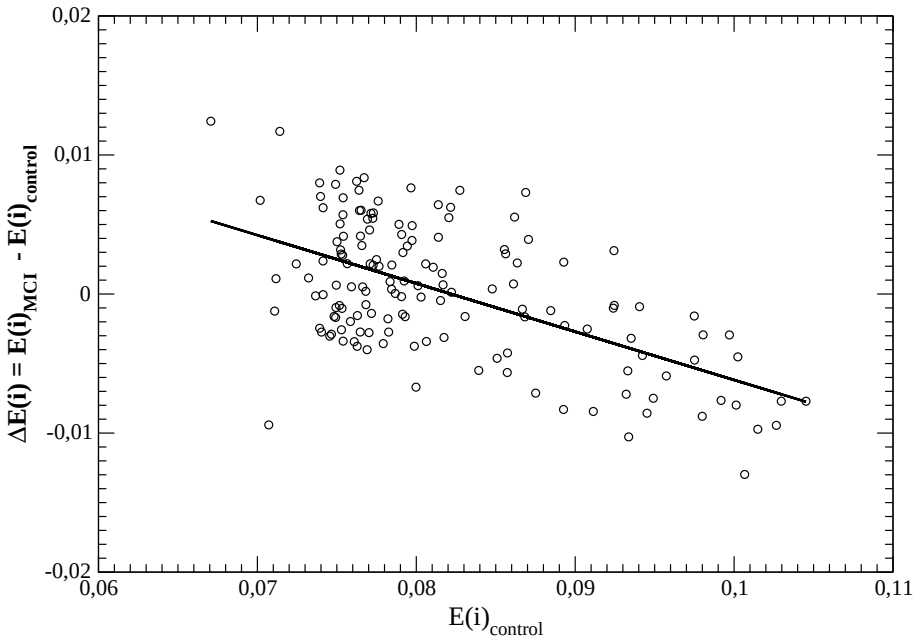

Figure 4.3: **Correlation between the eigenvector centrality $E(i)$ and its variation $\Delta E(i) = E(i)_{MCI} - E(i)_{control}$.** Note the negative correlation indicating that nodes with higher eigenvector centrality are those that are affected the most by the disease.

node (j). The former associates the importance of a node due to the lower values of the shortest paths a node i has. The more central a node is, the lower distances to other nodes in the network. Meanwhile, the later measures the ability of a node to act as transmitter of information through the network. $B(i)$, that was defined in previous chapters, accounts for the number of the shortest paths between every pair of nodes j and k that pass through node i, properly normalized by the total number of geodesic paths g_{jk} from j to k.

In Fig. 4.2B-C we plot the average values of $C(i)$ and $B(i)$ for control and MCI groups. While both measures have their proper characteristics, a common behavior appears in the high correlation present among the centralities of control and MCI for all nodes. The position of the network hubs perfectly matches when comparing the local measure of centrality $S(i)$ with $C(i)$, while $B(i)$ seems to suggest the existence of hubs but with a more noisy distribution. Interestingly, the highest peaks reported in the three distributions correspond to nodes placed at the occipital lobe (see node number in Fig. 4.2). Again, there are no significant differences in the centrality of the network hubs, and the most clear signature of MCI is an increase of centrality in the nodes belonging to the central lobe (from 1 to 40). This alteration is not captured by $B(i)$, thus indicating that it is not the most suitable measure to evaluate changes in network centrality.

It is worth noting that although $C(i)$ and $B(i)$ contain information about how weights are distributed within the network, they only refer to shortest paths distribution and disregard other structural properties of the network. To surpass this issue, we compute the eigenvector centrality $E(i)$ of the nodes. Note that any modification of the weight of the links, will result in a change of the matrix $\mathbf{W}$ and, therefore, will be reflected in the value of the eigenvector centrality $E(i)$. On the contrary, if an alteration of a link does not imply any modification in the distribution of shortest paths, it will not be captured by $C(i)$ or $B(i)$ centralities.

Figure 4.2D shows the eigenvector centrality $E(i)$ for both groups. It detects the position of the network hubs which, as in $S(i)$ and $C(i)$, are mainly placed at the occipital lobe. Interestingly, this measure captures a clear decay in the centrality of the hubs, as indicated by the decrease of the peaks height. The consequence of this decrease is a network were the hubs play a less relevant

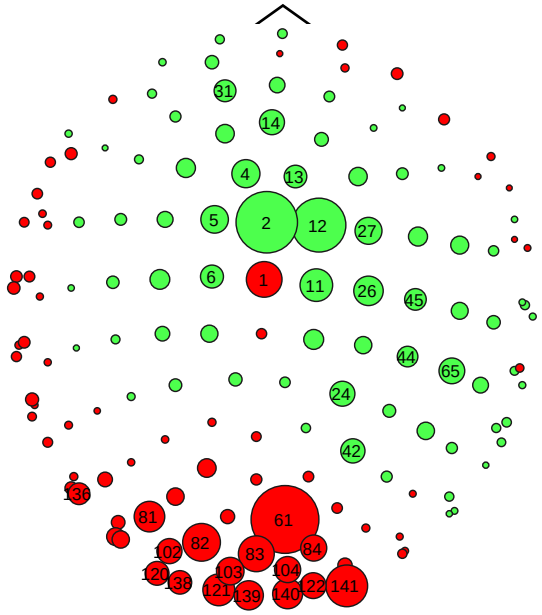

Figure 4.4: **Distribution of the variation of eigenvector centrality** $E(i)$. The size of the nodes is proportional to $|\Delta E(i)| = |E(i)_{MCI} - E(i)_{control}|$, while node color indicates an increase (green) or decrease (red) in the node centrality. Node number is indicated for those nodes with high $|\Delta E(i)|$.

role. In Fig. 4.3 we plot how the variation of the eigenvector centrality $\Delta E(i)$ due to MCI is related with the centrality of the control nodes. We can observe a negative correlation, indicating that those nodes with higher centrality are, in turn, the nodes that decrease its importance the most. It is also interesting to see what is the position of the nodes in the whole network. Figure 4.4 shows the increase (green) and decrease (red) of eigenvector centrality with the node size proportional to the value of $|\Delta E(i)|$. It is the occipital lobe the one that is mostly affected by the decrease of centrality, while the central lobe takes advantage of this reduction.

4.4 Discussion

The analysis of functional and anatomical brain networks using complex networks analysis have revealed interesting information about how these networks are organized [A30]. All studies agree on the fact that brain networks are highly heterogeneous, giving rise to the existence of hubs, i.e. leading nodes from the point of view of dynamics of the networks. We have shown a detailed analysis of how the importance of network hubs in a functional network associated with the execution of a memory task is affected by the emergence of MCI. We report how the disease particularly affects network hubs, reducing their importance in the network. This reduction is captured by all different measures of centrality, independently of whether they rely on the local or global properties of the network.

Among all centrality measures, eigenvector centrality $E(i)$ is the one that better captures the effect of the disease on the network hubs. The occipital region, containing the majority of the hubs in the case of healthy individuals, is the region where centrality decreased the most, while nodes belonging to the central lobe benefit from the hub deterioration. Interestingly, anatomical networks of patients suffering from schizophrenia also show a reduction of the hub importance, together with a dispersion in the location of network hubs [A18]. This reduction of hub centrality can be used as a signature of the existence of pathology since it is known that the hub structure is quite stable in healthy adult individuals [A114], [A271]. In addition, it reinforces the hypothesis that MCI

increases the randomness and homogeneity of the functional networks [A29], since the reduction of hubs importance leads to more homogeneous networks

The implications of hub deterioration are still unclear. For example, in Alzheimer's disease, it has been shown that amyloid-beta deposition in the locations of cortical hubs could act critically in the severity of the disease [A27]. In the case of anatomical networks in schizophrenia, the reduction of centrality of the frontal hubs has been related to the disorganization of the anatomical network. The reduction in hub centrality in posterior scalp regions could be related to the high levels of beta amyloid accumulation in those regions found in MCI and Alzheimer's disease. Conversely, the increased hub centrality found for anterior sensors could reflect enhanced engagement of frontal regions compensating for decreased capacity to tackle the demands of the memory task (see [A13] for a similar interpretation). We believe that our work will shed some light on the role played by hubs in brain networks, which may have strong influence on the network robustness [A6], cascading processes [A156] and network controllability [A228]. Similar studies could be carried out in other neurodegenerative diseases where the existence of functional hubs has been reported.

In summary, this first study focuses all attention in the dynamics of the brain, specifically when the brain can be viewed as a single large scale network. Nonetheless, the brain has evolved to be anatomically and functionally differentiated in two hemispheres. Thus a remarkable exploration of the brain must attest this fact, that is, given that we have two hemispheres we can assume each as different networks. The coming chapter attempts to unveil the dynamics of the brain network when it is viewed as a composite system of two networks, one for each hemisphere.

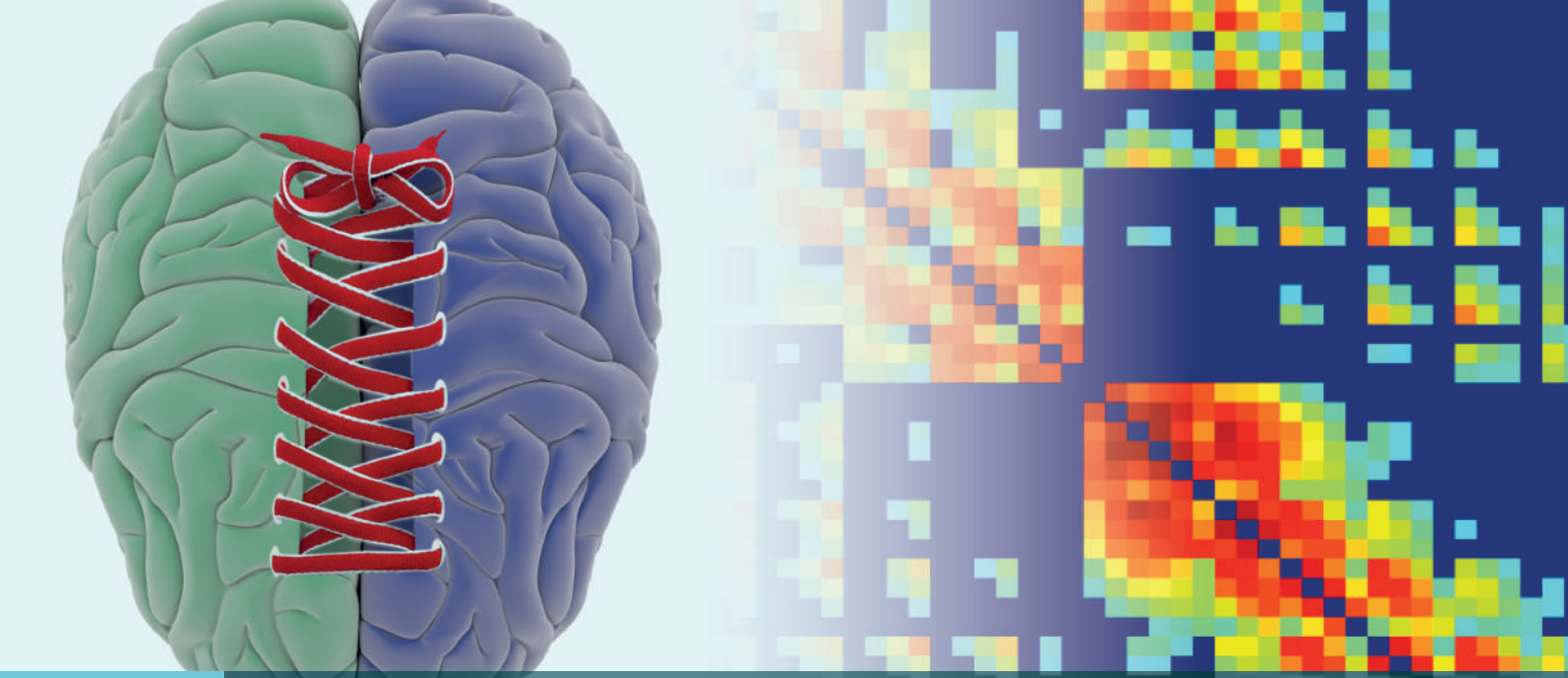

5 Hemispherical Balance

§

Network theory has been recently adapted to study the physiopathology of the human brain, which can be modelled as a graph where nodes represent different regions and links stand for statistical interaction between their activity as recorded by current neuroimaging techniques [A31], [A209], [A212]. Nevertheless, brain functioning, and any functional or anatomical network extracted from it, relies on a combination of a segregated and integrated activity, the former leading to the existence of modules, or sub-networks, and the latter to the existence of a *network-of-networks* (*NoN*) coordinating the activity of all its underlying components. For this reason, a careful study of the brain at the resting state condition would benefit from an inspection of how functional sub-networks interact between them. In this Chapter, we describe the brain as a system composed of two interacting networks, the left (L) and right (R) hemispheres, which struggle each other in order to remain central (i.e., important) in a functional NoN. In this way, we investigate how the fact that both hemispheres are interacting between them influences the distribution of centrality along the whole NoN. We will see how the distribution of centrality, not only between hemispheres, but also at the node level, strongly depends on the number of functional connections between hemispheres and the way these connections are distributed.

With this aim, we carried out a series of experiments recording brain signals from the scalp of 54 healthy adults in open/closed eyes conditions (EO and EC, respectively) by means of an electroencephalograph (EEG). Next, we used the noise-reduction imaginary coherence for evaluating the correlation between the recorded cortical activations for the classical $\theta(4-7Hz)$, $\alpha(8-13Hz)$, $\beta(14-29Hz)$ and $\gamma(30-40Hz)$ frequency bands. For each individual, we obtained two functional networks, one accounting for the 24 cortical regions of the left hemisphere, and the other with the other 24 regions of the right hemisphere. Both networks are composed of intra-links, accounting for the statistical correlations between regional activities within each hemisphere and inter-links, measuring the coordinated activity between nodes belonging to different hemispheres.

§This chapter is based on the unpublished work entitled: ***Connector Links Support Functional Centrality Distribution in Brain Hemispheres***. *A collaborative work from my academic stay in Paris in the group of Dr. M. Chavez*

Once the NoN and its sub-networks (i.e., hemispheres) were defined, we quantified the centrality of the nodes inside each hemisphere and studied what rules constrain the distribution of centrality among the whole functional NoN. By means of numerical simulations, we studied of how the distribution of inter-links promotes (or hinders) the leading role of an hemisphere over the other, by comparing the actual distribution of inter-links with the best/worst cases for each of the hemispheres. These simulations are based on identifying the strategies of the different rewiring processes of inter-hemispherical links that lead to the highest amount of centrality for each hemisphere. In this way, it is possible to define a competition parameter indicating how close the actual inter-hemispheric connections are from the optimal configuration of any of the hemispheres. Under this framework, variations of the hemispherical centralities and the competition parameter for both conditions (EO and EC) were obtained in all bands. Finally, we investigated the robustness of functional NoNs when facing node failures and discovered how, depending on the number of inter-hemispherical links, the hemispherical robustness could be highly sensitive to failures, in contrast to other network metrics such as the clustering or the average shortest path.

5.1 Introduction

The fact that brain networks are spatially embedded, i.e. each node of the network has a precise spatial position, results on a useful information that it is not always accessible in many kinds of real networks. In turn, closeness between nodes distributed along a spatial network leads in many cases to the formation of clusters, which rely on the spatial constrains of the network. This is, somehow, the case of the human brain, which consists of two large modules (i.e., the hemispheres), exhibiting different but complementary functions [A266], [A249].

An adequate interplay between both hemispheres is necessary for the correct functioning of the brain, and the way hemispheres interact can be roughly classified into two categories: (i) competition and (ii) cooperation [A76]. The role of these categories during cognitive control[1] has been widely investigated by means of fMRI data, showing that both cooperation and competition arise in the dynamics of the hemispherical interactions [A46] .

Notwithstanding, the competition/cooperation of hemispheres during the development of different cognitive tasks requiere to achieve high temporal resolutions, something difficult to reach using merely fMRI techniques. This fact motivates the use of EEG/MEG measurements, with a much higher temporal resolution, with the aim of obtaining more precise information on the different oscillatory behaviors of functional brain networks. In this way, and with the objective of better understanding the role of the functional interaction between the brain hemispheres, we are going to adopt a EEG-based network approach. The analysis of these functional networks, will allow us to evaluate to what extent hemispheres are engaged in a competitive behaviour in terms of nodal centrality, or whether they are in a functional trade-off demeanour, i.e., how the importance of each hemisphere relies on the connections between them. Specifically, we will focus our study on the case of the resting state of healthy individuals, in order to obtain a baseline of inter-hemispherical interactions, which could be used for further studies on how these interactions are modified during a cognitive task or due to the emergence of a certain impairment.

As we have explained in the previous Chapter, *eigenvector centrality* has been shown as an adequate indicator of the importance that a node plays in the topology of a brain network [A158]. One of the advantages of this measure of importance is that, once the functional network has been obtained, it can be easily calculated with the eigenvector associated to the largest eigenvalue of the (weighted) adjacency matrix of the network [B16]. In this way, we were able to measure the eigenvector centrality of the nodes belonging to the whole functional network, and quantify the centrality accumulated by each of the hemispheres as the sum of the centralities of their constituent

[1] Cognitive control associates the ability of adaptation regarding specific tasks.

nodes [A4]. Next, we analyzed how the centrality has been distributed between the hemispheres and how the inter-hemispherical links influence this distribution. Furthermore, we traced the differences between hemispherical centralities and evaluated the competition between brain hemispheres at the different frequency bands.

Our results show that, even at resting state, hemispheres are characterized by dynamical asymmetry, and by different connection patterns. Finally, we carried out a detailed study about the hemispheric robustness against failures of the individual nodes. Our analysis reveals how the centrality distribution is extremely sensitive to the failure of single nodes, while other parameters of the network topology such as the clustering and shortest path remain almost unaffected. These results open the way to a new characterization of the interactions between the two hemispheres that can be used to better understand organizational mechanisms in healthy and disease brain networks, specially when the role of the leading brain regions (i.e., hubs) is investigated.

5.2 Matherials and Methods

5.2.1 Experimental Setup

The database consists of $S = 54$ healthy subjects recorded in two different baseline conditions, i.e. 1-minute eyes opened (EO) and 1-minute eyes closed (EC), both at resting state. In each condition, subjects were comfortably seated on a reclining chair in a dimly lit room. During EO they were asked to avoid ocular blinks in order to reduce signal contamination. The EEG data were recorded on a commercial system (Brainproduct GmbH, Munich, Germany) with a sampling rate of 200 Hz. All the EEG signals were referenced to the mean signal gathered from electrodes on the ear lobes. Data were subsequently down-sampled to 100 Hz after applying a proper anti-aliasing low-pass filter to restrict the available frequency range up to 50 Hz. The electrode positions on the scalp followed the standard 10-10 montage [C6]. 5 electrodes are excluded and only 56 electrodes are retained for the subsequent analysis. From the previous, 8 electrodes associated to the sagittal plane were removed so as to differentiate between the two hemispheres. This way, the final amount of nodes used in this study was 48, 24 electrodes per hemisphere.

5.2.2 Imaginary Coherence

EEG signals come from tangential and radial oriented cortical sources respect to the scalp surfaces, but many different electric conductivities, i.e., skull, hair, skin, can influence the measurement of these sources, blurring the real EEG acquired data. This fact hinders the localization of the brain regions that are the real sources, leading to spurious links due to the volume conduction effects. To overcome this issue, the imaginary coherence ($iCoh_{i,j}(f)$) has been proposed as a satisfying method to assess brain connectivity based on the frequencies of the brain signals [A165]. This measure of functional connectivity has been proved to be effective to avoid the field spread and cross-talk residual effects in EEG data [A81], [A56]. Given two zero-mean time series x(t) and y(t) for channels X and Y respectively and their (complex) Fourier transforms $S_x(t,f)$ and $S_y(t,f)$ as defined in [A165]. Then we obtain the cross spectrum as $S_{X,Y}(t,f) = \langle S_X(t,f) \cdot S_Y^*(t,f) \rangle$, where $\langle \cdot \rangle$ is the expectation operator. Finally, the imaginary coherence $iCoh_{X,Y}(f)$ is defined as the imaginary part of the normalized cross spectrum:

$$iCoh_{X,Y}(f) = Im\{\frac{S_{X,Y}(f)}{\sqrt{S_{X,X}(f) \cdot S_{Y,Y}(f)}}\} \tag{5.1}$$

5.2.3 Functional Network Construction: Hemispheres and Interlinks

The imaginary coherence gives us a value that can be used as a *weight of communication* between two brain sites. In this way, we use the imaginary coherence to obtain a $N \times N$ bidirectional matrix

(with $N = 48$), which can be interpreted as a weighted adjacency matrix. Note that the matrix is symmetric and, in principle, all values are different from zero, i.e., we have a *fully connected network*. Initially, we are going to use the fully connected networks to maintain as many information as possible, which is contained in the weight of the links. Networks associated to each individual contain at the same time the information about two sub-networks L and R, corresponding to the left and right hemispheres, respectively. Each of these two sub-networks has $N_L = N_R = 24$ nodes. Finally, we define the matrix P as the inter-hemispherical block matrix containing only the interlinks that connect both hemispheres. In this way, the structure of the whole brain network-of-networks is defined by a supra connectivity matrix T:

$$T = \begin{pmatrix} L & P \\ P^\top & R \end{pmatrix} \tag{5.2}$$

Note that, T, L and R are intrinsically symmetric, meanwhile P is non-symmetrical. Also note that in the supra connectivity matrix, nodes numbered from $i = 1$ to $i = N_L$ belong to the left hemisphere, while nodes from $i = N_L + 1$ to $i = N_L + N_R$ belong to the right one. This way $N_T = N_L + N_R$.

5.2.4 Evaluating the node and hemisphere centrality

Following the methodology of [A4], the centrality accumulated by the L and R hemispheres, C_L and C_R, respectively, is obtained as the sum of the centrality of the nodes belonging to each hemisphere, i.e, $C_L = \frac{\sum_{i=1}^{N_L} u_T(i)}{\sum_{i=1}^{N_T} u_T(i)}$ and $C_R = \frac{\sum_{i=N_L+1}^{N_L+N_R} u_T(i)}{\sum_{i=1}^{N_T} u_T(i)}$, with u_T being the eigenvector centrality over the whole network. With such a normalization, the global centrality of T is shared between both hemispheres following the equation $C_L + C_R = 1$. Intra-hemispherical eigenvector centralities $u_{L,R}(i)$ of the non-connected hemispheres can also be calculated treating both sub-networks as if they were isolated from each other. In this way, we can also categorize the importance of cortical regions (i.e., nodes) inside their own hemisphere (i.e., sub-network). From now on, we will call *hubs* those nodes with the highest intra-hemisphere centrality, while those nodes with lower centrality will be designed as *peripheral* nodes.

We are going to investigate how the connections between hemispheres have been carried out and what is their influence on the distribution of centrality along the whole functional network. Furthermore, we will evaluate how the centrality would have been redistributed if different connections between hemispheres would have been created. By inspecting the consequences of the rewiring of the matrix P, we can gather the best strategies to optimize (maximize or minimize) the hemispherical centrality of a specific hemisphere and, in turn, evaluate how far the actual distribution is from any of the optimal cases.

The rewiring of P is based on a deterministic search of the inter hemispherical links p_{ij} that promotes the acquisition of centrality by one of the sub-networks forming a NoN, as explained in [A4]. If we compute the largest eigenvalue λ_1 of the connectivity matrices of two isolated networks (e.g., L and R), once we connect them, the network with higher λ_1 (suppose the dominant network is L) will be the one retaining more centrality (i.e., $C_L > C_R$). Nevertheless, there are two fundamental rules that can enhance/decrease the amount of centrality accumulated by a sub-network if the adequate connector nodes are selected (see box 5) [A4].

Box 5: Rules to enhance/decrease the accumulated centrality

Rules to enhance/decrease the centrality accumulated by a sub-network based on the adequate connector nodes:

1. The hemisphere that, in isolation, has a higher λ_1 will accumulate more centrality if the connection with the other network is carried out through the peripheral nodes.
2. The network with lower λ_1 benefits from connecting to the other network through the hubs, acquiring the highest possible centrality in this case (when compared with any other configuration).

A detailed demonstration of the above rules, both with theoretical and real applications, can be found in [A4].

Using these rules we analyzed the effects that the rewiring of P may have in the centrality accumulated by each hemisphere. The rewiring process is focused on obtaining the highest possible centrality of a given hemisphere, let us say L in this example (the same procedure is followed for R). With this aim, we remove all connector links from the matrix P and re-introduce them again starting with the one with the highest weight p_{ij}^{max} and finishing with the one with the lowest p_{ij}^{min}. The position of the weight p_{ij}^{max} will be the one that leads to the highest centrality of L. Once all positions of the matrix P have been inspected and the one leading to the highest C_L identified, we leave the weight p_{ij}^{max} in that position and repeat the procedure with the link with the second highest value of p_{ij}. Once all weights of matrix P have been relocated, we call C_{max}^L the value of the centrality accumulated in the L hemisphere, and conversely C_{min}^R the one accumulated by the R hemisphere, since $C_R = 1 - C_L$.

When the configuration of the inter-links associated to the highest and lowest centralities of the two hemispheres has been identified, we can define a competition parameter Ω that evaluates how the actual distribution of centrality is from the optimal cases of both hemispheres (see box 6).

Box 6: The competition parameter Ω

The Ω parameter, which depends on C^L, C_{max}^L, C_{min}^L, is given by $\Omega_L = \frac{2(C^L - C_{min}^L)}{C_{max}^L - C_{min}^L} - 1$. Note that Ω_L is normalized such as $-1 \leq \Omega_L \leq 1$. Values close to 1 (-1) indicate that the real distribution of centrality C^L ($C^R = 1 - C^L$) is close to the best case for the left (right) hemisphere. Importantly, values of Ω close to zero reveal that none of the hemispheres is optimally connected in terms of centrality distribution, indicating that the hemispheres are in a sort of functional balance.

5.2.5 Robustness against node failure

Our next objective is to evaluate the robustness of the hemisphere centrality when one of its nodes fails. We define the *hemispherical local impact* $l_{imp}^{L,R}$, which accounts for the loss of centrality that a hemisphere suffers when one of its nodes is removed from the functional network, calculated (in the left hemisphere) as

$$l_{imp}^{L}(i) = \left(\frac{C_*^L(i) - C^L}{C^L}\right) * 100\% \tag{5.3}$$

where i is the node that has been removed, and C^L and $C_*^L(i)$ are the centralities accumulated by the left hemisphere before and after the removal. The local impact in the right hemisphere would be obtained in the same way, just replacing L by R. It is also important to relate the local impact of a node with its centrality, since we can expect higher impacts when failures occur in the hemispherical

hubs. We define the local importance of a node as

$$lc^L(i) = \frac{u_T(i)}{\sum_i^{N_L} u_T(i)} * 100\% \tag{5.4}$$

which indicates the percentage of the hemispherical centrality that is captured by node i. The interplay between the local impact and the local importance will be crucial to evaluate the robustness of the functional network under node failure.

5.2.6 Thresholding the functional network

We will initially work with fully connected networks, i.e., all links will have a certain weight. Nevertheless, when analyzing functional networks it is common to remove those links whose weight adds spurious information about the coordination between brain sites. What links to remove or, more specifically, where to put a threshold to the links' weights is an unsolved problem [B4], [A262]. Here we will adopt one of the most extended solutions, which consists on removing all possible links, starting with those with the lowest weight, until the network is broken, and set the threshold at the value that guarantees the existence of a unique connected component.

When anayzing the impact of inter-hemispherical links, we will use this procedure to each of the hemispheres in isolation and, next, treat the removal/addition of the inter-hemispherical links as an independent problem.

5.3 Results

5.3.1 Node centrallity

The centrality accumulated by each of the brain hemispheres is just a consequence of the centrality accumulated by the nodes belonging to that hemisphere. Therefore, a preliminar step is to obtain the centrality of all nodes of the network in order to detect how it is distributed, what are its bounds and how it depends on both the experimental conditions (i.e., EO and EC) and the hemisphere the nodes belong to. Importantly, we have to distinguish between the centrality that a node has over the whole functional network-of-networks and the centrality at its hemisphere (i.e., within each sub-network). The former, the global centrality u_T, is obtained from the eigenvector associated to the largest eigenvalue of the matrix T, which is related to the full functional network. The latter, the local one $u_{L,R}$, is calculated from the eigenvectors associated to the largest eigenvalues of L and R when both hemispheres are in isolation. Note, that it would be reasonable to expect that the hubs of each hemispheres would also be the hubs of the full network, although this is not a necessary condition. Figure 5.1 shows the interplay between both centrality measures for each hemisphere and condition. We can observe how, as expected, all plots reveal a positive correlation between the global centrality u_T and the local centrality $u_{L,R}$, which holds for any frequency band.

These results indicate that the centrality of the nodes does not change significantly when hemispheres are connected/disconnected. Thus, it suggests that the functional inter-connections do not promote the scape of centrality from one hemisphere to the other, being both hemispheres in a kind of functional balance.

5.3.2 Evaluating the centrality distribution between hemispheres

We are going to further investigate the competition for centrality from the point of view of the hemispheres (and not their nodes) in the two aforementioned conditions, eyes closed (EC) and eyes opened (EO), and four frequency bands: θ, α, β, γ. First, we calculate how the centrality of the whole network-of-networks is distributed along the two hemispheres. For simplicity, we chose the left hemisphere as the reference and we compute the difference of hemispherical centrality ($C_L - C_R$) in both conditions, for each subject. In this way, we obtain the hemispherical centrality of

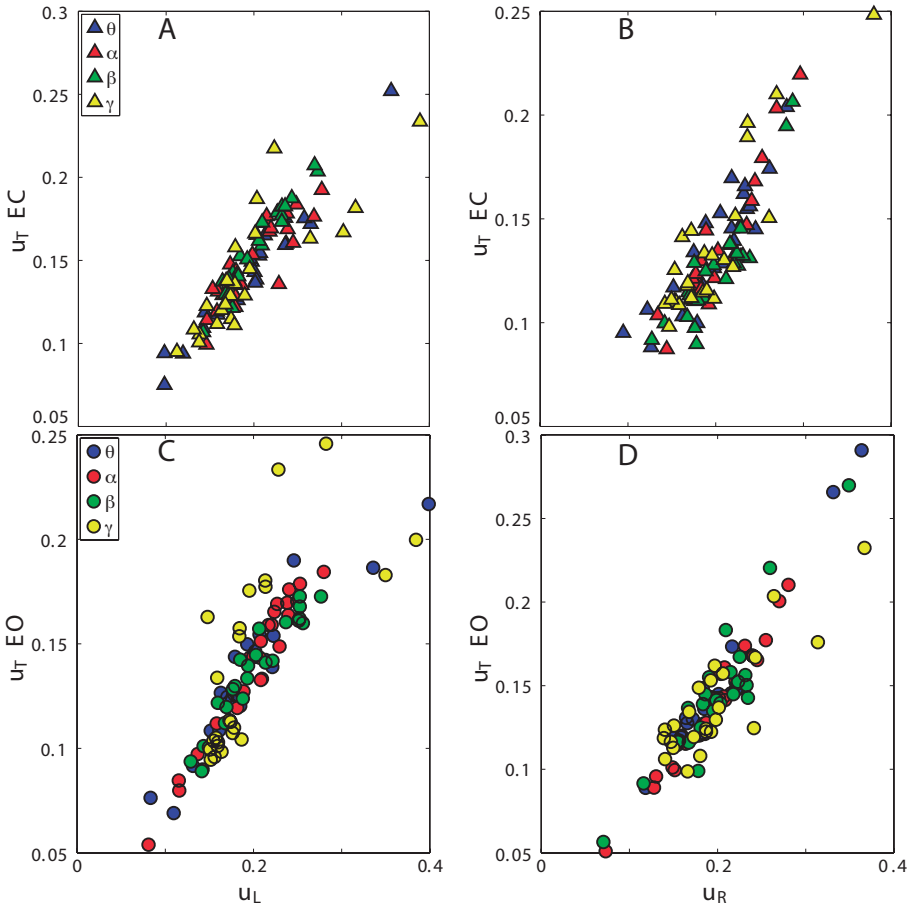

Figure 5.1: **Correlation between the global and local centrality of the nodes in EC and EO conditions.** Global centrality u_T is obtained from the complete matrix T, when both hemispheres are connected (vertical axes); while local centrality $u_{L,R}$ is extracted from the hemisphere matrices L and R when hemispheres are isolated (horizontal axes). Upper panel sows the EC condition for the left (**A**), and right (**B**) hemispheres. Bottom panel: the same as the upper panel but in the EO condition.

each of the 54 subjects and, then, average over the whole group in each condition. Results show that the centrality accumulated by both hemispheres is very similar. In Fig. 5.2 **A** we can observe how the difference of centrality is, in all cases, close to zero, indicating a situation close to a balance in the distribution of centrality between both hemispheres.

Nevertheless, the results of Fig. 5.2**A**, which are summarized in Tab. 5.1, also show slight differences in the hemispherical importance when both the EC and EO conditions are compared. We observe a higher concentration of centrality in the left hemisphere during the EC condition, for all bands, as indicated by values higher than zero. In contrast, a certain amount of centrality is transferred to the right hemisphere when individuals open their eyes (see 5.2**A** and second column of Tab. 5.1).

For all frequency bands, the difference of centralities between hemispheres are closer to zero in the EO condition, which indicates a more balanced situation (i.e., $C_L - C_R = 0$ would reflect an equal distribution of centrality), at least under the scope of the importance and hemisphere plays in the topology of the whole functional network-of-networks.

These results reveal a situation close to a balance in the EO condition, that shifts to benefit one of the hemispheres when eyes are closed. This latter fact, raises the question of what is the role of

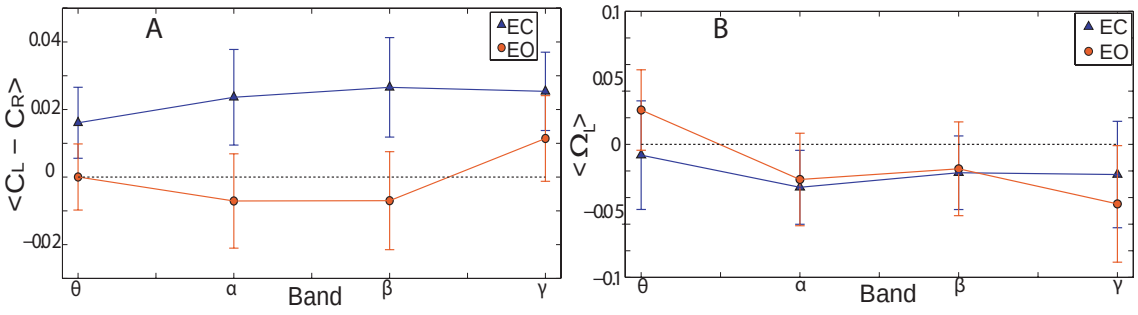

Figure 5.2: **Differences of centralities and Competition Parameter for left hemisphere**. EC conditions (triangles) and EO (circles) and four frequency bands: θ, α, β, γ. **A**. Average difference of the hemispherical centralities ($C_L - C_R$) along 54 subjects. **B**. Average of the Competition Parameter Ω_L for all subjects. In both plots, error bars are the standard deviation of the mean.

	$\langle \mathbf{C_L} - \mathbf{C_R} \rangle$		$\langle \Omega_L \rangle$	
Band	EC	EO	EC	EO
θ	0.016	0.0	−0.008	0.025
α	0.023	−0.007	−0.032	−0.026
β	0.026	−0.007	−0.021	−0.018
γ	0.025	0.011	−0.022	−0.044

Table 5.1: **Mean hemispherical centralities and competition parameter** Ω_L. Results of hemispherical differences between C^L and C^R and the competition parameter Ω_L for average of the 54 individuals in both conditions. Summary of the data shown in Figs. 5.2 and 5.3

the inter-hemispherical links, whether they are enhancing the centrality of one of the hemispheres or, on the contrary, if they are promoting a balance. To clarify this issue, we compute the competition parameter Ω_L which is an indicator of how the inter-hemispherical links favour one or the other hemisphere.

In order to calculate Ω_L we first need to obtain the highest/lowest possible centrality of each hemisphere according to the rewiring of the inter-hemispherical connections. In this context, the rewiring implies reconnecting all elements within the inter-hemispherical matrix P. Note that these rewirings are unreal, but they are necessary to asses whether the actual distribution of inter-links is close to the optimal or worst case situation for each hemisphere. In this way, we obtain a value of Ω_L for each individual and condition, and then average them to have a value for the overall population. Figure 5.3 shows an example of how the distribution of the inter-hemispherical links benefits/hinders the centrality captured by one of the hemispheres, in this case for the α band of an average brain network.

In Fig. 5.3 we have followed the rules explained in Box 5 about the role of the connector nodes of each hemisphere, which lead to the best/worst solutions. Specifically, we show the configuration for the inter-hemispherical links for three different cases: the highest centrality of L (Fig. 5.3A), the actual distribution of centrality (Fig. 5.3B) and the highest centrality of R (Fig. 5.3B). According to these values we obtain $\Omega_L = -0.006$, which revels that, for the example shown in Fig. 5.3, the actual distribution of inter-links promotes the balance of centrality between both hemispheres.

When $\langle \Omega_L \rangle$ is computed (as the average of the whole group) we obtain values very close to zero in all frequency bands and for both conditions (see Fig. 5.2B). Interestingly, α, β and γ bands have a $\langle \Omega_L \rangle$ that is slightly negative. Since the competition parameter is defined with regard

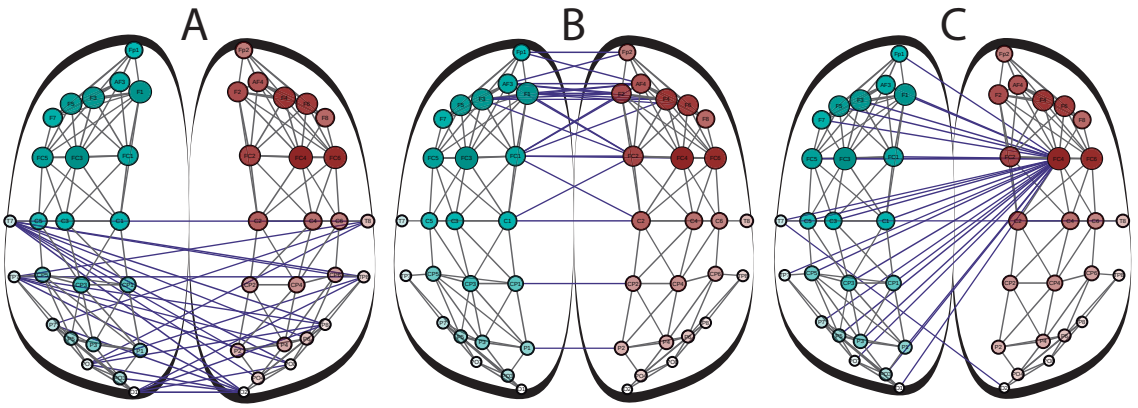

Figure 5.3: **Reshuffling the inter-hemispherical links**. Example of three different configurations of the inter-hemispherical links. Intra-hemispherical connections are colored in grey, while blue is used for the inter-hemispherical links. Nodes' sizes are proportional to their local eigenvector centrality before connecting both hemispheres. For visualization purposes, these networks have an arbitrary threshold that maintains the 16% of the links with the highest weight. Data is obtained from the α band of an average subject. In this example, **A**: Peripheral nodes are connected, resulting in the left hemisphere's optimal strategy for increasing its centrality (leading to $C^L_{max} \approx 0.7$); **B**: Actual distribution of inter-hemispherical connections, which leads to a balance of the centrality distribution as indicated by $C^L = 0.49$; **C**: Right hemisphere's optimal strategy is obtained through the connection of the hubs ($C^R_{max} \approx 0.8$). The competition parameter in the original configuration is $\Omega_L = -0.006$, indicating a balance between the optimal strategies of both hemispheres.

to the left hemisphere, the negative value of $\langle \Omega_L \rangle$ is a consequence of an inter-hemispheric link distribution that slightly benefits the right hemisphere. This behaviour is reported in both the EC and EO conditions (see also fourth column of Tab. 5.1).

From all above, it seems that there are no major distinctions between the centrality of brain hemispheres, despite the distribution of links slightly benefits the right hemisphere. This fact would indicate that hemispheres are close to a balance or a trade-off situation, at least with regard to the centrality distribution. Nevertheless, it is crucial to investigate to what extent this balance is a consequence of the particular topology of the network. Is the type of network topology responsible of this equal partition of the network centrality between hemispheres? And, furthermore, what is the role played by the inter-hemispherical links?

5.3.3 Inter-hemispherical links and the competition for centrality

In this section we are going to investigate how the number of inter-hemispherical links may be fundamental to the distribution of centrality between hemispheres, showing two clear regions that could be related to a "competition" and "cooperation" scenarios. Importantly, the results shown in the previous sections have been obtained, in all cases, when the analysis is carried out maintaining all weights of the links in the connection matrix. As a consequence, we have been working with fully connected matrices, despite the great part of the links have weights that are close to zero. However, as we have mentioned in the introductory Chapters, functional networks are ussally thresholded, maintaining only those links that are relevant for the topology of the functional networks, and, in the majority of cases, analyzing binary matrices [C3].

For this reason, we are going to introduce a threshold at both the matrices L and R and also at the network-of-networks T. The procedure is the following. First we are going the keep, for each hemisphere L and R, those links with higher weights that maintain each hemisphere as a connected component (i.e., without any isolated node). Note that following this procedure both hemispheres

may have different thresholds. Nevertheless, we select the lowest threshold of the two hemispheres in order to guarantee that none of them is favored among the other. We repeat this procedure for each functional network of each individual.

	Left-dominant population (%)			
Condition	θ	α	β	γ
EC	59.2	57.4	55.5	53.7
EO	37.0	50.0	50.0	55.0

Table 5.2: **Percentage of left-dominant individuals within the group of study**. The hemisphere dominance is defined according to the largest eigenvalue λ_1 of the hemispherical connectivity matrices: the hemisphere with the highest λ_1 is the one that dominates over the other (see Ref. [A4] for details).

Next, we compute the largest eigenvalue λ_1 of L and R and call the “strong" (“weak") hemisphere that with the highest (lowest) value of λ_1 (see a detailed explanation in Ref [A4]). We distinguish between groups of people that are *left-dominant* when the eigenvalue λ_1 of L is higher than the eigenvalue λ_1 of R, otherwise they are *right-dominant*. See table Tab. 5.2 summarizing the percentage of each kind of dominance according to the condition and frequency band.

Once the matrices of both hemispheres have been analyzed in isolation, we study the influence of adding the inter-hemispherical links. We take the matrix T and empty the inter-hemispherical block matrix P. Next, we introduce the inter-hemispherical link with the highest weight, compute the new value of the centrality distribution (i.e., C_L and C_R) and repeat the process until all inter-hemispherical links have been re-introduced. We repeat this procedure for each of the frequency bands of the 54 subjects, and for both the EC and EO conditions.

Figure 5.4 shows the evolution of C_L (note that $C_R = 1 - C_L$) with the addition of the inter-hemispherical links, distinguishing between left- and right- dominant individuals. We also obtain the values of $\langle C_L \rangle$ as the average of the centralities of L along all subjects, which are grouped according to the dominant hemisphere (see. Fig. 5.4). Interestingly, the inclusion of inter-hemispherical links shows a clear tendency in the hemispherical centrality: the hemisphere that has the “strong" position (i.e., it has a higher λ_1) accumulates a high amount of centrality when the number of inter-hemispherical links is low, but its centrality diminishes as the number of interlinks is increased. “Weak" hemispheres behave just in the opposite way.

Figure 5.4 evidences a crucial dependency of the hemispherical centrality on the amount of links that coordinate the activity between them, leading to two well-defined regions: (1) a region where the number of inter-hemispherical connections is low and the centrality accumulated by one of the hemisphere is very high and (2) a region where the number of inter-links is high and the centrality is evenly distributed between the two hemispheres.

The majority of studies investigating the role of the nodes within a functional network and, more specifically, the characterization of functional hubs, are based on a thresholding of the connectivity matrix where only the 3%-10% of the links are maintained [A171], [A31].

Nevertheless, the fact that the distribution of the overall centrality is strongly dependent on the number of inter-links has been commonly disregarded. This fact opens the door to two relevant issues: (1) To what extent is affected the role of the network hubs by the distribution of centrality between hemispheres and (2) is the functional balance of the hemispheres just a consequence of the high number of connections between them? Both questions deserve further attention in the future, and the results presented in this Chapter could be a starting point to understand how the distribution of centrality is influenced by the existence of functional communities in the brain. Furthermore, an

additional question naturally arises, what happens with such a centrality distribution in the case of failures in the functional network?

5.3.4 Hemispherical Robustness against node failures

Hitherto, our results analyze the distribution of centrality under normal conditions (i.e., EO and EC, resting state) but, what would happen if a subject suffers from a dysfunction? In other words, what would be the impact of the hemispherical centrality if an individual suffers from a cortical damage? And furthermore, which hemisphere is better prepared, in terms of centrality, to the corresponding node failure? In order to answer these questions we have investigated the consequences of node removal over both the hemispherical and whole network properties, focusing on the impact on the distribution of centrality. Node removal can be a way of modeling the effect of brain lesions (i.e. strokes) in a functional network and has been one of the most extended ways to evaluate the robustness of a network [A217], [A213], [A122], [A7].

The study of the network robustness against failures should be also inspected under the scope of the number of inter-hemispherical links since, as we have shown in the previous Section, centrality is strongly dependent on this issue. For this reason, we considered three different kinds of configurations, each of them accounting for a prototypical distribution of centrality. The first one assumes all inter hemispherical links between both hemispheres, keeping the same properties as the fully connected state. As we have seen, this state is associated with a balance in the amount of centrality retained by each hemisphere (see Fig. 5.5, stage 1). The second one is a condition where part of the low-weighted inter-hemispherical links have been removed and only around the 10% of the strongest links have been maintained (Fig. 5.5, stage 2). Finally, the third situation is just the opposite to the first one: we maintain only a small number of links (the highest 3, in this example), entering a region where the distribution of centrality is highly unequal, with the dominant hemisphere acquiring the main percentage (Fig. 5.5, stage 3).

Once these three regions are defined, we study the effects of node deletion by computing its impact on the hemispherical centrality, for each hemisphere, band and condition. Specifically, we remove a node from the left hemisphere and compute the new hemispherical centrality C^L_* without that node. Next, we estimate the percentage of network damage as the difference with the actual centrality of that hemisphere C^L. The local impact $l^L_{imp}(i)$ is defined as the percentage $l^L_{imp}(i) = \frac{(C^L_* - C^L)}{C^L} \times 100$. At the same time, we measure the local contribution $lc^L(i)$ of the node i being removed as the percentage of importance inside its hemisphere (see Section 5.2.5). The same procedure is repeated for analyzing the robustness of the right hemisphere. In this way, we measure the impact a node has when it is removed from the network as a function of its own importance.

Figure 5.6 shows the behaviour of $l^L_{imp}(i)$ vs. $lc^L(i)$ for all frequency bands, conditions and, importantly, for each of the three regions defined by the number of inter-hemispherical links. We plot a dashed line at $l^L_{imp}(i) = lc^L(i)$ in order to help the reader to evaluate if the impact of a node is higher/lower than its importance or, in other words, to see if a node with importance x has an impact higher or lower than x.

Interestingly, we can clearly differentiate between three different groups which perfectly fit with the aforementioned stages. In all plots of Fig. 5.6, stages 1, i.e., the impact of the removal when all inter-hemispherical links are considered, corresponds to the group of nodes lying above the dashed lines which is defined by $l^L_{imp}(i) = lc^L(i)$. This fact indicates that the impact on the local centrality is always lower than the importance of the node itself. The explanation of this behaviour is simple, once a node is removed, part of its centrality is still retained by the nodes belonging to its hemisphere. This phenomenon promotes the resilience of the hemisphere against random failures and also maintains the functional network-of-networks close to the balance reported in stage 1, at least in terms of the hemispherical centrality. At the same time, we observe a linear correlation between the local contribution of a node and its local impact (see Tabs. 5.3-5.4). This kind of

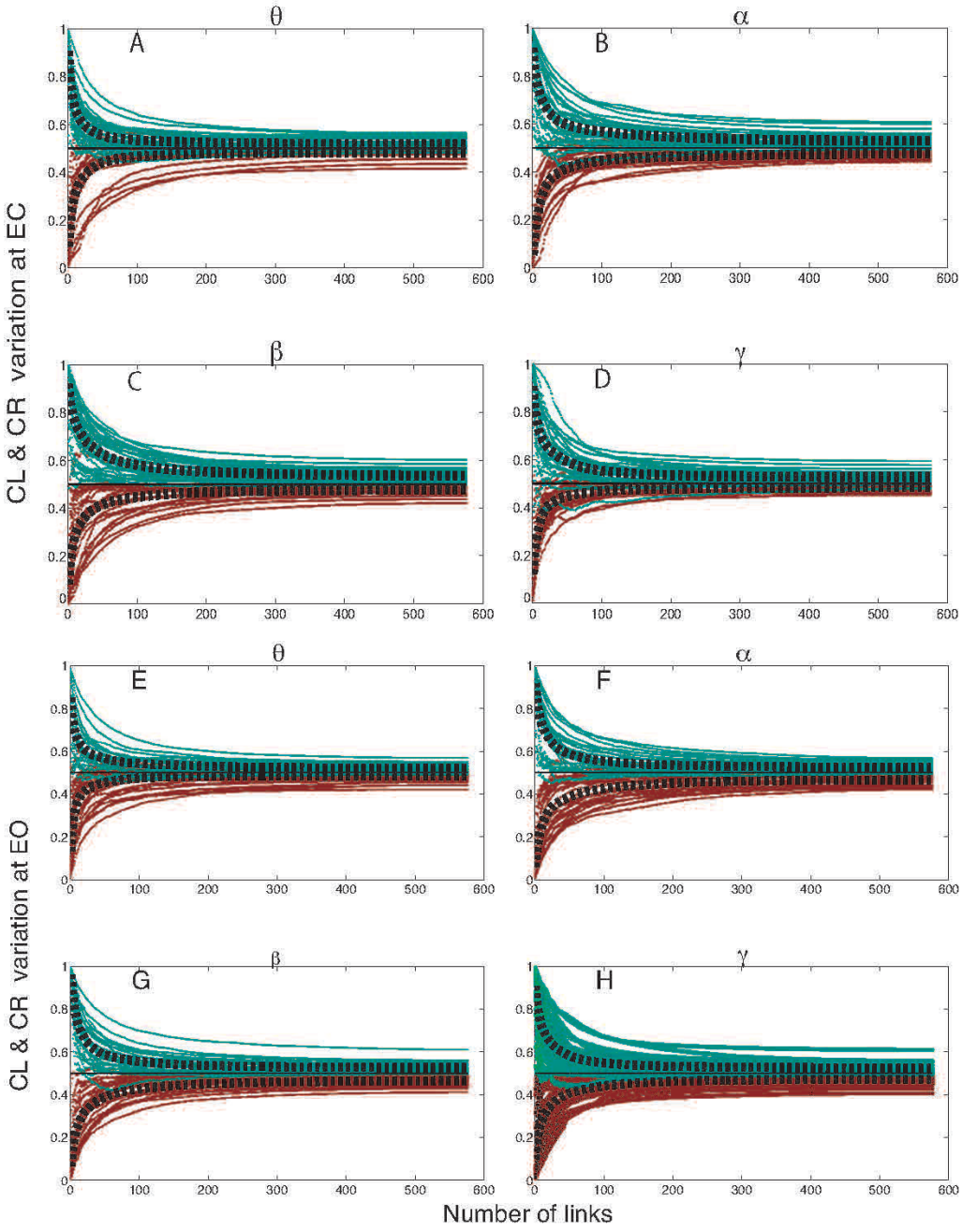

Figure 5.4: **Hemispherical centrality C_L vs. the number of inter-hemispherical links**. Each plot shows a different combination of a condition (EC or EO) and a frequency band (θ, α, β and γ). Line colors indicate whether the dominant hemisphere is the left (green) or the right one (red). The 54 curves corresponding to the C_L of all subjects are plotted together with the average over the left-dominant and right-dominant groups (dashed lines). Note how the fact that an hemisphere is dominant over the other (i.e., when it has higher λ_1) leads that hemisphere to retain more centrality, despite the ratio is strongly dependent on the number of inter-hemispherical links.

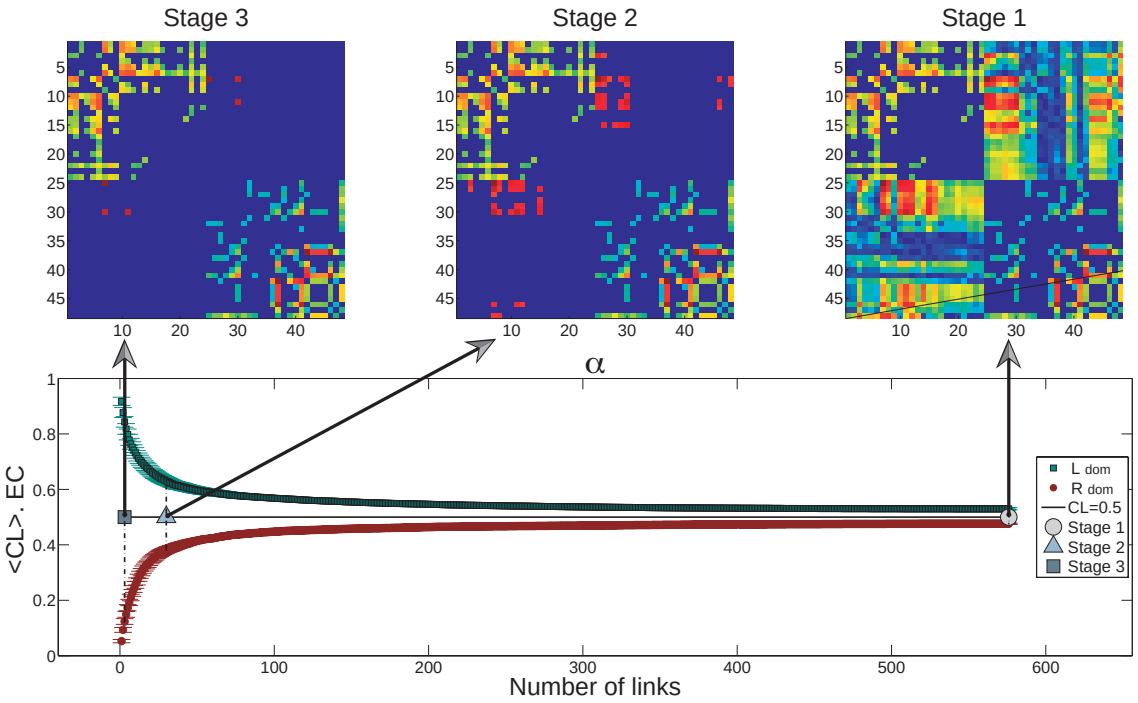

Figure 5.5: **The sparsity of the inter-hemispherical links leads to three different stages**. Example from an arbitrary subject in the α band and during the EC condition. The upper panel shows the weighted matrices for the three regions, according to the number of inter-hemispherical links, as explained in the main text. In these matrices, the left and right hemispheres keep those links with a weight higher than the threshold that guarantees that both L and R have a unique connected component when they are in isolation. Next, the number of links belonging to the inter-hemispherical connections is modified (i.e., those belonging to P). Stage 3 contains only the three inter-links with the highest weight; Stage 2 contains thirty inter-links (10.4% of the total); Stage 1 contains all inter-links. The bottom panel shows the value of C_L corresponding to the connectivity matrices of the upper panel, where red circles correspond to right-dominant individuals and green squares to left-dominant ones

correlation could be expected but, as we will see, the value of the slope is crucial to determine how important is that the failure occurs at a hub or at a peripheral node. In this case, the damage would be always lower than 5% no matter what node fails.

Stage 2 of Fig. 5.5 (the one maintaining the 10% of the links) corresponds to the cloud appearing in the middle of the four plots of Fig. 5.6. Despite the local importance of the nodes is maintained, we can observe how the damage in the centrality accumulated by hemispheres has increased (when compared to the previous stage). Now, the local impact of the nodes is close to its local contribution. At first sight, this result could be counter-intuitive, since the reduction of the number of inter-hemispherical links is making the centrality to better “escape" to the other hemisphere. Nevertheless, the explanation comes from the fact that, the lower the number of links, the farther we are from the balance in the centrality distribution (and the higher the centrality captured by one of the hemispheres). In addition, while the linear correlation between node contribution and impact is maintained, we observe and increase of the slope, indicating that differences between peripheral nodes and hubs are increasing (Tabs. 5.3-5.4).

Finally, stage 3, the one maintaining only 3 inter-hemispherical links, corresponds to the cloud of points placed at the lower part of all panels of Fig. 5.6. In this extreme situation, the damage due to node failure is dramatically increased, at least when compared with the previous results. Now

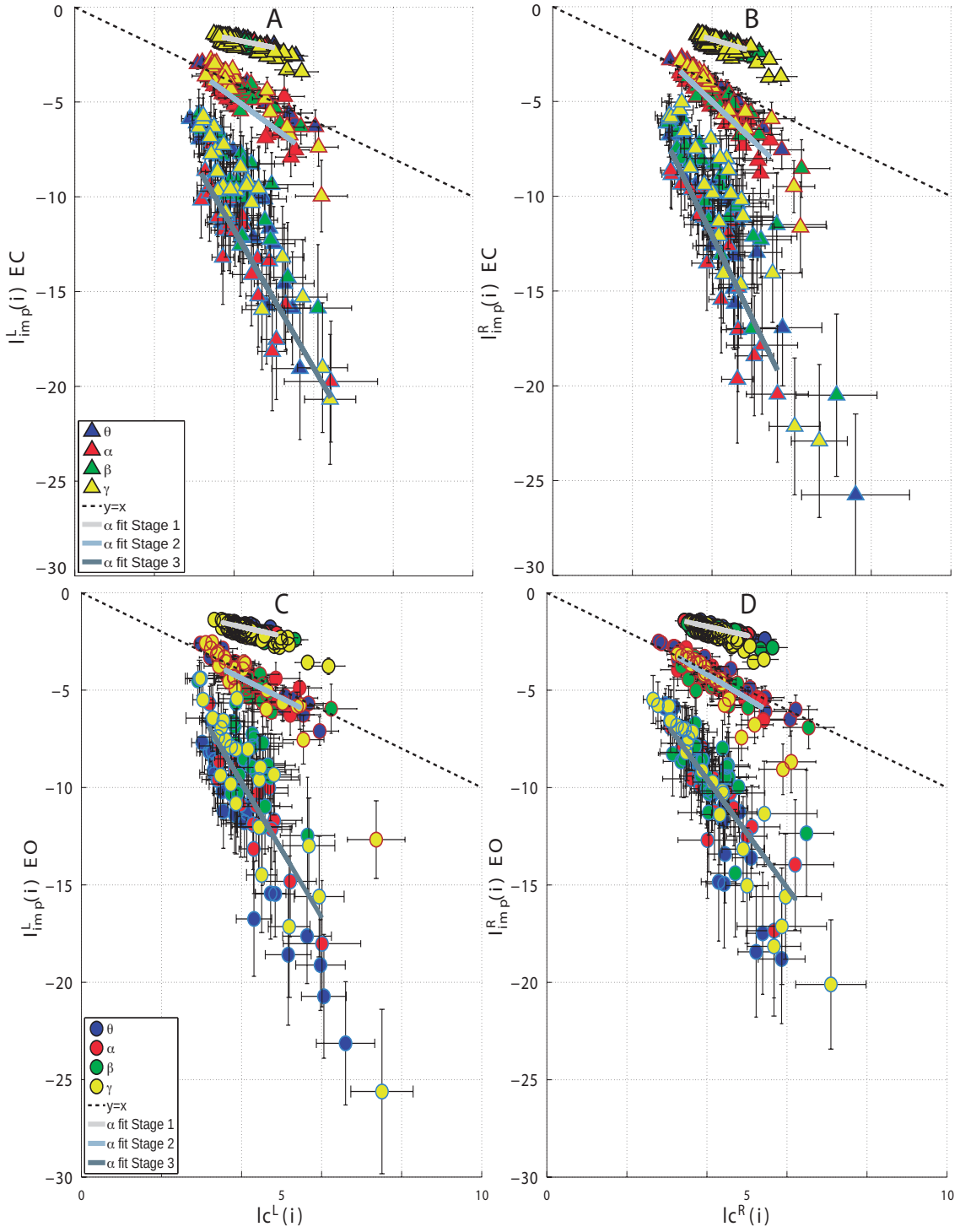

Figure 5.6: **Local impact $l^L_{imp}(i)$ vs. local contribution $lc^L(i)$ during a failure of node i.** In all plots, points correspond to single-node failures (i.e., a single node is removed from the functional network). Upper (bottom) plots refer to the EC (EO) condition and left (right) column to the impact in the left (right) hemisphere. In all panels, three groups of nodes can be identified: (1) Stage 1 corresponds to the upper cloud of nodes, (2) Stage 2 to the middlle cloud and (3) Stage 3 to the bottom group of nodes. See Fig. 5.5 for a definition of the three stages. The dashed line corresponds to $l^L_{imp}(i) = lc^L(i)$. For each stage, a solid line allows to better follow the linear correlation between the local contribution and the local impact. It has been obtained from the α band, but similar slopes are obtained for the rest of frequency bands. See Tabs. 5.3-5.4 for a detailed study.

Band	Stage 1		Stage 2		Stage 3	
	m_{EC_L}	m_{EO_L}	m_{EC_L}	m_{EO_L}	m_{EC_L}	m_{EO_L}
θ	-0.479	-0.537	-1.238	-1.357	-3.784	-4.296
α	-0.421	-0.465	-1.541	-1.021	-3.629	-3.466
β	-0.599	-0.631	-1.262	-1.082	-3.107	-2.416
γ	-0.686	-0.748	-1.857	-2.013	-4.034	-4.098

Table 5.3: **Correlation between the local impact and the local contribution (left hemisphere)**. Slopes of the linear fitting of l^L_{imp} vs. l^L_c (Fig. 5.6) for all bands, conditions and stages. Note the increase of the slope as we move from stage 1 to stage 3.

Band	Stage 1		Stage 2		Stage 3	
	m_{EC_R}	m_{EO_R}	m_{EC_R}	m_{EO_R}	m_{EC_R}	m_{EO_R}
θ	-0.623	-0.441	-1.759	-1.070	-3.942	-4.660
α	-0.608	-0.466	-2.000	-1.222	-4.322	-2.788
β	-0.532	-0.586	-1.653	-1.064	-3.118	-1.430
γ	-0.833	-0.933	-2.462	-2.240	-4.480	-3.534

Table 5.4: **Correlation between the local impact and the local contribution (right hemisphere)**. Slopes of the linear fitting of l^L_{imp} vs. l^L_c (Fig. 5.6) for all bands, conditions and stages. Note the increase of the slope as we move from stage 1 to stage 3.

the slope of the linear correlation is that high (Tabs. 5.3-5.4) that the damage in the hemispherical centrality can be more than three times the local contribution of a node. This way, damaging a node with a local centrality of 5% leads to a lose of centrality of more than 15%. The clonlussion is clear: the lower the number of inter-connections between hemispheres, the highest the centrality vulnerability of the hemispheres and, as a consequence, the farther we are from a balance situation. These results hold no matter what the hemisphere being attacked is, the condition under study or the frequency band being analyzed.

Figure 5.7 shows an example of how the impact of the node failure is strongly related to the amount of inter-hemispherical links. In this example, we plot a spatial distribution of the nodes, whose size and color indicates the percentage of local impact in the α band. We can observe that, when all inter-hemispherical links are considered, the local impact of the nodes is similar, no matter what their local centrality is (Fig. 5.7, left panel). On the contrary, when only few inter-hemispherical links are considered (Fig. 5.7, right panel), the local impact of all nodes drastically increases, but also differences between nodes are enhanced. Interestingly, those nodes with the highest impact are placed at the occipital region and are more vulnerable in the EC condition.

In view of all, we can affirm that the way the hemispheres are interconnected is crucial to understand the distribution of centrality and the local damage in a functional network-of-networks. Nevertheless, this point of view has been traditionally disregarded when analyzing functional brain networks. An explanation of this oversight may come from the impact on other network parameters, such as the clustering coefficient and the average shortest path. Is the same dependence on the inter-hemispherical links reported when calculating these two topological parameters? To answer this question, we computed the impact on the shortest path $l_{imp_d}(i)$ and the clustering coefficient $l_{imp_c}(i)$ when a node failure is introduced. Figures 5.8 and 5.9 show the behaviour of $l_{imp_d}(i)$ and

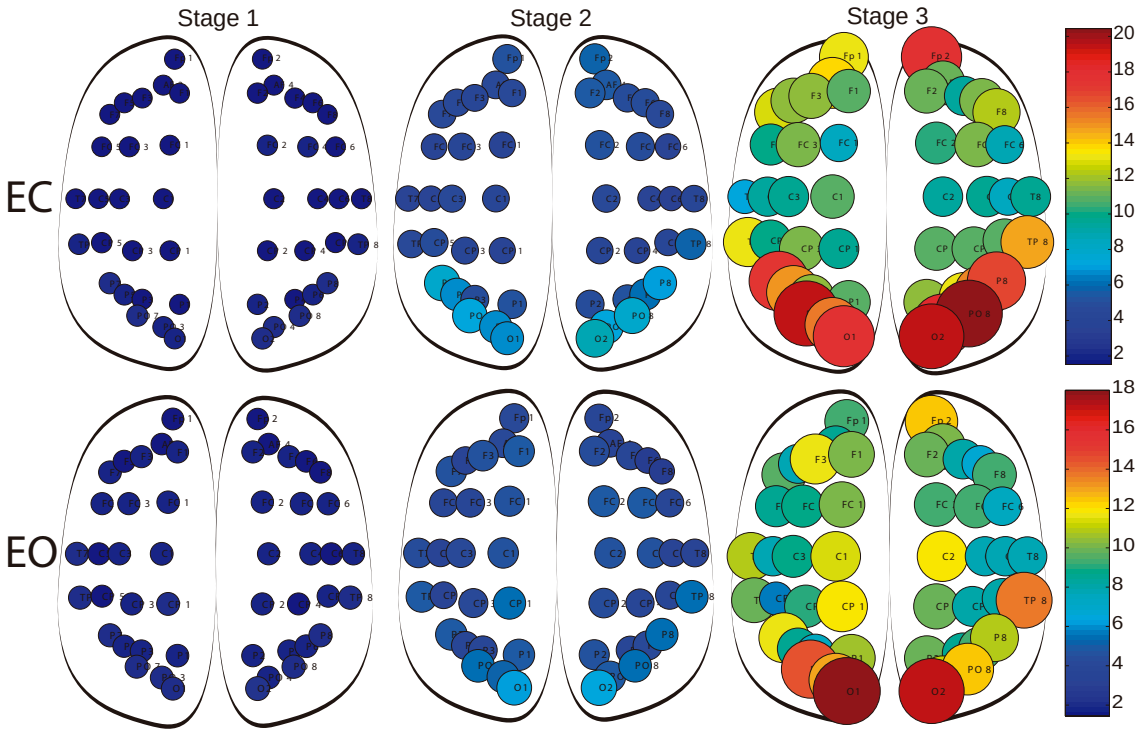

Figure 5.7: **Topological organization the local impact in the α band for EC and EO conditions**. Average local impacts in α band for the EC (upper panel) and EO (bottom panel) groups and for the three stages. The radius of each node is proportional to the local impact and represented by a color bar. Note how the local impact of the nodes increases as we move from stage 1 to stage 3.

$l_{imp_c}(i)$ for the EC and EO conditions, respectively. We have also included the local impact in terms of hemispherical centrality in order to ease the comparison between them. Results are quite surprising, since both the clustering and the shortest path remain almost unaltered when the number of inter-hemispherical links is modified (i.e., at the three different stages). Furthermore, the role of the node that suffers the failure is irrelevant in terms on the impact at the clustering (Figs. 5.8C-D and 5.9C-D) and has a slight positive correlation in the case of the average shortest path (Figs. 5.8E-F and 5.9E-F).

5.4 Discussion

In the current Chapter we have seen a study of how centrality is distributed in functional brain networks from a perspective that is different from classical approaches where the brain is treated as a single network. While a series of previous studies were based on the idea of using the eigenvector centrality as the metric to assess the importance of the nodes, this centrality parameter is strongly influenced by the fact that functional brain are composed by inter-connected hemispheres. It is important to say that all subjects are right-handed, however there is no clear evidence for left-handed with right dominant brain or vice versa.

Under this framework, we have found that the hemispherical centrality is a useful metric to better quantify whether brain hemispheres vie to acquire the highest possible amount of centrality or, conversely, if they are close to a functional trade-off. We have seen how the total centrality along the functional network-of-networks of the brain is fully distributed between hemispheres in almost equal proportions when considering all its inter-hemispherical links, including those whose weight seemed to be irrelevant. As a consequence, we report the existence of a functional balance that, in

the context of centrality, is merely a consequence of this hyperconnectivity between hemispheres. This trade-off is captured by the competition parameter Ω, which is close to zero in all conditions of study (i.e., eyes closed and eyes opened, both at resting state).

The fact that weaker links between hemispheres may represent spurious correlations among cortical regions, highlights the need to understand how the hemispherical centrality is modified as the level of connectivity decreases. In this context, we computed the percentage of the damage a cortical regions has due to single strokes (i.e., removing a node from the network), highlighting the resilience of the functional network when weakest links are maintained (stage 1). Nevertheless, when these links are disregarded, the local impact due to a node failure becomes more important (stages 2 and 3). This way, the functional network-of-networks goes from a tight-binding model to a fragile system due to absence of inter-hemispherical links. Interestingly, the cortical regions that lead to the most severe deterioration of the hemispherical centrality are located in the occipital lobe for all conditions.

In contrast to the centrality distribution, the effect of nodal failures on both the shortest path and clustering coefficient is not dependent on the number of inter-links. These results should be put in contrast when network-of-networks methods are applied to neuroscience, because it warns about the risks of investigating the robustness of multilayered systems only in terms of the typical topological features associated to information distribution, such as the average shortest path or the clustering coefficient. In this way, another take-home message is that a network-of-networks whose number of inter-links is decreased might be robust when dealing with information transport, meanwhile at the same time it may become vulnerable in terms of centrality.

In conclusion, despite topological studies of functional brain networks improve the understanding how the brain operates, it is important to remark that the brain cannot be analyzed as a single network. Furthermore, as many other biological complex systems, the brain continuously evolves in time, but this is another story, which will be the main goal of the next Chapter...

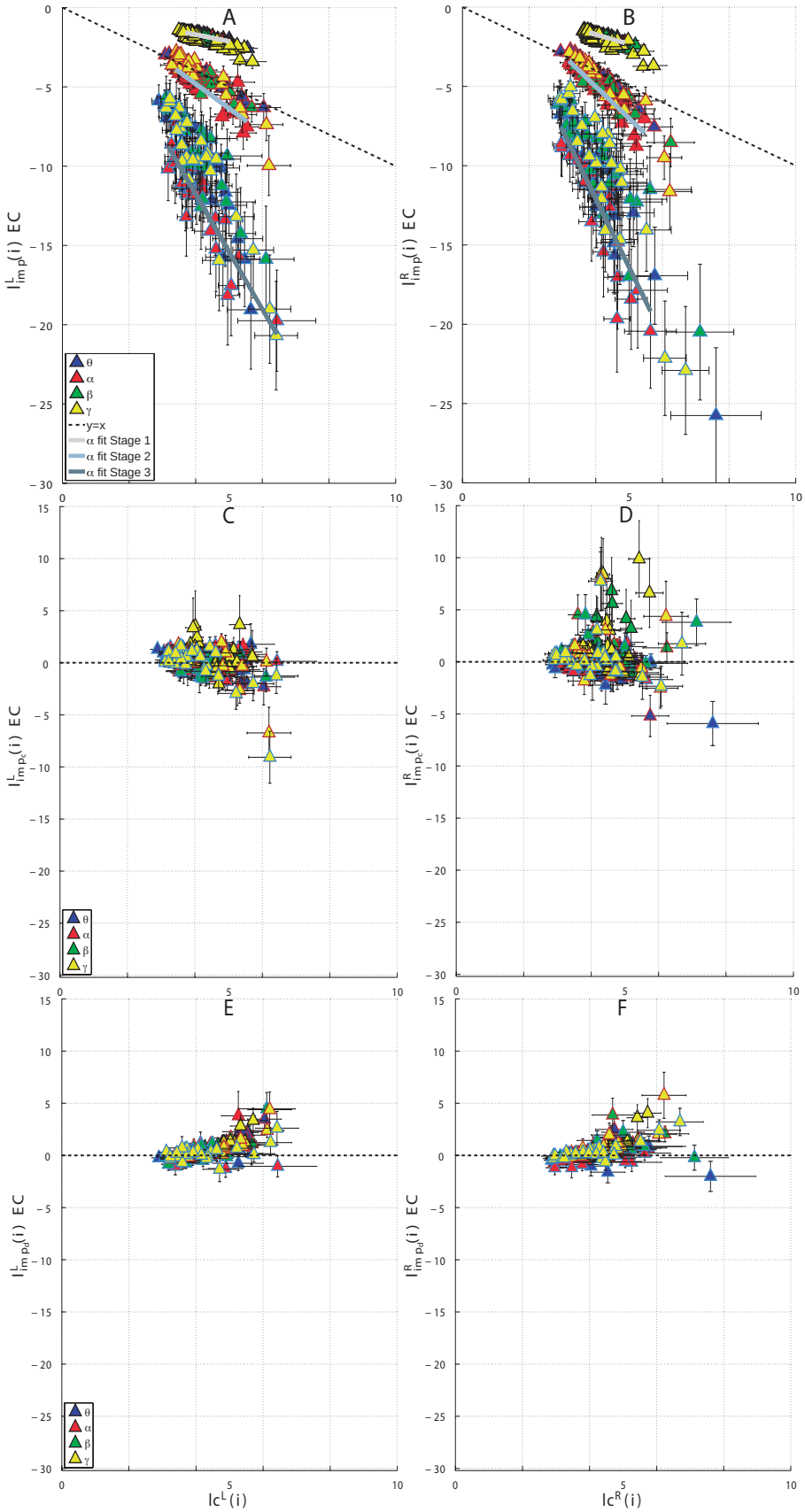

Figure 5.8: **Local impact on centrality, clustering and shortest path for the EC condition**. Upper panels: Local impacts on hemispherical centrality for the left (**A**), and right (**B**) hemispheres. Middle panels: Local impact on the clustering for the left (**C**) and right (**D**) hemispheres. Bottom panel: Local impact on the average shortest path for the left (**E**) and right (F) hemispheres.

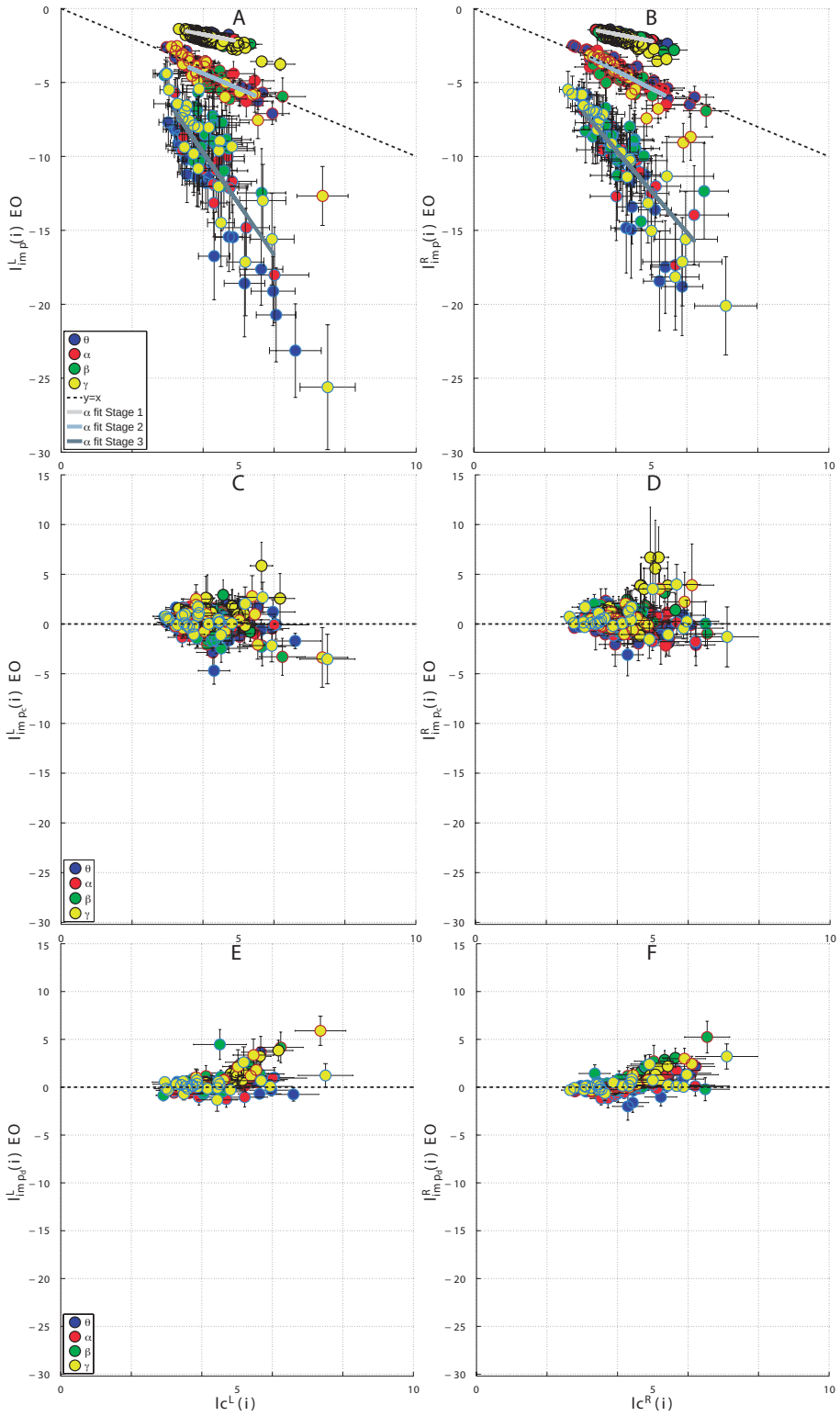

Figure 5.9: **Local impact on centrality, clustering and shortest path for the EO condition**. Same representation as the figure 5.8 but in this case for the EO condition.

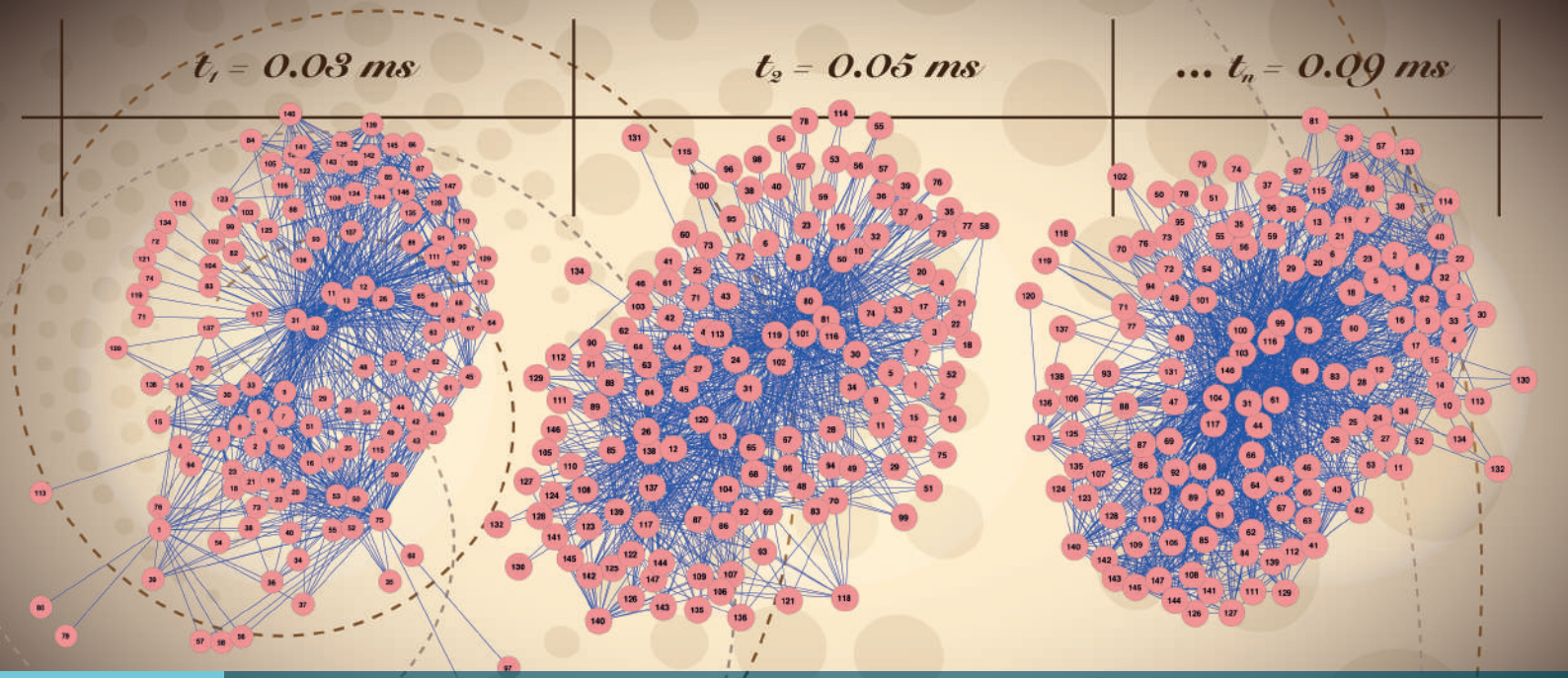

6 Evolving Networks

§

We have seen how the eigenvector centrality is useful to better understand the central role played by nodes in a single network and, to what extent the level of nodes simultaneously activated in different hemispheres categorizes the level of resilience of the brain when we see it as a system composed by two single networks. Nonetheless, the previous studies attend to static systems, that is, networks that simply do not evolve in time and concentrate their dynamics in a steady state. For this reason a profound study of networks that dynamically change their own topology is convenient to better understand what happens with the topological organization in different time-steps. In the present study we used graph theory analysis to investigate age-related reorganization of functional networks during the active maintenance of information that is interrupted by external interference. Additionally, we sought to investigate network differences before and after averaging network parameters between both maintenance and interference windows. We compared young and older adults by measuring their magnetoencephalographic recordings during an interference-based working memory task restricted to successful recognitions. Data analysis focused on the topology/temporal evolution of functional networks during both the maintenance and interference windows. We firstly observed that older adults require higher synchronization between cortical brain sites in order to achieve a successful recognition. Secondly we found the main differences between age groups arise during the interference window and we conclude that older adults show reduced ability to reorganize network topology when interference is introduced. Finally, we detected that averaging network parameters leads to a loss of sensitivity to detect age differences.

6.1 Introduction

Older adults show a decline in information-processing resources, such as working memory, and it is commonly accepted that ageing adversely affects memory abilities. In this regard, age-related difficulties to suppress irrelevant information from distractors are evident during the active rehearsal

§This chapter is based on my published paper: ***Evaluating the Effect of Aging on Interference Resolution with Time-Varying Complex Networks Analysis***. *Frontiers in human neuroscience*. **9**, 255 (Jan 2015). [A10]

of the to-be-remembered material [A83], [A140], [A190], [A101], [A203], [A204], [A205]. Compelling evidence from functional neuroimaging studies has suggested that the disproportionate susceptibility to interference in older individuals is accompanied by greater activity in prefrontal and parietal regions relative to their young counterparts. This over-recruitment is thought to be compensatory when it is accompanied by similar task performance across age groups [A91], [A35]. On the other hand, less activity in frontoparietal regions may also be shown in ageing as task demands increase, which is associated with a drop in performance [A182]. Despite extensive evidence on focal brain activity, the human brain is primarily a network and, complex cognitive functions, such as interference resolution, may be mediated by interactions among a set of functionally related areas rather than specific brain regions (McIntosh, 1999; Salami et al., 2014)[A144]. Functional connectivity [A78], [A190] refers to the interactions among spatially remote brain regions [A245] and connections within specific networks involved in high level cognitive processes seem to be altered with age, which in turn might affect behaviour [A44], [A90], [A190], [A9], [A92], [A52]. Specifically, a greater distractibility has been associated with reductions in connectivity between the prefrontal cortex and the parahippocampal area [A44], and within a more anterior network including the middle frontal gyrus, anterior cingulate and basal ganglia [A190]. Additionally, Geerligs et al [A85], compared connectivity changes between four different networks showing increased connectivity in older compared to young adults.

Altogether, current research suggests an age-related reorganization within and between specific networks. On the other hand, most of the studies have considered functional networks as static entities without investigating their evolution over time. Importantly, functional networks emerge, evolve and disappear according to the specific requirements of a given cognitive process and also in the absence of external stimulation, [A113]. Only a few studies to date have focused on the temporal evolution of different neural networks [A58], [A66], [A20], [A68]. Network reconfigurations at larger time scales have been shown to be strongly correlated with learning [A20]. Hence, the temporal evolution of simultaneous brain networks can help identifying the neural mechanisms promoting interference resolution with progressing age. This way, MEG technique is an ideal tool to explore the dynamical properties of whole-brain networks as it enables a direct measurement of brain magnetic fields from pyramidal neurons in the human cortex with optimal temporal resolution (i.e., milliseconds) [A99].

Two main principles might be considered when exploring the temporal dynamics of whole-brain networks, the so-called local specialization and global integration of functionally linked brain networks [A79], [A207], [A268], [A25], [A245], [A22], [A31], [A245]. Those studies have been able to demonstrate that the healthy brain is organized according to a small world architecture that favours cognitive performance [A202], which is characterized by high local specialization (high clustering coefficient, C) and high global integration (short topological distance between nodes or path length, L) [A246]. Additionally, deviant graph parameters have been used as markers for several pathological conditions (for a review, see [A95], [A17], [A245], [A215]), such as mild cognitive impairment and Alzheimer's disease [A104], [A61], [A212], [A202], [A30], [A178], [277] and also for healthy ageing [A149]. In this regard, healthy ageing generally leads to alterations in the topology of large-scale functional networks with connectivity patterns more similar to "random" networks [A149], [277] and, hence, deviating from the optimal small-world organization observed in healthy young individuals. However, only a few studies to date have examined age effects on task-related functional connectivity with graph approaches [A106], with only one of them focusing on memory processes [A245]. In this respect, the authors observed age-related disruptions of large-scale networks relevant to memory encoding and recognition. Specifically, older adults showed a widespread loss of long-range connections and longer path lengths in fronto-temporal and temporo-parietal regions with a few increases in posterior parietal regions.

The present study aimed at expanding limited previous work from graph approaches on age-

related disruptions of memory-based functional connectivity, with special emphasis on the temporal evolution of network topology. To address this important issue, we examined whole-brain temporal dynamics of large-scale functional networks with MEG during the performance of an interference-based working memory task in young and older adults. To this end, we calculated phase synchronization across whole-brain regions and computed complex network parameters within each age group for α, β and γ bands, observing that the α band was the one reporting significant differences between young and older individuals. We then compared the abovementioned complex network values between age groups for successful recognitions. We also focused on the ability of functional networks to evolve and adapt in time during both the maintenance and interference period. Finally, we investigated network differences before and after averaging network parameters between both maintenance and interference windows. In contrast with previous research that focused on memory encoding and recognition, we were interested in memory maintenance as it corresponds to the period in which distraction is presented and interference resolution takes place. The present work is built on an study who examined age-related changes in brain activations during memory maintenance. Here we demonstrated that interference resolution from distractors during the active maintenance of information requires greater neural resources for older adults in order to match the level of performance seen in young adults. Previous studies of network functionality in ageing [A140], [A148], hypothesized that older adults would demonstrate altered temporal dynamics in whole-brain functional networks during task performance compared to younger adults. To investigate this issue, we analysed how the topology of the functional networks of both young and old adults evolves during the experiment and we compare it with the classical analysis of the averaged functional networks, i.e. disregarding the fluctuations of the network topology along the experiment.

6.2 Materials and Methods

The sample comprised 20 healthy individuals divided into two groups according to their age, young and older adults (see, Table. 6.1 for a description of the sample). They were selected from the adults program at the Universidad Complutense de Madrid (UCM). All participants reported corrected to normal vision and hearing within the normal range. All participants underwent a screening evaluation including a semi-structured interview, the reduced Geriatric Depression Scale rGDS [A253], and the MiniMental State Examination MMSE [A75]. They were required to satisfy a number of inclusionary criteria: (I) No psychiatric diagnosis described by the American Psychiatric Association (DSM-IV-TR axis I or II disorder), (II) No chronic neurological disease (e.g., seizure disorder or dementia) or severe medical illness that requires medication (e.g., diabetes or cardiopathies), (III) A score < 5 on the rGDS, and (IV) A score > 27 on the MMSE. Informed consent was obtained prior to participation and approved by the Institutional Review Board at UCM.

	Female/Male	**Age**	**MMSE**	**rGDS**
Young	6/3	21.88 (3.40)	29.77 (0.44)	0.92 (1.38)
Older	9/2	64.45 (4.68)	29.17 (0.83)	1.58 (2.47)

Table 6.1: **Demography of the Sample**. Variables are included as mean values (standard deviations).

6.2.1 Cognitive Task and MEG Recordings

We performed an *interference-based working memory task*, composed of 120 trials [A203]. Stimuli were presented using E-Prime 1.2 software (Groningen, The Netherlands). The experimental design is schematically depicted in Fig. 6.1. It is divided into three stages: encoding, maintenance and recognition. A 'LEARN' yellow cue (500 *ms*) indicated the beginning of each trial, followed by a blank screen (200 *ms*). Two paired associates, each of them composed of a visual stimulus (face) plus an auditory stimulus (semantic attribute describing some aspect of the face, i.e. 'clever'), were subsequently shown during 2000 *ms*, separated by a blank screen (200 *ms*). Participants were instructed to memorize each pair.

Next, after a 500 *ms* blank screen, an interfering face of a famous person was presented during 3000 *ms*. Participants had to answer a yes/no question (i.e. 'Is he a writer?') pressing one of two response buttons, followed by a blank screen (500 *ms*). Next, a 'REMEMBER' white cue appeared (500 *ms*), followed by another blank screen (200 *ms*). Thereafter, two more paired associates were shown during 2000 *ms* each.

Finally, another blank screen appeared for 200 *ms*. Subjects were required to make a match/non-match button-press response with the index finger to each probe as quickly as possible without sacrificing accuracy. We used a specially designed button panel and left/right (yes/no) index finger assignment was counterbalanced across participants. All participants were right-handed as stated with the initial semi-structured interview. On 120 of the 240 probes, the two paired-associates had been presented previously during the encoding period (a cue visual stimulus plus a cue auditory attribute) and the order of cue paired-associates at recognition was randomized. For the other 120 probes, the two paired-associates were foils. Specifically, 60 of these 120 probes were two paired-associates consisting of a cue visual stimulus plus a novel auditory attribute, and the other 60 consisted of a novel visual stimulus plus a cue auditory attribute. The presentation of 'Old/New' paired-associates was randomized and counter-balanced across all trials.

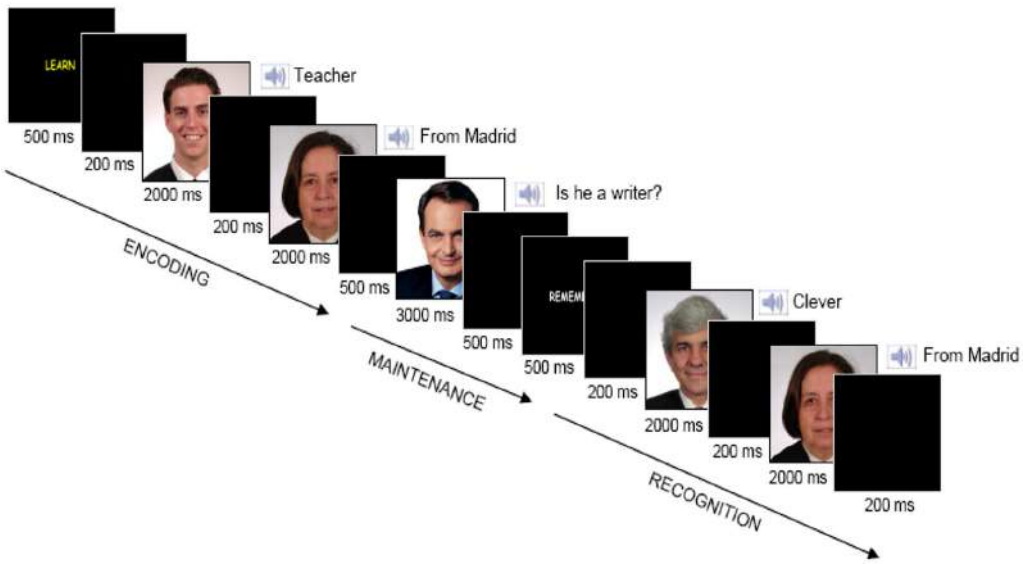

Figure 6.1: **Trial Structure**. Two paired associates were shown subsequently for 2000 *ms* each to memorize during the encoding stage. An interfering picture of a famous face was displayed for 3000 *ms* and subjects were asked about some attribute related to that picture during the maintenance stage. Two paired associates were presented subsequently for 2000 *ms* each during the recognition stage and subjects reported whether each of them had appeared during the encoding phase.

Visual stimuli consisted of coloured pictures of human faces from the MEG laboratory database

for faces. Sex and age were counter-balanced across all pictures. Age range was the same as the one employed in the selection of young and older participants (19-27 years for young participants, and 55-73 years for older participants). Famous faces were selected based on a preliminary behavioural study conducted with a different set of participants in which pictures were equally recognizable to young and older adults [A203]. Paired associates and famous faces at the maintenance period were novel across trials. The set of employed images consisted of 240 faces for the encoding stage, 120 for the maintenance, and 240 for the recognition stage. From those at the recognition state, 120 were target (faces presented at encoding) and the rest were distractors. From the set of distractors, half incorporated a novel auditory stimulus and the half matched those at the encoding stage, but incorporated a novel face. Gender and age showed a variety of neutral expressions and were controlled across pictures.

Auditory stimuli were stereo-recorded at a frequency of 44.1 KHz and 16 $bits$. The set of stimuli consisted of 300 words: 100 were adjectives taken from the dictionary of the Royal Academy of the Spanish Language; 100 were professions taken from the Spanish National Institute of Statistics; and the 100 remaining were places of residency taken from the Spanish National Institute of Statistics. Prior to the MEG scan, subjects undertook a 20 trial-training session with the same structure as described above.

MEG recordings

Magnetic fields were recorded using a 148-channel whole-head magnetometer (MAGNES® 2500 WH, 4-D Neuroimaging, San Diego, California, USA) confined in a magnetically shielded room. The sampling rate was set to 678.17 Hz. An online anti-aliasing bandpass filter between $0.1 - 100$ Hz was applied. Four electrodes were attached for the identification of blinks and eye movements; two of them near the left and right outer canthus and the other two above and below the right eye. Prior to the MEG measurements, the position of the magnetometers relative to the subject's head was determined utilizing five small radiofrequency coils. Responses at recognition were classified either as 'hits' (both answers were correct at recognition) or 'errors' (one answer or none of them were correct at recognition). We were interested in successful recognition; hence, we selected trials with hit responses for subsequent network analysis.

Data were pre-processed using a signal space projection (SSP) procedure that uses simultaneous recordings from nine reference channels. Baseline correction was applied on the basis of a pre-stimulus 100 ms window. Thereafter, the signal was submitted to a low-pass filter of 48 Hz. Ocular artifacts were corrected using BESA (version 5.1.6) (MEGIS Software GmbH, Gräfelfing, Germany), which is a standard artifact-correction tool. Datasets were then visually inspected for movement artifacts, and epochs with peak-to-peak amplitudes exceeding a threshold of3 pT were discarded from further analysis. In order to avoid any bias related to the different number of trials across subjects, we used a quality criterion referred to the minimum number of trials free of artefacts, which in the present study were 32. In individuals with more than 32 trials free of artefacts, we selected 32 of them randomly. From these trials, we segmented epochs of 1500 ms, including the blank-screen period prior to presentation of the interfering stimulus (500 ms) and the first 1000 ms after it. This segmentation was applied to avoid muscular artefacts coming from the button pressing while answering the interfering question. Hence, segmented epochs contained two different parts: 1) a memory maintenance window (500 ms) and b) and interference window (1000 ms).

6.2.2 Synchronization and Networks Analysis

The construction of the functional networks relies on the evaluation of the phase synchronization (PS) between brain regions. PS detects when the phases of two signals synchronize, even though their amplitudes remain uncorrelated [B17], [A174] and was quantified through the Phase Locking Value (PLV) [A129] using HERMES toolbox [A164]. Phases associated with the dynamics recorded

at each magnetometer were extracted using the Hilbert Transform [B17]. Next, we defined$\phi(t)$ as the difference between the two phases and calculate the *PLV* as:

$$PLV = \langle e^{i\phi(t)} \rangle == \sqrt{\langle \cos\phi(t) \rangle^2 + \langle \sin\phi(t) \rangle^2} \tag{6.1}$$

Higher PS between two signals relate to small differences between phases and high *PLV*, and vice versa for lower PS. We were interested in the temporal evolution and topology of the functional networks. This way, we split the 1500 *ms* epochs into time windows of 50 *ms* length each with no overlap and evaluate the *PLV* within each temporal window. The window length was set to a value low enough to guarantee a sufficient number of points to observe a non-stationary temporal evolution of the network structure, but large enough to allow an accurate *PLV*. *PLV*s were computed in ten frequency bands (from 8 Hz to 48 Hz, with central frequencies separated each 4 Hz) between pairs of the 148 magnetometers. Lower frequencies could not be considered due to edge effects after Hilbert transforms. Then, results were normalized with respect to a baseline (an open eyes resting state period of 100 *ms*). *PLV*s were then merged to form α $(8-12\ Hz)$, β $(12-30\ Hz)$ and low γ $(30-48\ Hz)$ frequency bands. Note that the length of the time windows to obtain the *PLV* is lower than the $\frac{1}{f_{min}}$ limit suggested by Leonardi and van de Ville [A133]. Nevertheless, the fact that we are analysing non-stationary signals allow us to reduce the length of the time window beyond this limit, as recently explained by Zalesky and Breakspear [A257]. Importantly, statistical differences between network parameters were only found at α band. Thus, we will focus on this frequency band in the forthcoming sections.

Complex network analysis

The *PLV* between all pairs of channels led to a NxN $(N = 148)$ symmetric matrix W, where its elements w_{ij} quantify the PS between node i and node j. Due to the time segmentation into 50 *ms* windows, we obtained a set of matrices $\{W\}$ for each individual, and we tracked how the topology of these matrices changed with time. With this aim, we computed a series of complex networks parameters for each matrix of the $\{W\}$ set: the network strength (S), outreach (O), weighted clustering coefficient (C_w), global efficiency (E_g) and average shortest path (SP). These parameters were obtained, first, for each node of the network and, second, averaged over the whole network. This procedure was followed for each individual and, finally, each network metric was averaged over individuals of the same group, leading to an average of the ensemble with its corresponding error.

We have also computed the average values for the memory maintenance, the interference and the whole experiment, in order to evaluate the information gained from the analysis of the evolution of the network parameters. Age-related differences in complex network parameters were calculated using non-parametric Kruskal-Wallis test [B22]. Reported p-values were corrected for multiple comparisons using a non-parametric permutation approach as elsewhere [A163]. Statistical significance was considered for p-values lower than 0.05.

6.3 Results

6.3.1 Functional Network Parameters in α Band

We have computed a group of classical network metrics over averaged and non-averaged functional networks in order to investigate functional activity. Our first approach was to obtain three different averages of the network parameters during: A) memory maintenance (MM), B) interference (I) and C) the whole experiment (MM+I). As we will see, the averaging of the network parameters leads in many cases to non-significant differences between groups, but we will use them as a reference to evaluate the advantages of analysing their temporal evolution.

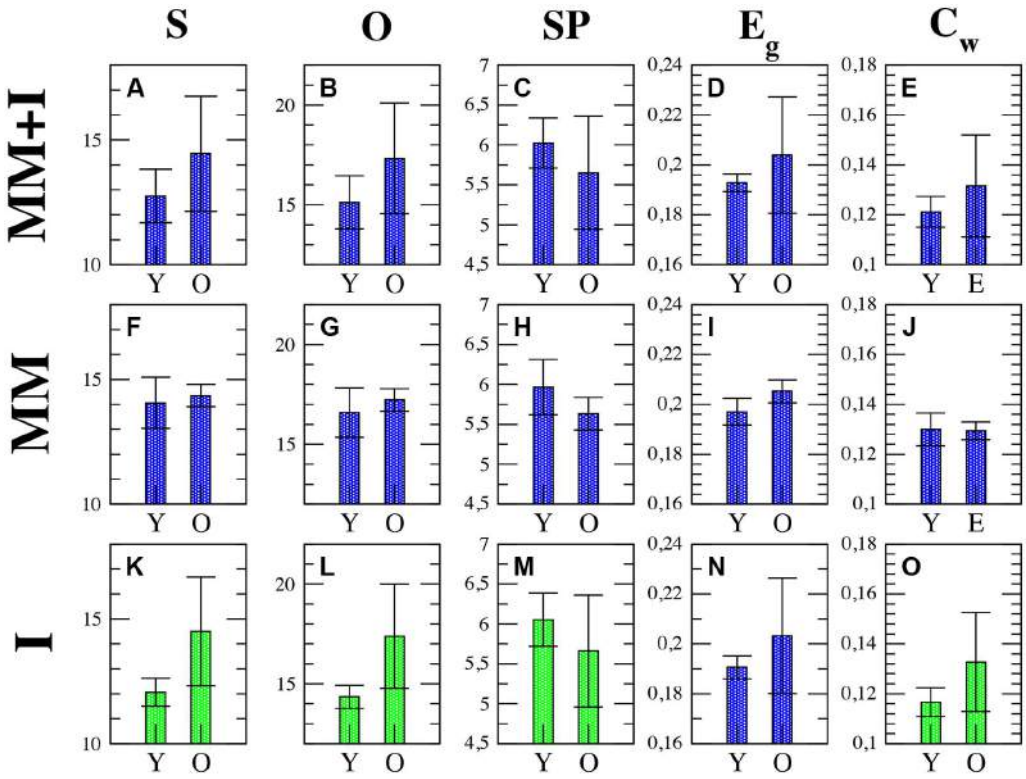

Figure 6.2: **Average network parameters obtained during the whole experiment (MM +I), memory maintenance (MM) and interference (I) windows**. strength (S), outreach (O), weighted clustering coefficient (Cw), global efficiency (Eg) and average shortest path (SP). Rows refer, respectively, to MM+I, MM and I. Statistically significant parameters ($p < 0.05$) are highlighted in green, see Tab. 6.2 summarizing the reported p-values. Black bars represent standard error of the mean. Y = young, O = old.

First row of Fig. 6.2 shows the network parameters of the functional network obtained for averaging the set of synchronization matrices W during the whole experiment (MM+I). We observed that the older adults group had a higher average of the network strength S (Fig. 6.2 **A**), indicating a more synchronous activity during the whole experiment. As a consequence, the outreach O, measuring how the synchronized activity is correlated with the physical length of the links, also had higher value in the older adults group (Fig. 6.2 **B**). Accordingly, the network shortest path SP was lower in the older group (Fig. 6.2 **C**), since the topological length of a link is obtained as the inverse of its weight (which, in turn, measures the synchronization). Thus, a higher value of S is translated into a lower average length of the network links, reducing the topological distance" between nodes and leading to a lower SP in the older group. Note that this does not necessary indicate a better/worse organization of the network structure (in terms of information processing) since the lower SP was just a consequence of having a larger S (i.e., higher average synchronization). The global efficiency E_g was obtained as the inverse of the harmonic mean of the shortest distances between nodes, and it normally correlates with the inverse of SP, which is the case of our experiment (Fig. 6.2 **D**). As explained before, the higher efficiency of the older group is just a consequence of having a higher average synchronization between cortical regions. Finally, we focused on the local properties of the network by inspecting the weighted clustering coefficient C_w, measuring how dense the connections are at the local level. We report a higher value in the older group (Fig. 6.2 **E**), which can be attributed again to a higher value in the average synchronization.

Second row of Fig. 6.2 shows the same network parameters but restricted to the memory

	S	O	SP	E_g	C_w
MM+I	0.0532	0.0524	0.0708	0.1008	0.0674
MM	0.8226	0.5496	0.3390	0.5026	0.8810
I	0.0230	0.0174	0.0476	0.704	0.0264

Table 6.2: **Comparisons between averaged graph metrics**. P-values of the comparisons between average graph metrics after correction for multiple comparisons through non-parametric permutations test.

maintenance window (MM). We observe similar results as in MM+I, with the exception of the clustering coefficient where average values of both groups remain very close. Nevertheless, although there are clear differences at the average value in the first panel, none of the network parameters had significant statistical differences between groups in the MM+I analysis (see first row of table, 6.2), i.e. when an averaged functional network is considered for the whole experiment. Likewise, the statistical analysis in the MM analysis leaded to the same results as in MM+I, that is, average differences between groups are not statistically significant.

Finally, in the third row of Fig. 6.2 the analysis is restricted to the interference window (I). In this case, S (Fig. 6.2 **K**), O (Fig. 6.2 **L**), SP (Fig. 6.2 **M**) and C_w (Fig. 6.2 **O**) show statistically significant differences (p<0.05) between young and older adults. The average strength S ($p = 0.0230$) during the interference period is higher for the older group, which suggests that they require a higher synchronization between cortical regions in order to successfully perform the memory task (note that only successfully recognized items were considered for the analysis). This fact is reflected in the differences in the SP: the increase of S reduces the topological distance between nodes, and SP now becomes statistically significant ($p = 0.0476$). Interestingly, the outreach is the network parameter showing the lower p-value ($p = 0.0174$) and, in turn, the largest difference between averages. When inspecting the local scale, we also obtain statistical significant differences in the clustering coefficient C_w ($p = 0.0264$). Only the E_g does not show enough differences to overcome the statistical test, although the differences between the average values between groups are larger than in the memory maintenance window.

Two general conclusions can be extracted from the analysis of the topology of the averaged functional networks. First, a division of the task into MM and I gives more interesting information about the functional network structure as compared to the average over the whole experiment (MM+I). This is somehow expected as we are considering two different cognitive processes: memory maintenance and interference. Second, age differences are more evident during the interference period, leading us to consider that older individuals require higher synchronization between brain regions in order to perform a successful recognition. However no correlations were observed between the averaged network metrics and the task behaviour, i.e. the percentage of correct answers.

6.3.2 Temporal Evolution of Functional Networks in α Band

The fact that the topology of functional networks is not static recommends a study of how their temporal evolution is. Thus, it is desirable to split the whole experiment into short time intervals, calculate the properties of the functional networks at each interval and track their evolution. The shorter the time intervals, the larger the number of points and the better the temporal resolution. Nevertheless, the minimum length required to compute the synchronization between cortical regions introduces a lower threshold when dividing each time series into short windows. In our case, we

have chosen a threshold of 50 *ms*, which leads to 30 points during the 1500 *ms* of each measurement.

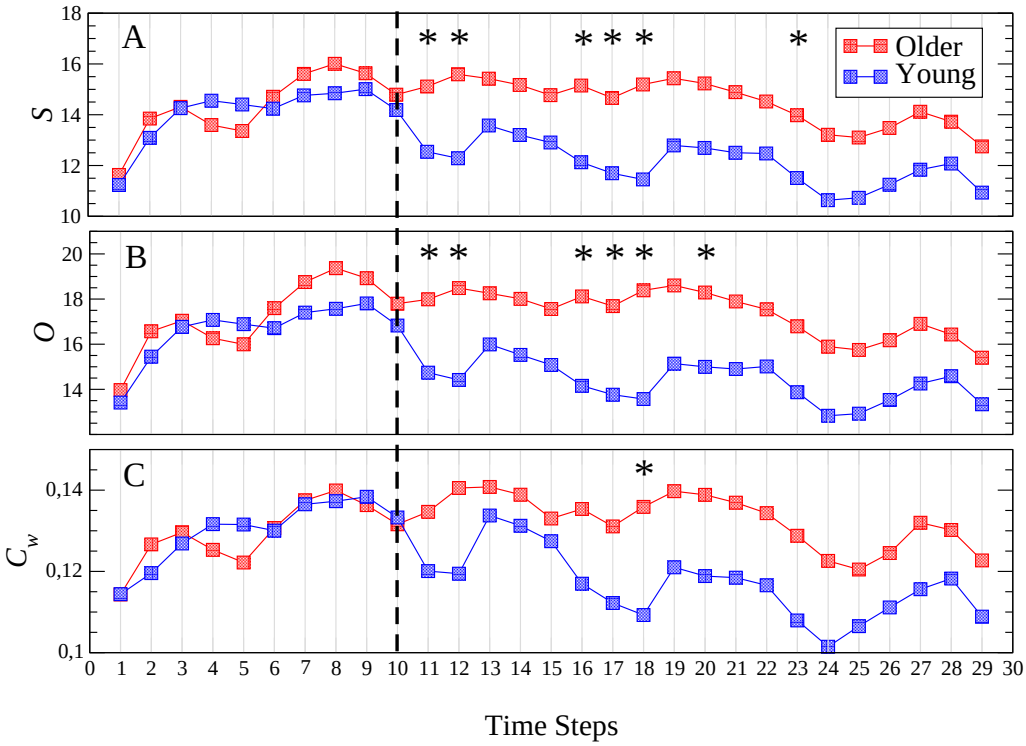

Figure 6.3: **Evolution of the network strength S (A), outreach O (B) and weighted clustering C_w (C) for young (blue squares) and older (red squares) groups**. The dashed line indicates the end of the memory maintenance period and the beginning of the interference period. Stars indicate those time steps where the strength of the functional network shows statistically significant differences (p<0.05) between both groups.

Next, we have obtained, and compared, all network parameters for each time step. Figure 6.3**A** shows the evolution of the network strength S during the whole experiment, with a dashed line indicating the end of the memory maintenance period and the beginning of the interference period. As we observed in the previous section, the average strength S was higher in older individuals. The phenomenon where $S_{older} > S_{young}$, is clearly reported in the interference time-window.

It is worth noting that those time steps where the functional network has statistically significant differences appear at the beginning of the interference period (see stars in Fig. 6.3**A**, indicating the time steps with a p-value p<0.05), vanishing after step 23 (700 *ms* after the beginning of the interference). Also note how the strength decreases during the interference period when compared with the memory maintenance period. This decrement is sharper at the beginning of the interference in the young group and much smoother in older individuals. Similar results are obtained with the outreach O parameter, as shown in Fig. 6.3**B**. Again the temporal evolution of the functional network reveals statistically significant differences between groups during the early stages of the interference period, in this case disappearing after 500 *ms* (step 20). For both groups, the outreach decreases in the interference period (See Fig. 6.2**G** and Fig. 6.2**L**) following a similar profile as the network strength S, as it can be seen by comparing 6.3**A** with Fig. 6.3**B**.

Interestingly, the weighted clustering coefficient C_w does not reveal such clear differences (see Fig. 6.3**C**). The number of points that have statistically significant differences (stars in Fig. 6.3**C**) decreases in just one time step located in the interference period. Again, the main differences are reported during interference and similar profiles to those of S and O are obtained, i.e., higher values during the memory maintenance in both groups and $C_{w(older)} > C_{w(young)}$ during the interference.

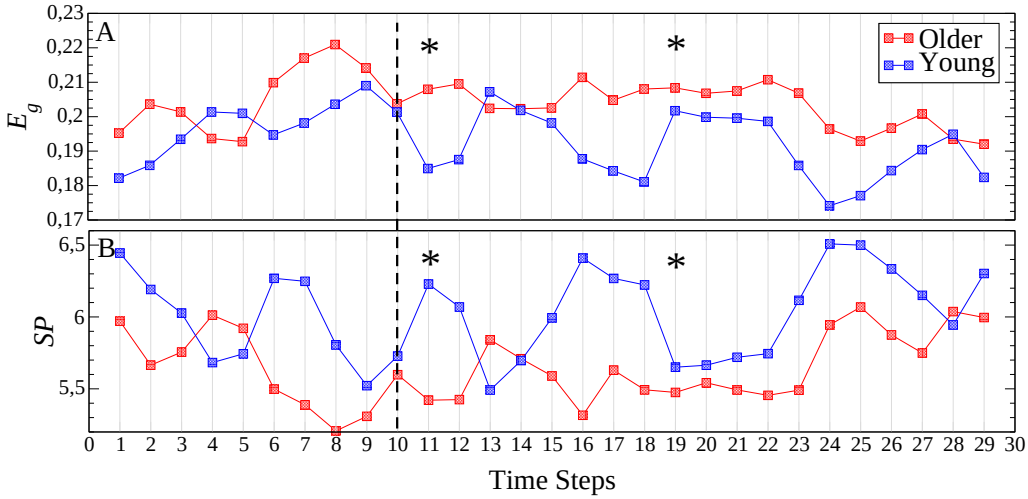

Figure 6.4: **Temporal evolution of the global efficiency E_g (A) and the average shortest path SP (B) for both the young (blue squares) and older (red squares) groups**. The dashed line indicates the end of the memory maintenance period and the beginning of the interference period. Stars indicate those time steps where the strength parameter shows statistically significant differences between both age groups.

Figures 6.4**A-B** account for the two parameters related with the global transmission of information along the network: global efficiency E_g and the average shortest path SP. As for the rest of parameters, differences between both groups are more evident in the interference period. In both measures, we only obtain two time steps with statistical differences in the interference region. The higher E_g reported in the older group (Fig. 6.4**A**) is a consequence of the higher value of S: the higher the synchrony between nodes, the higher the efficiency will be.

Note that E_g refers only to topological efficiency, and to the efficiency of the brain during the cognitive task. This decrease in network efficiency might indicate that older subjects require a higher synchronization between brain regions, which implies a higher energy demand, to achieve the same objective, in this case, a successful recognition after the inference. Finally, we observed that SP behaves in the opposite direction from the topological efficiency parameter (Fig. 6.4**B**). The increment of synchrony in the older adults group results in link weights of higher values that, in turn, lead to shorter paths between nodes (i.e., the higher the synchrony between two nodes, the shorter the distance between them).

6.3.3 Fluctuations of Network Parameters in α Band

We finally focused on the ability of functional networks to evolve and adapt in time during both the memory maintenance and the interference window. With this aim, we quantified the increment of the network strength S at every time step $\Delta S = |S_i - S_{i-1}|$ since, as seen in the previous section, this parameter influences the rest. We used ΔS as an indicator of how much the synchrony over the functional network is able to increase/decrease during the short time interval of 50 *ms* associated to each time step. Next, we computed the cumulative probability distribution $P_c(\Delta S)$ of having an increment of network strength higher than ΔS. $P_c(\Delta S)$ was obtained for both groups separately.

A comparison between memory maintenance and interference is plotted in Fig. 6.5. Interestingly, during the memory maintenance, fluctuations of the network strength are higher in the young adults group (Fig. 6.5**A**). When analysing the same distributions during the interference period, we observe that the situation is reversed. In this case, the older adults group shows higher fluctuations of the network strength, which can be clearly observed by looking at the difference between both

distributions (Fig. 6.5**B**).

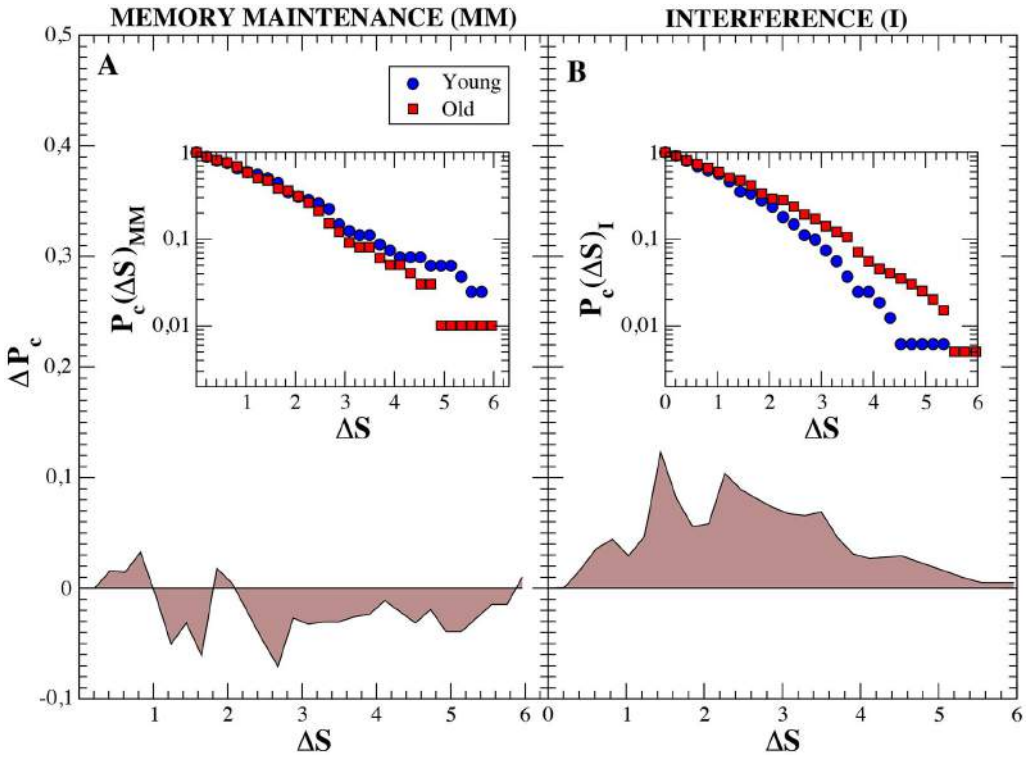

Figure 6.5: **Cumulative probability distributions of the increment of the network strength ΔS between consecutive time steps (insets) and differences between groups**. ΔS is defined as $\Delta S = |S_i - S_{i-1}|$. Blue circles refer to ΔS of individuals belonging to the young group and red squares to ΔS of old subjects. Both insets show the cumulative probability distributions $P_c(S)$ for the maintenance and interference regions (in log-linear scale), respectively. Main figures, (A) and (B) show the difference ($P_c^{Old} - P_c^{Young}$), in linear scale, between both groups. We observe how, during the memory maintenance the increments of the network strengths are higher in the young group. On the contrary, during the interference region, fluctuations are mush larger in old individuals.

We also analyse the fluctuations in strength at the nodal level. In Fig. 6.6**A-B** we show between-group differences, in the average strength of the nodes (i.e., $\Delta S_{old-young} = s_i^{old} - s_i^{young}$), for both the memory maintenance and the interference time windows. During memory maintenance, we observe that despite the average network strength S is higher in the older adults group (see Fig. 6.2**F**), this is not a generalized feature, since some nodes show a negative value of $\Delta S_{old-young}$ (Fig. 6.2**A**). In the interference time-window, with a higher average network strength S for the older group compared to the young group (see Fig. 6.2**K**), the majority of nodes have, accordingly, positive $\Delta S_{old-young}$, with values much higher than the ones in the memory maintenance window.

Finally, it is worth analysing strengths fluctuations at the node level during memory maintenance and interference. Figure 6.6**C-D** shows differences in strength fluctuations at the local level between both time windows (MM and I)for both age groups. This way, we first obtained strength fluctuations between two consecutive time steps $\Delta S = |S_i - S_{i-1}|$ and, next, we averaged this value within each time-window and computed the difference $\Delta S^{MM} - \Delta S^{I}$.

The results show how in the older adults group, differences between MM and I are more extreme at certain nodes placed at the frontal and occipital regions (Fig. 6.6 **D**), while differences in the young adults group are more homogeneous (Fig. 6.6**C**). In both cases, we have positive and negative deviations of $\Delta S^{MM} - \Delta S^{I}$, indicating that it is worth going to the level of nodes to

gain insights about how the fluctuations of the network strength are distributed among the cortical region.

6.4 Discussion

We have investigated how functional networks of young and older individuals modulate their structure during an interference-based working memory task. We have seen that averaging the network topology during the whole experiment or, splitting it into two parts corresponding to the memory maintenance and interference, hide the differences reported between groups when a full segmentation along the experiment is performed. The latter analysis allows observing the evolution of the network parameters on time, reporting significant differences between young and older individuals at the beginning of the interference period. These differences are more pronounced in parameters such as the strength S or outreach O, although they are also reported in the weighted clustering C_w, average shortest path SP and network global efficiency E_g. Interestingly, the ability of the network topology to reorganize is impaired in the older group, which shows lower variations of the network strength between consecutive time steps during the interference region when compared to the memory maintenance.

Complex networks' metrics have traditionally quantified the topological properties of networks with a unique and fixed value. This approximation is valid in those cases where the time scales of the network evolution are orders of magnitude higher than the dynamical processes occurring in them. For example, when evaluating anatomical brain networks, it is reasonable to assume that the topology of the network is fixed during the measurement of the network itself, despite it is known that the synaptic connections also evolve with time (although at much slower rates). On the contrary, during a cognitive task, the brain activity suffers drastic changes at really fast time scales, and it is reasonable to expect that the associated functional networks could modify their topology during the task. Thus, averaging the network properties during a whole task may hinder information about the real topology of the functional network. Despite these limitations, the majority of the studies analysing the topology of functional networks have dealt with, what we call averaged functional networks, which are obtained as the average of the activity during a cognitive process, e.g.: one memory task, one single functional network. Unfortunately, this approximation may not give enough accuracy to draw conclusions about how the topology of the functional network is and how it evolves in unison with the cognitive task. In addition, it can be expected that the analysis of the evolution of a functional network, if possible, would result on a deeper knowledge of how the network arises, evolves and disappears, thus leading to a better understanding of the interplay between the network topology and cognitive processes.

Only a few studies have focused on the evolution of the topology of functional networks, most of them analysing the effects of ageing or adaptation during learning ([A17][A58][A55]). The fact that the majority of real networks change their topology as time goes by is capturing the attention on scientist working on complex networks analysis and redefining classical measures in a way that they are able to capture the intrinsic evolution of the network structure.

In the current work, we use of this kind of methodologies in order to evaluate how young and older individuals perform an interference-based memory task and what are the consequences of undergoing an interference stimulus aiming to alter the memory maintenance. We show that calculating the parameters of the functional networks averaged along the whole experiment leads to differences between groups (young and older) that are not statistically significant. This fact reveals that, whenever it is possible, temporal averaging of the functional networks should be avoided. When the analysis is divided into two different stages, i.e., memory maintenance and interference, statistical differences between young and older individuals arise. Interestingly, it is only the interference window where the comparisons between network metrics show significant differences. This result indicates that at the whole-brain network level, the mechanism that allows to

the elder group to achieve a successful recognition appears during the interference period, and this seems to be related with a global increase of functional connectivity, as observed for the network strength and outreach in the two first time windows. This result is in agreement with previous evidence considering the increase of functional connectivity as a compensation mechanism.

Interestingly, the fact that an impaired functional network shows a higher synchronization between its nodes has been reported in mild cognitive impairment, a brain disease considered as Alzheimer's prodromal state. The network metrics reflect differences between groups when taking into account both the global organization, by means of the outreach parameter, and the local organization, through the network clustering. The older group showed higher values of both metrics, indicating a higher activity of their functional networks, despite, as in the case of network strength, only the interference period shows significant statistical differences. The fact that outreach parameter takes into account the physical length of the links indicates that the differences between groups are also influenced by geometrical constraints. Nevertheless, we must note that the increase of the network strength in the older group has consequences in the rest of the network parameters. Higher strength leads to shorter distances between nodes, since topological distance scales with the inverse of the weight of the links. Thus, an increase of$S$ is translated into a reduction (increase) in the SP (E_g). At the local scale, the clustering coefficient of the older group shows higher values than the young group, also capturing the enhancement of the synchronization in old individuals. As a general picture, the increase of the correlated activity of the older group modifies the network parameters accordingly, a fact that is mainly reported in the interference region.

In the present study, age-related differences in network topology are restricted to the alpha band. Converging evidence has demonstrated a central role of alpha oscillations in both the active processing necessary to memory maintenance ([A168][A193]) and functional inhibition [A116]. Both aspects are intrinsically linked to the notion of "top-down control", which refers to an attentional control function that focuses on task-relevant information and suppresses task-irrelevant information by means of inhibition [A179]. In this regard, our results support the importance of alpha in inhibitory top-down control to enhance the retention of the to-be-remembered material and the suppression of interference during the maintenance period.

All in all, it is worth mentioning how the functional networks adapt their values in time. We observed how the increment of the network strength between consecutive time steps behaves differently during the memory maintenance and the interference periods. While the fluctuations of the network strength are slightly higher in the young adults group during the memory maintenance, this situation is reversed during the interference period, where fluctuations of the strength of the older adults group are much higher. This fact suggests that the ability of functional networks to maintain (modify) its topology during interference is decreased (increased) with ageing, which may be related to inefficient top-down control, particularly, to deficits in inhibitory mechanisms necessary to override interference [A84]. These enhanced fluctuations of the network topology in order to compensate external disturbances might be of interest in the early diagnosis of neurodegenerative diseases such as Alzheimer's disease or other types of dementia. In addition, results are consistent with previous literature reflecting age related changes during recognition processes [A91], [A35].

Finally, this study offers another perspective to understand the dynamics of the functional networks on the basis of tracking the temporal evolution of the topology. Nonetheless, these kind of studies still let aside the possibility of knowing the inner dynamics associated to cortical regions, i.e., the intrinsic dynamics in the network. In this sense, the following study offers the way to understand how the inner dynamics of cortical regions may behave consistent/inconsistently in order to reorganize their own topology by themselves. That is to say, how the brain consistency can be captured by a new sub-type of functional network.

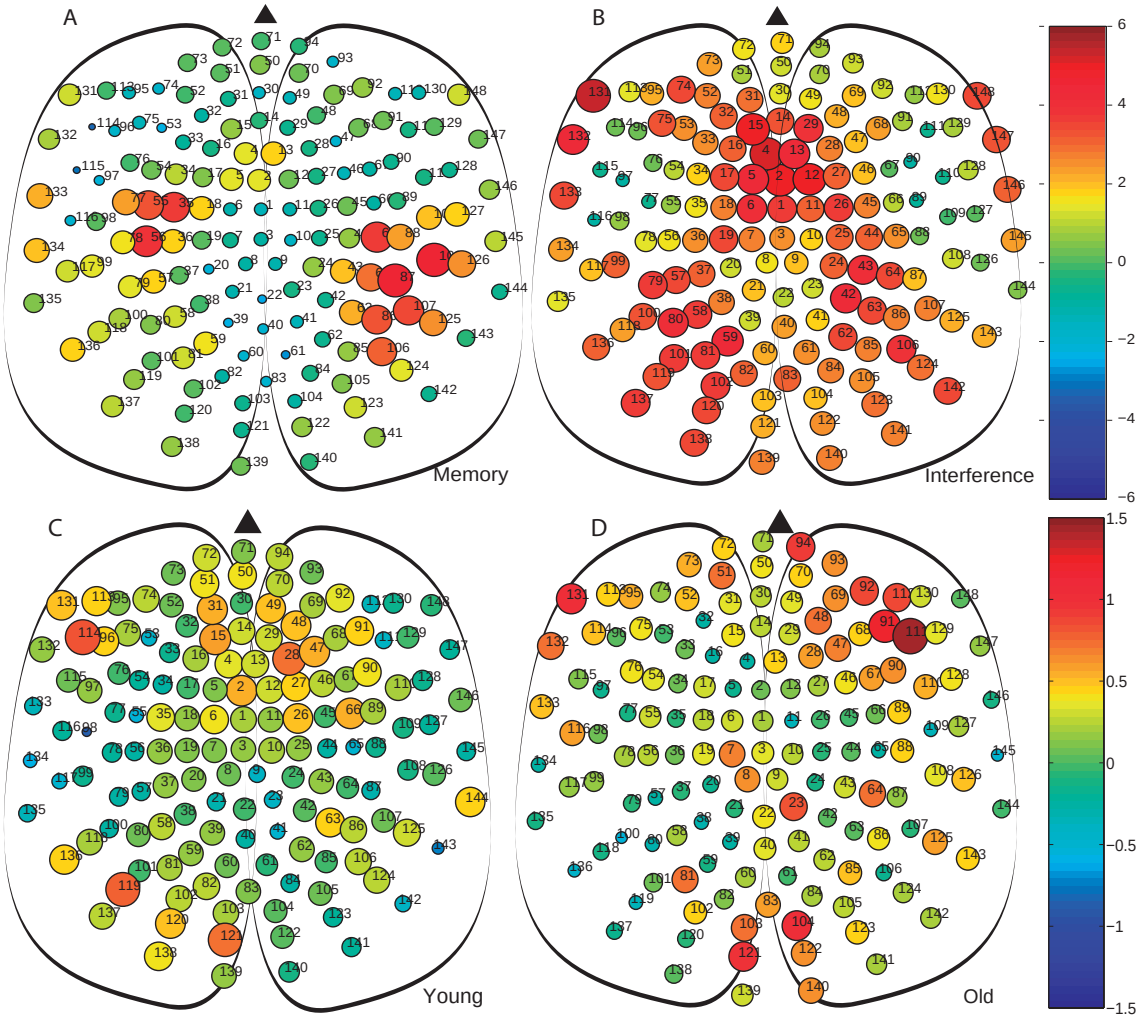

Figure 6.6: **Comparison of the strength of the nodes and their fluctuations during the memory maintenance and interference time windows**. (A) Comparison of nodal strengths si of both groups during memory maintenance ($s_i^{old} - s_i^{young}$). (B) Same as differences as (A) obtained during the interference period. In (A) and (B) node size is proportional to the average node strength. We can observe how, during the interference period, the strength, in this case at the node level is much higher in the old group. (C) and (D) Average differences of strength between consecutive time steps $\Delta S = |S_i - S_{i-1}|$ at the nodal level. Colours account for the difference of ΔS between the memory maintenance and interference regions, ie. $\Delta S^{MM} - \Delta S^{I}$. This way, we compare the value of the fluctuations within the same group at the different regions (MM - I): (C) Young group and (D) old group.

7 Anomalous Networks

§

The inner activity of the nodes makes feasible to study the dynamics in the networks, this way one can capture another different type of information about the brain networks different from that regarding multichannel interdependencies. i.e., the brain performance variability due to the local activations of cortical regions. In this sense, increased variability in performance has been associated with the emergence of several neurological and psychiatric pathologies. However, whether and how consistency of neuronal activity may also be indicative of an underlying pathology is still poorly understood. In this study we propose a novel method for evaluating consistency from non-invasive brain recordings. We evaluate the consistency of the cortical activity recorded with MEG in a group of subjects diagnosed with Mild Cognitive Impairment (MCI), a condition sometimes prodromal of dementia, during the execution of a memory task. We use metrics coming from nonlinear dynamics to evaluate the consistency of cortical regions. A representation known as *parenclitic networks* is constructed, where atypical features are endowed with a network structure, the topological properties of which can be studied at various scales. Pathological conditions correspond to strongly heterogeneous networks, whereas typical or normative conditions are characterized by sparsely connected networks with homogeneous nodes. The analysis of this kind of networks allows identifying the extent to which consistency is affected in the MCI group and the focal points where MCI is especially severe. To the best of our knowledge, these results represent the first attempt at evaluating the consistency of brain functional activity using complex networks theory.

7.1 Introduction

Excessive variability in performance negatively impacts people's ability to carry out activities of daily living. Increased short-term fluctuations, particularly in reaction times, that cannot be attributed to systematic effects, such as learning, have been associated with a wide range of cognitive disorders including impaired top-down executive and attentional control processes, and

§This chapter is based on my paper: ***Anomalous Consistency in Mild cognitive Impairment: A complex networks approach***. *Chaos, Solitons & Fractals*. **70** (Jan 2015). [A143]

with conditions including healthy ageing, and various neurological and psychiatric disorders ranging from Parkinson's disease [A36, A59], multiple sclerosis [A23], traumatic brain injury [A47], schizophrenia [A141] and various forms of dementia [A111, A234].

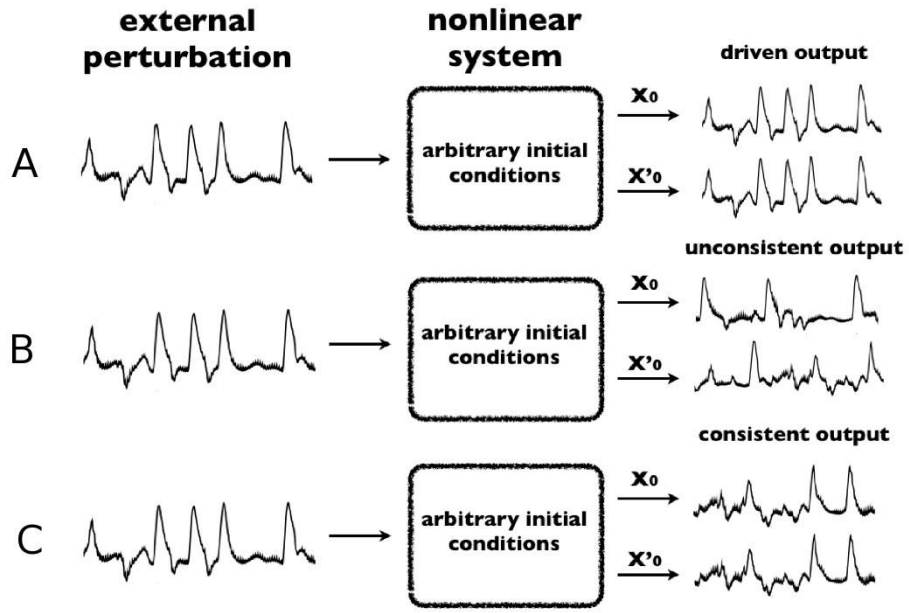

Figure 7.1: **The phenomenon of consistency.** The consistency of a dynamical system relies on its ability to respond in the same way when the the same external input is applied. In all panels (A, B, C), the same external perturbation is applied and the response of the system with two different initial conditions ($\vec{x}_0$ and $\vec{x}_0'$) is (qualitatively) shown. In A, we show an example of a driven system, where the output always behaves in the same way (as the external perturbation) due to a strong forcing of the input. In B, the external perturbation is not able to drive the output which responds in a different way when the same input is applied (due to different initial conditions). In C, we show an example of consistent dynamics. When the same input is applied, the system's output always behaves in the same way, despite not mimicking the driving dynamics.

A number of studies attest an association between behavioural inconsistency and structural and functional brain abnormalities. For instance, diffusion tensor imaging showed a relationship between intra-individual variability in reaction times and white matter integrity, with variability increasing with white matter degradation, pathway connectivity degradation and brain dysfunction [A73, A226, A230]. Behavioural inconsistency was also associated with neurotransmitter dysfunction, stress, and fatigue [A43, A67, A69, A157, A234].

However, whether and how behavioural consistency stems from a corresponding loss of consistency of functional brain activity is still unclear. For example, it has been shown that behavioural variability in the response time during a face recognition task negatively correlates with the brain signal variability, at least when children and adults are compared [A145], the latter having lower response time variability combined with higher signal variability. In the current study we will focus on the variability of brain dynamics when carrying the same (memory) task. We study whether the dynamics of the recorded signal at different cortical regions maintains (or not) its shape when the same memory task is carried out, and how the variability of each cortical region is related to that of

other regions.

In physics, *consistency* [A237] has been studied with a series of different dynamical models [A87, A176, A238]. The emergence of a consistent response requires a high synchronization between different outputs of a nonlinear system (i.e., different realizations with different initial conditions) when the same external input is applied. Nevertheless, consistency does not imply the observation of a synchronized state between the external input and the system's response as it is the case of an entrained or driven system. Figure 7.1 shows, qualitatively, the difference between a driven system and a consistent/inconsistent system.

Here we propose a new methodology for quantifying neuronal consistency that can be applied to noninvasive diagnostic procedures. This method involves constructing a *parenclitic network* representation [A260, A264] based on anomalous behaviour of a certain set of features. In our case, each node of the parenclitic network corresponding to a certain cortical region, is associated with a feature: its dynamical consistency during a memory task. We construct a network where nodes have a link between them with a weight that depends on how their consistency diverges from an expected value. The topological characteristics of the parenclitic networks can be used to extract information about how consistency is lost/maintained across the whole functional network. In such a representation, atypical or pathological conditions lead to the existence of a high number of links with large weights. Previous applications of this methodology to biological data have shown that parenclitic networks obtained from datasets associated with pathological conditions lead to strongly heterogeneous networks, i.e., networks where some nodes have a degree that is much higher than expected for links created at random, whereas typical or normative conditions are characterized by sparsely connected networks with homogeneous nodes [A260, A264]. In essence, a parenclitic representation equips the set of abnormalities of a system with a network characterization based on topological properties at various scales.

Specifically, we study the consistency of functional brain activity in a group of patients diagnosed with MCI. As it was mentioned in chapter 4, MCI is a clinical condition in which subjects experience memory loss to a greater extent than would be expected for age, who while not meeting the criteria for clinically probable Alzheimer's Disease (AD) are nonetheless at increased risk of developing it. Behavioural evidence shows that, compared to cognitively healthy ageing, MCI has been associated with increased response time variability and particularly in those subjects later developing AD [A43, A67, A69, A73, A89, A226]. Abnormal consistency in MCI may therefore represent a measure of functional integrity that may help identifying those patients who ultimately lapse into fully-fledged dementia.

On the other hand, recent studies have shown how the functional networks of MCI patients obtained during a memory test show differences in their topologies when compared to healthy subjects [A14, A29]. This fact indicates that a global reorganization of brain activity is occurring, raising the question of how the consistency of a brain network is affected by this reorganization. With the aim of studying the consistency of the whole brain network, we used MEG to record the brain activity of a group of patients suffering from MCI and a healthy control group as they carried out the Sternberg short-term memory task. We then computed the consistency of each brain site for each individual of each group and finally constructed the parenclitic network for the differences in consistency between MCIs and controls. The structure of the parenclitic networks highlights those regions whose consistency is most affected by the disease and suggests ways in which the effects of MCI may propagate through the functional brain network.

7.2 Materials and Methods

7.2.1 Subjects

It is important to remark that this study is based on the data set collected for the first study. Here, the only change is the number of subjects and the amount of magnetometers in the scalp of them (147 nodes). Specifically, fourteen right handed patients with MCI were recruited. In addition, fourteen age-matched elderly participants without MCI were included as the control group. A summarized demographical information is stored in Tab. 7.1.

GDS		**LM1**		**LM2**	
Controls	MCIs	Controls	MCIs	Controls	MCIs
1	3	42.5 ± 8	19.1 ± 5	26.7 ± 7	13.1 ± 6

Sample(Sex)		**Age**		**MMSE**	
Controls	MCIs	Controls	MCIs	Controls	MCIs
14(9 Female)	14(9 Female)	70.6 ± 8.1	74.7 ± 3.6	26.75 ± 0.9	25 ± 1

Table 7.1: **Demographic and clinical information of the Control and MCI groups** [A14]. **MMSE**: Mini Mental State Exam (maximum score is 30); **GDS**: Global Deterioration Scale; **LM1**: Logical Memory immediate recall; **LM2**: Logical Memory delayed recall

The details about the legal written consent and the type of psychiatric and psychological tests are described in the box 2 (Subjects), of chapter 4. In the same way MEG technique was used to record cortical signals from the subject's scalp. Details about the MEG devise and the Sternberg memory test can be found in boxes 3 (Recordings) and 4 (Task & Preprocessing), respectively. In sum, a total of 14 MCIs and 14 control was used in this study. 147 electrodes were used in located in their scalp in order to capture MEG signals and, after all preprocessing methodology we randomly selected thirty-five epochs from those individuals with a higher number of valid epochs.

7.2.2 Consistency and Network Construction

Now the first step is to quantify how consistent the output of each channel is. This can be done by computing how coherent the outputs of the same channel are when the same task is carried out. With this aim, for each individual, we calculate the Synchronization Likelihood (*SL*) [A14, A211] between each pair of MEG time series within the same channel. While other measures to evaluate linear or nonlinear correlation between time series could have been used [A173], *SL* has proven an adequate measure for capturing the interdependencies between MEG time series obtained during a short-term memory tests [A29].

This way, we evaluate if the cortical activity measured at each channel during a positive identification of a letter is consistent, e.g., has similar temporal evolution when repeating the same task, despite the initial conditions are intrinsically different. We calculate the average of the pairwise *SL* of all non-repeated permutations of the 35 time series recorded within each magnetometer in order to get the Channel Consistency (CC). Note that the 35 time series of each channel are not combined but compared between them to extract the CC. At this stage, we have a dataset based on 147 CC values for the 14 subjects of the two different groups (MCIs and controls), which were used to build the corresponding parenclitic networks [A264].

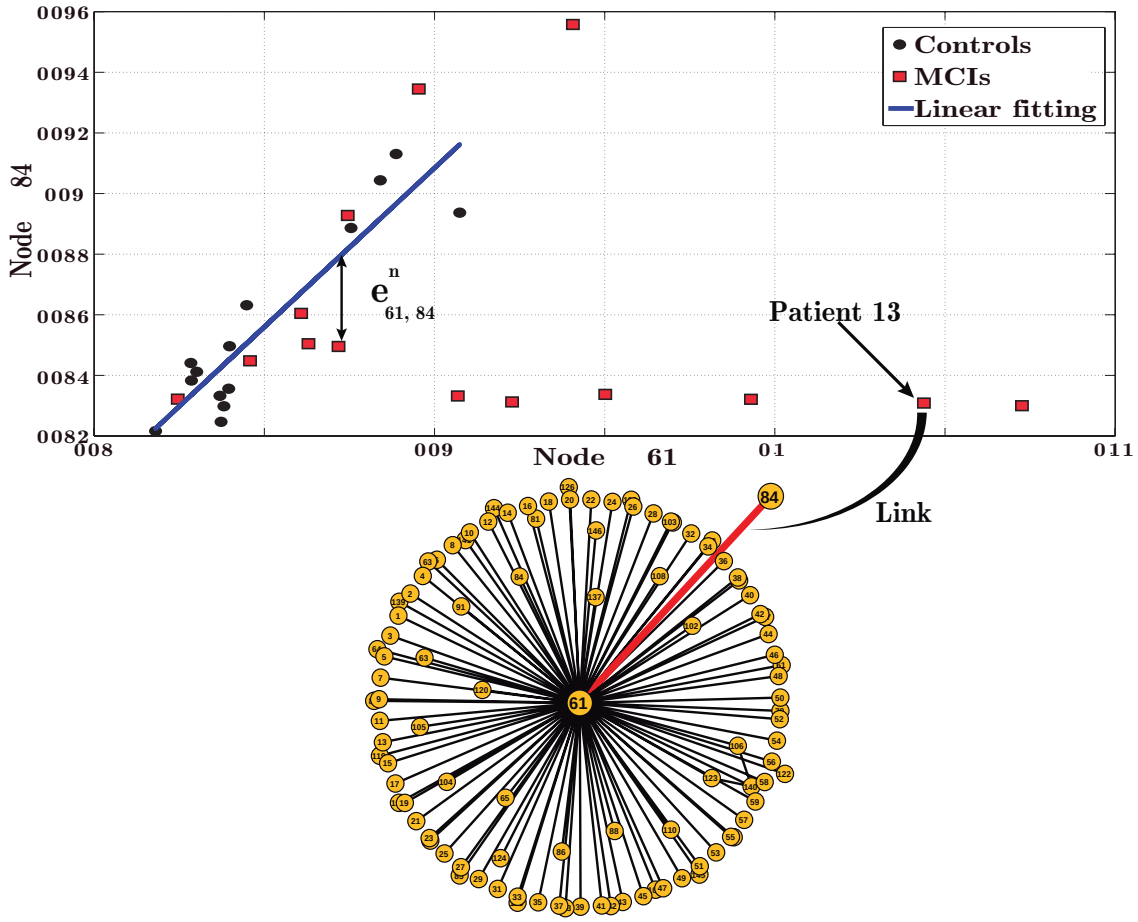

Figure 7.2: **Creating a parenclitic network.** The *channel consistency* (CC) of channels 61 and 84 (each one corresponding to a node of the parenclitic network) is plotted for the 14 controls (black circles) and the 14 patients suffering from MCI (red squares). A linear fitting of the CC pairs of the control group is calculated (blue line) and it will be taken as the reference for a normal behaviour. $e^n_{61,84}$ accounts for the deviation of CC from the reference value for the individual n. Each individual, will have its own parenclitic networks, where the weight of the link between nodes 61 and 84 is calculated as $Z^n_{61,84} = |e^n_{61,84}|/\sigma_{61,84}$, being $\sigma_{61,84}$ the standard deviation of the CC values from the reference line. This way, the larger the weight of the link the higher the deviation from the reference given by the control group. This procedure is repeated for each pair of channels, leading to a parenclitic network for each individual, whose links quantify how far is the consistency of a pair of channels from the normal behaviour. The bottom plot shows part of the parenclitic network of patient 13, specifically the neighborhood of node 61 once all pairs of channels underwent the same procedure.

The method for the network construction is explained in Fig. 7.2, which shows a specific example with channels $i = 61$ and $j = 84$. Black dots represent the CC of these two magnetometers for all control subjects and the blue line is their corresponding linear fitting. Note that there is no previous evidence that a linear correlation between the consistency of two independent channels exists, since, to the best of our knowledge, this is the first study obtaining networks from intra-channel consistency. Nevertheless, as we will see, assuming a linear correlation leads to a clear distinction between groups, based on statistical significant differences between the network parameters of the control and MCI groups.

Interestingly, assuming a correlation described by a second-order polynomial leads to the same qualitative results (not shown here). This is due to the fact that the number of points used to estimate the correlation function (fourteen in the absence of outliers) is low, since it is difficult to have large datasets of individuals. A combination of both kinds of correlations together with other non-linear methods to evaluate functional dependencies between nodes deserves its own study and it will probably depend on the kind of data and problem (disease) under investigation.

The errors of the control group are adjusted to a normal distribution in order to obtain its standard deviation $\sigma_{i,j}$. Once the standard deviation is obtained, we recalculate the correlation function excluding the outlier points of the control group. Individuals of the control group with an error higher than $2\sigma_{i,j}$ are assumed to be outliers and are not considered for the definition of the correlation function. This way we exclude 6030 outliers from all the $N(N-1)/2$ correlation diagrams, which represent the 4.2% of the total number of points. Importantly though, the outliers are considered when calculating the average properties of networks of the control. This allows taking into account variability inside the control group.

Red squares correspond to the CC of the same pair of channels for the 14 MCI patients. The deviation from the expected value given by the linear fitting is designated as the error $e_{i,j}$ of the joint consistency of channels i and j. The z-score of each pair of channels associated to a subject n will measure how far the consistency of both channels is from the expected value and it is obtained as $Z^n_{i,j} = |e^n_{i,j}|/\sigma_{i,j}$. The next step is to project the z-score dataset into a parenclitic network. In general, the links of a parenclitic network are created with a weight that is proportional to the deviations of a certain feature from an expected value [A264]. These networks are weighted and non-directed, and they unveil important topological differences between a reference group and a group with a certain anomaly [A260]. In our case, the nodes of the network will be the channels measuring the activity of a certain cortical region and the links between a pair of nodes i and j will be the z-score $Z^n_{i,j}$ measuring their deviation from its expected value.

The procedure followed to obtain the links and weights of nodes$i = 61$ and $j = 84$ is repeated for the CC of the $147 \times 146/2$ possible pairs of channels in order to obtain all links of the networks. This way, we obtain a weighted matrix which can be represented as a fully connected network. Finally, we need to apply a threshold in order to consider only those deviations that are relevant enough. The thresholding process consists in considering only the L links with higher weight, leading to a sparse matrix whose topology will be further analysed. Nevertheless, it is a delicate step, since a very low threshold will maintain spurious data that may hide the observation of the real network structure, while a very high threshold could dismiss valuable information.

In order to adequately set the threshold value, we repeated the analysis for different values of L and calculated the corresponding network parameters. Next, we identify the threshold that showed more differences between the network parameters of the control and the MCI groups [A263]. Specifically, we focused on the differences in the local $\bar{E}_l$ and global $\bar{E}_g$ efficiency, since the dependence of these parameters on the deletion of links is smoother than the clustering coefficient C or the shortest path length d [A131], and, in turn, showed a maximum difference around the same value of L.

After following this procedure, we finally consider only the $L = 400$ links with the largest $Z^n_{i,j}$ of each parenclitic network. This way, we obtain a set of weighted sparse networks for the control and MCI subjects with the same number of nodes N and links L. By computing a set of network metrics [B16], we are able to compare whether the networks differ in their topological organization and what are the kind of network structures associated to each group. All network metrics were statistically analysed on the basis of the mean differences between both populations and 5000 different permutations were performed in order to obtain the corresponding p value of each network metric.

7.3 Results

7.3.1 Degree, strength and hubs

Our first inspection of the network topology focuses on the local properties of its nodes. Specifically, we computed the highest degree K_{max} of the network, which is an indicator of the existence of network hubs. If we take into account the weight associated to the links, we can also compute the node strength $S(i)$. The maximum strength S_{max} and the average strength $\bar{S}$ of the networks are obtained as the maximum/average of $S(i)$ over all nodes.

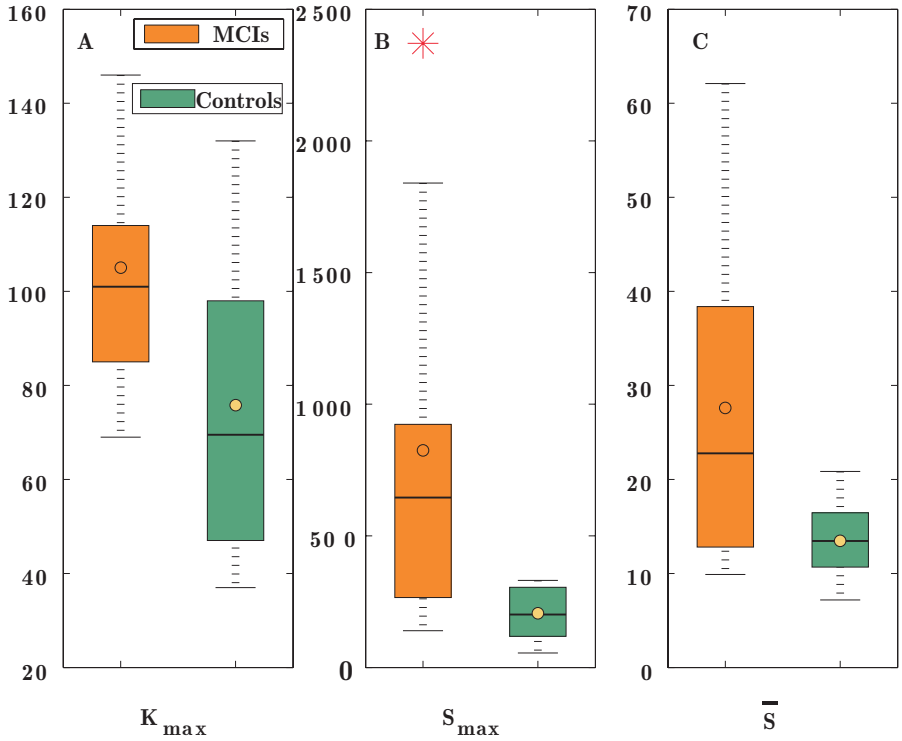

Figure 7.3: **Highest degree, maximum strength and average strength.** From left to right, box & whisker representation showing the first, second, third quartile and the average of: (A) the highest degree K_{max}, (B) maximum strength S_{max} and (C) average strength $\bar{S}$. Patient and control groups are orange and green, respectively. Red stars account for outlier values.

Figure 7.3 shows a comparison of the highest degree K_{max}, maximum strength S_{max} and the average strength $\bar{S}$ of the control and MCI groups. We use the *box & whisker* representation which highlights the main statistical quantities of the datasets, i.e., the first, second and third quartile and the mean. When looking at the highest degree K_{max} we can see how, in the MCI group, the mean, median (or second quartile), third quartile and, in general, all values are around 50 % higher than the corresponding values of the control group (Fig. 7.3A). This finding evidences the presence of hubs with higher number of links in the parenclitic network associated to the MCI group.

Figure 7.3B shows the maximum strength S_{max} for each group. Red stars are outliers that show that the maximum strengths of the MCI group follow not a normal but a skewed distribution. The behaviour of S_{max} remains similar to K_{max} and evidences that the existence of stronger hubs in the MCI group is reinforced when considering the weight of the links. Therefore both measures indicate the existence of certain nodes that accumulate large deviations in their expected value of consistency. Since the number of links is limited to $L = 400$ in both groups, the fact that large hubs

arise in the MCI networks also reveal the formation of more heterogeneous structures.

In Fig. 7.3C we plot the average strength $\bar{S}$ of the networks to confirm that the MCI patients have higher deviations from the reference value than the control individuals. As expected, the average strength of the MCI group $\bar{S}^{MCI} = 27.59$ is much higher than the control group ($\bar{S}^{control} = 13.49$), since the node strength accumulates the errors of all its links (i.e. the higher the strength of a node, the more anomalous its consistency is). The higher the value of $\bar{S}$, the larger the deviation of the overall consistency of the functional network. It is important to remark the difference between the maximum and average strength of both groups, which is much higher in the MCI group.

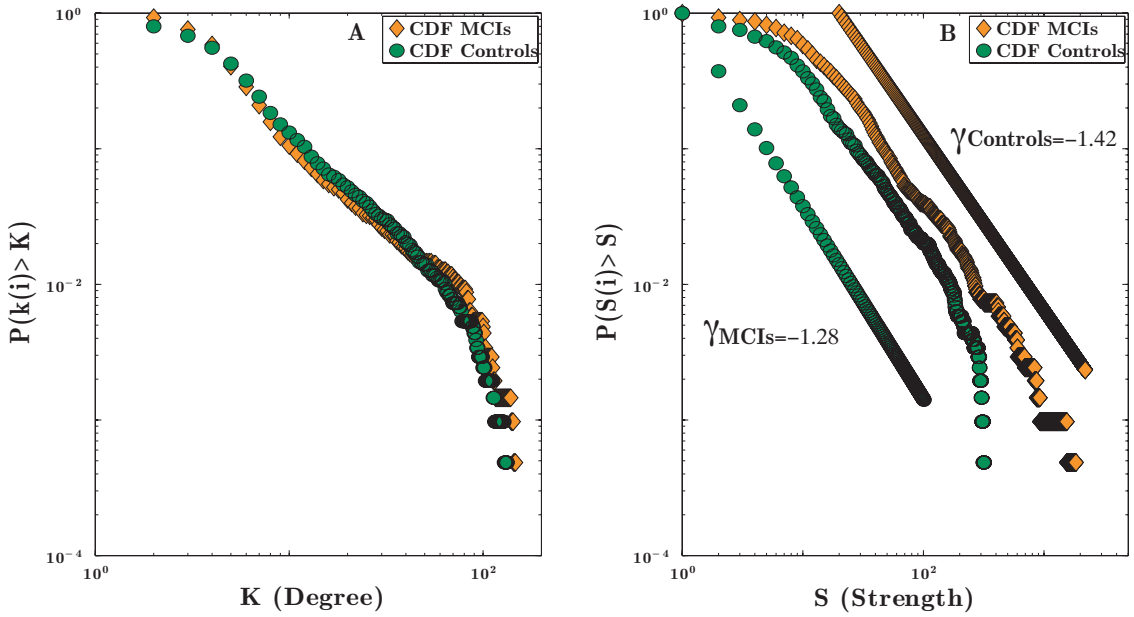

Figure 7.4: **CDF of the degree and strength distributions.** (A) Cumulative Distribution Functions (CDF) of the probability of finding a node with a degree (strength in (B)) higher than k (S in (B)). Green circles correspond to the control group and orange circles to the MCI group. When the strength of the nodes is considered (B), we obtain the power law distribution$P(S(i) \geq S) \sim S^{-\gamma}$ in both cases, as indicated by a straight line in the log-log scale.

Finally, we calculate the cumulative distribution function (CDF) of the degree and strength of the nodes both in the control and MCI groups. For each node i (i.e., a cortical region), we compute its corresponding average degree $\langle k(i) \rangle$. Next, we obtain the CDF by computing the percentage of nodes with a degree $\langle k(i) \rangle \geq k$. The same methodology is followed to calculate the CDF of the node strength $P(\langle S(i) \rangle \geq S)$. Both distributions are plotted in Fig. 7.4 with regard to the subjects of each group. Permutation t-test for the degree and strength CDFs was performed. Taking into account 5000 randomizations we found significant statistically differences in the strength distributions with a $p - value = 0.004$. Differences in the degree CDFs were not statistically significant ($p - value = 0.79$).

In figure 7.4A, we can observe how the degree distributions cross at $k_c = 40$ showing that nodes with a degree higher than k_c are more probable in the MCI group than in the control group. This confirms what the values of Kmax and Smax already suggested: a number of nodes in the parenclitic networks of the MCI group grossly deviate from their expected consistency.

The strength distribution spreads over three orders of magnitude and allows the CDF to show a power law decay $\sim k^{-\gamma}$. The exponent of the power law is lower in the MCI group ($\gamma^{MCI} = 1.28 < \gamma^{control} = 1.42$) which reveals the existence of hubs with a larger strength. These

hubs play a relevant role in the structure of the network, since they accumulate a higher percentage of the link weights: they are the core of the divergences with respect to the normal (healthy) values of consistency.

7.3.2 Local vs. Global Properties

Next, we calculate local (clustering coefficient $\bar{C}$ and local efficiency $\bar{E}_l$) and global (average path length $\bar{L}$ and global efficiency $\bar{E}_g$) properties of networks. Regarding to clustering, c_i is calculated using a generalization of this metric for weighted networks [A167].

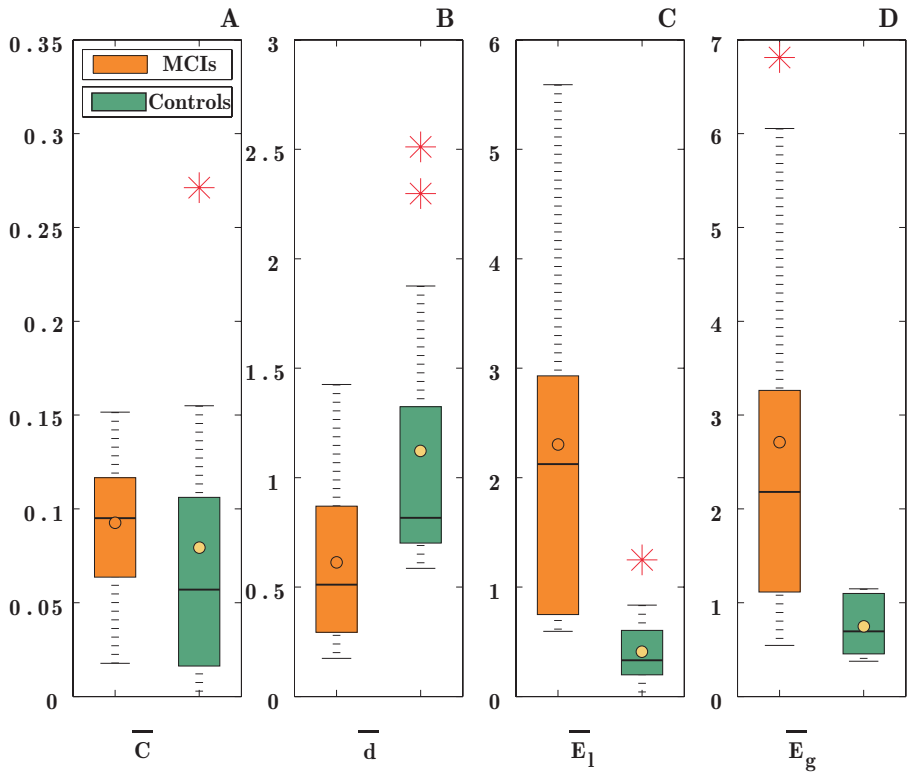

Figure 7.5: **Clustering, shortest path length, local efficiency and global efficiency.** Box & whisker representation of: (A) the clustering $\bar{C}$, (B) shortest path length $\bar{d}$, (C) local efficiency $\bar{E}_l$ and (D) global efficiency $\bar{E}_g$. Orange and green bars correspond, respectively, to the MCI and control groups. Red stars are the outlier values. P-values of the network parameters are given in Table 7.2.

c_i was then averaged over the whole network to obtain the clustering coefficient $\bar{C}$ per individual. Figure 7.5A shows $\bar{C}$ for the two groups under study. We can observe how the MCI network has a largest clustering coefficient, indicating a higher density of connections at the local level. Interestingly, the clustering coefficient is also an indicator of the network randomness since random networks have a value of $\bar{C}$ close to zero. Thus, the lowest value of $\bar{C}$ of the control group indicates that its network topology is closer to a random structure.

Now let us have a look at a global property of the network: the average shortest path $\bar{d}$. To obtain the value of $\bar{d}$ we first calculate the distance matrix D for all parenclitic networks. Each $d_{i,j}$ element of the D matrix is the shortest path between nodes i and j (i.e., the lowest combination of links' lengths to go from i to j), which is calculated using the Dijkstra's algorithm [A65]. Finally, the average shortest path $\bar{d}$ is just the average of all elements of matrix D. Figure 7.5B shows that the MCI group has a lower value of $\bar{d}$, which is a consequence of having higher weights (i.e.,

shorter distances), since, as we have seen, $\bar{S}^{MCI} > \bar{S}^{control}$. Parenclitic networks are capturing how alterations of the expected consistency are distributed over the whole network and, therefore, the low value of $\bar{d}$ reveals that the loss of consistency propagates with a shorter number of steps in the MCI group. That is not good news for the resilience of the consistency when MCI emerges.

Both parameters $\bar{C}$ and $\bar{d}$ can be reinterpreted in terms of how efficient is the network when transmitting information from one node to any other in the network. By other hand, high values of local/global efficiency indicate a good transmission of information (at the local/global scale) in terms of the number of steps.

Figures 7.5C-D show the local $\bar{E}_l$ and global $\bar{E}_g$ efficiency for both groups. We can observe how in both cases the efficiency is higher in the MCI networks, which indicates that the network of dysfunctions is better organized.

$\mathbf{K_{max}}$ ($p = 0.016$)		$\mathbf{S_{max}}$ ($p = 0.0002$)		$\bar{\mathbf{S}}$ ($p = 0.004$)	
Controls	MCIs	Controls	MCIs	Controls	MCIs
75.78	105	206.27	824.30	13.49	27.59

$\bar{\mathbf{C}}$ ($p = 0.562$)		$\bar{\mathbf{d}}$ ($p = 0.012$)		$\bar{\mathbf{E}}_\mathbf{l}$ ($p = 0.0002$)		$\bar{\mathbf{E}}_\mathbf{g}$ ($p = 0.0002$)	
Controls	MCIs	Controls	MCIs	Controls	MCIs	Controls	MCIs
0.08	0.09	1.12	0.61	0.40	2.30	0.74	2.70

Table 7.2: **Summary of the network metrics for the control and MCI groups**. Highest degree $\mathbf{K_{max}}$, maximum strength $\mathbf{S_{max}}$, average strength $\bar{\mathbf{S}}$, clustering $\bar{\mathbf{C}}$, average shortest path $\bar{\mathbf{d}}$, local efficiency $\bar{\mathbf{E}}_\mathbf{l}$ and global efficiency $\bar{\mathbf{E}}_\mathbf{g}$. The p-value of each metric is also indicated.

Table 7.2 summarizes the average of all network metrics. Note that despite the classical definition of C, d, E_l and E_g constrain the values of these to the interval [0,1] [B16], the fact that we are using weighted connectivity matrices, which contain more information about the interdependency between nodes, leads to values that can exceed this range [A188]. A comparison between control and MCIs group, for each network parameter, was developed via a non parametric Kruskal Wallis test, where we have computed the $p-values$ (5000 permutations each) that illustrate how significant the statistical differences are.

7.3.3 Localizing Focal Nodes

Anomalous networks allow detecting those nodes whose features (consistency in our case) diverge the most from the expected behaviour. This task is carried out by finding the network hubs and quantifying their importance. With this aim, we calculate the degree $k(i)$, strength $S(i)$ and eigenvector centrality $ec(i)$ of nodes belonging to both populations, all these metrics commonly used as quantifiers of the network hubs. The later one, $ec(i)$, is calculated from the eigenvector associated to the largest eigenvalue of the weighted connection matrix W whose elements are, in our case, $Z_{i,j}$.

We proceed as follows: two vectors $\vec{k}_{MCI}$ and $\vec{k}_{control}$ of length $N = 147$ (one element per node) contain the average degree of the nodes of each specified group. The difference of the elements of both vectors $\Delta\langle\vec{k}_{MCI,control}\rangle = \vec{k}_{MCI} - \vec{k}_{control}$ accounts for the difference of node degree between

both groups and reflects what nodes increase (or decrease) their importance in the network. Figure 7.6A shows $\Delta\langle\vec{k}_{MCI,control}\rangle$, where two peaks stand out over the rest of the degree variations. Nodes 32 and 61 have a much higher degree in the MCI parenclitic networks than in the control ones. This fact indicates that these two nodes accumulate the majority of variations related to the consistent behaviour.

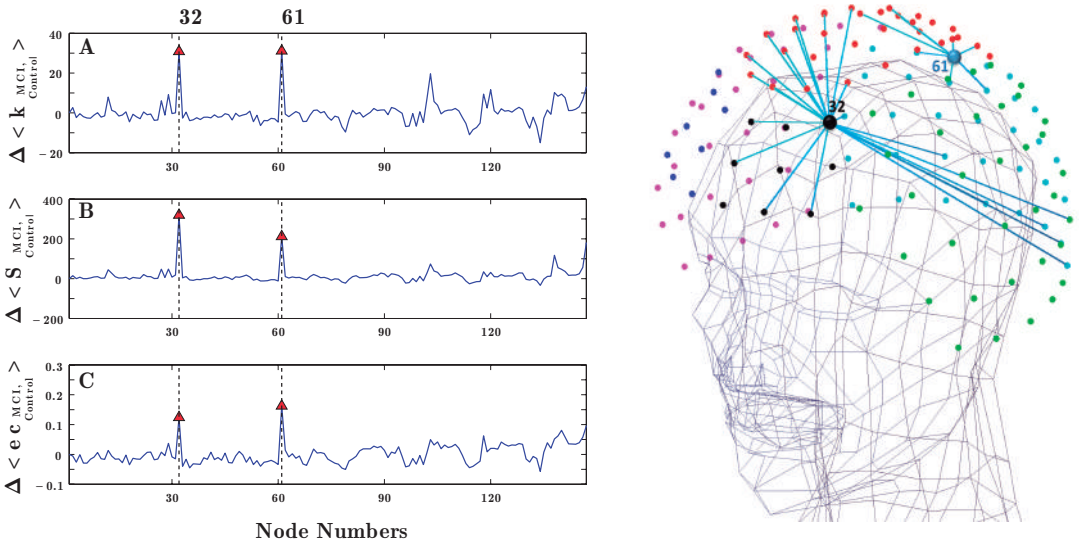

Figure 7.6: **Localizing focal nodes in the consistency impairment**. We calculate the differences in the node degree $k(i)$ (A), node strength $s(i)$ (B) and eigenvector centrality $ec(i)$ (C). In all cases, nodes 32 and 61 accumulate the highest variations, indicating that are the nodes whose consistency is affected the most by the disease. (We computed these same differences with another metrics but only the aforementioned ones showed relevant differences respect to control group) On the right plot, we show the position and the local network of connections of these two nodes, where only the 30 links with higher weights have been plot.

In a similar way, we obtain the variations of the strength $\vec{S}_{MCI,control}$ and eigenvector centrality $\vec{ec}_{MCI,control}$. Figure 7.6B-C shows the difference between groups of these two metrics $\Delta\langle\vec{S}_{MCI,control}\rangle$ (B), $\Delta\langle\vec{ec}_{MCI,control}\rangle$ (C). Independent of the metric, again two peaks appear at nodes 32 and 61, confirming that they are the nodes whose consistency is affected the most by the disease. It is worth noting that these two nodes are not necessarily those nodes whose consistency increased/decreased the most. Node 61 has an 8.14% variation in its consistency (#4 in the raking of consistency variations) and node 32 around 2.71% (#25 in the consistency variation ranking). This fact indicates that parenclitic networks go beyond the local changes of consistency and account for the way variations affect the interplay, based on consistency, between nodes.

In Fig. 7.6 we plot a 3D representation of these *focal nodes* together with their local network of interactions. This plot shows the local basin of influence of the network hubs and gives an idea about where the disease is being more severe, at least when consistency is taken into account. It is valuable to compare the position of the most affected nodes with previous results on how MCI affects functional networks. In Buldú et al. [A29], it was shown that both the frontal and the occipital lobes contain those nodes of the functional network whose synchronization with other parts of the network was most impaired. Interestingly, these two lobes also contain the two nodes that the consistency-based parenclitic networks revealed to be most affected by MCI. Comparing both results we observe that, despite being in the different lobes, nodes 32 and 61 are not the hub nodes of the functional network, nor are they the nodes whose local properties inside the

functional networks were most modified by the disease. This fact indicates that, with the projection of brain dynamics into parenclitic networks, we are evaluating a different effect of the disease on the functioning of the brain network.

7.4 Discussion

It is worth mentioning that although we assumed a linear correlation between the channel consistencies, we have not proved that this fitting is the one capturing the real interplay between the consistency of brain regions. Further studies should be devoted to investigating the existence, or co-existence, of higher order correlation functions, although we obtained similar results with a second-order polynomial adjustment (not shown here). In any case, we demonstrated that assuming a linear correlation leads to differences between groups and allows identifying the nodes whose topological properties are affected the most by the emergence of the disease.

In the current work, we are concerned with another type of consequences of the emergence of MCI: the loss of a consistent response [A237], i.e., in our case, the impairment of the ability of a cortical region to behave in the same way when undergoing the same cognitive task, despite having different initial conditions. We have taken advantage of a new kind of network representation, the parenclitic network [A264], where a link between two nodes quantifies the deviations of a certain feature of these nodes from an expected (healthy) behaviour. We have measured the consistency of 147 cortical brain regions by means of MEG and constructed a parenclitic network capturing dysfunctions of the expected consistency.

The analysis of the topological features of a control group of healthy individuals and a group of MCIs shows that the parenclitic networks can provide useful information to evaluate how disease alters the consistency between cortical regions. First, we report a higher network strength in the MCI group when the same number of links are considered in both groups. This fact indicates higher deviations from the expected consistency performance in the MCI group. Furthermore, we observe the appearance of strong hubs in the patients group, which reveals that the disease is specially severe at certain cortical regions. Specifically, nodes 32 (frontal lobe) and node 61 (occipital lobe) are detected to be the focal points of the consistency impairment.

Nevertheless, the loss of consistency is not restricted to certain specific regions. This is reflected by the fact that global network parameters such as the average path length or global efficiency also capture differences between the control and the MCI group. On the contrary, the number of steps needed to go from one node to any other in the parenclitic network is much lower in the MCI group, which indicates that the disease alters network consistency in quite a fundamental way.

At the local scale, the MCI group shows high values of clustering and local efficiency of the parenclitic network indicating that inconsistency does not emerge in isolated regions but in groups of densely interconnected nodes.

Finally, we have also seen that the networks associated to the control group are more random than those of the MCI group, which has been demonstrated to be a common signature of parenclitic networks in preliminary works [A260], [A264]. It is important to highlight that the control networks are not purely random in the sense of the definition given by Erdös-Renyi [B16], but their network properties are closer to random networks when compared with the MCI. Similarly, the MCI networks are closer to star-like networks, despite having more than one central hub and connections between their peripheral nodes.

To the best of our knowledge, this is the first result concerning the construction of parenclitic networks to understand brain functioning and specifically the effect of a neurodegenerative disease. We believe that this technique could be extremely useful to evaluate how different brain diseases deteriorate the normal functioning of the brain activity.

Although parenclitic networks unveil part of the inner dynamics of cortical regions, it is possible to account for another type of non linear metrics to better capture the dynamics of such cortical

regions. In fact, this is the topic of the last study in the next chapter, in which we consider to search for dynamical properties of such cortical activations that, independently from the network construction, correlate with the topological properties of the networks. In other words, we will evidence a correlation between the dynamics *of* the networks and the dynamics *on* the networks in a specific case.

8 Cognitive Reserve

§

The dynamics of the individual systems forming a network have been largely investigated through the combination of nonlinear dynamics and network science. More recently, the focus has been also put on the dynamics of networks themselves, consisting on studying how their structure and topology evolve in time. Nevertheless, despite several works on coevolutionary adaptive networks have analyzed the interplay between topology and dynamics, both innate characters of complex networks, have been commonly studied independently, disregarding the possible bridges between them. In this Chapter, we propose an analysis of functional brain networks that takes into account both the topological features of the nodes and their dynamical properties. We use brain signals obtained from magnetoencephalography (MEG) to investigate how the cognitive reserve, a neuropsichological construct associated to the ability of optimizing cognitive processes, is related to the level of studies a person has. With this aim, we compare the functional networks of two clinical datasets of healthy individuals with different educational attainments. On the one hand, we analyze the topological properties of their functional networks. On the other hand, we quantify two of the main dynamical properties of the times series of each individual: the entropy and the complexity. In this way, the Shannon's permutation entropy and the statistical complexity are calculated for all time series by means of temporal ordinal patterns. Next, we compare the topological and dynamical properties of the nodes of both groups of individuals. Interestingly, we report statistical significant differences between individuals with different level of studies both in the topological and dynamical parameters. At the same time, our results also show an interplay between the topological role a nodes has and its dynamical properties: hubs are prone to have higher entropy than peripheral nodes, while the complexity behaves in the opposite way.

§This chapter is based on the unpublished work entitled: ***Dynamics-Structural Interplay Patterns in Brain Networks Reveals Neural Correlates Organization in Cognitive Reserve.***. *A collaborative work with the Laboratory of Cognitive and Computational Neuroscience at Centre of Biomedical Technology. CTB-UPM.*

8.1 Introduction

Cognitive reserve consists on the ability of the brain to maintain its functionality when facing ageing or brain damage [A222]. The educational attainment has been one of the several factors related to the enhancement or maintenance of such a cognitive reserve [A223]. Notwithstanding, it has been difficult to quantify to what extent the educational level can postpone the consequences that ageing has on brain functioning. Epidemiological studies found that individuals with lower education levels had higher risk of developing Alzheimer's disease (AD), while individuals with higher education levels showed less chance of developing AD, however, more rapid decline of cognitive function when they got AD [A221]. Only recently, the analysis of the topology of the associated functional networks has been proposed as an alternative way of quantifying cognitive reserve [A250]. In that work, the existence of multiple paths between brain sites was shown to be related to the level of cognitive reserve. In this Chapter, we further investigate the interplay between the topology of functional brain networks and cognitive reserve, adding an additional point of view to better tackle the analysis: the dynamical features of brain regions. With this aim, we record the cortical activity of two groups of individuals with different educational level, in particular, nine Bachelor's graduate subjects (BG) and eleven School graduate individuals (SG). Both groups carry out a memory Sternberg task, where the subject has to recognize a letter from a previously memorized set of four letters [A224]. The cortical activity is recorded by means of a magnetoencephalograph, which has 148 magnetometers, each one acquiring the signal at different positions of the scalp. Recorded signals undergo two different analysis: (i) we construct and analyze their associated functional networks, reporting differences between both groups and (ii) we calculate the entropy and complexity of each brain region and correlate them with the topological properties of the nodes. As we will see, combining both analysis we found differences between both groups indicating that the higher cognitive reserve of the BG group can be quantitatively evaluated by the functional network parameters. Furthermore, we report a negative correlation between the topological importance of the nodes and the complexity of their associated signals. Conversely, when the entropy of the signal is analyzed, the correlation with the node importance becomes positive.

8.2 Materials and Methods

8.2.1 Subjects and Recordings

Again, the dataset comes from the same experiment performed and explained in Chapters 4 and 7. The details about the legal written consent and the type of psychiatric and psychological tests can be found in Box 2 (Subjects) of Chapter 4. Details about the MEG device and the Sternberg memory test can also be found in Boxes 3 (Recordings) and 4 (Task & Preprocessing), respectively. Here, the only difference is that we will only select a set of healthy people, which is divided according to their educational attainment. In this way, one group comprises 9 subjects with accomplished undergraduate studies (BG) and the other group has 12 individuals without undergraduate studies (SG). Individuals, with 148 magnetometers in their scalps, repeated 35 times (trials) the memory task, leading to 35 matrices containing 148 MEG time series, each of them with 230 sample points.

8.2.2 Building the functional networks

The construction of the functional networks associated to each individual requires a series of steps transforming brain signals into complex weighted networks. Specifically, the methodology is summarized in the following 3 steps:

1. We select a set of 35 trials for each individual, since it is the lowest number of successful trials for all subjects in the study. Each trial consists of the time series of 148 channels.

2. The coordination between all possible pairs of channels, within each trial, is quantified by means of the Synchronization Likelihood (*SL*) algorithm (see Material and Methods in Chapter 4 for details). All pairs of *SL* are then included into a correlation matrix $\mathbf{W}\{w_{ij}\}$ where w_{ij} have values comprised between ~ 0.05 and~ 0.5.
3. We apply a linear normalization that leads to a probability matrix $\mathbf{P}\{p_{ij}\}$, where the values of p_{ij} are obtained as $p_{ij} = \frac{w_{ij} - min[w_{ij}]}{max[w_{ij}] - min[w_{ij}]}$. In this way, the probability matrix $\mathbf{P}\{p_{ij}\}$, whose values are within the interval [0,1], reflects the probability of the presence of a link between nodes (brain regions) i and j. This normalization allows to adapt the classical methodologies of unweighted networks to their weighted counterparts and, as a consequence, the information included in the weak ties is maintained. In addition, the normalization facilitates the comparison among networks obtained from different individuals.

Following these three steps we arrive to a set of 9 networks (1 for individual) for the BG group and 12 for the SG group with $i = 1, 2, ..., 148$ nodes each. Next, we calculate a series of metrics related with the role of the nodes within the network: the strength $s(i)$, the weighted clustering $c_w(i)$, the eigenvector centrality $ec(i)$, the strength of the nearest neighbours $s_{nn}(i)$ and the outreach $o(i)$. Another parameters such as the within-module degree $z(i)$ (also kwon as the z-score) and the participation coefficient $p(i)$[A30, A94] are also computed using the community affiliation vector $C_{com}(i)$ extracted from the classical partition of the brain into six lobes: frontal-right, frontal-left, central, temporal-left, temporal-right and occipital. A series of global network features such as the global efficiency E_g and the average shortest path d were also calculated. The *node average* (average along the same node for all subjects within the same group) of several metrics was computed to obtain the following mean values: $\bar{s}(i)$, $\bar{c}_w(i)$, $\bar{ev}(i)$, $\bar{z}(i)$, $\bar{s}(i)_{nn}$ and $\bar{o}(i)$. Finally, network averages of the preceding features were also appraised in order to compare both groups.

8.2.3 Normalized network parameters

We will to construct a set of randomized versions of the former functional networks, in order to evaluate to what extent the deviation of the network parameters between groups are a consequence of a topological reorganization or, on the contrary, just a matter of the number of links and their weights. With this purpose, we generate a group of 100 networks for each of the functional network an individual has. The randomization maintains the value of the links' weights by reshuffling the components of the weighted probability matrix $\mathbf{P}\{p_{ij}\}$. In this way, we guarantee that the average strength of the network is maintained. Next, we calculate the network parameters for each of the randomized versions and obtain an average value of each metric. Finally, we normalize all network parameters with the average of the set of surrogate matrices, i.e., for a parameter X its normalized value would be $\hat{X} \sim \frac{X}{X_{ran}}$.

8.2.4 Evaluating the dynamical properties of the nodes

We are going to quantify the dynamical properties of the brain regions by computing the entropy and complexity of their associated time series. With this aim, each of the nodes of the network will be related to a times series comprising the 35 trials of the whole experiment. Since each trial has 230 time steps, we will obtain times series of $M = 8050$ points for each node of each functional network.

Next, we will apply the methodology introduced by Bandt and Pompe [A15] to quantify the dynamical properties of nonlinear dynamical systems. This methodology is based on the analysis of the probability distribution of symbol sequences associated to an order according to the amplitude of the signals (see section: Ordinal Patterns and Stochastic Analysis in Chapter 1). In this way, it is possible to capture "the memory" of the dynamical system implicitly encoded on its temporal patterns, which are also known as *ordinal patterns*. We chose a memory lapse of $D = 6$ to trace the ordinal patterns of each node. In other words, we select a value of the embedding dimension D

that defines the accessible states an ordinal pattern has, which could be repeated (or not) along the temporal evolution of the system. Once the ordinal patterns are calculated for the whole time series, the probability distribution P of these ordinal patterns is obtained.

In Chapter 1 we described how the dynamical properties of the node activity can be appraised through the use of the ordinal pattern measures $\{H,Q,C\}$ calculated upon the probability P. This set of measures quantifies both the stochasticity and complexity of a given time series [A180]. Normalized permutation entropy $H[P] = S[P]/Smax$ [A185], captures the level of uncertainty of a signal. Here, S is the Shannon's entropy and $Smax = \log(N)$ is the maximum level of entropy due to the assumption of an equilibrium distribution $\{Pe = \frac{1}{N}\}$,where N is the number of all possible ordinal patterns (appearing, or not, in the time series). The disequilibrium Q is a measure to evaluate how far the distribution of patterns is from a pure random distribution and it is computed using the Kulback divergence [A128]. In this way, $Q[P]$ discriminates between Pe and P distributions, being zero for a non discriminative observation between both distributions.

The product $C[P] = H[P]Q[P]$, known as the statistical complexity [A138], combines both the entropy of the ordinal pattern distribution with the disequilibrium. This measure has been shown to effectively quantify the complexity of different dynamical systems and it is specially robust for evaluating signals with a high amount of noise [A261]. Interestingly, these set of measures have been applied to characterize EEG signals [A254], but its application to MEG data has not been documented yet.

8.3 Results

8.3.1 Micro-scale: Differences at the node level.

We are going to evaluate the role a node plays within the functional network, for the two groups under study. We will pay special attention to the hubs of both groups, trying to find differences in the position of the leading nodes when both groups are compared.

Our first approach to characterize the role of the nodes is based on the calculation of the eigenvector centrality $\bar{ev}(i)^{BG,SG}$ of the nodes. Figure 8.1 shows the position of the 10 nodes with the highest eigenvector centrality in both groups.

At first sight, Figure 8.1 shows that both groups have the most influencing nodes placed at the same cortical region (i.e., at the occipital lobe). Nevertheless, we observe signs of a displacement of the node centrality toward the central and left-temporal lobes. In order to quantify the differences between groups, we obtained the average difference of the node centrality of both populations as $\Delta\bar{ev}(i) = \bar{ev}(i)^{BG} - \bar{ev}(i)^{SG}$. At the same time, we identified those nodes that had statistically significant differences between the $ev(i)$ of each group ($p_{val} \leq 0.05$, using a non parametric Kruskal-Wallis test). This procedure was also repeated for the averages of the within-module degree $z(i)$ and participation coefficient $p(i)$ of each node obtaining $\Delta\bar{z}(i)$, $\Delta\bar{p}(i)$, respectively.

We have summarized all these metrics in Fig. 8.2, where the 148 nodes of the functional network are plot in a two-dimensional space. In this figure, only those nodes with statistically significant differences ($p_{val} \leq 0.05$) have been marked with a circle, whose size is proportional to the values of $\Delta\bar{ev}(i)$ (**A**), $\Delta\bar{z}(i)$ (**B**) and $\Delta\bar{p}(i)$ (**C**). Green circles show those nodes where the average of BG population is higher than the SG group, otherwise nodes are circled in red. For example, Fig. 8.2A shows an increase of the eigenvector centrality of the BG group in the central lobe, near the parieto-occipital sulcus, as well as some tiny regions in frontal lobe (i.e., $\bar{ev}(i)^{BG} > \bar{ev}(i)^{SG}$ and subsequently, $\Delta\bar{ev}(i) > 0$). Conversely, cortical tissue placed at the left-temporal and occipital lobes increase their centrality in the SG population (i.e., $\Delta\bar{ev}(i) < 0$).

Panels showing $\Delta\bar{z}(i)$ (Fig. 8.2B) and $\Delta\bar{p}(i)$ (Fig. 8.2C) have less nodes with statistically significant differences, specially in the case of $\Delta\bar{p}(i)$. Nonetheless, there is a slight tendency of the lateral and posterior parts of brain to accumulate those regions that have statistically significant

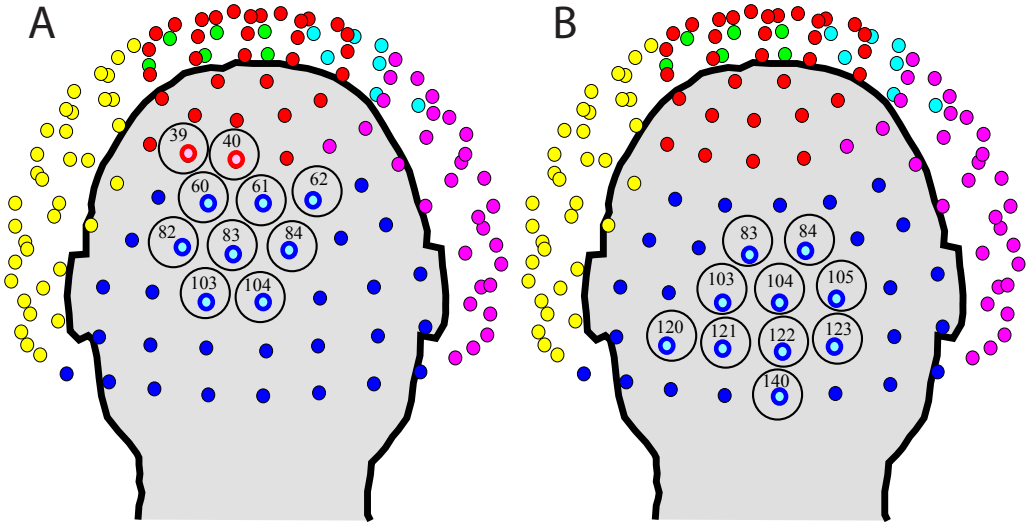

Figure 8.1: $\bar{ev}(i)$ **for BG and SG groups**. Back view for $\bar{ev}(i)^{BG}$ (**A**) and $\bar{ev}(i)^{SG}$ (**B**). Colors represent different brain lobes. Surrounded circles highlight the ten nodes with the highest $\bar{ev}(i)$. Note that they are localized close to the occipital lobe in the SG group and slightly shift toward the central lobe for the BG group.

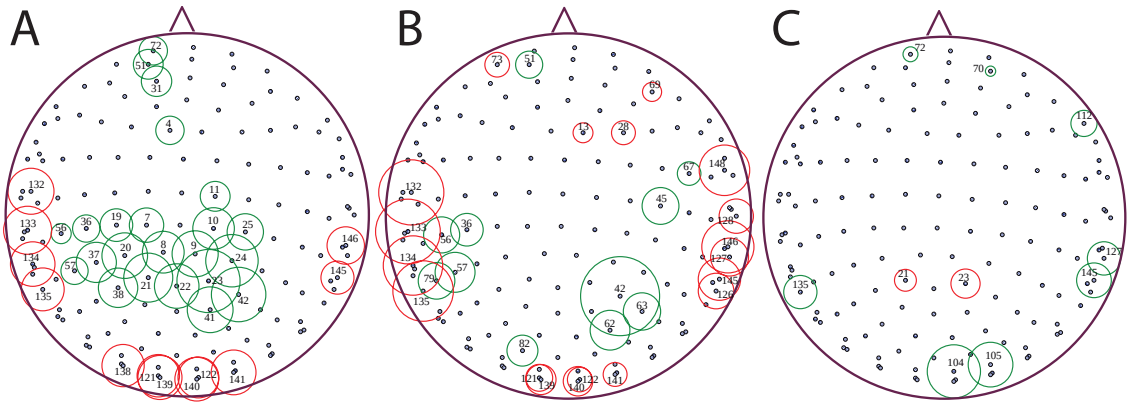

Figure 8.2: **Differences between BG and SG groups at the node level.** Black dots indicate the Euclidean position of the 148 magnetometers (nodes). Circles show those nodes with significant statistical differences in the: eigenvector centrality $\Delta\bar{ev}(i)$ (A), within-module degree z-score $\Delta\bar{z}(i)$ (B) and participation coefficient $\Delta\bar{p}(i)$ (C). Green (Red) circles represent nodes that have an increase (decrease) of the mean differences. Circle sizes are proportional to the absolute value of the differences.

differences. These results indicate the importance of the lateral (specially the lateral-left) and occipital lobes when a partition between lobes is considered (note that both $\bar{z}(i)$ and $\bar{p}(i)$ rely on this particular partition).

Still at the micro-scale, i.e. at the scale of the nodes and their properties, we have investigated how the strength of a node correlates with the strength of its neighbours, trying to quantify wether a correlation of the nodes' strengths exist. With this aim, we calculate the nearest neighbours strength $s_{nn}(i)$ as the average strength of a node's neighbours. Figure 8.3 shows the correlation between $\bar{s}_{nn}(i)$ and $\bar{s}(i)$, both for SG and BG groups of subjects. Also in Fig. 8.3 , we plot the $s_{nn}(i)$

obtained by a randomization of the original networks, to better observe how the topology of the real functional networks influences the value of $s_{nn}(i)$. We can observe the positive correlations of $\bar{s}_{nn}(i)$ vs. $\bar{s}(i)$, no matter what the level of studies is. The positive correlation reveals that nodes with higher strength are prone to be linked to nodes with higher strength, what is known as assortative mixing [A159]. This kind of behaviour is not reported in randomly distributed networks, as can be seen with the randomized version of the networks, where no correlation is reported (see Fig. 8.3). Note that, the only difference between both groups is that the SG has highest values of $s_{nn}(i)$, nevertheless, the fact that the slopes are similar suggests that this difference could be attributed just to an enhance of the average value of the network strength instead of being an effect of a reorganization of the network topology (which is actually the case, as we will see in the following Section).

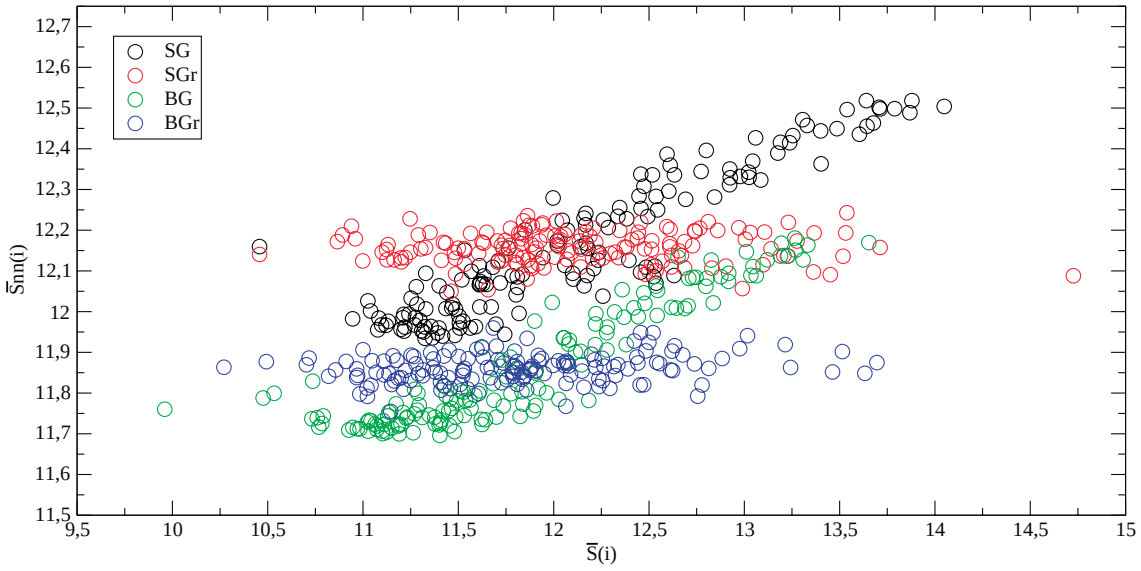

Figure 8.3: **Average strength of the nearest neighbours**. Correlation between the strength of a node $\bar{S}(i)$ and the strength of its nearest neighbours $\bar{S}_{nn}(i)$. Black circles represent the SG group, while green circles are the BG group. Red and blue circles are the average strengths of the randomized versions of the SG BG groups, respectively. We can observe a positive correlation in the case of the real functional networks, indicating that, in both groups, networks are assortative. (This is for the case of the average subject)

8.3.2 Macro-scale: Analyzing the topology of the whole network

Now let us move to a higher “topological" scale and analyze how the average network parameters are modified according to the level of studies an individual has. We have calculated six network parameters for each subject and obtained the average value for both the SG and BG groups. The six parameters under study are: the network strength $\bar{S}$, the outreach $\bar{O}$, the weighted clustering coefficient C_w, the average neighbour strength $\bar{S}_{nn}$, the global efficiency $\bar{E}_g$ and the average shortest path $\bar{d}$. Figure 8.4 shows the average network parameters for each group and their respective standard deviations. We can observe how the global strength, the outreach, the weighted clustering, the strength of the nearest neighbours and the global efficiency, have higher values in the SG group than in the BG group and, as a consequence the shortest path has lower ones (see Tab. 8.1). These increases of the former network parameters can be explained by the enhancement of the average network strength, which strongly determines the behaviour of the rest. The increase of

the average network strength in the group of individuals with lower level of studies reveals that a higher synchronization between cortical regions is requested in order to successfully perform the memory test. The increase of the average network strength have been already reported in individuals suffering from mild cognitive impairment and it has been associated to a higher energetic effort when carrying out a certain cognitive task [A30]. In this way, our results show how individuals with lower level of studies have a higher energetic cost when performing a memory task.

Nevertheless, due to the small size of the the group under study, it is important to check wether the results shown in Fig. 8.4 are statistically significant or not. With this aim, we carried out a Kurkal-Wallis test comparing both populations and summarized the results in Tab. 8.2. The p-values (p_{val}) are the percentages ($(1-p_{val})*100\%$) of significant differences between populations, e.g. a $p_{val} = 0.030$ in the network outreach indicates a 97.0% difference between the average outreach of both populations, reflecting that, according to the values of Tab. 8.1, $\bar{O}^{SG} > \bar{O}^{BG}$, is statistically significant. Therefore, the lower the p-value is, the more significant the differences between groups are. In the context of functional networks, parameters with p-values lower than 0.05 are accepted to be statistically significant. Thus, only the network outreach $\bar{O}$ and the average shortest path $\bar{d}$ successfully pass the statistical test, what makes these network parameters to be the most relevant when evaluating differences in the cognitive reserve of individuals with different level of studies.

Group	$\bar{S}$	$\bar{O}$	$\bar{C}_w$	$\bar{S}_{nn}$	$\bar{E}_g$	$\bar{d}$
SG	13.78	13.57	0.102	13.96	0.096	12.69
BG	12.65	12.29	0.093	12.76	0.089	14.12

Table 8.1: **Average network parameters for the SG and BG groups** Average network parameters for the School degree (SG) and Bachelor degree (BG) groups. Specifically, the network strength $\bar{S}$, the outreach $\bar{O}$, the weighted clustering coefficient C_w, the average neighbour strength $\bar{S}_{nn}$, the global efficiency $\bar{E}_g$ and the average shortest path $\bar{d}$.

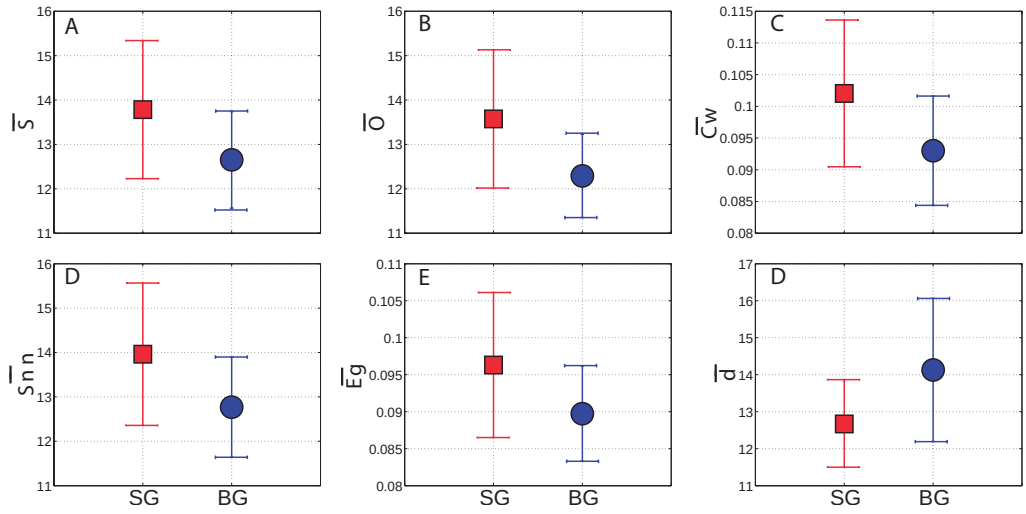

Figure 8.4: **Average network parameters for the SG and BG groups.** Average network parameters for the School degree (red squares for SG) and Bachelor degree (blue circles for BG) groups. Specifically, the network strength $\bar{S}$ (A), the outreach $\bar{O}$ (B), the weighted clustering coefficient C_w (C), the average neighbour strength $\bar{S}_{nn}$ (D), the global efficiency $\bar{E}_g$ (E) and the average shortest path $\bar{d}$ (F).

	$\bar{S}$	$\bar{O}$	$\bar{C}_w$	$\bar{S}_{nn}$	$\bar{E}_g$	$\bar{d}$
p_{val}	0.075	0.030	0.089	0.064	0.105	0.044

Table 8.2: **Statistical significance of the network parameters**. P-values (p_{val}) of the Kruskal-Wallis tests of the paramters shown in Fig. 8.4. Only the network outreach $\bar{O}$ and the average shortest path $\bar{d}$ have a $p_{val} < 0.05$.

8.3.3 Dynamical Analysis of MEG Time Series

Our next step leaves the topology of the functional network aside and concentrates on the dynamical properties of the nodes. We are going to quantify the entropy and complexity of each node (i.e., cortical region) and in the following Section we will try to find correlations between the topological and dynamical properties of the nodes. Between the diversity of methodologies to quantify both the entropy and complexity of a signal, we have selected a set of measures based on the occurrence of ordinal patterns within a time series. The use of ordinal patterns have been demonstrated to effectively work when analyzing signals with high amount of noise, as it is the case of our MEG recordings. We have created large times series for each brain region by connecting the 35 epochs recorded for each individual. Thus, we obtain series of $M = ||\{Xt\}|| = 230 \times 35 = 8050$ points. Next, we have to select the embedding dimension of the ordinal patterns, i.e. the number of consecutive points in the series whose ordering (according to its amplitude) is going to be analyzed. After a study of different lengths, we chose $D = 6$ since it is long enough to guarantee a high number of possible different patterns, specifically $D!$. Importantly, this embedding dimension also guarantees that the number of points in the time series is long enough to have enough statistics, since it fulfills the condition $M - D \gg D!$ (see section: Ordinal Patterns and Stochastic Analysis in Chapter 1. [A15]).

Once the ordinal patterns of each time series are obtained, we calculate their associated entropy $H(i)$ and complexity $C(i)$ for each node i and individual. As explained in the Materials and Methods Section 8.2.4, both measures rely on the probability P of finding certain ordinal pattern in the time series. With the aim of quantifying the differences between the SG and BG groups, we average $H(i)$ and $C(i)$ for each group. Finally, we identify those nodes with significant statistical differences between groups with a permutation test of 5000 randomizations of both $H(i)$ (or $C(i)$).

Interestingly, we find a group of brain regions with a $p_{val} < 0.05$ indicating statistical differences between the SG and BG groups, both for $H(i)$ and $C(i)$. In accordance with previous sections, the occipital lobe is the brain region that concentrates the highest amount of nodes with statistical differences (see Fig. 8.5). We obtain a group of 23 nodes whose entropy is always higher in the SG group. At the same time, when complexity is compared, we obtain a very similar group (only two nodes do not overlap) but the complexity of the signals is lower in the SG group (see Fig. 8.6). These results indicate that a higher level of studies could be associated to a brain dynamics with lower entropy and higher complexity.

Since the results shown in Figs. 8.5-8.6 seem to indicate that changes in the entropy and complexity come together, we are going to investigate if a correlation between the two dynamical properties exists. Fig. 8.7 shows a complexity-entropy diagram (H-C diagram) for all nodes, with the inset plotting only those nodes with statistical differences. We can observe a negative correlation between $H(i)$ and $C(i)$, revealing that those nodes with less entropy are, at the same time, those nodes with higher complexity. This result holds no matter what the level of studies is. The negative correlation between $H(i)$ and $C(i)$ has been previously reported in theoretical models [A269] but, to the best of our knowledge, it is the first evidence in brain dynamics.

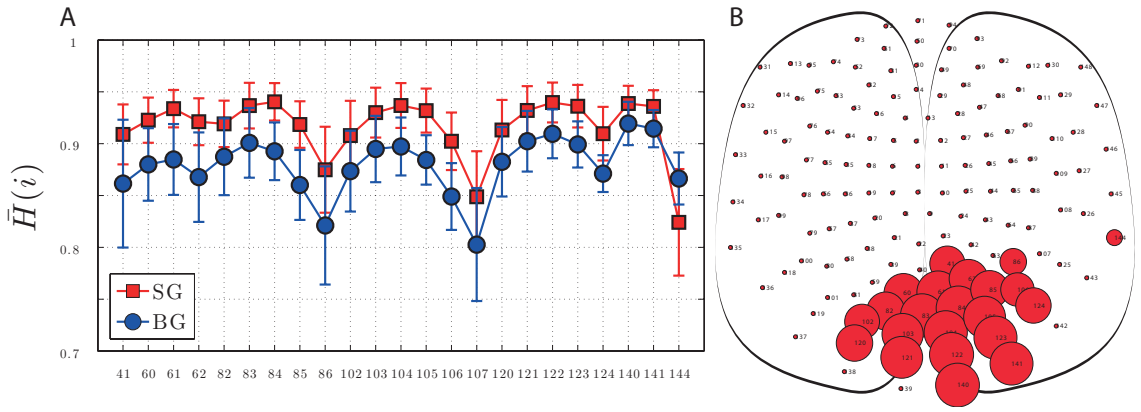

Figure 8.5: **Differences of entropy $H(i)$ between the SG and BG groups.** In A, entropy $H(i)$ of those nodes with statistically significant differences. Red squares (Blue circles) for SG (BG), respectively. $\bar{H}(i)^{SG}$ is higher than $\bar{H}(i)^{BG}$ for nearly all nodes. In B, position of the nodes with statistical differences. Node sizes are proportional to $\bar{H}(i)^{SG}$.

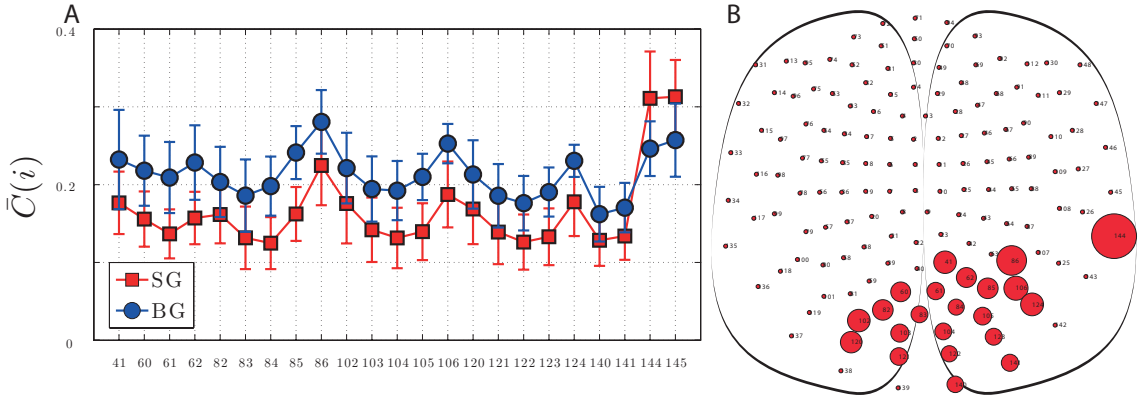

Figure 8.6: **Differences of complexity $C(i)$ between the SG and BG groups.** In A, complexity $C(i)$ of those nodes with statistically significant differences. Note that now, $\bar{C}(i)^{SG}$ is lower than $\bar{C}(i)^{BG}$ for all nodes. In B, position of the nodes with statistical differences. Node sizes are proportional to $\bar{C}(i)^{SG}$. Note that, as in the case of the node entropy, the majority of the nodes are placed at the occipital region.

8.3.4 Correlation between topology and dynamics

As we have seen in previous Sections, nodes located at the occipital lobe are, on one hand, the most relevant nodes for the topology characterization and, on the other hand, the nodes with statistically significant differences when the dynamical properties are compared. In view of this, it is reasonable to ask wether a certain interplay between the topological and dynamical properties of the nodes exists. With this aim, we have looked for correlations between the dynamic properties of the nodes (i.e., $\bar{H}(i)$, $\bar{C}(i)$) and two of their topological parameters, namely the node strength $\bar{S}(i)$ and the weighted clustering coefficient $\bar{C}_w(i)$. Figure 8.8 shows all posible combinations, i.e. $\bar{H}(i)$ vs. $\bar{S}(i)$ (A); $\bar{H}(i)$ vs. $\bar{C}_w(i)$ (C); $\bar{C}(i)$ vs. $\bar{S}(i)$ (B); $\bar{C}(i)$ vs. $\bar{C}_w(i)$ (D).

Fig. 8.8A shows the interplay between the entropy and the node strength. We can observe a monotonically dependence between $\bar{H}(i)$ and $\bar{S}(i)$ in both groups, which indicates that nodes with higher strength, i.e. the hubs of the network, are in turn those nodes with higher entropy at

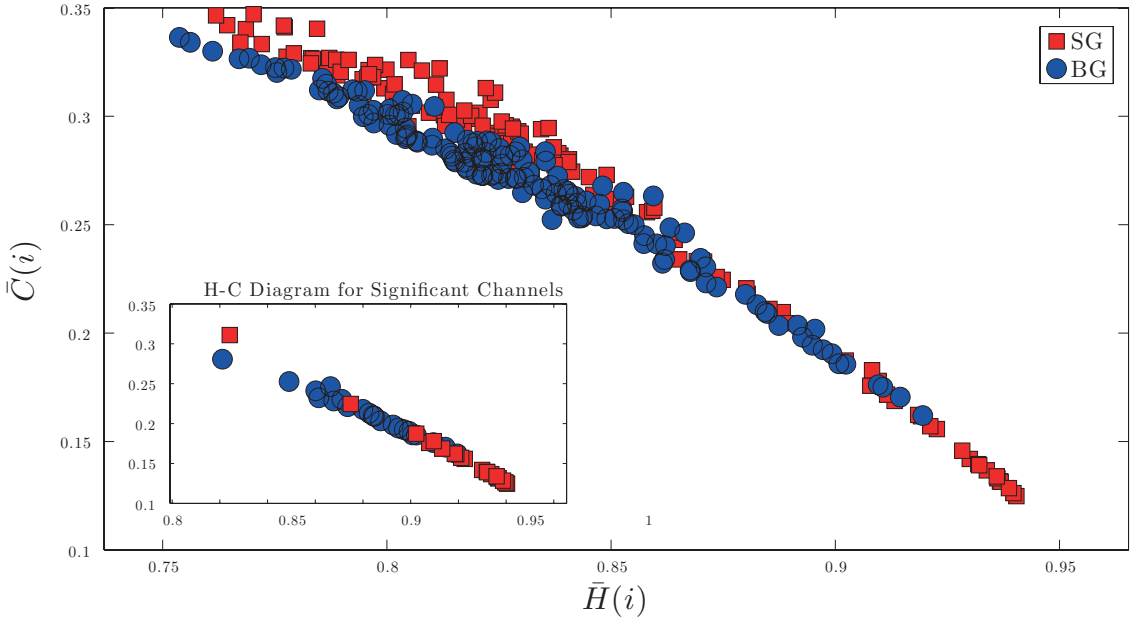

Figure 8.7: **Complexity-Entropy Diagram.** Red squares (blue circles) for **SG** (**BG**). Diagram of global complexity vs. global entropy for all 148 channels. Inset plot represent common channels with statistical significant differences.

their dynamics. The correlation between the node complexity and its strength is, on the contrary, negative (Fig. 8.8B), which could be expected from the results shown in the previous Section. In other words, the hubs of the network have the less complex dynamics, probably due to the high entropy of their signals.

The fact that the weighted clustering coefficient $\bar{C}_w(i)$ depends on the weight of the links a node has, leads to similar correlations when the clustering parameter is compared with the entropy and complexity of a node (see Fig. 8.8C-D). At any rate, the four panels of Fig. 8.8 lead to the conclusion that strong clusters of highly connected nodes are associated with dynamics with higher entropy and lower complexity. This behaviour is similar in both the SG and BG groups, nevertheless the fact that the SG group has nodes that reach higher strengths (see horizontal axis of Fig. 8.8A and B) makes this phenomenon more evident in individuals with lower level of studies.

8.4 Discussion

In this Chapter we have shown how the cognitive reserve, associated to the level of studies an individual has, leaves different fingerprints both in the dynamics of the cortical brain regions and the topology of their associated functional networks. Initially, we have seen how a group of people that reached the School level (SG) requires higher synchronization between brain regions in order to successfully perform a memory task, at least when compared with a group with the Bachelor degree (BG). This enhancement of synchronization leads to functional network with higher strengths. Nevertheless the network outreach is the parameter that better unveils the differences between both groups, which leads to the conclusion that there exists a reorganization of the network topology that goes beyond the increase of strength.

At lower scales, i.e. at the level of the network's nodes, the differences between groups also arise. Interestingly, the role of the hubs within each group show some differences, and the occipital and lateral regions of the brain increase their importance in the group with lower level of studies.

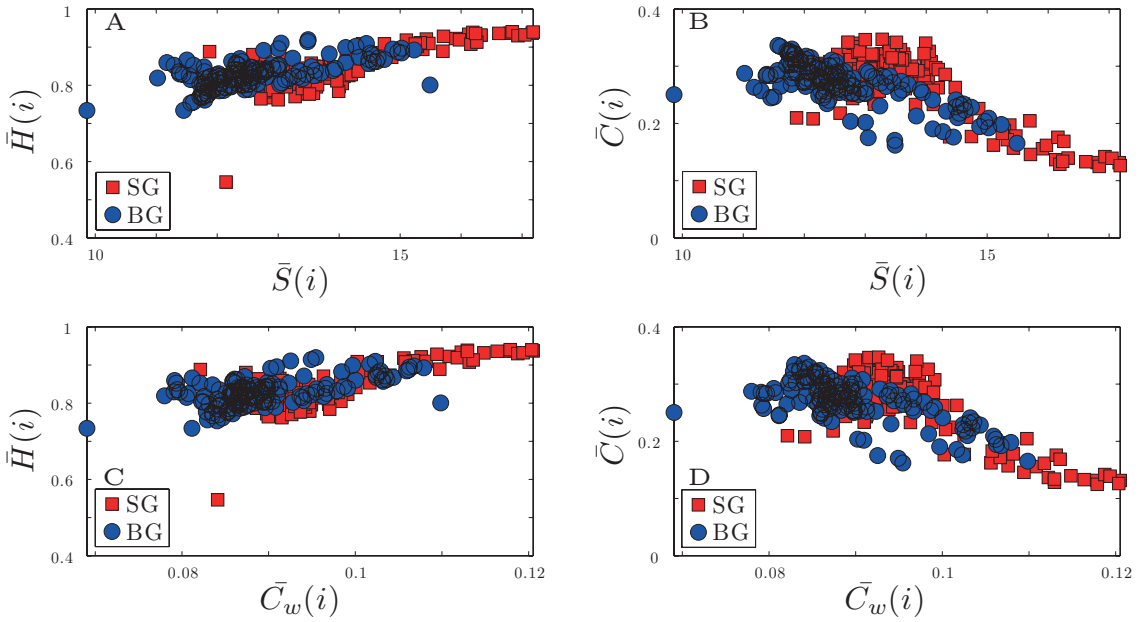

Figure 8.8: **Correlation between the topological and dynamical parameters.** Correlation plots for the global dynamical properties (entropy $\bar{H}(i)$ and complexity $\bar{C}(i)$) of the MEG time series and its corresponding topological features (strength $\bar{S}(i)$ and clustering $\bar{C}(i)$). Specifically, $\bar{H}(i)$ vs. $\bar{S}(i)$ (A); $\bar{H}(i)$ vs. $\bar{C_w}(i)$ (C); $\bar{C}(i)$ vs. $\bar{S}(i)$ (B); $\bar{C}(i)$ vs. $\bar{C_w}(i)$ (D). Red squares (blue circles) refer to the SG group (BG).

Differences in the occipital lobe are also reported when the dynamical properties of the cortical regions are investigated. In this way, it is the occipital lobe the one that accumulates the majority of regions with statistically significant differences between groups. But, what are these differences? They mainly consist of an increase of the entropy in the SG group, while, at the same time, individuals with higher level of studies show higher complexity in their signals.

Thus, both the topological and dynamical properties of the functional brain networks seem to capture differences between the level of studies and, in turn, in the associated cognitive reserve. Nevertheless, what is the interplay between both kind of indicators? As we have seen, the importance a node has within the functional network, measured as its strength, correlates with the entropy of the signals, while it is negatively correlated with the level of complexity. The fact that the network has been reported to be assortative and also the correlation between the clustering coefficient and the entropy, leads to the existence of a densely connected group of hubs, placed at the occipital lobe, with high entropy and low complexity. To the best of our knowledge, this is the first evidence of the existence of a topological-dynamical core, which we believe could be present in other kind of situations beyond the execution of memory tests. Thus, we hope that the results contained in this Chapter showing the interplay between topology and dynamics could be further adapted to other kind of cognitive or motor tasks, or even to the evaluation of brain impairment, shedding light on the understanding of functional brain networks.

III Discussion

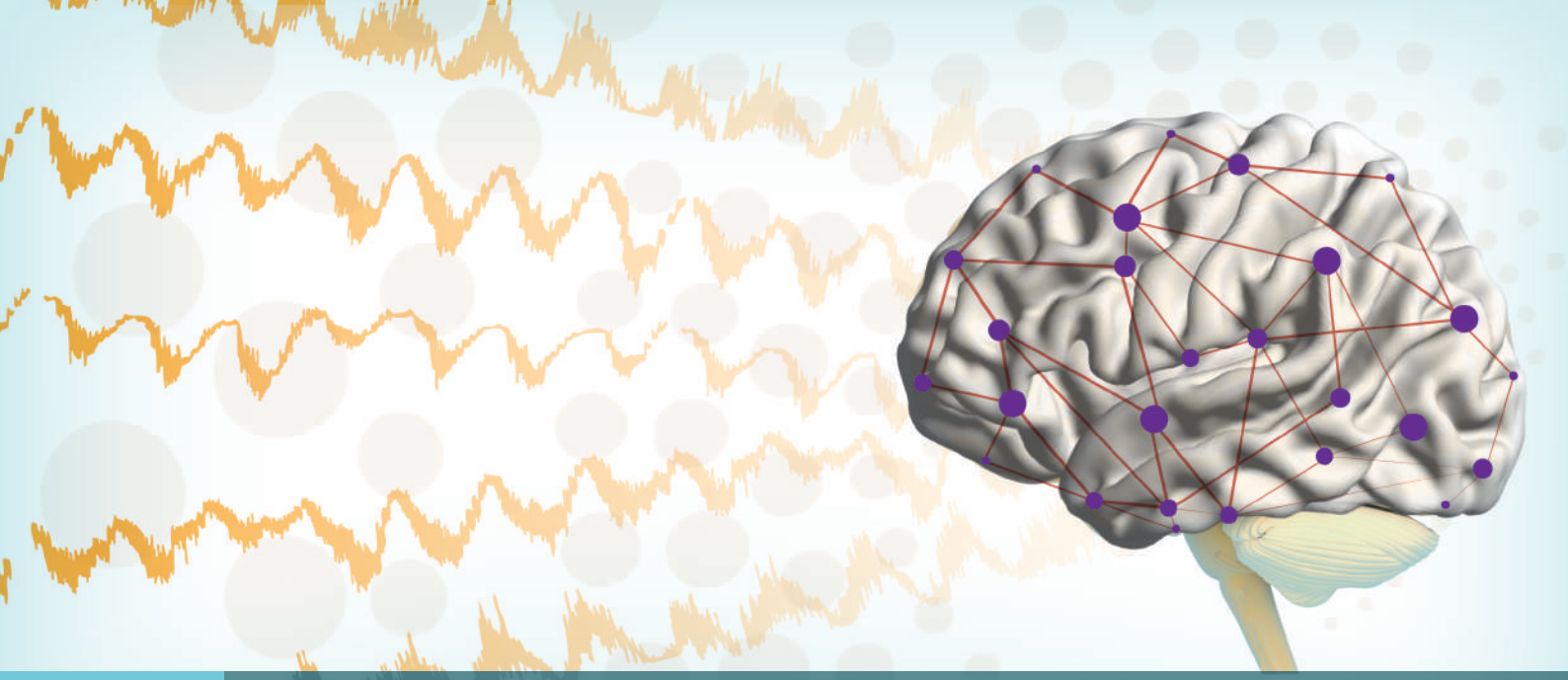

9 Conclusions and Future Perspectives

Mathematical methods developed under the paradigm of complexity have given priceless approaches to better understand nonlinear biological systems. Among them, the brain, probably the most complex system we are facing, has benefited from detailed studies that have shed light on many of its emergent behaviours. Within this framework, this PhD Thesis makes use of the new Science of Networks in order to better understand and characterize some of its emergent properties, all of that under the hypothesis that functional brain networks must be interpreted from their topological organization but also from their dynamical properties.

Along this PhD Thesis I have revisited key topics of complexity and neuroscience to understand the organization of coupled brain signals. Specifically, I have made use of Network Science to figure out how topological patterns appear in functional brain networks. Additionally, I characterized the rivalry/balance between brain hemispheres and traced how the organization of brain networks evolve in time. On the other hand, I unveiled the consistency of node dynamics and discovered how the inner dynamics of individuals suffering from a brain disease can be projected into an "anomalous network". Likewise, I analyzed the dynamics inside functional networks through the use of mathematical tools that allow to extract ordinal patterns from the brain activations. In this way, I captured the temporal content of information enclosed in brain signals so as to get statistical metrics containing the main features of nodes' dynamics. All of that was exposed through *five studies* devoted to the analysis of the dynamics in/of functional networks, showing how complex networks approach can be useful to the comprehension of the differences between groups of people under different cognitive conditions, as well as to demonstrate that by studying the dynamics in/of networks we can better understand the still-unclear relationship between topological and dynamical complexity.

In the *first study* I witnessed the brain as a network with high heterogeneity, giving rise to the existence of hubs. I showed a detailed analysis of how the importance of those hubs in functional networks was associated with the execution of a memory task, and how the emergence of mild cognitive impairment (MCI) affects the role of the network's hubs. I concluded that among all centrality measures, eigenvector centrality was the one that better quantifies the role of the hubs

and captures the impairment introduced by the neurodegenerative disease. Regarding the relevant cortical regions, the occipital region, containing the majority of the hubs in healthy individuals, was the one where centrality decreased the most, while nodes belonging to the central lobe benefited from the hub deterioration. For this reason, I concluded that the reduction of hub centrality could be used as a signature of the existence of certain brain diseases, since the hub structure is quite stable in healthy adult individuals.

The *second study* considered the brain not as a single network, but as a *network-of-networks* formed by two components (one per hemisphere) connected through a certain number of inter-links. I found that eigenvector centrality is a useful metric to evaluate wether the brain hemispheres of healthy individuals vie to reach a certain level of competition or, conversely, some functional trade-off. I found that the brain takes advantage of all links, including the weaker ones, to distribute the centrality in almost equally proportions in both brain hemispheres, a fact that is reflected in a competition parameter close to zero. I also computed the percentage of the damage an hemisphere has due to single strokes, highlighting to what extent the resilience of the brain is affected according to the number of inter-links between hemispheres. In this way, I evaluated how brain networks go from a tight-binding behaviour up to a fragile system when the number of inter-links is reduced. Interestingly, I found that the occipital lobe is the cortical region that suffers the most severe deterioration, for all conditions in the α band. I also found that while centrality is highly affected by strokes and removed inter-links, the shortest path and the averaged clustering coefficient were not dependent on the number of inter-hemispherical connections. This fact results of high importance, because it warns about the danger of investigating the robustness of network-of-networks only in terms of the typical topological features, such as the shortest path or clustering coefficient.

The *third study* emphasized the fact that functional networks are not static entities and focused on the analysis of how their topological features evolve and reorganize in time. I investigated how the functional networks of young and older individuals modulate their topology during an interference-based working memory task. This study allowed me to track the evolution of the network parameters, reporting significant differences between young and older individuals at the beginning of the interference period. These differences resulted more pronounced in parameters such as the network strength or outreach, despite they were also reported in the weighted clustering, average shortest path and network global efficiency. Interestingly, I found that the ability of the network topology to reorganize is impaired in the older group, which shows lower variations of the network strength between consecutive time steps during the interference region when compared to the memory maintenance. In addition, I found that while the fluctuations of the network strength are slightly higher in the young group during the memory maintenance, the situation is reversed during the interference period, where fluctuations of the strength of the older subjects are much higher. This fact suggests that the ability of functional networks to maintain (modify) its topology during interference is decreased (increased) with ageing. Importantly, I also showed that averaging the network topology during the whole experiment or, splitting it only into two parts, one corresponding to the memory maintenance and the other to interference, hides the differences existing between the two groups.

In the *fourth study* I focused on the dynamics in the network, i.e. I was concern about a dynamical process occurring in the network more than in the network topology itself. I studied how a dynamical property of dynamical systems called *consistency*, can be quantified with a new sub-type of functional networks, i.e., the *parenclitic networks*. In this kind of graph representation, the link between two nodes quantifies the deviations of the node consistency from an expected (healthy) behaviour. I demonstrated that, by assuming a linear correlation among the consistencies

of the nodes, the differences between a healthy group and a group suffering from MCI allowed to identify nodes whose topological properties were affected the most by the emergence of the disease. I reported a higher network strength for MCI group when the same number of links were considered in both groups. This fact indicated higher deviations from the expected consistency performance in the MCI group. Furthermore, I observed the appearance of strong hubs in the patients group, which revealed that the disease is specially severe at certain cortical regions. Specifically, node 32 (frontal lobe) and node 61 (occipital lobe) were detected to be the focal points of the consistency impairment. Nevertheless, the loss of consistency was not restricted to certain specific regions, as reflected by the fact that global network parameters (average path length or global efficiency) also captured differences between the control and the MCI group. On the other hand, I found that the number of steps needed to go from one node to any other in the parenclitic network is much lower in the MCI group, which indicates that the disease alters the network consistency in quite a fundamental way. I also showed that networks associated to the control group were more random than those of the MCI group, which has been demonstrated to be a common signature of parenclitic networks. To the best of our knowledge, this was the first result concerned about the construction of parenclitic networks to understand brain functioning and specifically the effect of a neurodegenerative disease.

Finally, in the *fifth study* I focused on how the topological features of functional brain networks can be interrelated with the dynamical properties of their nodes. I presented, for the first time, a study that takes advantage of the methodology of ordinal patterns in large-time-series to interrelate the dynamical properties of the nodes of a network with their topological features. Departing from the magnetoencephalographic recordings of two groups of individuals with different level of studies, I show the existence of differences between the topology and dynamics of their corresponding functional networks. These differences were specially evident in the occipital lobe, being the one that concentrated brain sites with higher statistical differences between both groups. Individuals with a lower level of studies showed higher levels of the node and network strengths, revealing a higher effort to attain the same level of performance during a memory test. The content of information in the temporal patterns also distinguished between both populations, again unveiling the occipital lobe to be the one with more differences between groups. In this context, subjects with higher educational attainment exhibited greater levels of complexity in the occipital brain sites. At the same time, nodes with higher levels of entropy were related to people with low educational levels. Finally, I reported a negative correlation between the strength of the nodes and the complexity of the signal, leading the hubs of the functional networks to be the nodes with lowest complexity and highest entropy. To the best of our knowledge, this is the first attempt to unveil the link between the topological and dynamical complexity in functional brain networks.

9.1 Future Perspectives

This Thesis offers different perspectives to understand how brain functional networks are organized, both from the topological and dynamical point of view. Future works related to the above-mentioned results should take into account other cognitive processes and/or other brain diseases in order to evaluate the generality of the results presented in this PhD Thesis. In general, the application of Network Science to understand the brain behaviour is still a pristine field with great expectations and challenges. Below, there is a list of those that I consider to be intimately related to the results contained in this PhD Thesis.

Applications to other brain diseases

Similar studies of statistical analysis of the hub deterioration could be carried out in other neurodegenerative diseases where the existence of functional hubs has been reported. For instance, not only

in the early symptoms of MCI, but actually in Alzheimer's Disease (AD). In the case of studying the hemispherical balance, further studies should be addressed to implement the procedure described in Chapter 2 to differentiate between individuals with a certain brain disease and a control group. A clear target could be those individuals who suffer from a malfunctioning in the hemispherical connectivity like, for example, agenesis of corpus callosum.

Applications to larger data sets

It is important to highlight that the sample size always represents a limitation when studying brain networks. Particularly, in the Chapter of time-evolving networks, although the results were statistically significant, subsequent similar studies should consider time series with larger sizes in order to get temporal networks with better statistics.

In the same way, in further works related to parenclitic networks, a larger data set of individuals would allow to test the existence of higher-order correlations among node features. A combination of both kinds of correlations (linear and higher order ones) together with other nonlinear methods would deserve its own study. Importantly, such combinations could depend on the size of the datasets and the disease under study.

Interplay between topology and dynamics

Future works should focus on the evaluation of the complexity and entropy of nodes' signals using different kinds of measures. Evidently the choice of one or another metric of entropy or complexity must be done carefully, because it depends on the task-related function and the particular dynamics within the time series. Additionally, larger signals would imply the access to longer memory when computing ordinal patterns, which would lead to a more accurate measurement of the probability distribution of the ordinal patterns.

This PhD Thesis started studying the topology of functional networks and then moved to the study of the dynamics in the network. In this way, I ultimately showed a correlation between the topological features of a node and its dynamics. This could be enclosed as a first approach to understand how functional networks act as adaptive networks. However I consider that future works should take into account correlations with other network features different (or more sophisticated) from the clustering and the strength. Additionally, the results concerning cognitive reserve came from a data set of healthy people, thus similar studies should take into consideration both a healthy group and a group with a certain disease in order to quantitatively measure the adaptativity of functional networks.

Finally, further studies should deepen into the aforementioned bridge between topology and dynamics of brain networks, since this kind of works could forward the application of Network Science to clinical uses, such as the early detection of certain brain diseases.

IV

Appendices

A Publications, Conferences & Others

Here I have listed the papers, conferences, seminars and, in summary, all the activities that I have carried out during the realization of this PhD Thesis.

A.1 Articles

Published: P. Ariza, E. Solesio-Jofre, **J. H. Martínez**, J. A. Pineda, G. Niso, F. Maestú, J. M. Buldú. *Evaluating the effect of ageing on interference resolution with time-varying complex networks analysis.* Frontiers in Human Neuroscience. Vol. **9**, 2015.

Published: A. Navas, D. Papo, S. Boccaletti, F. del-Pozo, R. Bajo, F. Maestú, **J. H. Martinez**, P. Gil, I. Sendiña-Nadal, J. M Buldú. *Functional Hubs in Mild Cognitive Impairment.* International Journal of Bifurcation and Chaos. Vol. **25**, No. 3. 2015.

Published: **J. H. Martínez**, P. Ariza, M. Zanin, D. Papo, F. Maestú, J. M. Pastor, R. Bajo, S. Boccaletti, J. M. Buldú. *Anomalous Consistency in Mild Cognitive Impairment: A Complex Networks Approach.* Chaos, Solitons & Fractals Journal. Vol. **70**. 2015.

Submitted: D. Papo, Zanin. M, **J. H. Martínez**, J. M. Buldú. *Beware of the small-world, neuroscientist!* Submitted to Trends in Cognitive Sciences. 2015.

Upcoming: **Martínez. J. H**, Buldú J. M, Papo. D, Chavez. M, de Vico Fallani. F. *Functional Centrality Distribution in Brain Hemispheres. A Resting State Study*. To be submitted to PNAS. 2015.

Upcoming: **J. H. Martínez**, J. Pineda, P. Ariza, J. M. Buldú *Correlation of Dynamics and Structural Activation Patterns Reveals Neural Correlates Reorganization in Cognitive Reserve* . To be submitted to Neuroimage. 2015.

A.2 Book Chapters

Published: Papo. D, **Martínez. J. H**, Ariza. P, Pineda J. A, Boccaletti. S, Buldú. J. M. *Las redes funcionales bajo la perspectiva de la teoría de grafos.* Book chapter in: Conectividad funcional y anatómica en el cerebro humano. ISBN-13: 978-8490225257. Ed: Elsevier. 2015.

A.3 Conferences and Workshops

Along those years I have attended several scientific events presenting oral and poster contributions:

Poster: **J. H. Martínez**, J. M. Buldú, M. Zanin, J. M. Pastor. *A Complex Network Model for Mild Cognitive Impairment Subject Characterization.* Congreso de Física Estadística XII. Proceedings ©, Congress. Mallorca, Spain, 2012.

Poster: **J. H. Martínez**, J. M. Pastor, M. Zanin, F. Maestú, R. Bajo, J. M. Buldú. *Consistency, complex networks and mild cognitive impairment.* XXXIII Dynamics Days Europe. Congress. ISBN: 978-84-15302-43-8 Legal Deposit: M-15935-2013, Madrid. Spain, June 2013.

Poster: **J. H. Martínez**, J. M. Pastor, M. Zanin, F. Maestú, R. Bajo, J. M. Buldú. *Anomalous Networks: An Application To Brain Diseases.* European Conferencce on Complex systems'13. Conference, ㏄, Barcelona. Spain, September 2013.

Poster: **J. H. Martínez** , D. de Santos, D. Papo, J. M. Pastor, E. Jover, I. Sendiña-Nadal, F. Maestú, J. M. Buldú. *Emergent Dynamical-Structural Interdependence in Hippocampus Cultures.* Net-works 2013. Conference, Madrid. Spain, December 2013.

Talk: **J. H. Martínez**, P. Ariza, J. Pineda, G. Niso, E. Solesio, F. Maestú, J. M. Buldú. *Evaluating Brain Resilience in Memory Ageing Based on Evolving Networks.* Net-works 2013. Conference, Madrid. Spain, December 2013.

Talk: **J. H. Martínez**, P. Ariza, D. Papo, J. Pineda, R. Bajo, F. Maestú, J. M. Buldú. *Utilizando patrones de orden y redes complejas para evaluar la reserva cognitiva.* NoLineal2014. Congress, Badajoz. Spain, June 2014.

Talk: **J. H. Martínez**, P. Ariza, J. M. Pastor, *et al Using Parenclitic Networks to Evaluate the Loss of Brain Consistency.* 10th AIMS Conference on Dynamical Systems Differential Equations and Applications, Special Session: How Do Complex Networks Improve Our Knowledge of Biology?. Conference, Madrid. Spain, July 2014.

Talk: **J. H. Martínez**, J. M. Buldú, D. Papo, M. Chavez, J. M. Pastor, de Vico Fallani. F *Hemisphere Competition in Functional Brain Networks.* NetSci2013. Conference, Zaragoza. Spain, June 2015.

Poster: **J. H. Martínez**, D. de Santos, D. Papo, J. M. Pastor, E. Jover, I. Sendiña-Nadal, F. Maestú, J. M. Buldú. *The Emergent Role of the Interplay Between Spikes Dynamical Properties and Structural Neural Networks.* Conference, Zaragoza. Spain, jun, 2015. Conference, Madrid. Spain, December 2013.

Talk: **J. H. Martínez**, J. M. Buldú, D. Papo, M. Chavez, J. M. Pastor, de Vico Fallani. F *Connector*

Links Support Functional Centrality Distribution in Brain Hemispheres. XIV LAWNP. Latin American Workshop on Nonlinear Phenomena. Workshop, Cartagena de Indias. Colombia, September, 2015.

A.4 Invited Seminars

Furthermore, I have been invited to give some talks, seminars, courses and tutorials related to my scientific activity in international schools and different universities:

Course: **J. H. Martínez**. *Introducción a Python en Cálculo Científico.* Given in Master of Physics on Complex Systems, Technical University of Madrid. Master Seminar, Madrid. Spain, April 2012.

Seminar: **J. H. Martínez**. *Complex networks Approach for MEG Time Sries. A Methodology for Data Classicfication.* Given in Advanced Seminars of Master of Physics on Complex Systems, Technical University of Madrid. Master Seminar, Madrid. Spain, October 2012.

Seminar: **J. H. Martínez**. *Competition in Resting State. An approach from complex networks.* Invited talk given in AramisLab Group Monthly Meeting at *Institut du Cerveau et de la Moelle Epinière (ICM), Universite Pierre et Marie Curie*. Seminar, Paris. France, April 2014.

Seminar: **J. H. Martínez**. *Introduction to Biological Complex Networks. A functional perspective from the complexity theory.* International School of Bioinformatic & Computational Neuroscience, School, Bogotá. Colombia, October 2014.

Course: **J. H. Martínez**. *How To Deal With My Own Brain And Not To Die In The Attempt?. The use of graph theory and complex systems for functional connectivity.* Given in School of Bioinformatic & Computational Neuroscience, Universidad Javeriana de Colombia, Also given at Universidad Central de Colombia. School, Bogotá. Colombia, October 2014.

Seminar: **J. H. Martínez**. *Prolegomenon to Functional Brain Complex Networks.* Seminario de Física Teórica del Departamento de Física at Universidad Nacional de Colombia, Capítulo Estudiantil MBES- Depto de Ingeniería Biomédica at Universidad de los Andes, Facultad de Ciencias Naturales y Matemáticas at Universidad de Ibagué, Neuros Research group at Universidad Rosario de Colombia and Technical University of Madrid. Seminars, Bogotá, Ibagué, Madrid. Colombia, Spain, September, October, November 2014; May 2015.

A.5 International Schools

As a PhD candidate I have attended the following international schools:

Talk: **J. H. Martínez**, J. M. Pastor, M. Zanin, F. Maestú, R. Bajo, J. M. Buldú. *Anomalous Networks: Unveiling an Intrinsic Behaviour in Mild Cognitive Impairment.* School of Biological Complex Networks: From the Cell to the Brain and Beyond. School, Natal. Brazil, jul, 2013.

Talk: **J. H. Martínez**, J. M. Pastor, M. Zanin, F. Maestú, R. Bajo, J. M. Buldú. *Anomalous Networks: An Application To Brain Diseases.* ECCS Warm-Up School on Complex Networks. School, Barcelona. Spain, sep, 2013.

Talk: **J. H. Martínez**, P. Ariza, D. Papo, M. Zanin, J. M. Buldú. *Do Our University Studies Increase our Brain Complexity?*. Mediterranean School of Complex Networks. School, Salina. Italy, jun, 2014.

Talk: **J. H. Martínez**, J. M. Buldú, D. Papo, M. Chavez, J. M. Pastor, de Vico Fallani. F *Dynamics-Structural Interplay Patterns in Brain Networks Reveals Neural Correlates Organization in Cognitive Reserve.* School on Fundamentals of Complex Systems and Applications to Neurosciences. School, São Paulo. Brazil, oct, 2015.

A.6 Conferences Committee

I have participated in the Organizing Committee of a Satellite of the NetSci2015 Conference:

Organizer: **J. H. Martínez**. *Brain Networks Satellite at NetSci Conference 2015.* NetSci2015. Satellite, Zaragoza. Spain, jun, 2015.

A.7 Academic Secondments

Finally, in order to improve my academic career, I have visited different universities and research centers:

London. UK: **Imperial College London**. Visit to the *Complexity & Networks Group* of Department of Mathematics. March 2011.

Southamptom. UK: **University of Southampton**. Visit to the *Adams & Graf Vision Labs* of Psychology Department. March 2011.

Paris. France: **Université Pierre et Marie Curie**. Scientific secondment at the *ARAMISlab* of Institute Du Cerveau Et De La Moelle Épinière (ICM). January-May, 2014.

Barcelona. Spain: **Universitat Politècnica de Catalunya**. Visit to the *Nonlinear Dynamics, Nonlinear Optics and Lasers. DONLL Group* of Department of Physcis and Nuclear Engineering. May 2015.

B Bibliography

Books

B1. Barrat, A., Barthlemy, M. & Vespignani, A. *Dynamical processes on complex networks* ISBN: 0521879507 (2008) (cited on pages 3, 17).

B2. Buzsáki, G. *Rhythms of the Brain* 448 (2006) (cited on page 30).

B3. Churchland, P. S. *Brain-wise: Studies in Neurophilosophy* ISBN: 026253200X (2002) (cited on pages 28, 31, 32).

B4. Cohen, M. X. *Analyzing Neural Time Series Data: theory and practice* 1st edition. ISBN: 978-0-262-01987-3 (The MIT Press, London, 2014) (cited on pages 5, 33, 64).

B5. Descartes, R. *Discours de la méthode, Les passions de l'âme, Lettres (Google eBook)* 280 (Éditions du Monde Moderne, 1637) (cited on page 27).

B6. Díaz, J. L. *La conciencia viviente* ISBN: 9681683528 (2008) (cited on page 31).

B7. Easley, D. & Kleinberg, J. *Networks , Crowds , and Markets : Reasoning about a Highly Connected World* 744 (Cambridge University Press, 2010) (cited on page 4).

B8. Érdi, P. *Complexity explained* 1–397 (Springer Berlin Heidelberg, 2008) (cited on page 28).

B9. Estrada, E., Estrada, P., in Complexity Science Ernesto, C., Prof & Knight, P. *A First Course in Network Theory* 272. ISBN: 0198726457 (Oxford University Press, 2015) (cited on page 6).

B10. Kandel, E. R., Schwartz, J. H. & Jessell, T. M. *Principles of Neural Science* 1414. ISBN: 0838577016. doi:10.1036/0838577016 (2000) (cited on page 30).

B11. Kantz, H. & Thomas, S. *Nonlinear time Series Analysis* 1st edition. ISBN: 978-0-521-82150-6 (Cambridge University Press, Cambridge, 2003) (cited on page 4).

B12. Kelso, J. A. S. *Dynamic Patterns: The Self-organization of Brain and Behavior* 334. ISBN: 0262611317 (MIT Press, 1997) (cited on page 5).

B13. Kuramoto, Y. *Chemical Oscillations, Waves, and Turbulence* ISBN: 978-3-642-69691-6. doi:10.1007/978-3-642-69689-3 (Springer Berlin Heidelberg, Berlin, Heidelberg, 1984) (cited on page 18).

B14. Luck, S. J. *An Introduction to the Event-Related Potential Technique* **3,** 388 (MIT Press, 2005) (cited on page 33).

B15. Marr, D. *Vision: A Computational Investigation into the Human Representation and Processing of Visual Information* ISBN: 0716715678 (1983) (cited on page 30).

B16. Newman, M. E. J. *Networks: An introduction.* (Oxford University Press, 2010) (cited on pages 6, 9, 11, 14, 40, 60, 98, 102, 104).

B17. Pikovsky, A., Rosenblum, M. & Kurths, J. *Synchronization A Universal Concept in Nonlinear Sciences* ISBN: 9780521533522 (Cambridge University Press, 2003) (cited on pages 5, 18, 35, 83, 84).

B18. Pines, D., Fe, S. F. I. S. & N.M. *Emerging syntheses in science: proceedings of the founding workshops of the Santa Fe Institute, Santa Fe, New Mexico* 237. ISBN: 0201156776 (Addison-Wesley, 1988) (cited on page 23).

B19. Rieke, F., Warland, D., De Ruyter Van Steveninck, R. & Bialek, W.*Spikes: Exploring the Neural Code* xvi, 395 p. (1997) (cited on page 33).

B20. Rolls, E. T. & Deco, G. *The Noisy Brain* (Oxford University Press, 2010) (cited on page 5).

B21. Shannon, C. E. & Weaver, W. *The Mathematical Theory of Communication* (eds Shannon, C. E. & Weaver, W.) *The Mathematical Theory of Communication* **4,** 117. ISBN: 0252725484. doi:10.2307/3611062 (University of Illinois Press, 1949) (cited on pages 21, 22, 33).

B22. Siegel, S. & Castellan, N. J. *Nonparametric statistics for the behavioral sciences (2nd ed.)* ISBN: 0-07-057357-3 (1988) (cited on page 84).

B23. Sporns, O. *Networks of the Brain* 1st edition. ISBN: 978-0-262-01469-4 (The MIT Press, Massachusetts, 2011) (cited on page 5).

Chapters

C1. A.Clauset. in *Network Analysis and Modeling CSCI 5352, Fall 2014* chapter 11 (2014) (cited on page 16).

C2. Barret, K., Brooks, H., Boitano, S. & Barma, S. in *Ganon's Medical Physiology* (eds Barret, K., Brooks, H., Boitano, S. & Barma, S.) 23rd edition, 79–157 (McGrawHill Medical, New York, 2010). ISBN: 0071605673 (cited on page 30).

C3. Papo, D., Buldú, J. & Boccaletti, S. in *Encyclopedia of Computational Neuroscience* chapter Network Theory in Neuroscience (Springer, 2014). doi:DOI10.1007/978-1-4614-7320-6\713-1 (cited on page 67).

C4. Papo, D. *et al.* in *Conectividad funcional y anatómica en el cerebro humano. Análisis de señales y aplicaciones en ciencias de la salud* (eds Maestú, F., Del-Pozo, F. & Pereda, E.) 81–91 (Elsevier Science Ltd, Madrid, 2015). ISBN: 8490225257, 978-8490225257 (cited on page 28).

C5. Smart, J. in *The Stanford Encyclopedia of Philosophy* (ed Zalta, E. N.) Winter 201 (Stanford, CA 94305, 2014). ISBN: 1095-5054 (cited on page 30).

C6. Srinivasan, R. in *Brain–Computer Interfaces: Principles and Practice* (eds Wolpaw, J. & Wolpaw, E. W.) 1st edition. Chapter 6 (Oxford Scholarship, 2012). ISBN: ISBN-13: 9780195388855. doi:10.1093/acprof:oso/9780195388855.001.0001 (cited on page 61).

Thesis

T1. Bialonski, S. *Inferring complex networks from time series of dynamical systems: Pitfalls, misinterpretations, and possible solutions* PhD thesis (Universität Bonn, 2012), 141. arXiv: arXiv:1208.0800v1 (cited on page 37).

T2. De Santos-Sierra, D. *Self-organizing cultured neural networks image analysis techiniques for longitudinal tracking and modeling of the underlying network structure* PhD thesis (Technical University of Madrid, 2015), 130 (cited on page 29).

T3. Gollo, L. L. *Dynamics and Synchronization of Motifs of Neural Populations in the Prescence of Delayed Interactions* PhD thesis (Universitat de les Illes Balears, 2012) (cited on page 33).

T4. Kraskov, A. *Synchronization and Interdependence Measures and their Applications to the Electroencephalogram of Epilepsy Patients and Clustering of Data (PhD Thesis)* PhD thesis (Oct. 2004) (cited on page 35).

T5. Sarpeshkar, R. *Efficient precise computation with noisy components : extrapolating from an electronic cochlea to the brain* PhD thesis (Aug. 1997) (cited on page 28).

Articles

A1. Acebrón, J. A., Bonilla, L. L., Vicente, C. J. P., Ritort, F. & Spigler, R. The Kuramoto model: A simple paradigm for synchronization phenomena. *Reviews of Modern Physics* **77,** 137–185. ISSN: 00346861 (2005) (cited on page 18).

A2. Achard, S. & Bullmore, E. Efficiency and cost of economical brain functional networks. *PLoS Computational Biology* **3,** 0174–0183 (2007) (cited on page 41).

A3. Achard, S., Salvador, R., Whitcher, B., Suckling, J. & Bullmore, E. A resilient, low-frequency, small-world human brain functional network with highly connected association cortical hubs. *The Journal of neuroscience : the official journal of the Society for Neuroscience* **26,** 63–72. ISSN: 0270-6474 (2006) (cited on pages 39, 49).

A4. Aguirre, J., Papo, D. & Buldú, J. M. Successful strategies for competing networks. *Nature Physics* **9,** 1–5. ISSN: 1745-2473 (2013) (cited on pages 61–63, 68).

A5. Albert, R. & Barabasi, A. L. Statistical mechanics of complex networks. *Reviews of Modern Physics* **74,** 47–97. ISSN: 1478-3967 (2002) (cited on page 16).

A6. Albet, R., Jeong, N. & Barabasi, A. L. Error and attack tolerance of complex networks (vol 406, pg 378, 2000). *NATURE* **409,** 542+. ISSN: 0028-0836 (2001) (cited on pages 54, 57).

A7. Alexander-Bloch, A. F. *et al.* Disrupted modularity and local connectivity of brain functional networks in childhood-onset schizophrenia. *Frontiers in systems neuroscience* **4,** 147 (2010) (cited on page 69).

A8. Amaral, L. A., Scala, A., Barthelemy, M. & Stanley, H. E. Classes of small-world networks. *Proceedings of the National Academy of Sciences of the United States of America* **97,** 11149–11152 (2000) (cited on page 39).

A9. Andrews-Hanna, J. R. *et al.* Disruption of Large-Scale Brain Systems in Advanced Aging. *Neuron* **56,** 924–935 (2007) (cited on page 80).

A10. Ariza, P. *et al.* Evaluating the effect of aging on interference resolution with time-varying complex networks analysis. English. *Frontiers in human neuroscience* **9,** 255. ISSN: 1662-5161 (Jan. 2015) (cited on page 79).

A11. Babiloni, C. *et al.* Fronto-parietal coupling of brain rhythms in mild cognitive impairment: A multicentric EEG study. *Brain Research Bulletin* **69,** 63–73. ISSN: 03619230 (2006) (cited on page 53).

A12. Babloyantz, A., Salazar, J. & Nicolis, C. Evidence of chaotic dynamics of brain activity during the sleep cycle. *Physics Letters A* **111,** 152–156 (1985) (cited on page 35).

A13. Bajo, R. *et al.* Functional connectivity in mild cognitive impairment during a memory task: Implications for the disconnection hypothesis. *Journal of Alzheimer's Disease* **22,** 183–193 (2010) (cited on pages 33, 53, 57).

A14. Bajo, R. *et al.* Functional connectivity in mild cognitive impairment during a memory task: Implication for the disconnection hypotesis. *J Alzheimers Dis* **22,** 183–193 (2010) (cited on pages 50, 95, 96).

A15. Bandt, C. & Pompe, B. Permutation Entropy: A Natural Complexity Measure for Time Series. *PRL* (2002) (cited on pages 19, 21, 109, 114).

A16. Barabási, A. Emergence of Scaling in Random Networks. *Science* **286,** 509–512. ISSN: 00368075 (Oct. 1999) (cited on pages 14, 16).

A17. Bassett, D. S. & Bullmore, E. Small-world brain networks. *The Neuroscientist : a review journal bringing neurobiology, neurology and psychiatry* **12,** 512–523. ISSN: 1073-8584 (2006) (cited on pages 80, 90).

A18. Bassett, D. S. *et al.* Hierarchical organization of human cortical networks in health and schizophrenia. *The Journal of neuroscience : the official journal of the Society for Neuroscience* **28,** 9239–48. ISSN: 1529-2401 (2008) (cited on pages 40, 54, 56).

A19. Bassett, D. S. *et al.* Efficient physical embedding of topologically complex information processing networks in brains and computer circuits. *PLoS Computational Biology* **6** (2010) (cited on pages 40, 41).

A20. Bassett, D. S. *et al.* Dynamic reconfiguration of human brain networks during learning. *Proceedings of the National Academy of Sciences of the United States of America* **108,** 7641–7646. ISSN: 1091-6490 (2011) (cited on page 80).

A21. Blankertz, B., Lemm, S., Treder, M., Haufe, S. & Müller, K. R. Single-trial analysis and classification of ERP components - A tutorial. *NeuroImage* **56,** 814–825. ISSN: 10538119 (2011) (cited on page 33).

A22. Bocaletti, S., Latora, V., Moreno, Y., Chavez, M. & Hwang, D. Complex networks: Structure and dynamics. *Physics Reports* **424,** 175–308 (2006) (cited on pages 7, 8, 12, 14, 17, 18, 80).

A23. Bodling, A. M., Denney, D. R. & SG., L. Individual variability in speed of information processing: An index of cognitive impairment in Multiple Sclerosis.*Neuropsychology* **26,** 357–367 (2012) (cited on page 94).

A24. Breakspear, M. & Terry, J. R. Nonlinear interdependence in neural systems: motivation, theory, and relevance. *The International journal of neuroscience* **112,** 1263–1284. ISSN: 00207454 (2002) (cited on pages 29, 49).

A25. Bressler, S. L. & Kelso, J. A. S. Cortical coordination dynamics and cognition. *Trends in Cognitive Sciences* **5,** 26–36. ISSN: 13646613 (2001) (cited on page 80).

A26. Büchel, C. & Friston, K. Assessing interactions among neuronal systems using functional neuroimaging. *Neural networks : the official journal of the International Neural Network Society* **13,** 871–82. ISSN: 0893-6080 (2000) (cited on page 38).

A27. Buckner, R. L. *et al.* Cortical hubs revealed by intrinsic functional connectivity: mapping, assessment of stability, and relation to Alzheimer's disease. *The Journal of neuroscience : the official journal of the Society for Neuroscience* **29,** 1860–1873 (2009) (cited on pages 49, 50, 54, 57).

A28. Bucolo, M., Fazzino, S., La Rosa, M. & Fortuna, L. Small-world networks of fuzzy chaotic oscillators. *Chaos, Solitons and Fractals* **17,** 557–565 (2003) (cited on pages 15, 41).

A29. Buldú, J. M. *et al.* Reorganization of functional networks in mild cognitive impairment. *PLoS One* **6,** e19584 (2011) (cited on pages 8, 41, 50, 52, 57, 95, 96, 103).

A30. Buldú, J. M. *et al.* Reorganization of functional networks in mild cognitive impairment. *PLoS ONE* **6** (2011) (cited on pages 50, 53, 54, 56, 80, 109, 113).

A31. Bullmore, E. & Sporns, O. Complex brain networks: graph theoretical analysis of structural and functional systems. *Nature reviews. Neuroscience* **10,** 186–98. ISSN: 1471-0048 (2009) (cited on pages 59, 68, 80).

A32. Butts, D. A. *et al.* Temporal precision in the neural code and the timescales of natural vision. *Nature* **449,** 92–5. ISSN: 1476-4687 (Sept. 2007) (cited on page 31).

A33. Buzsáki, G. & Draguhn, A. Neuronal oscillations in cortical networks. *Science (New York, N.Y.)* **304,** 1926–9. ISSN: 1095-9203 (June 2004) (cited on page 30).

A34. Buzug, T., Pawelzik, K., von Stamm, J. & Pfister, G. Mutual information and global strange attractors in Taylor-Couette flow. *Physica D: Nonlinear Phenomena* **72,** 343–350. ISSN: 01672789 (1994) (cited on page 50).

A35. Cabeza, R. *et al.* Age-related differences in neural activity during memory encoding and retrieval: a positron emission tomography study. *The Journal of neuroscience : the official journal of the Society for Neuroscience* **17,** 391–400. ISSN: 0270-6474 (1997) (cited on pages 80, 91).

A36. Camicioli, R. M., Wieler, M., de Frias, C. M. & Wayne Martin, W. R. Early, untreated Parkinson's disease patients show reaction time variability. *Neurosci Lett* **441,** 77–80 (2008) (cited on page 94).

A37. Castellano, C., Fortunato, S. & Loreto, V. Statistical physics of social dynamics. *Reviews of Modern Physics* **81,** 591–646. ISSN: 0034-6861 (May 2009) (cited on pages 4, 17).

A38. Chavez, M., Valencia, M., Navarro, V., Latora, V. & Martinerie, J. Functional Modularity of Background Activities in Normal and Epileptic Brain Networks. *Physical Review Letters* **104,** 118701. ISSN: 0031-9007 (Mar. 2010) (cited on page 41).

A39. Chen, S., Huang, W., Cattani, C. & Altieri, G. Traffic dynamics on complex networks: A survey. *Mathematical Problems in Engineering* **2012** (2012) (cited on page 17).

A40. Chen, Z. J., He, Y., Rosa-Neto, P., Germann, J. & Evans, A. C. Revealing modular architecture of human brain structural networks by using cortical thickness from MRI. *Cerebral cortex (New York, N.Y. : 1991)* **18,** 2374–2381. ISSN: 1460-2199 (2008) (cited on page 40).

A41. Cheng, E., Grossman, J. W. & Lipman, M. J. Time-stamped graphs and their associated influence digraphs. *Discrete Applied Mathematics* **128,** 317–335 (2003) (cited on page 24).

A42. Chou, K. C., Zhang, C. T. & Maggiora, G. M. Solitary wave dynamics as a mechanism for explaining the internal motion during microtubule growth. *Biopolymers* **34,** 143–53. ISSN: 0006-3525 (Jan. 1994) (cited on page 31).

A43. Christensen, H., Deart, K. B. G., Anstey, K. J., Parslow, R. A. & Sachdev P. Jorm, A. F. Within-occasion intraindividual variability and preclinical diagnostic status: Is intraindividual variability an indicator of mild cognitive impairment?. *Neuropsychology* **19,** 309–317 (2005) (cited on pages 94, 95).

A44. Clapp, W. C. & Gazzaley, A. Distinct mechanisms for the impact of distraction and interruption on working memory in aging. *Neurobiology of Aging* **33,** 134–148 (2012) (cited on page 80).

A45. Clauset, A. & Eagle, N. Persistence and periodicity in a dynamic proximity network. *October,* 1–5 (2007) (cited on page 24).

A46. Cocchi, L., Zalesky, A., Fornito, A. & Mattingley, J. B. Dynamic cooperation and competition between brain systems during cognitive control. *Trends in Cognitive Sciences* **17,** 493–501. ISSN: 13646613 (2013) (cited on page 60).

A47. Collins, L. F. & Long, C. J. Visual reaction time and its relationship to neuropsychological test performance. *Arch Clin Neuropsychol* **11,** 613–623 (1996) (cited on page 94).

A48. Corkin, S. What's new with the amnesic patient H.M.? *Nature reviews. Neuroscience* **3,** 153–160. ISSN: 14710048 (2002) (cited on page 27).

A49. Costa, L. d. F., Rodrigues, F. A., Travieso, G. & Villas Boas, P. R. Characterization of complex networks: A survey of measurements. *Advances in Physics* **56,** 167–242. ISSN: 0001-8732 (2007) (cited on pages 8, 10).

A50. Crick, F. & Koch, C. Towards a Neurobiological Theory of Consciousness. English. *Seminars in Neuroscience,* 2663–275 (1990) (cited on page 30).

A51. Damasio, A. R. Descartes' error revisited. *Journal of the history of the neurosciences* **10,** 192–194. ISSN: 0964-704X (2001) (cited on page 27).

A52. Damoiseaux, J. S. *et al.* Reduced resting-state brain activity in the "default network" in normal aging. *Cerebral Cortex* **18,** 1856–1864. ISSN: 10473211 (2008) (cited on page 80).

A53. De Vico Fallani, F., Richiardi, J., Chavez, M. & Achard, S. Graph analysis of functional brain networks: practical issues in translational neuroscience. *Philosophical transactions of the Royal Society of London. Series B, Biological sciences* **369,** 20130521–. ISSN: 1471-2970 (Oct. 2014) (cited on page 39).

A54. De Vico Fallani, F. *et al.* Cortical functional connectivity networks in normal and spinal cord injured patients: Evaluation by graph analysis. *Human brain mapping* **28,** 1334–46. ISSN: 1065-9471 (Dec. 2007) (cited on page 41).

A55. De Vico Fallani, F. *et al.* Cortical network dynamics during foot movements. *Neuroinformatics* **6,** 23–34 (2008) (cited on page 90).

A56. De Vico Fallani, F. *et al.* Community structure in large-scale cortical networks during motor acts. *Chaos, Solitons and Fractals* **45,** 603–610. ISSN: 09600779 (2012) (cited on pages 35, 61).

A57. De Vico Fallani, F. *et al.* Multiscale topological properties of functional brain networks during motor imagery after stroke. *NeuroImage* **83,** 438–49. ISSN: 1095-9572 (Dec. 2013) (cited on page 41).

A58. De Vico Fallani, F. *et al.* Persistent patterns of interconnection in time-varying cortical networks estimated from high-resolution EEG recordings in humans during a simple motor act. *Journal of Physics A: Mathematical and Theoretical* **41,** 224014. ISSN: 1751-8113 (2008) (cited on pages 80, 90).

A59. De Frias, C. M., Dixon, R. A. & Camicioli, R. Neurocognitive speed and inconsistency in Parkinson's disease with and without incipient dementia: An 18-month prospective cohort study. *J Int Neuropsychol Soc* **18,** 746–772 (2012) (cited on page 94).

A60. De Haan, W., Mott, K., van Straaten, E. C. W., Scheltens, P. & Stam, C. J. Activity Dependent Degeneration Explains Hub Vulnerability in Alzheimer's Disease. *PLoS Computational Biology* **8.** ISSN: 1553734X (2012) (cited on pages 50, 54).

A61. De Haan, W. *et al.* Functional neural network analysis in frontotemporal dementia and Alzheimer's disease using EEG and graph theory. *BMC neuroscience* **10,** 101. ISSN: 1471-2202 (2009) (cited on page 80).

A62. De Santos-Sierra, D. *et al.* Emergence of small-world anatomical networks in self-organizing clustered neuronal cultures. *PLoS One* **9,** e85828. ISSN: 1932-6203 (2014) (cited on page 39).

A63. Deco, G., Tononi, G., Boly, M. & Kringelbach, M. L. Rethinking segregation and integration: contributions of whole-brain modelling. *Nature reviews. Neuroscience* **16,** 430–9. ISSN: 1471-0048 (June 2015) (cited on page 5).

A64. Dickerson, B. C. *et al.* Increased hippocampal activation in mild cognitive impairment compared to normal aging and AD. *Neurology* **65,** 404–411. ISSN: 00283878 (2005) (cited on page 53).

A65. Dijkstra, E. W. A note on two problems in connexion with graphs. *Numerische Mathematik* **1,** 269–271 (1959) (cited on pages 11, 101).

A66. Dimitriadis, S. I. *et al.* Tracking brain dynamics via time-dependent network analysis. *Journal of Neuroscience Methods* **193,** 145–155 (2010) (cited on page 80).

A67. Dixon, R. A. *et al.* Neurocognitive markers of cognitive impairment: Exploring the roles of speed and inconsistency. *Neuropsychology* **21,** 382–399 (2007) (cited on pages 94, 95).

A68. Doron, K. W., Bassett, D. S. & Gazzaniga, M. S. Dynamic network structure of interhemispheric coordination. *Proceedings of the National Academy of Sciences of the United States of America* **109,** 18661–8. ISSN: 1091-6490 (2012) (cited on page 80).

A69. Duchek, J. M., Balota, D. A., Holtzman, D. M., Fagan AM. Tse, C.-S. & Goate, A. M. The utility of intraindividual variability in selective attention tasks as an early marker for Alzheimer's disease. *Neuropsychology* **23,** 746–758 (2009) (cited on pages 94, 95).

A70. Eguíluz, V. M., Chialvo, D. R., Cecchi, G. A., Baliki, M. & Apkarian, A. V. Scale-free brain functional networks. *Physical Review Letters* **94** (2005) (cited on pages 39, 40).

A71. Faure, P. & Korn, H. Is there chaos in the brain? I. Concepts of nonlinear dynamics and methods of investigation. *Comptes rendus de l'Académie des sciences. Série III, Sciences de la vie* **324,** 773–93. ISSN: 0764-4469 (Sept. 2001) (cited on page 4).

A72. Felleman, D. J. & Van Essen, D. C. Distributed Hierarchical Processing in the Primate Cerebral Cortex. *Cerebral Cortex* **1,** 1–47. ISSN: 1047-3211 (Jan. 1991) (cited on page 37).

A73. Fjell, A. M., Westlye, L. T., Amlien, I. K. & Walhovd, K. B. Reduced white matter integrity is related to cognitive instability. *J Neurosci* **31,** 18060–18072 (2011) (cited on pages 94, 95).

A74. Fletcher, P., McKenna, P. J., Friston, K. J., Frith, C. D. & Dolan, R. J. Abnormal cingulate modulation of fronto-temporal connectivity in schizophrenia. *NeuroImage* **9,** 337–342 (1999) (cited on page 41).

A75. Folstein, M. F., Folstein, S. E. & McHugh, P. R. "Mini-mental state". *Journal of Psychiatric Research* **12,** 189–198. ISSN: 00223956 (1975) (cited on page 81).

A76. Fornito, a., Harrison, B. J., Zalesky, A. & Simons, J. S. Competitive and cooperative dynamics of large-scale brain functional networks supporting recollection. *Proceedings of the National Academy of Sciences* **109,** 12788–12793. ISSN: 0027-8424 (2012) (cited on page 60).

A77. Friston, K. J. The labile brain. I. Neuronal transients and nonlinear coupling. *Philosophical transactions of the Royal Society of London. Series B, Biological sciences* **355,** 215–236 (2000) (cited on page 29).

A78. Friston, K. J., Frith, C. D., Liddle, P. F. & Frackowiak, R. S. Functional connectivity: the principal-component analysis of large (PET) data sets. *Journal of cerebral blood flow and metabolism : official journal of the International Society of Cerebral Blood Flow and Metabolism* **13,** 5–14. ISSN: 0271-678X (1993) (cited on page 80).

A79. Friston, K. Functional integration and inference in the brain. *Progress in Neurobiology* **68,** 113–143 (2002) (cited on page 80).

A80. Fujisaka, H. & Yamada, T. Stability Theory of Synchronized Motion in Coupled-Oscillator Systems. *Progress of Theoretical Physics* **69,** 32–47. ISSN: 0033-068X (Jan. 1983) (cited on page 35).

A81. García Domínguez, L., Stieben, J., Pérez Velázquez, J. L. & Shanker, S. The Imaginary Part of Coherency in Autism: Differences in Cortical Functional Connectivity in Preschool Children. *PLoS ONE* **8.** ISSN: 19326203 (2013) (cited on pages 35, 61).

A82. Gautreau, A., Barrat, A. & Barthélemy, M. Microdynamics in stationary complex networks. *Proceedings of the National Academy of Sciences of the United States of America* **106,** 8847–8852 (2009) (cited on page 24).

A83. Gazzaley, A. *et al.* Age-related top-down suppression deficit in the early stages of cortical visual memory processing. *Proceedings of the National Academy of Sciences of the United States of America* **105,** 13122–6. ISSN: 1091-6490 (Sept. 2008) (cited on page 80).

A84. Geerligs, L., Saliasi, E., Maurits, N. M. & Lorist, M. M. Compensation through Increased Functional Connectivity: Neural Correlates of Inhibition in Old and Young. *Journal of Cognitive Neuroscience* **24,** 2057–2069 (2012) (cited on page 91).

A85. Geerligs, L., Saliasi, E., Renken, R. J., Maurits, N. M. & Lorist, M. M. Flexible connectivity in the aging brain revealed by task modulations. *Human Brain Mapping* **35,** 3788–3804. ISSN: 10970193 (2014) (cited on page 80).

A86. Girvan, M. & Newman, M. E. J. Community structure in social and biological networks. *Proceedings of the National Academy of Sciences of the United States of America* **99,** 7821–7826 (2002) (cited on pages 10, 12).

A87. Goldobin, D. S. Coherence versus reliability of stochastic oscillators with delayed feedback. *Phys. Rev. E* **78,** 060104(R) (2008) (cited on page 95).

A88. Gong, G. *et al.* Mapping anatomical connectivity patterns of human cerebral cortex using in vivo diffusion tensor imaging tractography. *Cerebral cortex (New York, N.Y. : 1991)* **19,** 524–536. ISSN: 1460-2199 (2009) (cited on page 37).

A89. Gorus, E., De Raedt, R., Lambert, M., Lemper, J.-C. & Mets, T. Reaction times and performance variability in normal aging, mild cognitive impairment, and Alzheimer's disease. *J Geriatr Psychiatry Neurol* **21,** 204–218 (2008) (cited on page 95).

A90. Grady, C. L. Functional brain imaging and age-related changes in cognition. *Biological psychology* **54,** 259–281. ISSN: 0301-0511 (2000) (cited on page 80).

A91. Grady, C. L. *et al.* Age-related changes in cortical blood flow activation during visual processing of faces and location. *The Journal of neuroscience : the official journal of the Society for Neuroscience* **14,** 1450–1462. ISSN: 0270-6474 (1994) (cited on pages 80, 91).

A92. Grady, C. L. *et al.* A Multivariate Analysis of Age-Related Differences in Default Mode and Task Positive Networks Across Multiple Cognitive Domains. *Cerebral Cortex* **20,** 1432–1447 (2011) (cited on page 80).

A93. Granger, C. W. J. Investigating Causal Relations by Econometric Models and Cross-spectral Methods. *Econometrica* **37,** 424–438 (1969) (cited on page 35).

A94. Guimera, R. & Amaral., L. Functional cartography of complex metabolic networks. *Nature* **433,** 895–900 (2005) (cited on pages 10, 50, 109).

A95. Guye, M., Bettus, G., Bartolomei, F. & Cozzone, P. J. Graph theoretical analysis of structural and functional connectivity MRI in normal and pathological brain networks. *Magma (New York, N.Y.)* **23,** 409–421. ISSN: 1352-8661 (2010) (cited on page 80).

A96. Hagmann, P. *et al.* Mapping human whole-brain structural networks with diffusion MRI. *PLoS ONE* **2** (2007) (cited on pages 37, 41).

A97. Hagmann, P. *et al.* Mapping the structural core of human cerebral cortex. *PLoS biology* **6,** e159. ISSN: 1545-7885 (July 2008) (cited on pages 37, 40).

A98. Hagmann, P. *et al.* Mapping the structural core of human cerebral cortex. *PLoS Biology* **6,** 1479–1493 (2008) (cited on page 40).

A99. Hämäläinen, M., Hari, R., Ilmoniemi, R. J., Knuutila, J. & Lounasmaa, O. V. Magnetoencephalography—theory, instrumentation, and applications to noninvasive studies of the working human brain. *Reviews of Modern Physics* **65,** 413–497. ISSN: 0034-6861 (1993) (cited on page 80).

A100. Hameroff, S., Nip, A., Porter, M. & Tuszynski, J. Conduction pathways in microtubules, biological quantum computation, and consciousness. *BioSystems* **64,** 149–168 (2002) (cited on page 31).

A101. Hasher, L. & Zacks, R. T. Working Memory, Comprehension, and Aging: A Review and a New View. *Psychology of Learning and Motivation - Advances in Research and Theory* **22,** 193–225. ISSN: 00797421 (1988) (cited on page 80).

A102. Haynes, J.-D. & Rees, G. Decoding mental states from brain activity in humans. *Nature reviews. Neuroscience* **7,** 523–34. ISSN: 1471-003X (2006) (cited on pages 30, 32, 34).

A103. He, Y., Chen, Z. J. & Evans, A. C. Small-world anatomical networks in the human brain revealed by cortical thickness from MRI. *Cerebral cortex (New York, N.Y. : 1991)* **17,** 2407–19. ISSN: 1047-3211 (Oct. 2007) (cited on page 41).

A104. He, Y., Chen, Z., Gong, G. & Evans, A. Neuronal networks in Alzheimer's disease. *The Neuroscientist : a review journal bringing neurobiology, neurology and psychiatry* **15,** 333–350. ISSN: 1073-8584 (2009) (cited on page 80).

A105. Heinrich, S. P. A primer on motion visual evoked potentials. *Documenta Ophthalmologica* **114,** 83–105. ISSN: 00124486 (2007) (cited on page 34).

A106. Heitger, M. H. *et al.* Bimanual motor coordination in older adults is associated with increased functional brain connectivity–a graph-theoretical analysis. *PloS one* **8,** e62133. ISSN: 1932-6203 (2013) (cited on page 80).

A107. Hermoso de Mendoza, I., Pachón, L. A., Gómez-Gardeñes, J. & Zueco, D. Synchronization in a semiclassical Kuramoto model. *Physical Review E* **90,** 052904. ISSN: 1539-3755 (Nov. 2014) (cited on page 19).

A108. Hilgetag, C. C., Burns, G. A., O'Neill, M. A., Scannell, J. W. & Young, M. P. Anatomical connectivity defines the organization of clusters of cortical areas in the macaque monkey and the cat. *Philosophical transactions of the Royal Society of London. Series B, Biological sciences* **355,** 91–110. ISSN: 0962-8436 (Jan. 2000) (cited on page 40).

A109. Holme, P., Edling, C. R. & Liljeros, F. Structure and time evolution of an Internet dating community. *Social Networks* **26,** 155–174. ISSN: 03788733 (2004) (cited on page 24).

A110. Holme, P. & Saramäki, J. Temporal networks. *Physics Reports* **519,** 97–125 (2012) (cited on page 24).

A111. Hultsch, D. F., MacDonald, S. W. S., Hunter, M. A., Levy-Bencheton, J. & Strauss, E. Intraindividual variability in cognitive performance in older adults: Comparison of adults with mild dementia, adults with arthritis and healthy adults. *Neuropsychology* **14,** 588–598 (2000) (cited on page 94).

A112. Humphries, M. D. & Gurney, K. Network 'small-world-ness': A quantitative method for determining canonical network equivalence. *PLoS ONE* **3** (2008) (cited on page 12).

A113. Hutchison, R. M., Womelsdorf, T., Gati, J. S., Everling, S. & Menon, R. S. Resting-state networks show dynamic functional connectivity in awake humans and anesthetized macaques. *Human Brain Mapping* **34,** 2154–2177. ISSN: 10659471 (2013) (cited on page 80).

A114. Hwang, K., Hallquist, M. N. & Luna, B. The development of hub architecture in the human functional brain network. *Cerebral cortex (New York, N.Y. : 1991)* **23,** 2380–93. ISSN: 1460-2199 (Oct. 2013) (cited on pages 49, 56).

A115. Iturria-Medina, Y. *et al.* Characterizing brain anatomical connections using diffusion weighted MRI and graph theory. *NeuroImage* **36,** 645–660 (2007) (cited on page 37).

A116. Jensen, O. & Mazaheri, A. Shaping functional architecture by oscillatory alpha activity: gating by inhibition. *Frontiers in human neuroscience* **4,** 186 (2010) (cited on page 91).

A117. Joyce, K. E., Laurienti, P. J., Burdette, J. H. & Hayasaka, S. A new measure of centrality for brain networks. *PLoS ONE* **5** (2010) (cited on page 49).

A118. Just, M. A., Cherkassky, V. L., Keller, T. A. & Minshew, N. J. Cortical activation and synchronization during sentence comprehension in high-functioning autism: Evidence of underconnectivity. *Brain* **127,** 1811–1821 (2004) (cited on page 41).

A119. Kaiser, M. & Hilgetag, C. C. Optimal hierarchical modular topologies for producing limited sustained activation of neural networks. *Front Neuroinform* **4,** 8 (2010) (cited on page 41).

A120. Kaiser, M. & Hilgetag, C. C. Edge vulnerability in neural and metabolic networks. *Biological Cybernetics* **90,** 311–317 (2004) (cited on page 41).

A121. Kaiser, M. & Hilgetag, C. C. Nonoptimal component placement, but short processing paths, due to long-distance projections in neural systems. *PLoS Computational Biology* **2,** 0805–0815 (2006) (cited on page 40).

A122. Kaiser, M., Martin, R., Andras, P. & Young, M. P. Simulation of robustness against lesions of cortical networks. *European Journal of Neuroscience* **25,** 3185–3192 (2007) (cited on pages 41, 69).

A123. Kirschner, M. & Gerhart, J. Evolvability. *Proceedings of the National Academy of Sciences* **95,** 8420–8427. ISSN: 0027-8424 (July 1998) (cited on page 29).

A124. Kitzbichler, M. G., Henson, R. N. A., Smith, M. L., Nathan, P. J. & Bullmore, E. T. Cognitive effort drives workspace configuration of human brain functional networks. *The Journal of neuroscience : the official journal of the Society for Neuroscience* **31,** 8259–8270 (2011) (cited on page 40).

A125. Kolmogorov, A. N. Three Approaches to the Quantitative Definition of Information. *Problemy Peredachi Imformatsii* **1,** 3–11 (1965) (cited on page 22).

A126. Kostal, L., Lansky, P. & Rospars, J. P. Neuronal coding and spiking randomness. *European Journal of Neuroscience* **26,** 2693–2701. ISSN: 0953816X (2007) (cited on page 31).

A127. Kuhnert, M. T., Geier, C., Elger, C. E. & Lehnertz, K. Identifying important nodes in weighted functional brain networks: A comparison of different centrality approaches. *Chaos* **22.** ISSN: 10541500 (2012) (cited on page 49).

A128. Kullback, S. & Leibler, R. On Information and Sufficiency. *Annals of Mathematical Statistics* (1951) (cited on pages 19, 22, 110).

A129. Lachaux, J. P., Rodriguez, E., Martinerie, J. & Varela, F. J. Measuring phase synchrony in brain signals. *Human Brain Mapping* **8,** 194–208. ISSN: 10659471 (1999) (cited on pages 35, 83).

A130. Lago-Fernández, L. F., Huerta, R., Corbacho, F. & Sigüenza, J. A. Fast response and temporal coherent oscillations in small-world networks. *Physical review letters* **84,** 2758–2761 (2000) (cited on pages 15, 39, 41).

A131. Latora, V. & Marchiori, M. Efficient behavior of small-world networks. *Physical Review Letters* **87,** 198701 (2001) (cited on pages 11, 12, 40, 98).

A132. Laughlin, S. B. & Sejnowski, T. J. Communication in neuronal networks. *Science (New York, N.Y.)* **301,** 1870–1874. ISSN: 0036-8075 (2003) (cited on page 28).

A133. Leonardi, N. & Van De Ville, D. On spurious and real fluctuations of dynamic functional connectivity during rest. *NeuroImage* **104,** 430–6. ISSN: 1095-9572 (Jan. 2015) (cited on page 84).

A134. Li, A. *et al.* Micro-optical sectioning tomography to obtain a high-resolution atlas of the mouse brain. *Science (New York, N.Y.)* **330,** 1404–1408 (2010) (cited on page 37).

A135. Lobo, A. & Et˜al. Cognocitive mini-test (a simple practical test to detect intellectual changes in medical patients). *Actas luso-españolas de neurologia, psiquiatria y ciencias afines* **7(3),** pp.189–202 (1979) (cited on page 51).

A136. Lohmann, G. *et al.* Eigenvector centrality mapping for analyzing connectivity patterns in fMRI data of the human brain. *PLoS ONE* **5** (2010) (cited on page 49).

A137. Long, K. J. & Allen, N. Abnormal Brain-Stem Auditory Evoked Potentials Following Ondine's Curse. *Archives of Neurology* **41,** 1109–1110. ISSN: 0003-9942 (Oct. 1984) (cited on page 34).

A138. López-Ruiz, R., Mancini, H. L. & Calbet, X. A Statistical Measure of Complexity. *PRA* (1995) (cited on pages 19, 23, 110).

A139. Lynall, M.-E. *et al.* Functional connectivity and brain networks in schizophrenia. *The Journal of neuroscience : the official journal of the Society for Neuroscience* **30,** 9477–9487 (2010) (cited on page 40).

A140. Madden, D. J., Whiting, W. L., Cabeza, R. & Huettel, S. A. Age-related preservation of top-down attentional guidance during visual search. *Psychology and aging* **19,** 304–309 (2004) (cited on pages 80, 81).

A141. Manoach, D. S. Prefrontal cortex dysfunction during working memory performance in schizophrenia: Reconciling discrepant findings. *Schizophr Res* **60,** 285–298 (2003) (cited on page 94).

A142. Markesbery, W. R. Neuropathologic alterations in mild cognitive impairment: A review. *Journal of Alzheimer's Disease* **19,** 221–228 (2010) (cited on page 53).

A143. Martínez, J. *et al.* Anomalous consistency in Mild Cognitive Impairment: A complex networks approach. *Chaos, Solitons & Fractals* **70,** 144–155. ISSN: 09600779 (Jan. 2015) (cited on page 93).

A144. McIntosh, A. R. Mapping cognition to the brain through neural interactions. *Memory (Hove, England)* **7,** 523–48. ISSN: 0965-8211 (cited on page 80).

A145. McIntosh, A. R., Kovacevic, N. & Itier, R. J. Increased brain signal variability accompanies lower behavioral variability in development. *PLoS Comput Biol* **4(7),** e1000106 (2008) (cited on page 94).

A146. McShea, D. W. Complexity and evolution: What everybody knows. *Biology and Philosophy* **6,** 303–324 (1991) (cited on page 23).

A147. Meunier, D., Achard, S., Morcom, A. & Bullmore, E. Age-related changes in modular organization of human brain functional networks. *NeuroImage* **44,** 715–723. ISSN: 10538119 (2009) (cited on page 41).

A148. Meunier, D., Lambiotte, R., Fornito, A., Ersche, K. D. & Bullmore, E. T. Hierarchical modularity in human brain functional networks. English. *Frontiers in neuroinformatics* **3,** 37. ISSN: 1662-5196 (Jan. 2009) (cited on pages 40, 81).

A149. Micheloyannis, S. *et al.* The influence of ageing on complex brain networks: A graph theoretical analysis. *Human Brain Mapping* **30,** 200–208. ISSN: 10659471 (2009) (cited on pages 41, 80).

A150. Milgram, S. The small-world problem. *Psychol Today* **1,** 61–67 (1967) (cited on page 15).

A151. Milo, R. *et al.* Network motifs: simple building blocks of complex networks. *Science (New York, N.Y.)* **298,** 824–827 (2002) (cited on page 10).

A152. Miltner, W. H., Braun, C., Arnold, M., Witte, H. & Taub, E. Coherence of gamma-band EEG activity as a basis for associative learning. *Nature* **397,** 434–436. ISSN: 0028-0836 (1999) (cited on page 29).

A153. Mitchell, A. J. Is it time to separate subjective cognitive complaints from the diagnosis of mild cognitive impairment?. *Age and ageing* **37(5),** pp.4979 (2008) (cited on page 51).

A154. Montemurro, M. A., Rasch, M. J., Murayama, Y., Logothetis, N. K. & Panzeri, S. Phase-of-firing coding of natural visual stimuli in primary visual cortex. *Current biology : CB* **18,** 375–80. ISSN: 0960-9822 (Mar. 2008) (cited on page 31).

A155. Moreno, C. B., Díaz, J.-L. & Martínez, J. Petri Net Modeling of the Brain Circuit Involved in Aggressive Behavior. *Salud Mental.* arXiv: 1209034 (2015) (cited on page 31).

A156. Motter, A. E. & Lai, Y. C. Cascade-based attacks on complex networks. *Physical Review E - Statistical, Nonlinear, and Soft Matter Physics* **66** (2002) (cited on pages 54, 57).

A157. Moy, G. *et al.* Magnetic resonance imaging determinants of intraindividual variability in the elderly: Combined analysis of grey and white matter. *Neuroscience* **186,** 88–93 (2011) (cited on page 94).

A158. Navas, A. *et al.* Functional Hubs in Mild Cognitive Impairment. *International Journal of Bifurcation and Chaos.* **25,** 10 (July 2015) (cited on pages 49, 60).

A159. Newman, M. E. J. Assortative mixing in networks. *Physical review letters* **89,** 208701 (2002) (cited on page 112).

A160. Newman, M. E. J. The Structure and Function of Complex Networks. *SIAM Review* **45,** 167–256. ISSN: 0036-1445 (2003) (cited on pages 8, 16, 17).

A161. Newman, M. E. J. Power laws, Pareto distributions and Zipf's law (2005) (cited on pages 8, 14).

A162. Newman, M. Modularity and community structure in networks. *Proceedings of the National Academy of ...* **103,** 8577–82. ISSN: 0027-8424 (2006) (cited on page 10).

A163. Nichols, T. E. & Holmes, A. P. Nonparametric permutation tests for functional neuroimaging: A primer with examples. *Human Brain Mapping* **15,** 1–25 (2002) (cited on page 84).

A164. Niso, G. *et al.* HERMES: Towards an integrated toolbox to characterize functional and effective brain connectivity. *Neuroinformatics* **11,** 405–434. ISSN: 15392791 (2013) (cited on pages 35, 83).

A165. Nolte, G. *et al.* Identifying true brain interaction from EEG data using the imaginary part of coherency. *Clinical Neurophysiology* **115,** 2292–2307. ISSN: 13882457 (2004) (cited on pages 35, 61).

A166. Odom, J. V. *et al.* Visual evoked potentials standard (2004). *Documenta Ophthalmologica* **108,** 115–123 (2004) (cited on page 34).

A167. Onnela, J. P., ASaramaki, J., Kertesz, J. & Kaski, K. Intensity and coherence of motifs in weighted complex networks. *Phy Rev E Stat Nonliinear Soft Matter Phys* **71** (2005) (cited on pages 10, 101).

A168. Palva, J. M., Palva, S. & Kaila, K. Phase synchrony among neuronal oscillations in the human cortex. *The Journal of neuroscience : the official journal of the Society for Neuroscience* **25,** 3962–3972. ISSN: 1529-2401 (2005) (cited on page 91).

A169. Pan, R. K., Chatterjee, N. & Sinha, S. Mesoscopic organization reveals the constraints governing Caenorhabditis elegans nervous system. *PLoS ONE* **5** (2010) (cited on page 40).

A170. Pan, R. K. & Saramäki, J. Path lengths, correlations, and centrality in temporal networks. *Physical Review E - Statistical, Nonlinear, and Soft Matter Physics* **84** (2011) (cited on page 24).

A171. Papo, D., Zanin, M., Pineda-Pardo, J. A., Boccaletti, S. & Buldú, J. M. Functional brain networks: great expectations, hard times and the big leap forward. *Philosophical transactions of the Royal Society of London. Series B, Biological sciences* **369.** ISSN: 1471-2970. doi:10.1098/rstb.2013.0525 (Oct. 2014) (cited on page 68).

A172. Pecora, L. M. & Carroll, T. L. Master Stability Functions for Synchronized Coupled Systems. *Physical Review Letters* **80,** 2109–2112. ISSN: 0031-9007 (Mar. 1998) (cited on page 12).

A173. Pereda, E., Quiroga, R. Q. & Bhattacharya, J. Nonlinear multivariate analysis of neurophysiological signals. *Progress in neurobiology* **77(1-2),** 1–37 (2005) (cited on pages 36, 96).

A174. Pereda, E., Quiroga, R. Q. & Bhattacharya, J. Nonlinear multivariate analysis of neurophysiological signals. *Progress in Neurobiology* **77,** 1–37 (2005) (cited on pages 35, 83).

A175. Pereira, F., Mitchell, T. & Botvinick, M. Machine learning classifiers and fMRI: a tutorial overview. *NeuroImage* **45,** S199–S209. ISSN: 10959572 (2009) (cited on page 32).

A176. Pérez, T. & Uchida, A. Reliability and synchronization in a delay-coupled neuronal network with synaptic plasticity. *Phys. Rev. E* **83,** 61915 (2011) (cited on page 95).

A177. Petersen, R. C. Mild cognitive impairment as a diagnostic entity. *Journal of Internal Medicine* **256,** 183–194 (2004) (cited on pages 51, 53).

A178. Pineda-Pardo, J. A. *et al.* White Matter Damage Disorganizes Brain Functional Networks in Amnestic Mild Cognitive Impairment. *Brain connectivity* **00,** 1–11. ISSN: 2158-0022 (2014) (cited on page 80).

A179. Pinsk, M. A., Doniger, G. M. & Kastner, S. Push-pull mechanism of selective attention in human extrastriate cortex. *Journal of neurophysiology* **92,** 622–629 (2004) (cited on page 91).

A180. Plastino, A. & Rosso, O. A. Entropy and Statistical Complexity in Brain Activity. *Europhysics News* (2005) (cited on pages 19, 25, 110).

A181. Ponten, S. C., Bartelomei, F. & Stam, C. J. Small-world networks and epilepsy: graph theoretical analysis of intracerebrally recorded mesial temporal lobe seizures.*Clin Neurophysiol* **118,** 918–927 (2007) (cited on page 41).

A182. Reuter-Lorenz, P. A. & Cappell, K. A. Neurocognitive aging and the compensation hypothesis. *Current Directions in Psychological Science* **17,** 177–182 (2008) (cited on page 80).

A183. Rodriguez, E. *et al.* Perception's shadow: long-distance synchronization of human brain activity. *Nature* **397,** 430–433. ISSN: 0028-0836 (1999) (cited on page 29).

A184. Rosenblum, M. G. & Pikovsky, A. S. Detecting direction of coupling in interacting oscillators. *Physical review. E, Statistical, nonlinear, and soft matter physics* **64,** 045202. ISSN: 1063-651X (2001) (cited on page 35).

A185. Rosso, O. A. & et al Larrondo, H. A. Distinguish Noise from Chaos. *PRL* (2007) (cited on pages 19, 21, 110).

A186. Rosso, O. A., Vicente, R. & Mirasso, C. R. Encryption test of pseudo-aleatory messages embedded on chaotic laser signals: An information theory approach. *Physics Letters, Section A: General, Atomic and Solid State Physics* **372,** 1018–1023 (2008) (cited on page 18).

A187. Rosso, O. A. Entropy changes in brain function. *International journal of psychophysiology : official journal of the International Organization of Psychophysiology* **64,** 75–80. ISSN: 0167-8760 (2007) (cited on page 18).

A188. Rubinov, M. & Sporns, O. Complex network measures of brain connectivity: Uses and interpretations. *NeuroImage* **52,** 1059–1069 (2010) (cited on page 102).

A189. Rulkov, N. F., Sushchik, M. M., Tsimring, L. S. & Abarbanel, H. D. I. Generalized synchronization of chaos in directionally coupled chaotic systems. *Physical Review E* **51,** 980–994 (1995) (cited on page 35).

A190. Salami, A., Rieckmann, A., Fischer, H. & Bäckman, L. A multivariate analysis of age-related differences in functional networks supporting conflict resolution. *NeuroImage* **86,** 150–163. ISSN: 10538119 (2014) (cited on page 80).

A191. Sancho, M., Quesada, F. S. & Bajo, R. Magnetoencefalografía y exploración de la dinámica cerebral. *Revista Española de Física* **21.** ISSN: 0213-862X (Jan. 2011) (cited on pages 33, 34).

A192. Satarić, M. V., Tuszyński, J. A. & Akula, R. B. Kinklike excitations as an energy-transfer mechanism in microtubules. *Physical Review E* **48,** 589–597. ISSN: 1063651X (1993) (cited on page 31).

A193. Sauseng, P. *et al.* EEG alpha synchronization and functional coupling during top-down processing in a working memory task. *Human Brain Mapping* **26,** 148–155. ISSN: 10659471 (2005) (cited on page 91).

A194. Scannell, J. W., Burns, G. A. P. C., Hilgetag, C. C., O'Neil, M. A. & Young, M. P. The connectional organization of the cortico-thalamic system of the cat. *Cerebral Cortex* **9,** 277–299 (1999) (cited on page 37).

A195. Scheff, S. W., Price, D. A., Schmitt, F. A., Dekosky, S. T. & Mufson, E. J. Synaptic alterations in CA1 in mild Alzheimer disease and mild cognitive impairment. *Neurology* **68,** 1501–1508. ISSN: 00283878 (2007) (cited on page 53).

A196. Schneider, J. A., Arvanitakis, Z., Leurgans, S. E. & Bennett, D. A. The neuropathology of probable Alzheimer disease and mild cognitive impairment. *Annals of Neurology* **66,** 200–208 (2009) (cited on page 53).

A197. Schöner, G. & Kelso, J. A. Dynamic pattern generation in behavioral and neural systems. *Science (New York, N.Y.)* **239,** 1513–1520. ISSN: 0036-8075 (1988) (cited on page 5).

A198. Shanahan, M. The brain's connective core and its role in animal cognition. **367,** 2704–2714 (2012) (cited on page 40).

A199. Shefi, O., Golding, I., Segev, R., Ben-Jacob, E. & Ayali, a. Morphological Characterization of in Vitro Neuronal Networks. *Phys. Rev. E* **66,** 21905. ISSN: 1063-651X (2002) (cited on page 39).

A200. Shiner, J. S., Davison, M. & Landsberg, P. T. Simple measure for complexity. *Physical Review E* **59,** 1459–1464. ISSN: 1063-651X (Feb. 1999) (cited on pages 22, 23).

A201. Singer, W. Putative functions of temporal correlations in neocortical processing (1994) (cited on pages 29, 41).

A202. Smit, D. J. A. *et al.* The Brain Matures with Stronger Functional Connectivity and Decreased Randomness of Its Network. *PLoS ONE* **7,** e36896 (2012) (cited on page 80).

A203. Solesio, E. *et al.* Retroactive interference in normal aging: A magnetoencephalography study. *Neuroscience Letters* **456,** 85–88 (2009) (cited on pages 80, 82, 83).

A204. Solesio-Jofre, E. *et al.* Age effects on retroactive interference during working memory maintenance. *Biological Psychology* **88,** 72–82 (2011) (cited on page 80).

A205. Solesio-Jofre, E. *et al.* Age-related effects in working memory recognition modulated by retroactive interference. *Journals of Gerontology - Series A Biological Sciences and Medical Sciences* **67 A,** 565–572 (2012) (cited on page 80).

A206. Song, C., Havlin, S. & Makse, H. A. Self-similarity of complex networks. *Nature* **433,** 392–395 (2005) (cited on page 41).

A207. Sporns, O., Tononi, G. & Edelman, G. M. Connectivity and complexity: The relationship between neuroanatomy and brain dynamics. *Neural Networks* **13,** 909–922 (2000) (cited on page 80).

A208. Sporns, O., Chialvo, D. R., Kaiser, M. & Hilgetag, C. C. Organization, development and function of complex brain networks. **8,** 418–425 (2004) (cited on page 41).

A209. Sporns, O., Honey, C. J. & Kötter, R. Identification and classification of hubs in brain networks. *PLoS ONE* **2** (2007) (cited on pages 49, 59).

A210. Sporns, O. & Zwi, J. D. The small world of the cerebral cortex. *Neuroinformatics* **2,** 145–162. ISSN: 1539-2791 (2004) (cited on page 36).

A211. Stam, C. J. & Dijk, B. Synchronization likelihood: an unbiased measure of generalized synchronization in multivariate data sets. *Physica D* **163,** 236–251 (2002) (cited on page 96).

A212. Stam, C. J., Jones, B. F., Nolte, G., Breakspear, M. & Scheltens, P. Small-world networks and functional connectivity in Alzheimer's disease. *Cerebral cortex (New York, N.Y. : 1991)* **17,** 92–99. ISSN: 1047-3211 (2007) (cited on pages 41, 59, 80).

A213. Stam, C. J., Jones, B. F., Nolte, G., Breakspear, M. & Scheltens, P. Small-world networks and functional connectivity in Alzheimer's disease. *Cerebral Cortex* **17,** 92–99. ISSN: 10473211 (2007) (cited on pages 41, 69).

A214. Stam, C. J. & Van Dijk, B. W. Synchronization likelihood: An unbiased measure of generalized synchronization in multivariate data sets. *Physica D: Nonlinear Phenomena* **163,** 236–251 (2002) (cited on pages 35, 50, 52).

A215. Stam, C. J. & van Straaten, E. C. W. The organization of physiological brain networks. *Clinical Neurophysiology* **123,** 1067–1087 (2012) (cited on pages 41, 80).

A216. Stam, C. J. *et al.* Magnetoencephalographic evaluation of resting-state functional connectivity in Alzheimer's disease. *NeuroImage* **32,** 1335–1344. ISSN: 10538119 (2006) (cited on page 50).

A217. Stam, C. J. *et al.* Graph theoretical analysis of magnetoencephalographic functional connectivity in Alzheimer's disease. *Brain* **132,** 213–224 (2009) (cited on pages 40, 69).

A218. Stam, C. J. *et al.* Graph theoretical analysis of magnetoencephalographic functional connectivity in Alzheimer's disease. *Brain : a journal of neurology* **132,** 213–224. ISSN: 1460-2156 (2009) (cited on pages 41, 50, 54).

A219. Stein, R. B., Gossen, E. R. & Jones, K. E. Neuronal variability: noise or part of the signal? *Nature reviews. Neuroscience* **6,** 389–397. ISSN: 1471-003X (2005) (cited on page 31).

A220. Stephan, K. E. & Friston, K. J. Models of effective connectivity in neural systems. **2007,** 303–325 (2007) (cited on page 38).

A221. Stern, Y., Albert, S., Tang, M. X. & Tsai, W. Y. Rate of memory decline in AD is related to education and occupation: cognitive reserve? *Neurology* **53,** 1942–7. ISSN: 0028-3878 (Dec. 1999) (cited on page 108).

A222. Stern, Y. What is cognitive reserve? Theory and research application of the reserve concept. *Journal of the International Neuropsychological Society : JINS* **8,** 448–460 (2002) (cited on page 108).

A223. Stern, Y. Cognitive reserve in ageing and Alzheimer's disease. *The Lancet Neurology* **11,** 1006–1012 (2012) (cited on page 108).

A224. Sternberg, S. High-speed scanning in human memory. *Science* **153,** 652–654 (1966) (cited on page 108).

A225. Strogatz, S. H. Exploring complex networks. *Nature* **410,** 268–276. ISSN: 0028-0836 (2001) (cited on pages 15, 41).

A226. Tamnes, C. K., Fjell, A. M., Westlye, L. T. & Østby, Y. W. K. B. Becoming consistent: developmental reductions in intraindividual variability in reaction time are related to white matter integrity. *J Neurosci* **32,** 972–982 (2012) (cited on pages 94, 95).

A227. Tang, J., Scellato, S., Musolesi, M., Mascolo, C. & Latora, V. Small-world behavior in time-varying graphs. *Physical Review E - Statistical, Nonlinear, and Soft Matter Physics* **81** (2010) (cited on page 24).

A228. Tang, Y., Gao, H., Zou, W. & Kurths, J. Identifying controlling nodes in neuronal networks in different scales. *PLoS ONE* **7.** ISSN: 19326203 (2012) (cited on page 57).

A229. Tass, P. *et al.* Detection of n : m Phase Locking from Noisy Data: Application to Magnetoencephalography. *Physical Review Letters* **81,** 3291–3294. ISSN: 0031-9007 (Oct. 1998) (cited on page 35).

A230. Teipel, S. J. *et al.* Longitudinal changes in fiber tract integrity in healthy ageing and mild cognitive impairment: A DTI followup study. *J Alzheimers Dis* **22,** 507–522 (2010) (cited on page 94).

A231. Tiana, J., Torrent, M. C. & et al Rosso, C. Quantifying the statistical complexity of low-frequency fluctuations in semiconductor lasers with optical feedback. *PRA* (2010) (cited on page 18).

A232. Tononi, G., Sporns, O. & Edelman, G. M. A measure for brain complexity: relating functional segregation and integration in the nervous system.*Proceedings of the National Academy of Sciences of the United States of America* **91,** 5033–5037 (1994) (cited on page 41).

A233. Tononi, G., Edelman, G. M. & Sporns, O. Complexity and coherency: Integrating information in the brain. **2,** 474–484 (1998) (cited on page 41).

A234. Tractenberg, R. E. & Pietrzak, R. H. Intra-individual variability in Alzheimer's disease and cognitive aging: Definitions, context, and effect sizes.*PLoS One* **6(4),** e16973 (2011) (cited on page 94).

A235. Tuszynski, J. a., Brown, J. a. & Sept, D. Models of the Collective Behavior of Proteins in Cells: Tubulin, Actin and Motor Proteins. *Journal of Biological Physics* **29,** 401–428. ISSN: 00920606 (2003) (cited on page 31).

A236. Tuszyński, J. *et al.* Molecular dynamics simulations of tubulin structure and calculations of electrostatic properties of microtubules. *Mathematical and Computer Modelling* **41,** 1055–1070. ISSN: 08957177 (May 2005) (cited on page 31).

A237. Uchida, A. & McAllister, R. Consistency of Nonlinear System Response to Complex Drive Signals. *Phys. Rev. Lett* **93,** 244102 (2004) (cited on pages 95, 104).

A238. Uchida, A., Yoshimura, K., Davis, P., Yoshimori, S. & Roy, R. Local conditional Lyapunov exponent characterization of consistency of dynamical response of the driven Lorenz system. *Phys. Rev. E* **78,** 36203 (2008) (cited on page 95).

A239. Van den Heuvel, M. P., Kahn, R. S., Goni, J. & Sporns, O. From the Cover: High-cost, high-capacity backbone for global brain communication. **109,** 11372–11377 (2012) (cited on page 40).

A240. Van den Heuvel, M. P., Stam, C. J., Boersma, M. & Hulshoff Pol, H. E. Small-world and scale-free organization of voxel-based resting-state functional connectivity in the human brain. *NeuroImage* **43,** 528–539 (2008) (cited on page 39).

A241. Van Putten, M. Application of a neural complexity measure to multichannel EEG. *Physics Letters A* **281,** 131–141. ISSN: 03759601 (2001) (cited on page 41).

A242. Van Gerven, M. *et al.* The brain-computer interface cycle. *Journal of neural engineering* **6,** 041001. ISSN: 1741-2560 (2009) (cited on pages 32, 33).

A243. Varshney, L., Chen, B., Paniagua, E., Hall, D. & Chklovskii, D. Structural properties of the Caenorhabditis elegans neuronal network. *PLoS computational biology* **7,** e1001066. ISSN: 1553-7358 (2011) (cited on page 37).

A244. Vigo, R. Complexity over uncertainty in generalized representational information theory (GRIT): A structure-sensitive general theory of information. *Information (Switzerland)* **4,** 1–30. ISSN: 20782489 (2013) (cited on page 21).

A245. Wang, L., Li, Y., Metzak, P., He, Y. & Woodward, T. S. Age-related changes in topological patterns of large-scale brain functional networks during memory encoding and recognition. *NeuroImage* **50,** 862–872. ISSN: 10538119 (2010) (cited on page 80).

A246. Watss, D. J. & Strogatz, S. H. Collective dynamics of small word networks. *Nature* **393** (1998) (cited on pages 9, 15, 80).

A247. Watts, D. J. & Strogatz, S. H. Collective dynamics of 'small-world' networks. *Nature* **393,** 440–442. ISSN: 0028-0836 (1998) (cited on page 41).

A248. White, J. G., Southgate, E., Thomson, J. N. & Brenner, S. The Structure of the Nervous System of the Nematode Caenorhabditis elegans. *Philosophical Transactions of the Royal Society B: Biological Sciences* **314,** 1–340 (1986) (cited on page 37).

A249. Whitehouse, A. J. O. & Bishop, D. V. M. Hemispheric division of function is the result of independent probabilistic biases. *Neuropsychologia* **47,** 1938–43. ISSN: 1873-3514 (July 2009) (cited on page 60).

A250. Wook Yoo, S. *et al.* A Network Flow-based Analysis of Cognitive Reserve in Normal Ageing and Alzheimer's Disease. en. *Scientific reports* **5,** 10057. ISSN: 2045-2322 (Jan. 2015) (cited on page 108).

A251. Wu, S., Amari, S.-I. & Nakahara, H. Population coding and decoding in a neural field: a computational study. *Neural computation* **14,** 999–1026. ISSN: 0899-7667 (2002) (cited on page 31).

A252. Xia, M., Wang, J. & He, Y. BrainNet Viewer: a network visualization tool for human brain connectomics. *PloS one* **8,** e68910. ISSN: 1932-6203 (Jan. 2013) (cited on page 29).

A253. Yesavage, J. A. & Brooks, J. O. On the importance of longitudinal research in Alzheimer's disease. *Journal of the American Geriatrics Society* **39,** 942–4. ISSN: 0002-8614 (Sept. 1991) (cited on pages 51, 81).

A254. Yi, G. *et al.* Ordinal Pattern Based Complexity Analysis for EEG Activity Evoked by Manual Acupuncture in Healthy Subjects. en. *International Journal of Bifurcation and Chaos* (Mar. 2014) (cited on page 110).

A255. Young, K. & Schuff, N. NIH Public Access.*NeuroImage* **39,** 1721–1730 (2009) (cited on page 31).

A256. Yu, S., Huang, D., Singer, W. & Nikolić, D. A small world of neuronal synchrony. *Cerebral Cortex* **18,** 2891–2901 (2008) (cited on page 41).

A257. Zalesky, A. & Breakspear, M. Towards a statistical test for functional connectivity dynamics. *NeuroImage* **114,** 466–70. ISSN: 1095-9572 (July 2015) (cited on page 84).

A258. Zamora-López, G., Zhou, C. & Kurths, J. Cortical hubs form a module for multisensory integration on top of the hierarchy of cortical networks. *Frontiers in neuroinformatics* **4,** 1. ISSN: 1662-5196 (Jan. 2010) (cited on pages 40, 49).

A259. Zanin, M. & Boccaletti, S. Complex networks analysis of obstructive nephropathy data. *Chaos* **21.** ISSN: 10541500 (2011) (cited on page 29).

A260. Zanin, M. & Boccaletti, S. Complex networks analysis of obstructive nephropathy data. *Chaos* **21,** 33103 (2011) (cited on pages 95, 98, 104).

A261. Zanin, M., Zunino, L., Rosso, O. A. & Papo, D. Permutation Entropy and Its Main Biomedical and Econophysics Applications: A Review. en. *Entropy* **14,** 1553–1577. ISSN: 1099-4300 (Aug. 2012) (cited on page 110).

A262. Zanin, M. *et al.* Optimizing Functional Network Representation of Multivariate Time Series. *Scientific Reports* **2** (2012) (cited on pages 37, 64).

A263. Zanin, M. *et al.* Optimizing Functional Network Representation of Multivariate Time Series. *Sci Rep ; 2.* **630,** 1–6 (2012) (cited on page 98).

A264. Zanin, M. *et al.* Parenclitic networks' representation of data sets. *arXiv:1304.1896 [physics.soc-ph]* (2013) (cited on pages 95, 96, 98, 104).

A265. Zanin, M. *et al.* How does the forest's look depend on what trees you plant? Connectivity metrics reveal different aspects of functional brain organization. *Cerebral Cortex* **Unpublishe** (2015) (cited on page 34).

A266. Zeier, H. Complementary functions of the two brain hemispheres: comparisons with earlier conceptions and implications for individual and society. *The International journal of neuroscience* **47,** 175–9. ISSN: 0020-7454 (July 1989) (cited on page 60).

A267. Zhou, D., Thompson, W. K. & Siegle, G. MATLAB toolbox for functional connectivity. *NeuroImage* **47,** 1590–1607 (2009) (cited on page 35).

A268. Zhu, W. *et al.* Changing topological patterns in normal aging using large-scale structural networks. *Neurobiology of Aging* **33,** 899–913 (2012) (cited on page 80).

A269. Zunino, L., Zanin, M., Tabak, B. M., Pérez, D. G. & Rosso, O. A. Complexity-entropy causality plane: A useful approach to quantify the stock market inefficiency. *Physica A: Statistical Mechanics and its Applications* **389,** 1891–1901 (2010) (cited on page 114).

A270. Zunino, L. *et al.* Permutation entropy of fractional Brownian motion and fractional Gaussian noise. *Physics Letters, Section A: General, Atomic and Solid State Physics* **372,** 4768–4774. ISSN: 03759601 (2008) (cited on page 18).

A271. Zuo, X. N. *et al.* Network centrality in the human functional connectome. *Cerebral Cortex* **22,** 1862–1875. ISSN: 10473211 (2012) (cited on page 56).

Index

I

L

M

N

O

P

R

S

W